New Methods for Predicting Critical Tensile Strains in an M-E Framework

by

Mary Marjorie Robbins

A dissertation submitted to the Graduate Faculty of
Auburn University
in partial fulfillment of the
requirements for the Degree of
Doctor of Philosophy

Auburn, Alabama
May 4, 2013

Keywords: Asphalt concrete, pavement design,
mechanistic-empirical design

Approved by

David Timm, Chair, Brasfield & Gorrie Professor, Civil Engineering
Rod E. Turochy, Associate Professor, Civil Engineering
Randy West, Director, National Center for Asphalt Technology
John Fulton, Associate Professor, Biosystems Engineering

Abstract

As mechanistic-empirical pavement design comes to the forefront of design, the accurate prediction of critical tensile strains at the bottom of the asphalt concrete (AC) becomes increasingly more important to predict fatigue cracking. Current methods of predicting tensile strains typically rely solely on dynamic modulus (|E*|) of the AC to predict strain from which pavement performance is predicted. In doing so, vehicle speed is represented by loading frequency. However, a relationship between loading frequency in the lab and vehicle speed in the field has yet to be fully validated. As a result tensile strains are inaccurately predicted, leading to erroneous performance predictions and potential for inefficient pavement designs. A potential solution is to calibrate AC modulus to field-measured strain. This investigation pairs field measured strain from instrumented test sections at the National Center for Asphalt Technology (NCAT) Test Track from both the 2006 and 2009 test cycles with the modulus required to achieve those strains using a Layered Elastic Analysis (LEA) method. These sections represent a wide variety of AC mixtures including reclaimed asphalt pavement (RAP), warm-mix asphalt (WMA), high RAP, RAP and WMA combinations, highly polymer modified asphalt, sulfur-modified warm-mix and other, more conventional, mixtures. Utilizing the method for development of a master curve outlined in AASHTO PP 61-09, a field-based master curve was developed for the calibrated modulus using vehicle speed rather than loading frequency. Based on this sigmoidal fit function, a model was then developed to

predict modulus using vehicle speed, shape parameters for the |E*| master curves for the associated mixtures, as well as shape parameters for |G*| for the associated binders, gradation and volumetrics of the mixtures involved. This model enables the prediction of critical tensile strain within LEA at a given pavement temperature and vehicle speed.

Acknowledgments

The author would like to express deep appreciation to the author's advisor, Dr. David Timm for granting her this opportunity and for his guidance, wisdom and patience. The author thanks her family and friends who have always supported her in her endeavors with patience and love, and for being a voice of reason throughout this journey. She is also grateful for the guidance and support offered by her advisory committee, Dr. Randy West, Dr. Rod Turochy and Dr. John Fulton.

The author would like to thank the National Center for Asphalt Technology for the use of their facilities and support for this research. The author acknowledges the following state departments of transportation for their support and cooperation: Alabama, Florida, Mississippi, Missouri, North Carolina, South Carolina, Oklahoma, and Tennessee. The author also acknowledges the Federal Highway Administration, Kraton Performance Polymers, Inc., Lake Asphalt of Trinidad and Tobago (1978) Ltd., and Shell Oil Products U.S.A for their support and cooperation.

Computer software used: Microsoft Word, Microsoft Excel, WESLEA Version 3.0, Mechanistic-Empirical Pavement Design Guide Version 1.0, DataFit Version 9.0, EVERCALC

TABLE OF CONTENTS

Abstract ii

Acknowledgements iv

LIST OF TABLES xi

LIST OF FIGURES xiii

LIST OF ABBREVIATIONS xvi

CHAPTER 1 1

INTRODUCTION 1

1.1 BACKGROUND 1

1.2 OBJECTIVES 6

1.3 SCOPE 7

1.4 ORGANIZATION OF DISSERTATION 7

CHAPTER 2 9

LITERATURE REVIEW 9

2.1 INTRODUCTION 9

2.2 DETERMINATION OF |E*| 10

2.2.1 Laboratory Testing 10

2.2.2 Predictive Models 13

2.2.2.1 Witczak 1-37A 14

2.2.2.2 Hirsch Model 16

2.2.2.3 Witczak 1-40D 18
2.3 FACTORS AFFECTING |E*| 20
2.3.1 Effect of Aggregate Properties 21
2.3.2 Effect of Binder Properties 22
2.4 APPLICATION OF |E*| 24
2.4.1 Master Curve Construction 24
2.4.1.1 Master Curve Construction: AASHTO TP 62-07 24
2.4.1.2 Master Curve Construction: AASHTO TP79-09/PP 61-09 26
2.4.1.3 Comparison of Master Curve Construction 27
2.4.2 Use in MEPDG 29
2.4.2.1 Master Curve Construction in MEPDG 32
2.5 TRANSLATION OF |E*| TO FIELD CONDITIONS 33
2.5.1 Loading Frequency in the Field 34
2.5.1.1 Time of Loading 34
2.5.1.2 Time-Frequency Relationship 37
2.5.2 Loading Conditions and LVE Region 38
2.6 FACTORS INFLUENCING STRAIN 40
2.7 SUMMARY 42
CHAPTER 3 44
METHODOLOGY OVERVIEW AND TESTING FACILITIES 44
3.1 INTRODUCTION 44
3.2 METHODOLOGY OVERVIEW 45
3.3 NCAT TEST TRACK 48

3.3.1 2006 Structural Study 50
3.3.1.1 Pavement Cross-sections: 2006 Structural study 50
3.3.2 2009 Structural Study 52
3.3.2.1 Pavement Cross-sections: 2009 Structural Study 53
3.3.3 Instrumentation 55
3.3.4 Traffic 59
3.3.5 Data Acquisition 60
3.3.6 Performance Monitoring 60
3.3.7 FWD Testing 61
3.4 IN-PLACE PROPERTIES FROM NCAT TEST TRACK 62
3.4.1 Volumetric and Gravimetric Properties 63
3.4.2 Backcalculated Moduli 65
3.5 LABORATORY TESTING 67
3.5.1 Dynamic Modulus Testing 67
3.5.1.1 Dynamic Modulus Master Curves 70
3.5.2 Dynamic Shear Modulus Testing 74
3.5.2.1 Dynamic Shear Modulus Master Curve 76
3.6 SUMMARY 77
CHAPTER 4 79
MODULUS-STRAIN RELATIONSHIPS 79
4.1 INTRODUCTION 79
4.2 MEASURED PAVEMENT RESPONSE 79
4.3 STRAIN ASSOCIATED WITH DAMAGE 81

4.4 NON-ELASTIC STRAIN 85
4.4.1 Strain as a Function of Time and Temperature 86
4.4.2 RMSE as an Indicator of Non-elastic Behavior 89
4.4.3 Difference between Maximum and 95th Percentile Strain 92
4.4.4 Gauge Functionality 93
4.5 MODULUS-STRAIN RELATIONSHIP 97
4.5.1 Structure 98
4.5.2 Loading 98
4.5.3 Evaluation 99
4.5.4 Slip Condition 99
4.5.5 Modulus-strain Relationship 100
4.6 SUMMARY 104
CHAPTER 5 106
FIELD-CALIBRATED MASTER CURVES 106
5.1 INTRODUCTION 106
5.2 MASTER CURVE CONSTRUCTION 107
5.2.1 Calculated Speed 109
5.2.2 Composite Parameters 112
5.3 RESULTS 120
5.4 SUMMARY 123
CHAPTER 6 125
MODEL DEVELOPMENT AND PERFORMANCE 125
6.1 INTRODUCTION 125

6.2 PARAMETER SELECTION 127
6.3 MODEL CALIBRATION 131
6.4 COMPREHENSIVE MODEL PERFORMANCE 137
6.5 SUMMARY 153
CHAPTER 7 155
CONCLUSIONS AND RECOMMENDATIONS 155
7.1 SUMMARY 155
7.2 CONCLUSIONS 161
7.3 RECOMMENDATIONS 163
REFERENCES 165
APPENDIX A 174
AS-BUILT PROPERTIES 174
APPENDIX B 219
DYNAMIC MODULUS MASTER CURVE PARAMETERS 219
APPENDIX C 222
DYNAMIC SHEAR MODULUS MASTER CURVE PARAMETERS 222
APPENDIX D 225
FIELD-CALIBRATED MASTER CURVES 225

LIST OF TABLES

Table 2.1: Recommended testing temperatures and loading frequencies, AASHTO PP 61-09 13

Table 2.2: Asphalt |E*| estimation at different hierarchical input levels for new and reconstruction design (ARA, Inc. 2004) 30

Table 2.3: Recommended frequencies and temperatures for |E*| and |G*|, at level one design (ARA Inc. 2004) 31

Table 3.1: Location of Thermistors 59

Table 3.2: Spacing Between Axles (Taylor 2008) 60

Table 3.3: Axle Weight by Truck (Taylor 2008) 60

Table 3.4: Surveyed Layer Thickness Used for Backcalculation 66

Table 3.5: Average Backcalculated Moduli for Unbound Layers 67

Table 4.1: Performance summaries for 2009 structural sections 85

Table 4.2: Summary of cut-off dates for strain 97

Table 4.3: Coefficients for modulus-strain relationships in a full bond condition 104

Table 5.1: Field-calibrated master curve inputs for S9 trial 114

Table 5.2: In-place VMA and VFA for each lift, S9 114

Table 5.3: Composite VMA and VFA, S9 114

Table 5.4: Fitting parameters and fit statistics for field-calibrated master curve, S9 115

Table 5.5: Results from speed study and resulting composite moduli, S9 116

Table 5.6: Summary of field master curve fitting parameters and fit statistics 122

Table 6.1: Volumetric and gravimetric properties of composite AC layer 128

Table 6.2: Aggregate gradation properties for composite AC layer 128

Table 6.3: Dynamic modulus master curve fitting parameters for composite AC layer. 130

Table 6.4: Dynamic shear modulus master curve fitting parameters for composite AC layer 131

Table 6.5: Fit statistics for fitting parameter models 136

Table 6.6: Correlation matrix for log $E_{comp,min}$ 136

Table 6.7: Correlation matrix for β_{comp} 136

Table 6.8: Correlation matrix for γ_{comp} 136

Table 6.9: Correlation matrix for $E_{a,|E^*|}$ 137

Table 6.10: Fit statistics for field-calibrated master curve and comprehensive model for composite AC modulus 138

Table 6.11: Calculated R^2 for strain predictions 150

Table 6.12: Percent differences for strain prediction methods..... 153

Table 7.1: Fit statistics for fitting parameter models 160

LIST OF FIGURES

Figure 1.1: Phase lag between sinusoidal stress and induced strain (Muench 2003)..... 3

Figure 1.2: MEPDG iterative procedure for loading time (*after* ARA 2003)..... 5

Figure 2.1: Master curve fitting parameters. 26

Figure 2.2 Load Duration Definitions. 35

Figure 3.1: General methodology..... 46

Figure 3.2: Aerial view of the NCAT Test Track. 49

Figure 3.3: Triple trailer truck. 49

Figure 3.4: 2006 Structural Study Test Sections (Timm 2009). 51

Figure 3.5: 2009 Structural Study Test Sections. 54

Figure 3.6: Standard Configuration for Gauges (Timm 2009)..... 56

Figure 3.7: Geokon model 3500 earth pressure cell..... 57

Figure 3.8: CTL strain gauge. 58

Figure 3.9: Random locations and FWD testing scheme. 62

Figure 3.10: The AMPT and close up of specimen..... 69

Figure 4.1: Illustration of peak tensile strain used for investigation. 80

Figure 4.2: Crack maps for sections N1 and N2 (Timm et al. 2009). 83

Figure 4.3: Rut depths for section S11. 85

Figure 4.4: Crack map for N9 for 2009 test cycle. 85

Figure 4.5: Strain and mid-depth temperature with time, section N6. 87

Figure 4.6: Strain with mid-depth temperature, section N6. 88

Figure 4.7: Example of strain trace removed. 89

Figure 4.8: RMSE over time for section N1. 90

Figure 4.9: Plot of temperature and RMSE with time, section N6. 92

Figure 4.10: Strain and mid-depth temperature with time, N9 (2009). 94

Figure 4.11: Strain and mid-depth temperature with time, N7. 95

Figure 4.12: Strain and mid-depth temperature with time, S12. 96

Figure 4.13: Strain and mid-depth temperature with time, N10. 97

Figure 4.14: Slip conditions investigated. 100

Figure 4.15: Modulus-strain relationship, S9, full bond condition. 101

Figure 4.16: AC moduli for fully bonded condition, S9. 102

Figure 4.17: AC moduli for slip and partial slip conditions, S9. 102

Figure 4.18: Backcalculated AC moduli and AC moduli for full-slip condition, S9..... 104

Figure 5.1: Time between steer axle at pressure plate 13 and pressure plate 14. 110

Figure 5.2: Distribution of speed for 2009 test sections 118

Figure 5.3: Comparison of composite moduli for geometric mean method, applied to speed study. 118

Figure 5.4: Comparison of composite moduli for weighted average method, applied to speed study. 119

Figure 5.5: Comparison of composite moduli for method to blend G_{sb}, applied to speed study. 119

Figure 5.6: Field-calibrated master curve, N5..... 122

Figure 6.1: Strain-temperature relationships for section N9 from 2006 and 2009. 141

Figure 6.2: Predicted composite AC moduli from comprehensive model and measured composite AC moduli for N8. 144

Figure 6.3: Predicted composite AC moduli from comprehensive model and measured composite AC moduli for N11 144

Figure 6.4: Predicted composite AC moduli from comprehensive model and measured composite AC moduli for S9..... 144

Figure 6.5: Predicted composite AC moduli from comprehensive model and measured composite AC moduli for N9 (2009 test cycle) 144

Figure 6.6: Composite modulus predicted by model with measured composite modulus.147

Figure 6.7: Predicted strain from predicted composite modulus against measured strain.149

Figure 6.8: Predicted strain against measured strain, section N7..... 151

Figure 6.9: Comparison of strain values for N9 (2006 test cycle) (after Robbins 2009).153

Figure 7.1: General approach to developing a new method for predicting critical tensile strains. 157

LIST OF ABBREVIATIONS

AASHTO: American Association of State Highway and Transportation Officials

AC: Asphalt Concrete

AMPT: Asphalt Mixture Performance Tester

ARAN: Automate Road Analyzer

ESAL: Equivalent Single Axle Load

FWD: Falling Weight Deflectometer

HMA: Hot-Mix Asphalt

IRI: International Roughness Index

LEA: Layered Elastic Analysis

M-E: Mechanistic-Empirical

MEPDG: Mechanistic-Empirical Pavement Design Guide

NCAT: National Center for Asphalt Technology

NCHRP: National Cooperative Highway Research Program

RAP: Reclaimed Asphalt Pavement

RMSE: Root Mean Square Error

SBS: Styrene Butadiene Styrene

TLA: Trinidad Lake Asphalt

WESLEA: Waterways Experiment Station Layered Elastic Analysis

WMA: Warm-Mix Asphalt

CHAPTER 1

INTRODUCTION

1.1 BACKGROUND

Pavement design has progressed over the years into the more robust mechanistic-empirical (M-E) design framework. Pavement responses are calculated within an M-E framework based on known mechanistic relationships from which pavement performance can be predicted. In doing so, the M-E framework can be applied to a range of materials for which the mechanistic relationships hold true, an improvement over the earlier design systems that used empirical relationships developed for a limited set of materials and traffic. Within the M-E framework three major inputs are required: climate, traffic, and the materials and their properties to be used in the cross-section. Climate encompasses the range of temperatures over the design period as well as rainfall events. Design speed is a critical input in traffic, as well as load spectra which characterizes the types and frequency of axle weights. Material properties may include resilient moduli of unbound materials and dynamic modulus of asphalt concrete (AC) layers as well as viscosity or dynamic shear modulus of the asphalt binder. Through mechanistic computations, the stress and strain at various points in the pavement can be predicted. In turn, these predicted stresses and strains can be related empirically through transfer functions to critical pavement distresses such as bottom-up fatigue cracking and

rutting. The thicknesses of the materials can then be altered to achieve a cross-section that meets specified distress thresholds.

The primary objective of any pavement design is to minimize pavement distresses and maximize cost effectiveness. An M-E design framework combines mechanistic analysis through the application of known stress-strain relationships for various material properties with empirically derived functions for those relationships that either cannot be described mechanistically or are unknown. This is the case with pavement distress and pavement response, thus transfer functions have been developed to empirically relate these two parameters. These functions tend to perform best when applied to the same materials and conditions for which the function was developed. One approach to improving pavement distress predictions is to calibrate the transfer functions for local materials and conditions. The current and soon-to-be widely adopted M-E design framework, the Mechanistic-Empirical Pavement Design Guide (MEPDG), is a software program that was developed under the National Cooperative Highway Research Program (NCHRP) Project 1-37A. The MEPDG is currently available through the American Association of State Highway and Transportation Officials (AASHTO) under its new name, DARWin M-E, although it will be referred throughout this dissertation as MEPDG. Within the MEPDG it is explicitly stated that a local calibration is necessary: "Without calibration, the results of mechanistic calculations cannot be used to predict rutting, fatigue cracking, and thermal cracking with any degree of confidence….This damage must be correlated with actual cracking in the field" (ARA 2004(a)). The transfer functions embedded in the MEPDG were nationally calibrated using the Long-Term Pavement Performance Program (LTPP) database. However, it is

recognized in the guidance document that "this national calibration may not be entirely adequate for specific regions of the country and a more local or regional calibration may be needed" (ARA 2004(a)).

A local calibration was performed for the default transfer functions in the MEPDG for the materials and conditions at the NCAT Test Track (Timm et al. 2012). When level one site-specific parameters (climate, traffic and material properties specific to the Test Track) were input into the MEPDG, poor correlations were found between predicted distresses (fatigue cracking and rutting) and distresses measured at the Test Track. A calibration was attempted by adjusting the coefficients in each transfer function to minimize the error between predicted and measured distress. Although the rutting transfer function was improved through this local calibration, the fatigue cracking could not be improved (Timm et al. 2012). If fatigue cracking predictions cannot be improved through local calibration, the mechanisms behind this distress need to be further evaluated.

It has been well-established that bottom-up fatigue cracking is a function of the tensile strains at the bottom of the AC layers. In an M-E framework, the prediction of tensile strains within the AC layers relies heavily on dynamic modulus ($|E^*|$), of each AC layer. $|E^*|$, as defined by Equation 1.1, is the ratio of maximum applied stress to peak recoverable axial strain. It captures the viscoelastic nature of AC through its dependency on both temperature and frequency. Illustrated in Figure 1.1, the phase angle, ϕ, represents the time lag between applied sinusoidal stress and induced axial strain and is a function of angular frequency, illustrated in Equation 1.2. In turn, shown in Equation 1.3, angular frequency is related to loading frequency.

$$|E^*| = \sqrt{\left(\frac{\sigma_0}{\varepsilon_0}\cos\phi\right)^2 + \left(\frac{\sigma_0}{\varepsilon_0}\sin\phi\right)^2} = \frac{\sigma_0}{\varepsilon_0} \quad (1.1)$$

where:

|E*| = dynamic Modulus (psi)

σ_0 = stress amplitude (psi)

ε_0 = strain amplitude ($\mu\varepsilon$)

ϕ = phase angle (radians)

$$\phi = \omega \Delta t \quad (1.2)$$

where:

ω = angular frequency (radians/sec)

Δt = change in time (sec)

$$\omega = 2\pi f \quad (1.3)$$

where:

f = loading frequency (Hz)

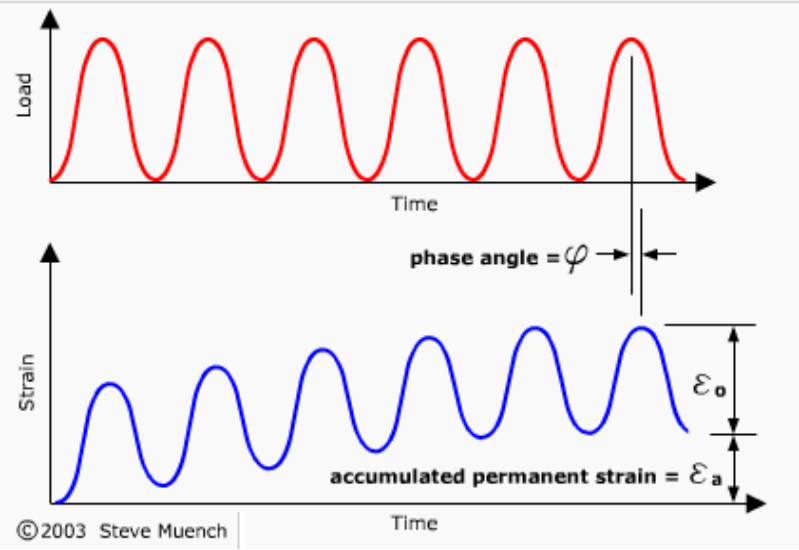

Figure 1.1: Phase lag between sinusoidal stress and induced strain (Muench 2003).

In the recently developed Mechanistic-Empirical Pavement Design Guide (MEPDG), now referred to as DARWin-ME, the |E*| of each AC layer is selected by first iterating on loading time as shown in Figure 2 (ARA 2003). To determine time of loading, an initial time is estimated and then converted to frequency. Time of loading is then calculated using the subgrade modulus, height of each layer, effective length of the load pulse (L_{eff}), effective depth of load pulse (Z_{eff}), contact radius of the tire (a_c) and vehicle speed (v_s). Using |E*| master curves, the modulus of each layer, $|E_i^*|$, is then selected based on that frequency and the given temperature. Once the time of loading has been determined, frequency is again calculated and an |E*| is selected for each layer. Using layered elastic analysis, |E*| is then used to predict tensile strains within the AC layers.

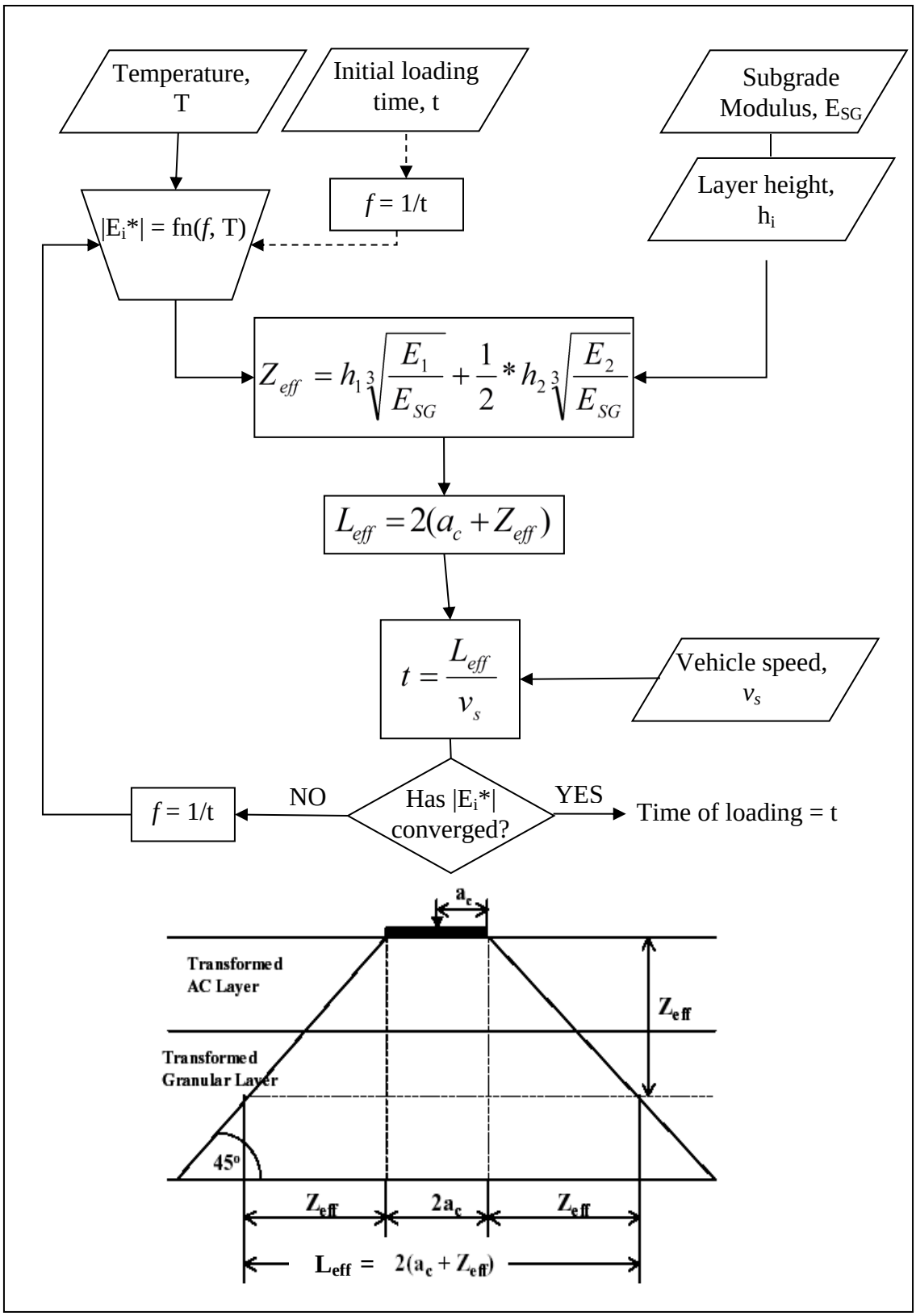

Figure 1.2: MEPDG iterative procedure for loading time (*after* ARA 2003).

In following this procedure for time of loading and using a corresponding measured |E*| to estimate strains with a layered elastic analysis program, strains based on measured responses in the field were found to be twice that of predicted strains at the National Center for Asphalt Technology (NCAT) Test Track (Robbins 2009). Other cases of large differences between measured strain and predicted strain have also been reported in the most recent research cycle at the Test Track for a sulfur-modified warm-mix cross-section (Timm et al. 2009, Timm et al. 2011) in which differences were on the order of 600 με or roughly 60% higher than the predicted strain.

Strain is a critical parameter in design and dictates the estimated pavement performance. By underpredicting strain, pavement performance may erroneously be over-predicted leading to early pavement failure. Thus, a method to more accurately predict tensile strains at the bottom of the AC layer is necessary. Furthermore, these under-predictions highlight the inability to accurately characterize and design for material properties in the field under current design practices. This is of importance particularly with the increasing use of warm-mix, reclaimed asphalt pavement (RAP) and other unconventional materials.

1.2 OBJECTIVES

The primary objective of this dissertation was to refine the current method of determining critical strains to more accurately predict field tensile strains for use in M-E pavement design using layered elastic analysis. A secondary objective was to develop a model to predict in-place AC modulus using field conditions and known material properties.

1.3 SCOPE

To meet the objectives of this research, data from both the 2006 and 2009 research cycles of the NCAT Test Track were utilized. The Test Track is located near Opelika, Alabama. It is a 1.7 mile track consisting of 46 test sections trafficked by heavy trucks operating at 45 mph. During these research cycles, pavement responses were measured in particular test sections using embedded instrumentation. Data included in this analysis were the strain responses in conjunction with the weekly performance data (rut depths, International Roughness Index (IRI) and crack maps) and hourly average pavement temperatures of each section. Laboratory testing was completed on the mixtures placed as part of the 2006 and 2009 structural studies. Laboratory testing included the characterization of the AC mixtures through dynamic modulus testing and binder characterization through dynamic shear modulus testing. Rudimentary gradation and volumetric testing were combined with as-built properties (density, volumetrics, etc.,) of the structural test sections to determine in-place properties of the AC layers. Additionally, falling weight deflectometer (FWD) testing allowed for the backcalculation of the unbound material materials. These datasets were necessary to characterize the AC layers of each test section. Additionally, these datasets were necessary to develop relationships between material behavior and field conditions using known in-place material properties.

1.4 ORGANIZATION OF DISSERTATION

Chapter Two serves as the literature review necessary to support the objectives of this dissertation. It documents the methods for determination of |E*| as well as the role of |E*| in predicting tensile strains at the bottom of the AC layers in an M-E framework.

Chapter Three provides a brief overview of the methodology utilized to improve tensile strain predictions. This chapter also provides details on the testing facility (the NCAT Test Track) as well as the methods for determining in-place properties of the pavement cross-sections, and laboratory characterization of the AC mixtures and binders. In Chapter Four the method followed to develop strain-modulus relationships using a layered elastic analysis program (WESLEA) is documented. This chapter also details the procedure followed to ensure that the strains used in this investigation were elastic in nature and associated with undamaged pavement sections. The procedure developed to construct master curves calibrated to field measured strain using vehicle speed and measured temperatures is described in Chapter Five. The models developed to relate the parameters of the field calibrated master curve to known laboratory and in-place properties is discussed in Chapter Six of this dissertation. This chapter also documents the proposed comprehensive model for predicting in-place modulus and the improvement that resulted when used to predict tensile strains in WESLEA. Lastly, Chapter Seven summarizes the findings of this dissertation and provides recommendations for the implementation of the proposed model.

CHAPTER 2

LITERATURE REVIEW

2.1 INTRODUCTION

The current design system, the MEPDG, utilizes a procedure for determining time of loading which is then used to select a representative |E*| value for use in predicting tensile strain, described by Figure 1.2. A 2009 study at the NCAT Test Track found that when this time of loading procedure was followed for a 14-inch AC layer under varying speeds and temperatures, the resulting calculated strain was only half of the tensile strain measured in the field (Robbins 2009). Strain is a critical parameter in design and dictates the estimated pavement performance. By underpredicting strain, pavement performance may erroneously be over-predicted leading to early pavement failure, specifically through bottom-up fatigue cracking. Although local calibration is encouraged in the guidance document for the MEPDG to improve pavement performance predictions (ARA 2004), it was found to be futile for the fatigue cracking transfer function when a local calibration was performed at the NCAT Test Track (Timm et al. 2012). When applied to the NCAT Test Track, the fatigue cracking transfer function performed poorly, underestimating cracking for some sections and overpredicting for others. The local calibration aimed to optimize the coefficients of the fatigue transfer function to more accurately predict fatigue cracking at the NCAT Test Track; however it was found that the poor performing transfer function could not be improved by optimizing the

coefficients. These findings were the basis for evaluating the mechanisms behind strain predictions. Given that strain is typically predicted by dynamic modulus (|E*|), it was necessary to further investigate, through this literature review, the determination and application of |E*| to understand reasons for the gap between measured and predicted strains. Additionally, field conditions that influence tensile strain are also summarized.

2.2 DETERMINATION OF |E*|

|E*| is a complicated property that can be difficult to accurately capture and is often unrepresentative of field conditions. However, it is necessary to describe the time and temperature dependent responses of asphalt concrete under dynamic loading. |E*| can be determined in the laboratory following the most recent procedures, AASHTO TP 62-07 and AASHTO TP 79-09 or through empirical predictive equations.

2.2.1 Laboratory Testing

|E*| laboratory testing has evolved from the original test developed at the Ohio State University in the 1960s (Papazian 1962) and later adopted by the Asphalt Institute. Early testing included compressive haversine loading on a cylindrical specimen at varying loading frequencies and has since evolved into |E*| testing outlined in the current AASHTO TP 62 and 79 methods.

Although the first and current methods utilize a cylindrical specimen under compressive loading, a two-point bending test developed for the Shell Laboratories in the 1970s used trapezoidal specimens (Bonnaure et al., 1977). From the two-point bending test, |E*| could be determined in two ways. First, |E*| could be determined from a simple calculation using the measured applied force and the measured displacement at the free end of the specimen. The second method utilized measured strain and the

applied stress to calculate |E*|. By testing multiple mixes at three frequencies (4, 40, and 50Hz) and three temperatures (-15, 9, and 30ºC) Bonnaure et al. found that loading time and temperature were "significant parameters for the bending strains of asphalt mixes since, under standard service conditions the stiffness may vary from 1,400 to 6,000,000 psi (1977)." It was reported that increasing the temperature or loading time resulted in a decrease in stiffness (1977).

The ASTM specification, "D3497-79 (2003) Standard Test Method for Dynamic Modulus of Asphalt Mixtures" (2003) was the standard testing protocol since its inception in 1979 but was withdrawn in 2009. This method required the application of a haversine compressive stress pulse to a cylindrical specimen at three temperatures, 41, 77, and 104ºF, as well as three frequencies, 1, 4, and 16 Hz. The sinusoidal load was applied to the specimen for a minimum of 30 seconds, but not to exceed 45 seconds. Strain gauges bonded to the mid-height of the specimen measured axial strain from which the dynamic modulus was computed as the ratio of axial stress to recoverable axial strain.

Further progress in |E*| testing came with the AASHTO TP62-07: Standard Test Method for Determining Dynamic Modulus of Hot-Mix Asphalt (HMA). In this test a cylindrical specimen is used to which haversine axial compressive stress is applied at a given temperature and frequency to induce strains in the range of 75-125 με. Specimens are compacted to air voids of 7% ±0.5% with a height of 150 mm and diameter of 100 mm. Five temperatures, 14, 40, 70, 100, and 130ºF and six frequencies, 0.1, 0.5, 1.0, 5, 10, and 25 Hz are specified for testing. Linear variable differential transformers (LVDT) are mounted, as a minimum, in two locations to measure axial deformation, from which

recoverable strain is calculated. Dynamic modulus is defined in this procedure as the ratio of the stress magnitude to average strain magnitude. Furthermore, phase angle computations are outlined in this procedure.

The most recent protocol is AASHTO TP 79-09: Determining the Dynamic Modulus and Flow Number for Hot Mix Asphalt (HMA) Using the Asphalt Mixture Performance Tester (AMPT). AASHTO TP 79 refined the TP 62 method but is still based on axial strain measurements under the application of a controlled sinusoidal (haversine) compressive load at various frequencies and temperatures over a specimen of 100 mm in diameter and 150 mm in height. This protocol is intended for use with an AMPT as opposed to the AASHTO TP 62 which can be used with any general servo-hydraulic loading equipment. The magnitude of the cyclic loading must be such that the axial strain is between 75 and 125 με for unconfined tests and 85 to 115 με for tests run with confining pressure. AASHTO PP 60-09: Preparation of Cylindrical Performance Test Specimens Using the Superpave Gyratory Compactor (SGC) is the standard practice for preparing samples for use in the AASHTO TP 79 test procedure. This protocol for preparation requires that the specimen be compacted to target air voids of 7.0% with ±0.5% tolerance. Additional requirements for specimen preparation include dimension tolerances. Although dimension tolerances were outlined in AASHTO TP 62, additional requirements were added in AASHTO PP 60-09 which included end flatness of the specimens of less than or equal to 5 mm and end perpendicularity of less than or equal to 1.0 mm. Recommended temperatures and frequencies are listed in AASHTO PP 61-09: Developing Dynamic Modulus Master Curves for Hot Mix Asphalt (HMA) Using the Asphalt Mixture Performance Tester (AMPT). Temperatures should include 4

and 20ºC with one additional high temperature based on the performance grade (PG) of the binder, as outlined in Table 2.1. According to AASHTO PP 61-09, loading frequencies should include 10, 1, and 0.1 Hz with additional frequencies tested at the high temperature based on the PG of the binder in the AC.

Table 2.1: Recommended testing temperatures and loading frequencies, AASHTO PP 61-09

PG 58-XX and softer		PG 64-XX and PG 70-XX		PG 76-XX and stiffer	
Temperature (ºC)	Loading Frequencies (Hz)	Temperature (ºC)	Loading Frequencies (Hz)	Temperature (ºC)	Loading Frequencies (Hz)
4	10, 1, 0.1	4	10, 1, 0.1	4	10, 1, 0.1
20	10, 1, 0.1	20	10, 1, 0.1	20	10, 1, 0.1
35	10, 1, 0.1, 0.01	40	10, 1, 0.1, 0.01	45	10, 1, 0.1, 0.01

2.2.2 Predictive Models

Dynamic modulus can also be estimated through predictive models requiring rudimentary volumetric measurements and Superpave binder characteristics. Predictive models are sometimes more attractive than laboratory determination due to the expense of lab tests, equipment and specialized training that coincides with |E*| testing. Additionally the parameters used to predict |E*| are common parameters that are already measured for mix design and Superpave requirements. Three recent models include the Witczak 1-37A model stemming from NCHRP Project 1-37A (Andrei et al. 1999), the Hirsch model developed by Christensen, Pellinen and Bonaquist (2003) and the Witczak 1-40D model produced by the NCHRP Project 1-40D (Bari and Witczak 2006). Although there are more recent predictive models, these three are currently the most commonly used. Furthermore, both Witczak predictive models are currently being used in the MEPDG to predict |E*| at level 2 and 3 designs and given that the MEPDG is the

leading M-E design system it is necessary to have an understanding of these models. The Hirsch model is applied in the AASHTO PP 61-09 method for constructing |E*| master curves, therefore, it is necessary to review this model as well.

2.2.2.1 Witczak 1-37A

The Andrei, Witczak and Mirza's revised model was developed in 1999 (called the Witczak 1-37A model from this point forward), as an update to the previous |E*| predictive equation, by Witczak and Fonseca in 1996 (Andrei et al. 1999). This model considers the binder properties by means of the asphalt viscosity, and effective asphalt content. The model also includes the loading frequency as an input variable. Other input parameters include air voids, and aggregate gradation information. Laboratory |E*| test results were used to re-calibrate the previous model by the addition of various mix properties including modified asphalt binders. The resulting Witczak 1-37A model is shown in Equation 2.1 (Bari and Witczak, 2006). As shown in Equation 2.1, the same factors as used for the previous model were utilized for the revised predictive equation. It should be noted that the equation listed in Equation 2.1 was reported by Bari and Witczak in the most recent document regarding the revised Witczak E* predictive equations and it appears that the sixth coefficient is contrary to other sources.

$$\log|E^*| = 3.750063 + 0.02932\rho_{200} - 0.001767(\rho_{200})^2 - 0.002841\rho_4 - 0.058097V_a - 0.802208\frac{V_{be}}{V_{be}+V_a} + \frac{3.871977 - 0.0021\rho_4 + 0.003958\rho_{38} - 0.000017(\rho_{38})^2 + 0.005470\rho_{34}}{1+e^{(-0.603313 - 0.313351\log(f) - 0.393532\log(\eta))}} \quad (2.1)$$

where:

|E*| = dynamic modulus of mix (10^5 psi)

η = viscosity of binder (10^6 poise)

f = loading frequency (Hz)

ρ_{200} = % passing #200 sieve

ρ_4 = cumulative % retained on #4 sieve

ρ_{38} = cumulative % retained on 3/8 in. sieve

ρ_{34} = cumulative % retained on 3/4 in. sieve

V_a = air voids (% by volume)

V_{be} = effective binder content (% by volume)

For use in this model (Andrei et al., 1999), the viscosity of the binder is determined by a linear relationship between log-log viscosity and log temperature, illustrated by Equation 2.2 (Bari and Witczak 2006). In plotting the log-log of the viscosity versus the log of temperature, the slope of the line is the parameter VTS, and the intercept is A. If viscosity information is not obtainable, viscosity can be determined by the relationship with the binder shear complex modulus and binder phase angle, shown in Equation 2.3 (Bari and Witczak 2006).

$$\log\log\eta = A + VTS\log T_R \tag{2.2}$$

where:

η = viscosity of binder, centipoise (cP)

A, VTS = regression parameters

T_R = temperature, ºRankine

$$\eta = \frac{|G^*|}{10}\left(\frac{1}{\sin\delta}\right)^{4.8628} \tag{2.3}$$

where:

|G*| = dynamic shear modulus of binder, psi

δ = phase angle of |G*|, degrees

2.2.2.2 Hirsch Model

The Hirsch model for estimating AC modulus is based on a law of mixtures for composite materials (Christensen et al. 2003). The law of mixtures, called the Hirsch model, was developed by T.J. Hirsch in the 1960s and combines phases of a material by the arrangement of its elements (Christensen et al. 2003). The elements of a material may be in parallel or series arrangement. The Hirsch model allows for the prediction of a material property (commonly the modulus) of a composite material from the sum of the same material property of two separate phases of the material, shown in Equation 2.4 in parallel, and Equation 2.5 in series.

$$E_c = \nu_1 E_1 + \nu_2 E_2 \tag{2.4}$$

$$1/E_c = \nu_1 / E_1 + \nu_2 / E_2 \tag{2.5}$$

where:

E_c = modulus of the composite material

ν_1, ν_2 = the volume fraction of a given phase

E_1, E_2 = moduli of each phase

In applying the Hirsch model to AC, Christensen et al. (2003) developed a model to predict the modulus of AC, |E*|, from the shear modulus of the binder, |G*|, and volumetric properties of the mix, shown in Equation 2.6. This model was developed in part to meet the objectives of NCHRP Projects 9-25 and 9-31 for Superpave requirements, and to analyze the effects of air voids, voids in mineral aggregate (VMA) and other volumetric properties on |E*| (Christensen et al. 2003). According to

Christensen et al. (2003), the Hirsch model was selected for application to AC because "asphalt concrete tends to behave like a series composite at high temperature, but more like a parallel composite at low temperatures." The resulting model for estimating AC modulus is for "a simple three-phase system of aggregate, asphalt binder, and air voids (Christensen et al. 2003)." The aggregate phase in the parallel portion of the model represents that portion of the aggregate particles in intimate contact with each other, termed aggregate contact volume, Pc (Christensen et al. 2003). Temperature dependency of AC is partially represented by Pc, such that high values of Pc are related to mixtures with high stiffness and strength, typical at low temperatures, whereas low values of Pc represent mixtures with low strength and stiffness, typical at high temperatures (Christensen et al. 2003). In addition to a predictive equation for |E*|, an equation to predict the phase angle was also developed, although it is not presented here.

$$|E^*| = Pc\left[4{,}200{,}000\left(1-\frac{VMA}{100}\right)+3|G^*|\left(\frac{VFA\times VMA}{10{,}000}\right)\right]+$$
$$(1-Pc)\left[\frac{1-(VMA/100)}{4{,}200{,}000}+\frac{VMA}{3VFA|G^*|}\right]^{-1} \qquad (2.6)$$

where:

$$Pc=\frac{\left(20+\frac{VFA\times 3|G^*|}{VMA}\right)^{0.58}}{650+\left(\frac{VFA\times 3|G^*|}{VMA}\right)^{0.58}}$$

where:

$|E^*|$ = dynamic modulus (psi)

VMA = voids in mineral aggregate (% by volume)

VFA = voids in aggregate filled with asphalt (% by volume)

$|G^*|$ = dynamic shear modulus of binder (psi)

In comparison with the Witczak 1-37A predictive equation this model is much simpler, requiring only three parameters (|G*|, VMA and VFA). Rather than incorporating frequency and temperature directly into the Hirsch predictive equation, they are inherent to the shear modulus of the binder. Also, the need to translate viscosity data to shear modulus is eliminated, which not only simplifies the equation but is also intuitive given the Superpave Performance Grading system for which |G*| testing is conducted.

2.2.2.3 Witczak 1-40D

Upon the expansion of the database used to enhance the original Witczak predictive model, resulting in the Witczak 1-37A model, Witczak discovered a decrease in accuracy of the 1-37A model (2006). As a result of this decrease, $R^2 = 0.88$ compared to $R^2 = 0.94$ for the development of the 1-37A model, a new model was developed from the expanded database, called the Witczak 1-40D predictive equation from this point forward. The 1-40D model is presented in Equation 2.7. It should be noted that according to Bari and Witczak (2006) the loading frequency (in Hz) used in dynamic shear mode is not equivalent to the loading frequency (in Hz) used in dynamic compression mode, but rather, is related as shown in Equation 2.8. Thus, the frequency at which |G*| was tested must be converted to compression mode frequency for use in this model.

$$\log E^* = -0.349 + 0.754\left(|G^*|^{-0.0052}\right) \times \begin{pmatrix} 6.65 - 0.032\rho_{200} + 0.0027(\rho_{200})^2 + 0.011\rho_4 \\ -0.0001(\rho_4)^2 + 0.006\rho_{38} - 0.00014(\rho_{38})^2 \\ -0.08V_a - 1.06\left(\frac{V_{be}}{V_a + V_{be}}\right) \end{pmatrix}$$

$$+ \frac{2.56 + 0.03V_a + 0.71\left(\frac{V_{be}}{V_a + V_{be}}\right) + 0.012\rho_{38} - 0.0001(\rho_{38})^2 - 0.01\rho_{34}}{1 + e^{(-0.7814 - 0.5785\log|G^*| + 0.8834\log\delta)}} \quad (2.7)$$

where:

|E*| = dynamic modulus of mix (psi)

$|G^*|$ = dynamic shear modulus of binder (psi)

ρ_{200} = % passing #200 sieve

ρ_4 = cumulative % retained on #4 sieve

ρ_{38} = cumulative % retained on 3/8 in. sieve

ρ_{34} = cumulative % retained on 3/4 in. sieve

V_a = air voids (% by volume)

V_{be}= volume of effective binder (%)

$$f_c = 2\pi f_s \quad (2.8)$$

Where:

f_c = frequency in compression mode (Hz)

f_s = frequency in shear mode (Hz)

The combined database used to develop the 1-40D model expanded the mix properties and incorporated various aging conditions including short-term oven aging, laboratory aging, plant aging, and field aging (Bari and Witczak 2006). This was an improvement from the previous database that included only un-aged laboratory blended

mixes. Discrepancies in the accuracy of the 1-37A model for the combined database were believed to be due to the representation of stiffness of the binder and extrapolation of the model beyond the initial range of variables (Bari and Witczak 2006).

The 1-37A model requires viscosity by means of the A-VTS relationship shown in Equation 2.2, however, this relationship, as Bari and Witczak (2006) state, "does not consider the effect of loading frequency (or time) on the stiffness of the binder itself." This was accounted for in the 1-40D model by replacing the viscosity by means of the A-VTS relationship with a direct input of the complex shear modulus of the binder, |G*|, which "can more effectively take care of the binder rheology with changing temperature and loading rate (Bari and Witczak 2006)." Furthermore, the associated binder phase angle, δ, was also incorporated into the new model.

2.3 FACTORS AFFECTING |E*|

|E*| has been sufficiently proven to be dependent on two parameters: temperature and frequency. The decrease in |E*| with an increase in temperature and decrease in loading frequency has been consistently reported by researchers for many years (e.g., Bonnaure et al. 1977; Flintsch et al. 2007, Tashman and Elangovan 2007, Mohammad et al. 2007). Looking at the test specimen itself, it is evident that there are many parameters that may present variability in the dynamic modulus. AC has two main components: aggregate and binder. Each component has numerous properties which influence the overall response of the mixture. Thus, it is only logical that the properties of each component may further influence dynamic modulus.

This sentiment was echoed in research findings at the Virginia Tech Transportation Institute (VTTI) (Flintsch et al. 2007). Dynamic modulus tests produced

different master curves for the various mixtures tested, causing Flintsch and colleagues to conclude that "the dynamic modulus test is sensitive to variation in the mix properties" (Flintsch et al. 2007). In similar research conducted for the Washington State Department of Transportation (WSDOT) different mixes were found to possess statistically significantly different dynamic moduli (Tashman and Elangovan 2007). Because these mixtures were tested using the same procedure, AASHTO TP-62-03 (e.g. same temperatures and frequencies), it was concluded that the differences in the aggregate properties, as well as the differences in asphalt properties may account for the variations in dynamic moduli.

2.3.1 Effect of Aggregate Properties

Previous investigations into dynamic moduli revealed that some aggregate properties are more influential than others. At the very simplest level, the amount of aggregate significantly influences the mix design and its performance. Likewise, Bonnaure and colleagues found that the percent of aggregate by volume also influences the stiffness (dynamic modulus) of the mix (Bonnaure et al. 1977). The percent by volume of air voids was also observed to influence the stiffness of the mix (Bonnaure et al. 1977). A look into asphalt mixtures in Louisiana revealed that nominal maximum aggregate size (NMAS) contributed to variations in dynamic moduli (Mohammad et al. 2007). A the trend of increasing dynamic moduli among mixes with larger NMAS was reported. Mixes with a 25 mm NMAS were found to have higher dynamic moduli than those mixes with a 19 mm or 12.5 mm NMAS within each mixture category. Mohammad and colleagues attributed this trend to the stronger stone-to-stone contact among larger aggregates (Mohammad et al. 2007).

Aggregate interactions were found to also influence the phase angle associated with the dynamic moduli. In research conducted at VTTI, phase angles were found to increase up to a certain frequency, and beyond that frequency, phase angles began to decrease for a temperature of 100ºF (Flintsch et al. 2007). Whereas at 130ºF, phase angles consistently increased with increased frequencies. "The predominant effect of aggregate interlock" was credited for the observed behavior (Flintsch et al. 2007).

In addition to aggregate gradation, shape, and interaction, the type of aggregate was also found to contribute to variations in dynamic modulus values of asphalt mixtures. Research at the Florida Department of Transportation (FDOT) was conducted on several mixes in which the binder type remained constant, while aggregate properties varied (Ping and Xiao 2007). Because the binder type was consistent among all mixes, the differences in AC stiffness were attributed to the different aggregate types (Ping and Xiao, 2007). Asphalt mixtures containing either granite or RAP were found to be stiffer (higher E*) than the limestone mixtures (Ping and Xiao 2007).

2.3.2 Effect of Binder Properties

Some properties associated with the asphalt binder used in AC mixtures have been found to influence the dynamic modulus values. The PG grade of an asphalt binder is related to its performance under certain temperature ranges. Higher binder grades are generally stiffer to prevent deformation under hot weather conditions. The stiffer binder would likely contribute to the overall stiffness of the mix. Findings from Huang (2008) and his associates were consistent with this, as an increase in dynamic moduli was observed as the PG grade progressed from PG 64-22 to PG 70-22 to PG 72-22 for a given temperature. However for a different type of aggregate (gravel rather than

limestone), they found the trend was reversed, such that the dynamic moduli decreased with an increase in binder grade. Further investigation on the Tennessee plant-produced mixes revealed that the asphalt content was influencing the stiffness of the mix as well (Huang et al. 2008). The mixes containing gravel had different asphalt contents for each binder grade used, and overall higher binder contents than the limestone mixes. It was found that the lower dynamic moduli values were associated with higher asphalt contents, leading them to conclude that small variations in binder content influenced the dynamic modulus values (Huang et al. 2008).

The sensitivity of the dynamic modulus to asphalt content found in Tennessee mixes was consistent with findings at VTTI (Flintsch et al. 2007). By comparing mixes of the same type, Flintsch et al. (2007) also found that the mix with the highest asphalt content exhibited the lowest dynamic modulus. The findings by both these researchers reiterate those from early research by Bonnaure et al. (1977), in which sensitivity to the percent of bitumen, the hardness of the bitumen and the temperature susceptibility of the bitumen in the mix were reported.

Reclaimed asphalt pavement (RAP) is often used in mixes across the country to reduce costs. Using RAP in a mixture reduces the amount of new binder required in the mix because of the contributing asphalt content of the RAP. The aged binder (and therefore higher binder stiffness) from the RAP has been credited with contributing to higher dynamic modulus for Louisiana AC mixtures (Mohammad et al. 2007).

2.4 APPLICATION OF |E*|

Given that |E*| is the driving force behind strain predictions in the current MEPDG, it is necessary to understand how |E*| is applied in M-E design regardless of whether those values are measured or predicted.

2.4.1 Master Curve Construction

In developing a new method for determining |E*| in the laboratory, Bonnaure and colleagues discovered that an equivalency among temperature and loading frequency existed. From this he found that stiffness curves from different temperatures and frequencies could be superimposed (referred to as time-temperature superposition), enabling a master curve to be created for a reference temperature (1977). Master curves have since become a useful tool to translate laboratory results to one reference temperature, as is done in the MEPDG. The master curve allows for the prediction of |E*| at any frequency or temperature within the range tested, ideally spanning the whole range of typical in-service temperatures and vehicle speeds. Associated with the two laboratory testing protocols for |E*| are two slightly different methods of master curve construction.

2.4.1.1 Master Curve Construction: AASHTO TP 62-07

Master curve development for testing using the AASHTO TP 62-07 is described by Equations 2.8 and 2.9. The shift factor, log a(T), can be determined through regression of a second order polynomial, shown in Equation 2.10. The master curve is defined by a sigmoidal fit function such that δ represents the limiting minimum modulus in Figure 2.1 and $\delta+\alpha$ represent the limiting maximum modulus. Fitting parameters, γ and β help

define the shape of the curve, shown in Figure 2.1. For application to test results from TP 62, the functional form of the master curve and shift function are assumed as shown in Equations 2.8 and 2.10. Using the Solver function in Excel, the fitting parameters, δ, α, β, γ, and regression coefficients for the shift factor are determined through best-fit optimization. Because testing is conducted at the low temperature range, 14ºF, the limiting maximum modulus is easily optimized (Underwood et al. 2011).

$$\log(|E*|) = \delta + \frac{\alpha}{1+e^{\beta-\gamma\log(fr)}} \quad (2.8)$$

where:

|E∗| = Dynamic modulus (psi)

δ, α, β, γ = Fitting parameters

f_r = Reduced frequency (Hz)

$$\log(f_r) = \log(f) + \log[a(T)] \quad (2.9)$$

where:

f_r = reduced frequency (Hz)

f = test frequency (Hz)

a(T) = shift factor

T = Test temperature (ºC)

$$\log \alpha_T = \alpha_1(T^2 - T_r^2) + \alpha_2(T - T_r) \quad (2.10)$$

where:

α_1, α_2 = fitting parameters

T_r = reference temperature (ºC)

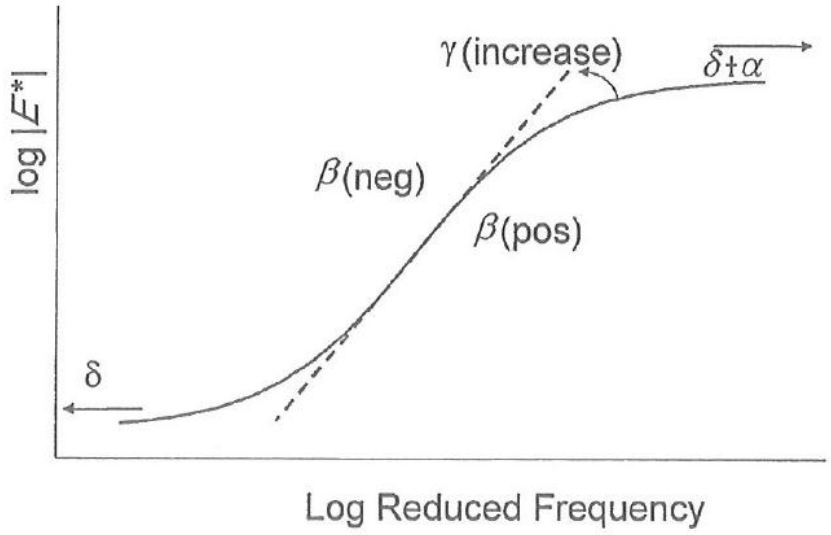

Figure 2.1: Master curve fitting parameters.

2.4.1.2 Master Curve Construction: AASHTO TP79-09/PP 61-09

The procedure for constructing a master curve from the results of the TP 79 procedure is outlined in AASHTO PP 61-09. Testing at a minimum of three frequencies and three temperatures enables the use of the time-temperature superposition principle to create a master curve similar to Figure 2.1 and of the form shown in Equation 2.11 when used with the Arrhenius shift factor defined in Equation 2.13. Rather than regressing on the limiting maximum modulus, the PP 61 method uses the Hirsch model (Christensen et al. 2003) with an assumed maximum binder modulus of 145,000 psi or 1 GPa, as shown in Equation 2.12. Due to the reduced number of temperatures tested, there are uniqueness issues in the Solver function that reduce the overall optimization reliability and by calculating the limiting maximum modulus using Equation 2.12, the shortcomings are resolved (Underwood et al. 2011). Also due to abbreviated testing temperatures and frequencies, a simpler shift factor in the form of the Arrehenius shift factor is used.

$$\log(|E*|) = \log|E*|_{min} + \frac{\log|E*|_{max} - \log|E*|_{min}}{1+e^{\beta+\gamma(\log f_r)}} \quad (2.11)$$

where:

$|E^*|_{min}$ = limiting minimum modulus (psi), treated as a fitting parameter

β, γ = fitting parameters

$|E^*|_{max}$ = limiting maximum modulus (psi), see Equation 2.12

$$|E*|_{max} = P_c\left[4{,}200{,}00\left(1-\frac{VMA}{100}\right)+435{,}000\left(\frac{VMA\times VFA}{10{,}000}\right)\right]+\frac{1-P_c}{\left[\frac{\left(1-\frac{VMA}{100}\right)}{4{,}200{,}000}+\frac{VMA}{435{,}000(VFA)}\right]} \quad (2.12)$$

where:

$$P_c = \frac{\left(20+\frac{435{,}000(VMA)}{VFA}\right)^{0.58}}{650+\left(\frac{435{,}000(VMA)}{VFA}\right)^{0.58}}$$

VMA = Voids in mineral aggregate (%)

VFA = Voids filled with asphalt (%)

$$\log a(T) = \frac{\Delta E_a}{19.17142}\left(\frac{1}{T}-\frac{1}{T_r}\right) \quad (2.13)$$

where:

ΔE_a = Activation energy, treated as fitting parameter

T = Temperature (°K)

T_r = Reference temperature (°K)

2.4.1.3 Comparison of Master Curve Construction

In a study conducted by Underwood and colleagues, comparisons were drawn between modulus values measured from TP 62 testing at 14°F and 130°F between 25 and 0.1 Hz

with modulus values calculated at the same temperatures following the PP 61 procedure (Underwood et al. 2011). It was found that for the mixes studied, the PP 61 method tends to under-predict moduli at temperatures lower than 40F for with differences ranging between 7 and 34%. Underprediction at 130ºF was also found, although substantially lower. The authors contributed the under-prediction at 130ºF to errors in extrapolation of the time-temperature shift factor function, as shift factors were found to be smaller at 130°F for the PP 61 procedure than they were for the TP 62 method. The authors explained that the smaller shift factors would lead to reduced frequencies and given that the master curve is a decreasing function with reduced frequency, would result in smaller |E*| values. In comparing the measured modulus values determined from TP 62 testing with predict modulus values following the master curve construction for TP 62 testing, errors were also found in fitting the master curve at the extreme temperatures (14 and 130ºF). Although the errors were much smaller than reported for the comparison between PP 61 predicted values and TP 62 measured values, only 3.5%, the differences indicated that "the sigmoidal function is not a perfect representation of the |E*| master curve" (Underwood et al. 2011).

In addition to studying the difference in master curves for the two protocols, Underwood and colleagues also investigated the impact of using measured values from either protocol on pavement performance as predicted by the MEPDG (Underwood et al. 2011). The largest difference in pavement performance between the two master curve protocols was for predicted top-down cracking, however in its current state, the embedded model in the MEPDG is unreliable (NCHRP 2006). Differences were also

found to exist in the predicted fatigue cracking predictions, although the largest percent differences were associated with fatigue cracking predictions of 1-2% of the lane cracked (Underwood et al. 2011).

2.4.2 Use in MEPDG

The MEPDG offers three levels of design which are dependent on the user's available data and desired accuracy of the design. One significant difference in the three levels of design is the determination of the dynamic modulus. Upon the determination of |E*|, a master curve is created at a reference temperature of 70ºF. The degree of complexity required for material property inputs is dictated by the level of design chosen. A brief description of the methods to estimate |E*| at each level is listed in Chapter Two of Part Two of the Guide for the MEPDG, presented in Table 2.2 (ARA Inc., 2004). At the highest level of complexity, level one requires laboratory |E*| and |G*| results. At levels two and three, laboratory test results for |E*| are replaced by the estimation of |E*| from either the 1-37A or 1-40D Witczak predictive equation. At the current stage of development of the MEPDG, the user can select which |E*| predictive model is run.

Table 2.2: Asphalt |E*| estimation at different hierarchical input levels for new and reconstruction design (ARA, Inc. 2004)

Input level	Description
1	• Conduct |E*| (dynamic modulus) laboratory test (NCHRP 1-28A) at loading frequencies and temperatures of interest for the given mixture • Conduct binder complex shear modulus (|G*|) and phase angle (δ) testing on the proposed asphalt binder (AASHTO T315) at ω = 1.59 Hz (10 rad/s) over a range of temperatures. • From binder test data estimate Ai-VTSi for mix-compaction temperature. • Develop master curve for the asphalt mixture that accurately defines the time-temperature dependency including aging.
2	• No |E*| laboratory test required. • Use |E*| predictive equation. • Conduct |G*|-δ on the proposed asphalt binder (AASHTO T315) at ω = 1.59 Hz (10 rad/s) over a range of temperatures. The binder viscosity of stiffness can also be estimated using conventional asphalt test data such as Ring and Ball Softening Point, absolute and kinematic viscosities, or using the Brookfield viscometer. • Develop Ai-VTSi for mix-compaction temperature. • Develop master curve for asphalt mixture that accurately defines the time-temperature dependency including aging.
3	• No |E*| laboratory testing required. • Use |E*| predictive equation. • Use typical Ai-VTS – values provided in the Design Guide software based on PG viscosity, or penetration grade of the binder. • Develop master curve for asphalt mixture that accurately defines the time-temperature dependency including aging.

For a level one design, |E*| laboratory testing must be completed for a range of frequencies and temperatures. |G*| testing on RTFO-aged binder must also be completed, however, at a fixed loading frequency of 1.59 Hz for a range of temperatures. The recommended temperatures and frequencies for these tests are listed in Table 2.3.

Table 2.3: Recommended frequencies and temperatures for |E*| and |G*|, at level one design (ARA Inc. 2004)

	Mixture |E*| and δ				
Temperature (ºF)	0.1 Hz	1 Hz	10 Hz	25 Hz	Binder |G*| and δ, 1.59 Hz
10	X	X	X	X	
40	X	X	X	X	X
55					X
70	X	X	X	X	X
85					X
100	X	X	X	X	X
115					X
130	X	X	X	X	X

In Table 2.2, the A-VTS relationship is mentioned as a requirement for a level one design, as well as levels two and three. The A-VTS relationship is described by Equation 2.2 and characterizes the effect of temperature on viscosity for a particular binder. It is used mainly in a level one design to complete the master curve. To obtain viscosity, conventional binder testing can be completed, or Equation 2.3 can be used to convert |G*| test results (at f = 1.59 Hz) to viscosity. Once viscosity is obtained the A-VTS relationship is obtained through a linear regression on the viscosity-temperature data, allowing the determination of viscosity at any temperature.

A level two design uses one of the two models previously discussed to estimate |E*|, requiring volumetric properties, gradation information and depending on which model is selected, either |G*| testing or viscosity testing. For the Witczak 1-37A model, viscosity is required and can be obtained in the same manner as described above for a level one design. Although |G*| testing (at f = 1.59 Hz) can be used for the Witczak 1-37A model, it is not required. For a level two design using the Witczak 1-40D model, |G*| is necessary. Rather than testing at a fixed loading frequency, |G*| testing must be

completed for a range of frequencies and temperatures which can be obtained by developing a |G*| master curve from a |G*| frequency sweep.

A level three design also utilizes volumetric properties, and gradation information, however no laboratory testing is required. If the user selects the Witczak 1-37A model to estimate |E*|, viscosity values are estimated from typical temperature-viscosity relationships, programmed into the MEPDG, for the selected binder grade. Similarly, the Witczak 1-40D E* model selects typical |G*| values from the temperature-viscosity relationship for the binder grade.

2.4.2.1 Master Curve Construction in MEPDG

For a level one design, using measured |E*| values, a master curve is constructed for |E*| in the MEPDG using a sigmoidal fit function, similar to the one shown in Equation 2.8 at a reference temperature of 70°F. One important difference exists: time of loading at the reference temperature, t_r, shown in Equation 2.14, is used to replace reduced frequency, f_r (ARA 2004(a)). The shift factor function is described in Equations 2.15 and 2.16, where time of loading is put in terms of viscosity and *c* is treated as a fitting parameter determined through non-linear optimization as are the fitting parameters, δ, α, β, γ for the master curve. Although the units of the parameters shown in Equations 2.14-2.16, were not explicitly stated in the MEPDG documents, they were assumed to be consistent with the Witczak 1-37A model. The master curve is used to select |E*| values for a given temperature and time of loading representative of vehicle speed, following the procedure describe in Chapter One and Figure 1.2. For levels two and three designs, the master curve is computed directly from the predictive equations. When applied to

the Witczak 1-37a model in Equation 2.1, the fitting parameter, "*c"*, for the shift factor function is 1.255882 (ARA 2004(a)).

$$t_r = \frac{t}{a(T)} \tag{2.14}$$

where:

t_r = time of loading at reference temperature (sec)

t = time of loading (sec)

$a(T)$ = shift factor

T = temperature (°F)

$$\log(t_r) = \log(t) - \log[a(T)] \tag{2.15}$$

$$\log(t_r) = \log(t) - c\big(\log(\eta) - \log(\eta_{T_r})\big) \tag{2.16}$$

where:

c = fitting parameter

η = viscosity of binder (10^6 poise)

η_r = viscosity at reference temperature, (10^6 poise)

2.5 TRANSLATION OF |E*| TO FIELD CONDITIONS

Regardless of the means used to determine |E*|, |E*| is a function of loading frequency and pavement temperature. To translate |E*| to field conditions requires loading, frequency and temperature to be accurately defined in the field. With this several challenges arise; frequency is difficult to measure in the field and furthermore, the testing parameters (loading and induced strain) in the laboratory differ from field conditions.

2.5.1 Loading Frequency in the Field

Loading frequency is challenging, if not impossible, to measure in the field. However, loading frequency is necessary to capture the viscoelastic effect of truck speed on AC modulus. As a result, researchers have relied on time-frequency relationships to provide frequency since loading time can be measured from stress or strain pulses under traffic loading. Although time can be measured from either strain gauge responses or pressure plates embedded in the pavement, there has been disagreement on the correct definition of time of loading.

2.5.1.1 Time of Loading

Historically, time of loading has been defined by either a stress pulse or a strain pulse and found to be dependent on speed and depth. Through the use of finite element and elastic layer theory, Barksdale (1971) estimated the shape and length of compressive stress pulses under a rolling wheel load. He concluded that compressive stress pulse durations are a function of pavement depth and vehicle speed and could be characterized by either a sinusoidal or triangular pulse for vehicle speeds up to 45 mph depending on the depth within the pavement. Further investigation by Brown extended Barksdale's research to stress pulses in three directions, using elastic layered theory and sinusoidal curves to estimate the length of such pulses (Brown, 1973).

Measuring load durations in the field has presented challenges in defining the boundaries of the load pulse. More recent research by Loulizi et al. (2002) at the Virginia Smart Road facility characterized the effects of speed, depth and temperature on measured vertical compressive stress pulse times. Stress pulse durations were

measured for truck speeds ranging from 8 km/h (5 mph) to 72 km/h (45 mph) at various pavement depths. Similar testing conducted at a later date was used for temperature comparisons, resulting in maximum in-situ temperature differences between test dates of 13.2ºC (55.8ºF) and 6.8ºC (44.2ºF) for the two pavement types investigated. Due to the lack of symmetry in the stress pulses, the loading time was taken to be twice the time of the rising normalized vertical compressive stress pulse beginning at a normalized stress of 0.01 (Loulizi et al., 2002). This is described in Figure 2.2 as twice the "Duration (a)" as applied to a stress pulse.

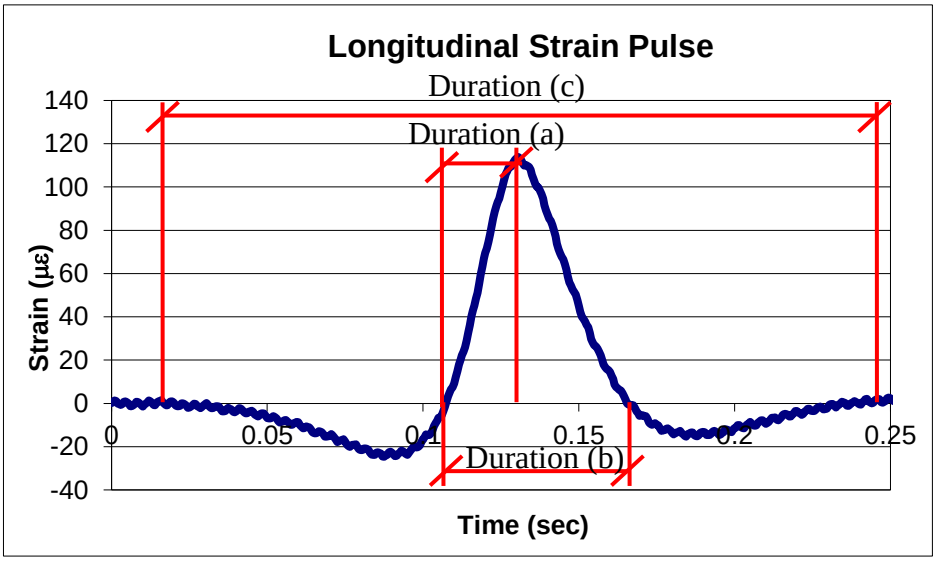

Figure 2.2 Load Duration Definitions.

In 2008, Garcia and Thompson (2008) utilized strain pulses to measure the loading times, reporting that load durations for strain pulses were also influenced primarily by load speed and pavement thickness. A traffic load simulator, the Advanced Transportation Loading Assembly (ATLAS), was employed to apply loads under a single tire inflated to 110 psi (Garcia and Thompson, 2008). For the strain measurements recorded during ATLAS testing, the longitudinal and transverse strain pulses were of

different shapes, requiring two different definitions for strain pulse duration. In the longitudinal direction, it was taken to be the time that the pavement experienced only tensile strain, whereas in the transverse direction, it was taken to be twice the rising portion (in the tensile region) of the pulse using the unloaded condition as a reference point described in Figure 2.2 by "Duration (b)" and "Duration (a)", respectively.

A study conducted in 2009 on an instrumented highway in Wisconsin had similar findings and strain pulse definitions, in which strain pulse durations were defined separately depending on orientation (Hornyak and Crovetti 2009). For this study strain pulse duration in the longitudinal direction was also defined by the time it was in tensile strain, or "Duration (b)" in Figure 2.2. In the transverse direction, a definition was used similar to that used by Garcia and Thompson (2008). However, a strain threshold of 1 με was used, such that the strain pulse measurement began at this threshold, rather than in the unloaded state (or baseline value) (Hornyak and Crovetti 2009).

A 2009 study at the NCAT Test Track investigated strain pulse durations. The entire duration, from departure from the baseline value to full return, described by "Duration (c)" in Figure 2.2, was considered (Robbins 2009). However, similar to findings by Garcia and Thompson (2008), it was difficult to identify the beginning and end of the strain pulse duration due to the asymptotic nature of signal responses. This definition is further complicated by close axle spacings preventing a full return to a local baseline. As a result, this study used the time associated to tensile strain only ("Duration (b)"), in both the longitudinal and transverse directions.

2.5.1.2 Time-Frequency Relationship

Due to the ability to measure time of loading in the field, rather than frequency, researchers have had to rely on time-frequency relationships to estimate loading frequency in the field. Although there is disagreement in the definition and accurate measurement of time of loading, the real difficulty in relating loading frequency in lab to loading frequency in the field lies in the conversion of loading time to frequency. Within the MEPDG, the proposed relationship is simply $t = 1/f$, where f is loading frequency and t is loading time (ARA 2003). However, based on a survey completed by Dongre and colleagues (Dongre et al. 2006), others suggest that the correct conversion is $t = 1/\omega$, based on the field of rheology, where ω is angular frequency and this can be expanded to read as $t = 1/(2\pi f)$. Others have proposed alternative relationships for converting loading frequency to time of loading such as $t = 0.1f$ and $t = 0.08f$ (Dongre et al. 2006). Dongre et al. (2006) went on to explore the differences in |E*| values using $t = 1/f$ and $t = 1/\omega$ as applied to the shift factor. Results showed large differences in |E*| values at the same reduced time, with percent differences ranging between 37 and 123% (Dongre et al. 2006). At present, no research has been found to corroborate these time-frequency relationships under field conditions.

A study was completed at the NCAT Test Track that investigated the impact of time of loading on predicted tensile strains (Robbins 2009). The iterative procedure outlined in the MEPDG for determining time of loading was examined as well as measured strain pulse durations from embedded strain gauges at the NCAT Test Track. The time-frequency relationship used in the MEPDG, $f = 1/t$, was used for converting

time of loading to frequency for which |E*| values were selected for use in a Layered Elastic Analysis (LEA) program to predict strain. When predicted strain was compared with measured strain in the field, it was found that both methods significantly under-predicted strain, suggesting that the time-frequency relationship utilized in the MEPDG inaccurately describes the time-frequency relationship in the field (Robbins 2009).

2.5.2 Loading Conditions and LVE Region

The discrepancies between predicted strain and measured strain could be due to the difference between |E*| laboratory testing conditions and field conditions. A haversine compressive stress pulse is applied in |E*| testing to achieve strains within the linear-elastic range of AC. There have been disagreements among researchers on whether measured stress or strain pulses should be investigated for application to field measurements as discussed above. One researcher has found field measured stress pulses exhibit shapes similar to haversine pulses (Loulizi et al. 2002); however, those studying strain pulses have not found a haversine function to fit pulses measured by embedded strain gauges (Garcia and Thompson 2008). Furthermore, in the laboratory the compressive load pulses are applied in a continuous fashion for each frequency tested. However, load pulses are not continuous in the field due to axle configurations and vehicle spacing.

Stress is applied in accordance with AASHTO TP 79-09 to achieve compressive strains between 75 and 125 με for unconfined tests and 85 to 115 με for tests run with confinement. These strain levels are meant to maintain testing within the linear-(visco)elastic range of AC (Witczak et al. 2002). Previous research has been conducted

to determine the linear viscoelastic (LVE) range of AC. Mehta and Christensen (2001) found that AC mixtures subjected to a relaxation test followed by a creep test at low temperatures were found to meet both the proportionality and superposition requirements. By meeting these requirements, the AC mixtures tested were found to be within the linear viscoelastic region (LVE) at 150 με for -20ºC and up to 300 με for -10ºC (Mehta and Christensen 2001). Given that tensile strains are critical at low temperatures, this would suggests that 150 με would be a conservative value for LVE behavior under loading at higher temperatures. Although tensile strains are critical at low temperatures, Pellinen and Witczak (2002) have suggested that at high temperatures and high strain levels the AC behaves in a stress dependent fashion rather than stress independent as is the case at high temperatures and low strain levels. Pellinen and Witczak (2002) noted the large accumulation of plastic strain under high temperatures and high strains (resulting in non-linear behavior) whilst measuring relatively moderate resilient strains from which |E*| is calculated, indicating that plastic strain at high temperatures could be masked by the test. Echoing this finding, Tran and Hall (2006) found permanent strain accumulation at high temperatures with induced strains between 100 and 150 με.

Although, the 100 to 150 με strain limit has been widely accepted as the LVE boundary for |E*| testing and even though others have found permanent strain accumulation at lower strain levels, strains have been measured in the field that far-surpass this boundary while maintaining good pavement performance. Willis and Timm (2009) documented strain levels beyond this 100-150 με level in several good

performing sections from the 2003 and 2006 structural studies. Multiple sections (7 and 9-inches thick) at the 2009 Test Track have experienced tensile strains of 900 με and upwards of 1400 με (Timm et al. 2011). It should be noted that laboratory measured |E*| values were used in the design process for these 2009 Test Track sections. The control section (S9) and two sulfur-modified warm-mix asphalt (WMA) sections (N5 and N6) were designed to meet distress thresholds using the MEPDG, resulting in a predicted 90th percentile tensile strain of 375 με for S9 and between 200 and 275 με for N5 and N6 (Timm et al. 2009). After nearly 10 million ESALs these sections are performing well with no cracking evident and minor rutting. Although the LVE region has been clearly defined in the laboratory, it is difficult to do so in the field. Therefore, it is difficult to assess whether the moduli and resulting master curve determined in the laboratory are appropriate for predicting field strains.

2.6 FACTORS INFLUENCING STRAIN

Pavement responses, specifically tensile strain, can be difficult to characterize due to the viscoelastic nature of AC. Because of its viscous properties, AC responses are time-dependent, such that as a load is applied, a response is not immediately induced throughout the pavement. Additionally, it is dependent on temperature, causing increased flexibility under warmer temperatures and increased stiffness under colder temperatures. The prediction model becomes increasingly complex when the pavement is under dynamic loading, such as the loading that occurs with live traffic.

Researchers and engineers have characterized these time-temperature relationships both theoretically and through physical measurement. Although developing

a temperature-strain relationship was not the primary area of investigation in Mateos and Snyder's (2002) validation of a response model from the Minnesota Road Research (Mn/ROAD) test facility, a trend of increasing strain with increasing pavement temperatures was illustrated in their findings. Observations from the National Center for Asphalt Technology (NCAT) Test Track have reported that an increase in temperature has resulted in an increase in horizontal tensile strain. This relationship was found to be well-modeled by a power function of the mid-depth pavement temperature (Priest and Timm, 2006). A study, completed in 2009, at the NCAT Test Track echoed these findings in which mid-depth pavement temperature significantly influenced the magnitude of the tensile strain responses at the bottom of the AC layers (Robbins 2009).

Investigations at the PACCAR Technical Center into the effects of vehicle speed on strain have revealed a reduction in tensile strain with increasing speed (Chatti et al., 1996). For tensile strain in the longitudinal direction at the bottom of the AC layer, a maximum reduction of 30-40% was reported as vehicle speeds were increased from creeping motion to 64 km/h (Chatti et al. 1996). Similarly, transverse strain at the bottom of the HMA layer was also reported to decrease with speed, although not as significantly (Chatti et al. 1996). Mateos and Snyder (2002) also recorded a decrease in tensile strains in both the transverse and longitudinal direction with changes in vehicle speed. Similar findings were reported by Robbins (2009) during the 2009 Test Track research cycle which found tensile strains to increase as vehicle speeds were reduced from 45 mph incrementally to 15 mph. This study found strain to be a function of the natural logarithm of vehicle speed.

2.7 SUMMARY

The primary objective of this dissertation was to develop a method to improve tensile strain predictions to more accurately reflect strains measured in the field. In M-E design, strain is predicted primarily through the use of |E*|, a material property that describes the viscoelastic behavior of AC through it's time and temperature dependency. Therefore, this chapter served in discussing research findings related to |E*| and its relevance to field conditions, as well as field conditions influencing strain.

|E*| can be determined in the laboratory through the application of sinusoidal compressive stress pulses applied at varying frequencies and temperatures. By measuring |E*| at a wide range of frequencies and temperatures, master curves can be constructed which enable the prediction of |E*| at any frequency and temperature. There are currently two methods for constructing master curves that are associated with the current testing protocols. Additionally, the MEPDG prescribes a method for constructing a master curve that is dependent on time of loading and binder viscosity. |E*| can also be determined through one of many predictive equations that are reliant on binder and aggregate properties as well as mix volumetrics. Currently, the MEPDG relies on one of two predictive models to estimate |E*| for level 2 and 3 designs.

In addition to loading frequency and temperatures, a variety of factors have been found to influence |E*| measurements. Intuitively, aggregate and binder properties significantly impact |E*| measurements as do mix type. It was important to understand the various parameters that influence |E*| measurements, as they will likely also influence in-place modulus.

The testing conditions for |E*| measurements were evaluated relative to field conditions to gain a better understanding of why tensile strains predicted through the use of |E*| do not accurately match field-measured strains. It was found that strain levels that define the LVE region in the laboratory may be smaller than the current strain levels being used for |E*| testing, although field strains related to well-performing pavements tend to be much larger. Additionally, it was found that although loading time can be determined, an accurate time-frequency relationship has yet to be validated for field conditions making it difficult to understand the relationship between loading frequency in the laboratory and loading rate (vehicle speed) in the field. Lastly, field measured strains were found to be largely influenced by vehicle speed and pavement temperature, thus, highlighting the need to incorporate field conditions in the method selected for improving tensile strain predictions.

CHAPTER 3

METHODOLOGY OVERVIEW AND TESTING FACILITIES

3.1 INTRODUCTION

To meet the objectives of this study, a model was developed to predict in-place composite AC modulus from a variety of known parameters. This model was developed to improve the prediction of strain to more closely match those tensile strains measured in the field at the bottom of the AC layers when utilized in a LEA program. This chapter provides a general overview of the methodology used to develop this model as well as the laboratory testing and the testing facility utilized to complete the field testing necessary for the development of this model. In the following chapters, the steps necessary to complete the model are discussed in more detail.

In developing this model, strain and temperature were measured at the NCAT Test Track for a variety of pavement cross-sections as part of the 2006 and 2009 structural studies using embedded instrumentation, as discussed in more detail in Section 3.3 titled, "NCAT Test Track". In addition to field measured strain and temperatures, laboratory testing was completed to determine the mix and binder properties that were utilized in the model, as discussed in Section 3.5, "Laboratory Testing". Lastly, knowledge of in-place properties of the AC layers and unbound materials were necessary in creating this model. Properties of the in-place AC layers

were determined by combining laboratory mix properties and field measured compaction. Furthermore, moduli for the unbound materials in the 2006 and 2009 structural sections were determined through backcalculation of measured deflections from Falling Weight Deflectometer (FWD) testing at the Test Track, as described in Section 3.4, "In-Place Properties from NCAT Test Track."

3.2 METHODOLOGY OVERVIEW

To improve predictions of tensile strain at the bottom of the AC layer, a model for in-place AC modulus was developed that is calibrated to field measured strains from test sections at the NCAT Test Track (discussed in the following section). This model estimates the composite modulus of the AC layers for field conditions through the use of known parameters that combine in-place properties with laboratory determined properties. The general approach is illustrated in Figure 3.1. Using a LEA program, for a given section, tensile strain was predicted at the bottom of the AC layer by varying the AC modulus to cover a wide range of moduli (and conditions). The resulting calculated strain was then plotted against the AC moduli to develop modulus-strain relationships for each section. Then by applying the measured strain in the field to the developed relationships, the modulus required to achieve that strain in the field can be determined. Relationships with the modulus required to achieve that strain can then be developed with field conditions (pavement temperature (T) and vehicle speed (v)), laboratory properties and in-place volumetrics and gradations.

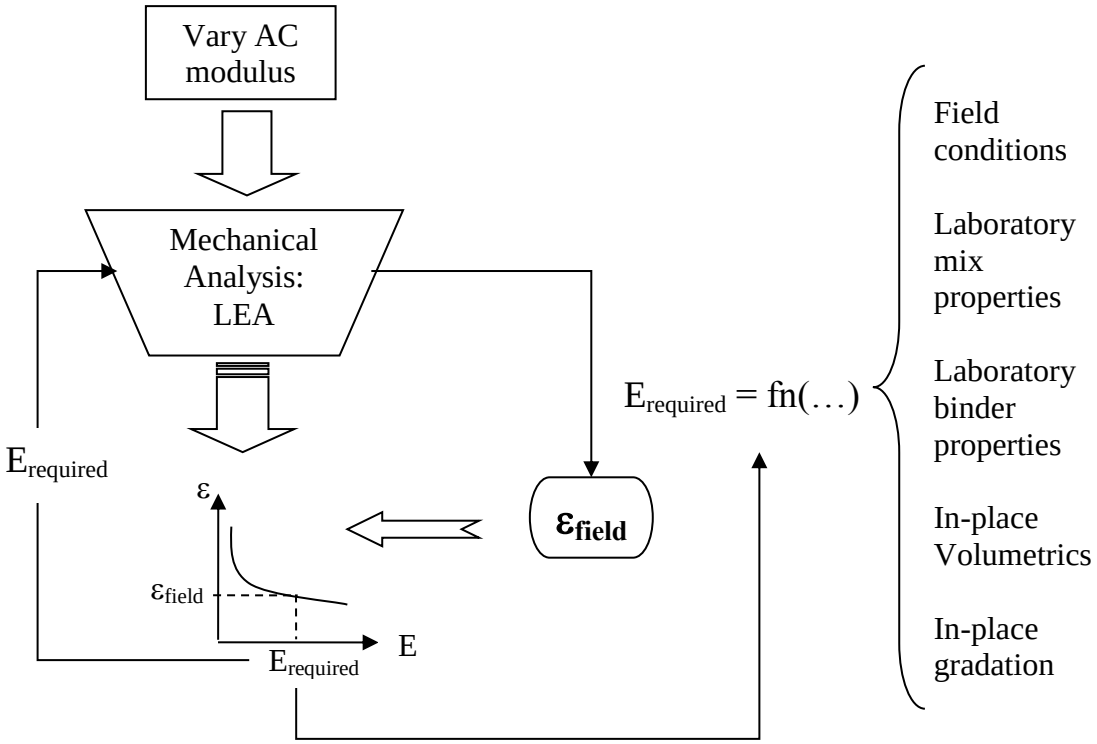

Figure 3.1: General methodology.

To calibrate the composite AC modulus to field measured tensile strains, the first step was to determine the relationship between strain and composite AC modulus. To be consistent with the objective to provide a simplistic method to achieve realistic strain level predictions, layered elastic analysis was selected for use in developing the strain-modulus relationships. For each of the test sections that were included in this study the surveyed lift thicknesses and backcalculated moduli for the unbound materials, discussed in more detail in the Section 3.4 of this chapter, were entered into a LEA software program, Waterways Experiment Station Layered Elastic Analysis (WESLEA). By varying the composite AC modulus, relationships were developed for each section by plotting composite AC modulus against predicted tensile strain at the bottom of the

AC layer and fitting a regression model to the data. Then, by knowing the strain measured in the field, the composite modulus required to achieve that strain could be determined by the observed relationship. This step of the procedure is discussed in more detail in Chapter 4 of this dissertation.

Since it has been well-established that strain is influenced by vehicle speed and pavement temperature, the next step was to express the required modulus for each measured strain in terms of the field conditions at which the strain was measured. To do so, a master curve calibrated to field conditions and field-measured strain was created for each test section. This was done by applying a sigmoidal fit function, consistent with the form described in AASHTO PP 61-09 for creating dynamic modulus master curves (discussed further in the Section 3.5 of this chapter) using vehicle speed (mph) rather than testing frequency (Hz) and mid-depth pavement temperature, to the moduli required to achieve the strain measured in the field. The development of the field calibrated master curves are described in more detail in Chapter 5 of this dissertation.

The last step was to pool all of the sections together and develop models to relate the fitting parameters of the field calibrated master curves to known field and laboratory measured properties. As a result, four individual models were developed that incorporated in-place volumetrics and gradations; and laboratory-determined dynamic modulus and dynamic shear modulus (discussed further in "Laboratory Testing" of this chapter). These individual models were then input into the form of the field calibrated master curve to provide a comprehensive model. Chapter 6 of this dissertation documents the development of these individual models and the performance of the

comprehensive model in predicting tensile strain from the relationships previously established for each section using WESLEA.

3.3 NCAT TEST TRACK

The National Center for Asphalt Technology (NCAT) at Auburn University has a full-scale accelerated pavement testing facility for the evaluation of flexible pavements under live traffic. The test facility is located in Opelika, Alabama, and consists of a 1.7 mile oval test track, shown in Figure 3.2, with applied traffic similar to open access highways using live traffic. The Test Track is comprised of 46 200-ft pavement sections with varying cross-sections. Some sections, referred to as structural sections, have embedded instrumentation for the evaluation of pavement response and mechanistic-empirical analysis. Four testing cycles have been completed with embedded instrumentation that were constructed in the years 2000, 2003, 2006, and 2009. For this investigation, only data from the structural sections in the third (2006) and fourth cycles (2009) were utilized. Research cycles are three years in length and consist of a 2-year traffic period and 1-year forensic study and reconstruction period. Live traffic is applied at the Test Track on a daily basis, operating at a target vehicle speed of 45 mph. Heavy trucks are manually operated for 16-hours a day, 5 days a week, totaling approximately 10 million equivalent single axle loads (ESALs) in the 2-year traffic period. The trucks have approximately a 12-kip steer axle, 40-kip tandem axle, and 5 trailing 20-kip single axles. A photograph of one of the triple trailer trucks is shown in Figure 3.3.

Figure 3.2: Aerial view of the NCAT Test Track.

Figure 3.3: Triple trailer truck.

The performance of each test section was also assessed through weekly performance measurements that included international roughness index (IRI), rut depth and crack maps. In addition to performance monitoring, frequent falling weight deflectometer (FWD) testing was conducted on structural test sections.

3.3.1 2006 Structural Study

The third test cycle (2006-2009) included eleven test sections as part of the structural study. The eleven test sections were equipped with embedded instrumentation to capture pavement response under live loading and temperatures throughout the cross-sections. Of the eleven sections, five (N3, N4, N5, N6, and N7) were left in place from the 2003-2006 test cycle to continue evaluation under additional traffic, and six sections (N1, N2, N8, N9, N10, and S11) were newly constructed with embedded instrumentation in 2006 (Timm 2009). Additionally, N5 was milled and inlaid with 2 inches of asphalt concrete to correct previous top-down cracking in the section. Under normal testing operations, pavement responses were captured on a weekly basis throughout the testing cycle for analysis. Also, the surface performance of each test section was monitored on a weekly basis.

3.3.1.1 Pavement Cross-sections: 2006 Structural study

Each of the eleven test sections was designed based on the individual sponsor's need and common practices. As a result, the cross-sections varied by the AC mixtures and unbound materials utilized in the structures. The cross-sections of each are shown in Figure 3.4, labeled with its associated sponsor and whether it was left in place from the 2003-2006 test cycle or newly constructed in 2006.

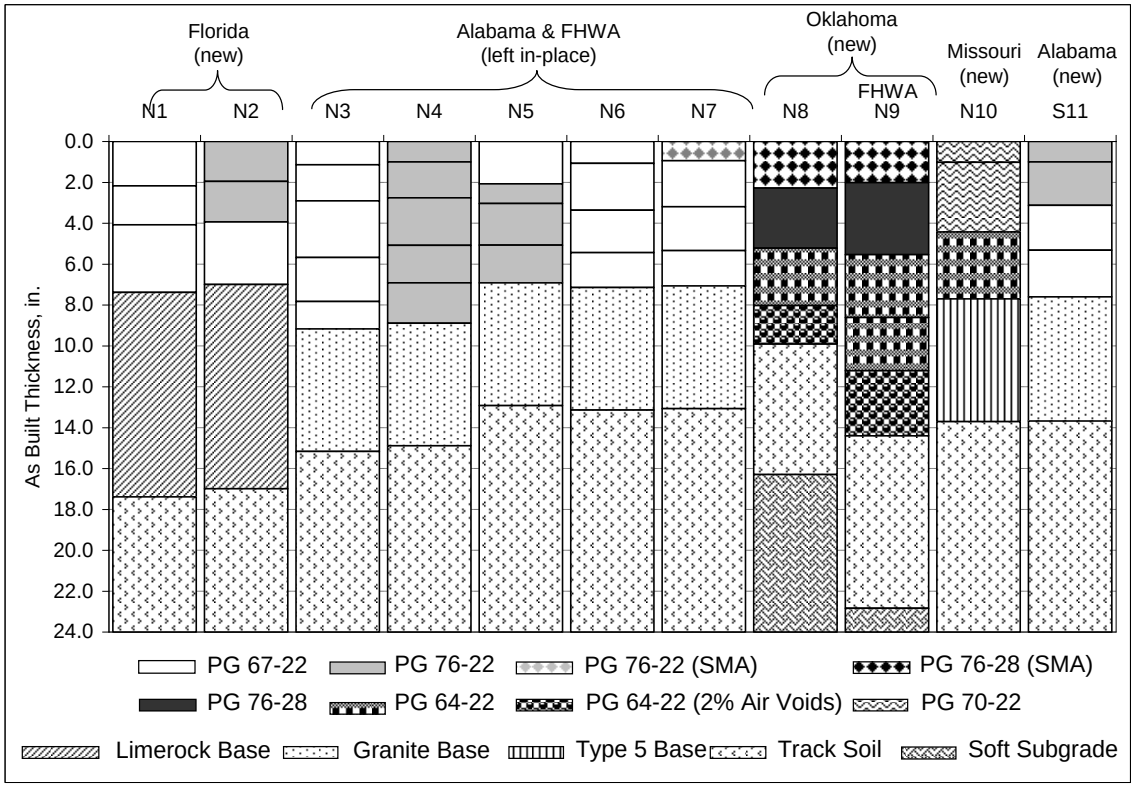

Figure 3.4: 2006 Structural Study Test Sections (Timm 2009).

One commonality among the test sections was the local unbound material used to construct the sections. All eleven pavement sections utilized the local soil at the Test Track, referred to as "Track soil," which is classified as an AASHTO A-4(0) soil containing large cobbles and stones (Timm 2009). Excluding section N8 and N9, all of the test sections utilized this material as a compacted subgrade. Sections N8 and N9 instead used a compacted soft subgrade material, on top of the uncompacted Track soil (not shown in Figure 3.4) and the compacted Track soil as a base material. The soft subgrade material was imported from Seale, Alabama and had a high clay content which closely replicates subgrade materials typically encountered in Oklahoma. A limerock base quarried in Florida and typically used by the Florida DOT was placed in sections N1 and N2. The granite base used in sections N3-N7, and S11 was quarried in

Columbus, Georgia, and is typically utilized by ALDOT for road construction in the Southeastern part of Alabama. Section N10 used a Missouri Type 5 base material.

In terms of AC mixtures, five different binder types were used to create unique mixes by varying aggregate gradations, air voids, and binder contents. AC layers in seven sections, N1, N2, N3, N5, N6, N7, and S11 employed a performance grade (PG) 67-22 unmodified binder. The PG 76-22 binder used in the AC layers in sections N2, N4, N5, and S11 was modified with styrene-butadiene-styrene (SBS). The surface course of N7 also used a PG 76-22; however it was a stone-matrix asphalt (SMA) mix. PG 76-28 binder was used in sections N8 and N9 in the surface course SMA and in the second AC layers. These sections used PG 64-22 binder in the bottom two AC layers. Although the binder type was common to both layers, the bottom layer was designed for only 2% air voids, referred to as a "rich bottom" layer. Lastly, the PG 70-22 binder was used for one AC layer in section N10. As-built properties of each layer were recorded, as well as the design properties (Timm 2009). For the sections constructed in 2006, including the top layer of section N5, binder testing was completed to determine the dynamic shear moduli, |G*| and associated phase angles. Additionally, laboratory tests were completed to determine the dynamic moduli, |E*|, and associated phase angles of the AC layers.

3.3.2 2009 Structural Study

The 2009 structural study consisted of sixteen structural sections. Of those sections, only three were left in place from previous research cycles, N3, N4 and N9. N3 and N4 were originally constructed in 2003 and N9 was constructed in 2006, shown in Figure 3.2. At

the conclusion of the 2009 cycle, N3 and N4 were subjected to over 30 million ESALs and N9 to 20 million. New sections for this study highlighted innovative technology and unconventional materials.

3.3.2.1 Pavement Cross-sections: 2009 Structural Study

The cross-sections included in the 2009 structural study are shown in Figure 3.5. In addition to the three sections left in place from previous cycles, there were three other sections, N1, N2 and N8 that were constructed in previous cycles and rehabilitated for use in the 2009 study. Sections N1 and N2 were originally constructed in 2006 and saw severe distresses during the 2006 study at which point they were rehabilitated. For the 2009 study, these sections were again rehabilitated by milling off the top two lifts and using spray paver technology for the construction of the surface lifts to mitigate de-bonding of AC layers. Although N8 was originally constructed in 2006, it saw severe distresses in the top five inches and was rehabilitated using a high polymer (7.5% SBS modification) AC mixture.

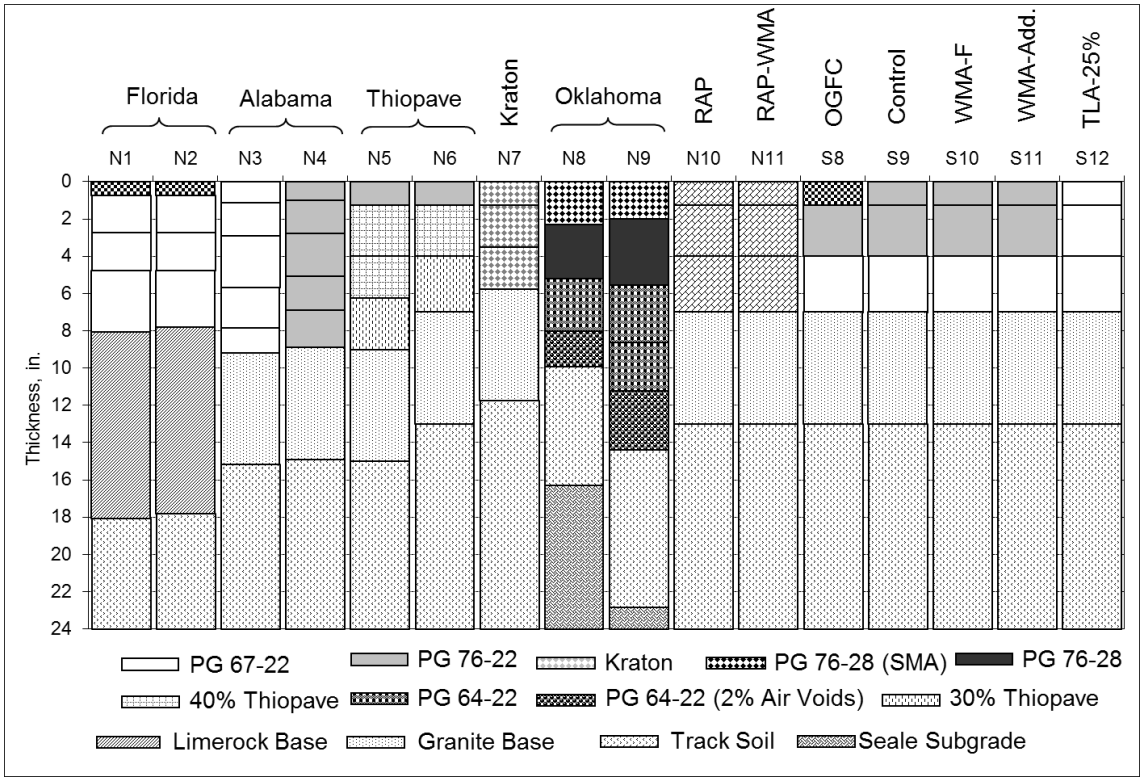

Figure 3.5: **2009 Structural Study Test Sections.**

Ten sections were newly constructed in 2009 with various technologies and unconventional materials. Sections N5 and N6 were constructed with sulfur-modified warm-mix asphalt (WMA) in the binder and base courses with a typical surface course used in Alabama, designed at 9 and 7 inches thick, respectively. These sections utilized sulfur pellets to replace 30-40% of the virgin binder by weight. Section N7 was a 5.75-inch section constructed entirely with high polymer (7.5% SBS) modified AC. Sections N10 and N11 were both 7-inch sections constructed with 50% RAP in each lift, with the difference being that N11 utilized the foaming technique to produce it at as a WMA while the other was produced at typical production temperatures for hot-mix asphalt. S8 also utilized RAP, but was used in a lower proportion (15%) and was only used in the porous friction course (PFC) which replaced the typical PG 76-22 dense-graded surface

course; the remainder of the 7-inch section was identical to the control section. S9, the control section, was a 7-inch section with typical Superpave AC mixtures including a PG 76-22 (SBS modified) surface and binder lift with a PG 67-22 (unmodified) base lift. Sections S10 and S11 were 7-inch sections constructed with warm-mix technologies, such that S10 utilized foaming technology and S11 contained additives to reduce the viscosity during production. Lastly, section S12 used a base binder of PG 67-28 for all lifts throughout with 25% of the virgin binder replaced with pellets of naturally occurring asphalt produced by Trinidad Lake Asphalt (TLA).

3.3.3 Instrumentation

To characterize pavement response, instrumentation was embedded within each structural section at the time of construction, providing extensive information on temperature, stress and strain within the structures. Embedded within each of the structural sections were a pair of earth pressure cells, twelve strain gauges, and four temperature probes. Based on the research objectives of the corresponding sponsors, some sections included more extensive instrumentation. Figure 3.6 illustrates the standard arrangement of the pressure cells and strain gauges for the structural sections. This standard arrangement was utilized for all of the structural sections with the exception of N7, constructed in 2003, and N9, constructed in 2006; those arrangements are shown in Figures 3.5 and 3.6, respectively.

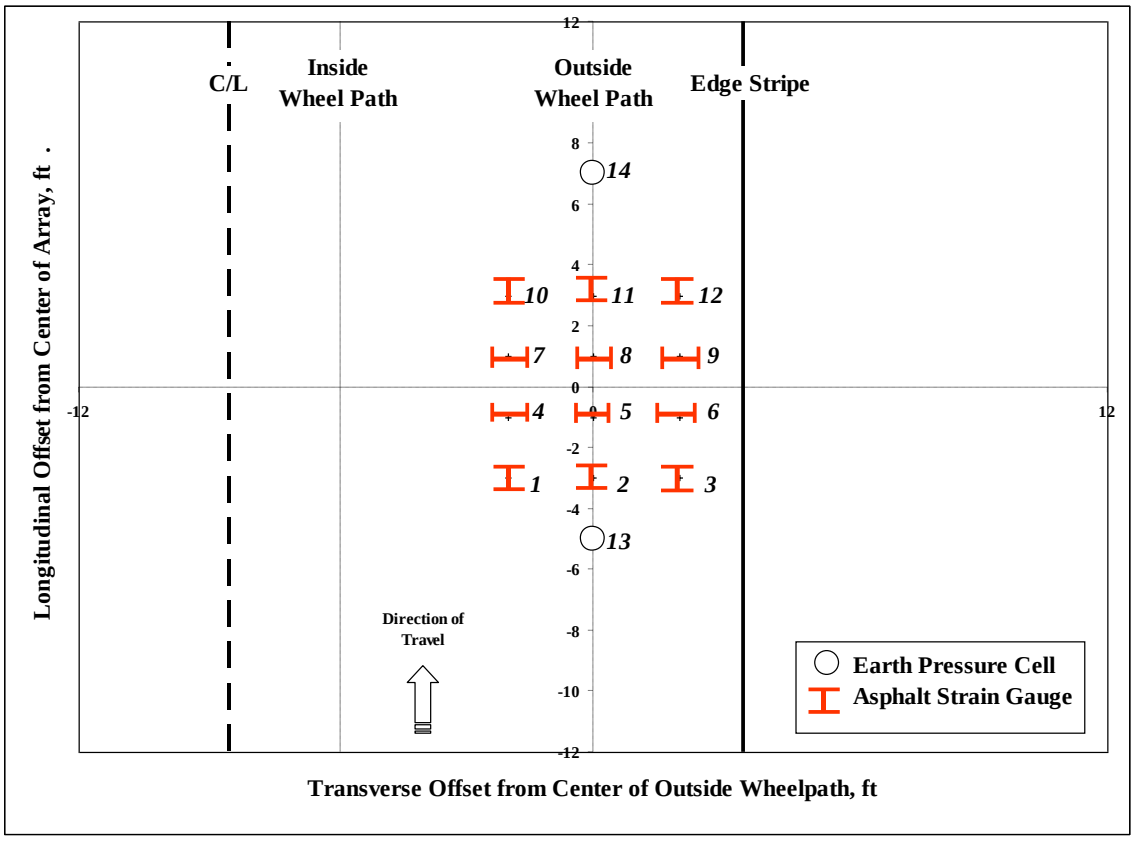

Figure 3.6: Standard Configuration for Gauges (Timm 2009).

Two earth pressure cells were installed in each section, one at the top of the subgrade and the other at the top of the base material. Geokon model 3500 earth pressure cells, shown in Figure 3.7, with a capacity of 36.3 psi, were used. As the vertical pressure changed, a change in fluid pressure inside the cell was induced, which was converted to an electrical signal and read as a change in voltage. Using the calibration factors determined from the on-site calibration procedure, described elsewhere (Timm 2009), the change in voltage was then converted to pressure.

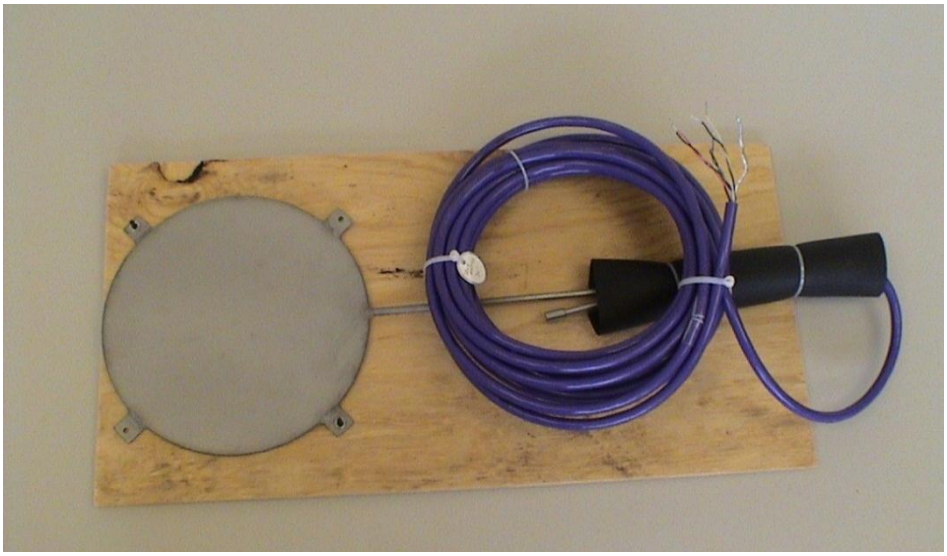

Figure 3.7: Geokon model 3500 earth pressure cell.

Strain gauges were installed to capture the induced tensile strain in both the longitudinal and transverse directions. Construction Technologies Laboratories, Inc. (CTL) asphalt strain gauges, shown in Figure 3.8, were used in each section. They were designed for pavement cross-sections with a maximum range of 1,500 με, well within typical strain magnitudes experienced in most pavement cross-sections (Timm 2009). Strain was measured with these gauges by converting the change in resistance over the embedded 350Ω Wheatstone Bridge to an electrical signal and applying the required excitation voltage and known gauge factor to calculate strain. A strain gauge array, gauges 1 through 12 in Figure 3.6, was installed in each of the sections at the bottom of the AC layers. The gauges were installed in groups of three by direction, oriented either longitudinally or transversely. Within a group, one gauge was aligned with the centerline of the outside wheel path, and the remaining two were offset two feet on center to the right and left of the outside wheel path. Doing so helped to account for wheel wander, allowing the best hit to be captured. Two groups of strain gauges were

installed in both the longitudinal and transverse directions to create redundancy in the system.

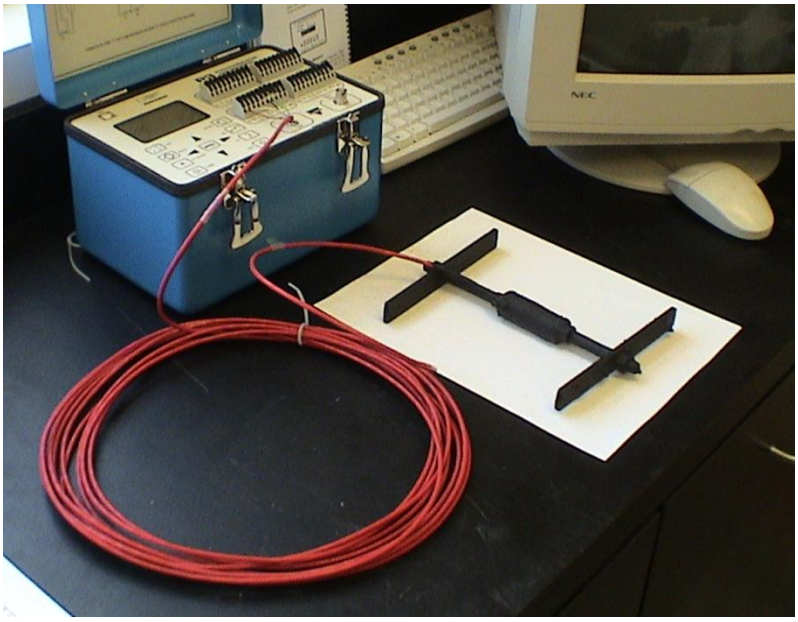

Figure 3.8: CTL strain gauge.

Temperature probes were installed at various depths within the structure, creating a complete temperature profile for each. For consistency, Campbell-Scientific model 108 temperature thermistors were installed in each test cycle. Four thermistors were placed as a minimum in each section, as listed in Table 3.1. Sections N3-N7 (those left in place from the 2003-2006 cycle) were installed at consistent depths, regardless of the cross-section. However, for the sections constructed in 2006, one thermistor each was installed at the surface, mid-depth and bottom of the AC layer and three inches into the base layer (Timm 2009).

Table 3.1: Location of Thermistors

	Depth of Probe, inches			
Section (2006)	T1	T2	T3	T4
N1	0.0	3.7	7.4	10.4
N2	0.0	3.5	7.0	10.0
N3	0.0	2.0	4.0	10.0
N4	0.0	2.0	4.0	10.0
N5	0.0	2.0	4.0	10.0
N6	0.0	2.0	4.0	10.0
N7	0.0	2.0	4.0	10.0
N8	0.0	5.0	10.0	13.0
N9	0.0	7.2	14.4	17.4
N10	0.0	3.9	7.7	10.7
S11	0.0	3.8	7.6	10.6
Section (2009)	T1	T2	T3	T4
N5	0.0	4.3	8.7	11.7
N6	0.0	3.5	7.1	10.1
N7	0.0	2.5	5.0	8.0
N10	0.0	3.8	7.5	10.5
N11	0.0	3.6	7.1	10.1
S8	0.0	3.5	7.0	10.0
S9	0.0	3.4	6.8	9.8
S10	0.0	3.4	6.8	9.8
S11	0.0	3.4	6.9	9.9
S12	0.0	3.3	6.6	9.6

3.3.4 Traffic

Live traffic was applied at the Test Track on a daily basis. Heavy trucks were operated at approximately 45 mph by truck drivers for 16-hours a day, 5 days a week, totaling nearly 10 million ESALs in the 2-year traffic period. The Test Track operates five different trucks with the following axle spacing and axle weights listed in Tables 3.2 and 3.3.

Table 3.2: Spacing Between Axles (Taylor 2008)

Distance Between Axles (ft)

Truck #	Steer	Front Tandem	Rear Tandem	Single 4	Single 5	Single 6	Single 7	Single 8
1	0.0	13.6	4.3	18.7	11.2	20.0	11.2	20.0
2	0.0	13.6	4.3	17.1	17.0	17.0	17.0	17.0
3	0.0	13.6	4.3	17.1	17.0	17.0	17.0	17.0
4	0.0	13.6	4.3	17.1	17.0	17.0	17.0	17.0
5	0.0	13.6	4.3	14.8	12.4	17.2	11.0	17.2

Table 3.3: Axle Weight by Truck (Taylor 2008)

Axle Weights (lb)

Truck	Steer	Front Tandem	Rear Tandem	Single 4	Single 5	Single 6	Single 7	Single 8
1	9,400	20,850	20,200	20,500	20,850	20,950	21,000	20,200
2	11,200	20,100	19,700	20,650	20,800	20,650	20,750	21,250
3	11,300	20,500	19,900	20,500	20,500	21,000	20,650	21,100
4	11,550	21,200	19,300	21,000	21,050	21,000	20,750	20,800
5	11,450	20,900	19,400	20,100	20,450	21,000	20,050	20,650

3.3.5 Data Acquisition

Wireless data transmission was utilized in the 2006 and 2009 Test Track structural studies to transmit pavement response measurements. For normal operations, data were collected on each of the structural sections on a weekly basis. Weekly data collection consisted of recording strain responses under three passes of live traffic and the in-situ pavement temperatures at the time of collection. Data collection was alternated each week from morning to afternoon to capture strain and pressure at a variety of temperatures.

3.3.6 Performance Monitoring

The heavy triple trailer trucks were operated Tuesday through Saturday, allowing for the track to be shut down on Mondays, allowing for performance monitoring. Pavement

performance was evaluated by International Roughness Index (IRI), rut depth measurements and crack maps. Pavement performance was evaluated over the middle 150-ft of each test section to minimize effects of the transition areas on either end. IRI, reported in inches/mile, was measured using the Automatic Road Analyzer (ARAN) van, a high-speed inertial profiler capable of taking roughness measurements in each wheel path. The ARAN van was also equipped with rear-mounted lasers that allowed for rut depth measurements. Visual inspection of each section was performed manually, at which time any cracks that were detected were marked as were the progressive growth of any existing cracks. From this, crack maps were created and maintained, enabling a very useful and visual representation of formation and progression of cracking in a section relative to the traffic level.

3.3.7 FWD Testing

Once construction was completed and trafficking commenced, FWD testing was conducted several times per month on each section during both test cycles. The testing was performed in the middle 75% (150 ft) of each 200-ft test section, within this area, four random locations (RL) were chosen for testing. Figure 3.9 shows a schematic detailing the typical testing locations (not to scale). The RL 1-3 were randomly selected from each 50-ft subsection of the middle 150-ft of the section. The fourth random location was placed in the center of the gauge array. The random testing stations (numbered 1 through 12) were located such that testing was conducted at three offsets: outside, inside and between the wheelpaths (OWP, IWP and BWP respectively). Testing

was conducted at four drop heights representing four load levels: 6, 9, 12, and 16 kips, with three drops conducted at each drop height.

The FWD was a Dynatest Model 8000 FWD with a 5.91 in. radius split plate. Nine sensors were used to measure pavement deflection and were spaced at 0, 8, 12, 18, 24, 36, 48, 60, and 72 inches from the center of the load plate. Pavement temperatures were recorded at the time of each test.

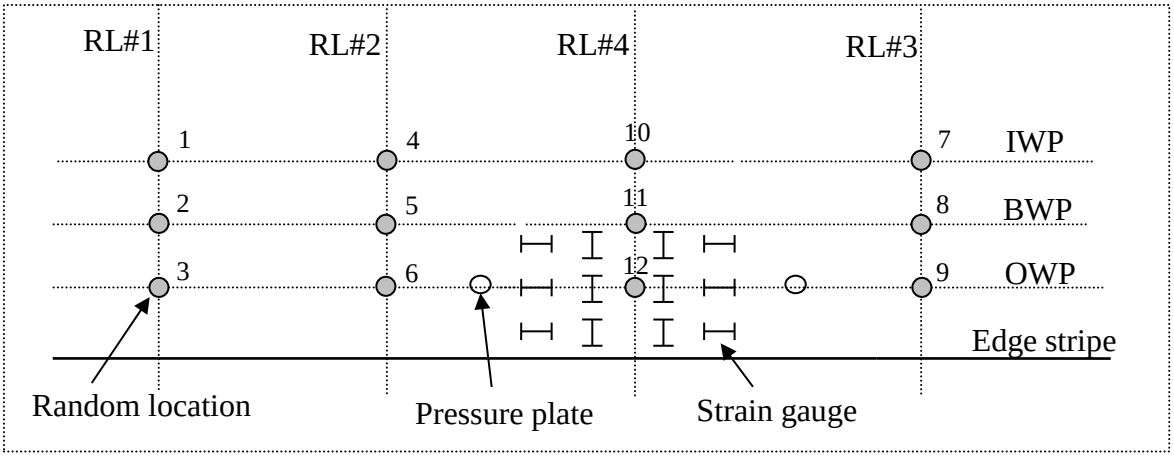

Figure 3.9: Random locations and FWD testing scheme.

3.4 IN-PLACE PROPERTIES FROM NCAT TEST TRACK

As discussed previously, the type of testing and the conditions tested in the laboratory for AC modulus do not reflect the conditions and loading typically seen in the field. This investigation aimed to close the gap between laboratory determined properties and in-place properties to improve predictions of tensile strains at the bottom of the AC layer. To do so required the use of in-place material properties. During construction of the test sections, plant produced mix was sampled for quality control (QC) purposes. From these samples, volumetric and gravimetric properties were determined. When combined with the known mat compaction that was determined during construction, the volumetrics

and gravimetric properties of the in-place AC layers were able to be determined. Due to the extensive FWD testing that was completed for each test section, the in-place moduli of the bound and unbound materials were also determined.

3.4.1 Volumetric and Gravimetric Properties

QC testing was completed on the sampled plant produced AC mixtures during construction. Included in the QC testing was the maximum specific gravity of the mix, G_{mm}, particle size distribution of the extracted aggregate, percent binder from extractions, P_b, and bulk specific gravity of the blended aggregate, G_{sb}. Additionally, plant produced samples were compacted in a Superpave gyratory compactor, consistent with the number of gyrations used in design. From these QC pills, the percent air voids, V_a, voids in mineral aggregate (VMA), voids filled with asphalt (VFA) and bulk specific gravity of the mix, G_{mb}, were determined. In addition to QC testing of the plant-produced mix, mat compaction was determined at various locations in the section from which an average was computed and recorded. During the construction of the 2009 structural sections, the four random locations discussed previously under "FWD Testing" were established and used as locations for testing mat compaction as well. Mat compaction was determined through the use of a nuclear density gauge for each AC layer placed. These values in addition to the plant settings during production of the mix are shown in Appendix A for each AC layer in the sections included in this investigation.

QC pills were compacted following design gyrations resulting in air voids of approximately 4%, which is typical of Superpave mix design. However, mixtures compacted in the field typically have an initial air voids closer to 7%, therefore it was

necessary to have the G_{mb} and volumetrics of the in-place AC layers to appropriately reflect the field conditions, as relationships were drawn with field strain. To be consistent with the location of the strain measurements, the mat compaction was taken from the random location in the gauge array, RL 4, in the outside wheel path. It should be noted that although four random locations were established in both the 2006 and 2009 test cycles, the fourth random location was not established during construction of the 2006 test cycle. Therefore, for the 2006 structural studies, the average mat compaction for the entire 150-ft study area was utilized. The in-place V_a were determined by subtracting the percent mat compaction from 100%. From the known G_{mm} (determined through QC testing) and the in-place V_a, the in-place G_{mb} was determined for each lift using Equation 3.1. In-place VMA, VFA, and dust proportion (DP) were also calculated following Equations 3.2, 3.3, and 3.4, respectively.

$$G_{mb} = G_{mm}\left(1 - \frac{V_a}{100}\right) \quad (3.1)$$

$$VMA = 100 - \frac{G_{mb}(100 - P_b)}{G_{sb}} \quad (3.2)$$

$$VFA = 100 \times \frac{VMA - V_a}{VMA} \quad (3.3)$$

$$DP = \frac{\rho_{200}}{P_{be}} \quad (3.4)$$

where:

P_b = Percent binder (%)

ρ_{200} = Percent passing the #200 sieve (%)

P_{be} = Percent of effective binder (%)

3.4.2 Backcalculated Moduli

Backcalculation of the deflection basins measured from FWD testing was completed for each section using EVERCALC 5.0. EVERCALC is a pavement analysis software program that estimates the elastic modulus of each pavement layer from measured deflections under FWD testing, using layered elastic analysis. A three-layer pavement section (AC over aggregate base over subgrade) was simulated. Surveyed layer thicknesses at each offset and random location were used in the backcalculation process, however, only the backcalculated moduli in the OWP of the random location in the gauge array was considered for this investigation. It should be noted that although four random locations were established in both the 2006 and 2009 test cycles, the fourth random location was not established during construction of the 2006 test cycle. As a result, the layer thicknesses at RL 4 were not surveyed; they were either taken from another RL in close proximity, or interpolated from layer thicknesses at the surrounding random locations. The layer thicknesses utilized for backcalculation for the sections used in this study are listed in Table 3.4. For section N9, RL 2 was relatively close to the gauge array and therefore the surveyed layer thicknesses for RL 2 in the OWP were utilized for backcalculation during the 2006 Test Track cycle. However, in the 2009 Test Track, the interpolated layer thicknesses at RL 4 were utilized during routine backcalculation which resulted in a slightly thicker AC layer and slightly thinner granular base layer. For this reason and due to the age of the section, N9 in 2009 was considered to be a separate section from N9 in 2006.

Table 3.4: Surveyed Layer Thickness Used for Backcalculation

Test Cycle	Section	AC Thickness (in.)	Granular Base Thickness (in.)
2006	N1	7.46	9.96
2006	N2	7.01	9.93
2006	N8	9.44	6.52
2006	N9	13.92	9.60
2009	N5	8.69	5.78
2009	N6	7.08	5.40
2009	N7	5.04	5.37
2009	N9	14.32	9.00
2009	N10	7.50	3.37
2009	N11	7.10	4.62
2009	S9	6.83	6.22
2009	S10	6.80	7.02
2009	S11	6.86	6.26
2009	S12	6.65	5.16

Although backcalculation was completed for all load levels and dates, the average modulus for each the granular base and subgrade at the 9-kip load level was used for this investigation. The 9-kip load level best represents the 20-kip single axles on the triple trailer trucks used to traffic the sections. Additionally, only backcalculated moduli that fell below the standard root mean square error (RMSE) threshold of 3% were used. The average moduli for the granular base and subgrade layers are listed in Table 3.5. Although the subgrade consistently returned higher moduli than the granular base material, this is consistent with findings from previous cycles at the Test Track (Timm 2009 and Taylor 2008). The Track soil which is utilized for the compacted subgrade is classified as an AASHTO A-4(0) soil and contains large stones and cobbles which contributed to the high backcalculated moduli. Sections N8 and N9 utilized the Track soil as a base material and a thick layer soft Seale subgrade was placed on top of the uncompacted Track soil. The very high subgrade moduli shown in Table 3.6 are

consistent with findings from a previous study on backcalculation of unbound materials at the Track when a three layer simulation was used (Taylor 2008).

Table 3.5: Average Backcalculated Moduli for Unbound Layers

Test Cycle	Section	Granular Base Modulus (psi)	Subgrade Modulus (ksi)
2006	N1	7,200	37,350
2006	N2	7,724	31,750
2006	N8	2,607	28,263
2006	N9	2,909	57,717
2009	N5	2,300	35,741
2009	N6	3,255	34,926
2009	N7	2,421	29,010
2009	N9	2,834	71,488
2009	N10	1,555	48,504
2009	N11	3,347	36,553
2009	S9	2,271	27,720
2009	S10	1,779	26,868
2009	S11	1,438	27,019
2009	S12	1,363	26,334

3.5 LABORATORY TESTING

To support the objectives of this study, laboratory testing was completed to characterize the AC mixtures through dynamic modulus (|E*|) and the asphalt binder through dynamic shear modulus (|G*|). By testing at the prescribed number of frequencies and temperatures the time-temperature superposition principle was applied to create a master curve for each AC mixture as well as each asphalt binder. The master curve allows for the prediction of |E*| at any frequency or temperature within the range tested, spanning the whole range of typical in-service temperatures and vehicle speeds.

3.5.1 Dynamic Modulus Testing

|E*| testing was conducted on plant produced mixtures, sampled during construction of both the 2006 and 2009 test cycles, from which |E*| and the associated phase angle, δ, were measured. Dynamic modulus is an important parameter in pavement design and is essential to current M-E designs, particularly the MEPDG. Therefore, |E*| values for the

mixtures included in the 2006 and 2009 test sections were incorporated in the development of the model resulting from this investigation. Those sections placed in 2003 and left in place were tested for |E*| by a third party using an older testing protocol that is no longer being used. As a result, those sections were excluded from this study. Additionally, not all of the AC mixtures placed in the 2006 structural study were tested, therefore, only sections that had |E*| testing completed for all of the AC layers included in the section were included in this study. Due to updates in the testing protocols two different protocols were followed, albeit similar, for mixtures placed in 2006 and 2009.

Regardless of testing protocol, plant produced mixtures were compacted in the laboratory, using a Superpave gyratory compactor. Once compacted, cylindrical specimens were cored from the gyratory compacted sample and trimmed to achieve a height of 150 mm and diameter of 100 mm. Volumetrics of the specimens were then determined with a target air void content of 7% within ±0.5%. As mentioned above, testing protocols were updated between the 2006 and 2009 research cycles, therefore specimens from the 2009 Test Track mixtures were subjected to additional requirements such as flatness and perpendicularity, as outlined in AASHTO PP 60-09.

For mixtures placed in 2006, testing was conducted under the guidance of the AASHTO TP 62-07 protocol. An Asphalt Mixture Performance Tester (AMPT), formerly called the Simple Performance Testing machine (SPT), shown in Figure 3.10, was utilized to apply haversine compressive loading to an unconfined specimen such that induced strain was within the range of 50-150 microstrain, in accordance with AASHTO TP 62-07. Due to complications in getting reliable data at the extreme temperatures, testing was conducted only at the three intermediate temperatures, 40, 70

and 100°F (4.4, 21.1, and 37.8°C). At each temperature the specimens were tested at seven frequencies, 0.5, 1, 2, 5, 10, 20, and 25 Hz. A minimum of three replicate specimens were tested for each mixture.

Mixtures placed in 2009 were tested in accordance with the updated protocol, AASHTO TP 79-09. For this procedure, the AMPT was utilized to apply a haversine compressive loading to unconfined specimens producing strains in the range of 75-125 microstrain, as outlined in AASHTO TP 79-09. For each mixture, testing was conducted at 39.2 and 68°F (4 and 20°C) and an additional high temperature, depending on the PG of the binder in the mix. For the 2009 Test Track mixtures, the high temperature was either 104 or 113°F (40 or 45°C). At each temperature, testing was completed at three frequencies, 0.1, 1 and 10 Hz, with an additional frequency of 0.01 Hz at the high temperature. A minimum of two replicates were tested for each mixture, as required by the AASHTO TP 79-09.

Figure 3.10: The AMPT and close up of specimen.

3.5.1.1 Dynamic Modulus Master Curves

Master curve development for testing using the AASHTO TP 62-07 is described by Equations 3.5 and 3.6. It should be noted that shift factor, log *a*(T), can be determined through regression of a second order polynomial, shown in Equation 3.7.

$$\log(|E*|) = \delta + \frac{\alpha}{1+e^{\beta-\gamma\log(f_r)}} \quad (3.5)$$

where:

|E∗| = Dynamic modulus (psi)

δ, α, β, γ = Fitting parameters

f_r = Reduced frequency (Hz)

$$\log(f_r) = \log(f) + \log[a(T)] \quad (3.6)$$

where:

f_r = Reduced frequency (Hz)

f = Test frequency (Hz)

a(T) = Shift factor

T = Test temperature (°C)

$$\log \alpha_T = \alpha_1(T^2 - T_r^2) + \alpha_2(T - T_r) \quad (3.7)$$

where:

α_1, α_2 = fitting parameters

T_r = reference temperature (°C)

Similarly, master curve generation is outlined in AASHTO PP 61-09 for testing completed with the AASHTO TP 79-09 protocol. The master curve generated under the AASHTO PP 61-09 procedure is of the form shown in Equation 3.8 where reduced frequency is also defined by Equation 3.6 (with temperature in °K). In addition to β and

γ, log $|E^*|_{min}$ is also treated as a fitting parameter. Although the log of the limiting minimum modulus is a regression term, the PP 61-09 procedure utilizes the Hirsch model (Christensen et al. 2003) to define the limiting maximum modulus. As illustrated in Equation 3.9, the Hirsch model used to define the maximum limiting modulus is modified to fix the |G*| term seen in the original Hirsh model (Christensen et al., 2003) to a value of 145,000 psi, which is the commonly accepted value for the glassy modulus of binder, G_g, (1 GPa). Rather than using a 2nd order polynomial, PP 61-09 utilizes the Arrhenius shift factor, shown in Equation 3.10, where only activation energy, (ΔE_a) is a fitting parameter.

$$\log(|E*|) = \log|E*|_{min} + \frac{\log|E*|_{max} - \log|E*|_{min}}{1+e^{\beta+\gamma(\log f_r)}} \quad (3.8)$$

where:

$|E^*|_{min}$ = limiting minimum modulus (ksi)

β, γ = fitting parameters

$|E^*|_{max}$ = limiting maximum modulus (ksi), see Equation 3.9

$$|E*|_{max} = \frac{P_c}{1000}\left[4{,}200{,}000\left(1-\frac{VMA}{100}\right)+435{,}000\left(\frac{VMA\times VFA}{10{,}000}\right)\right]+\frac{1-P_c}{\left[\frac{\left(1-\frac{VMA}{100}\right)}{4{,}200{,}000}+\frac{VMA}{435{,}000(VFA)}\right]} \quad (3.9)$$

where:

$$P_c = \frac{\left(20+\frac{435{,}000(VMA)}{VFA}\right)^{0.58}}{650+\left(\frac{435{,}000(VMA)}{VFA}\right)^{0.58}}$$

VMA = Voids in mineral aggregate (%)

VFA = Voids filled with asphalt (%)

$$log\ a\ (T) = \frac{\Delta E_a}{19.17142}\left(\frac{1}{T} - \frac{1}{T_r}\right) \quad (3.10)$$

where:

ΔE_a = Activation energy, treated as fitting parameter

T = Temperature (°K)

T_r = Reference temperature (°K)

To be consistent between testing cycles, one master curve procedure was selected and utilized for all mixtures. It should be noted that other procedures for generating an |E*| master curve exist, such as the method deployed in the current version of the MEPDG (ARA 2004(a)). This method uses viscosity and determines the viscosity-temperature relationship at a reference temperature using the linear A-VTS relationship, shown in Equation 3.11. The data are then shifted by applying a fitting parameter and given temperature to the known viscosity-temperature relationship. Rather than considering frequency, time of loading, t, is utilized, which requires a conversion from frequency, using the common f = 1/t relationship. As part of the standard testing regime for the Test Track, binder was characterized by |G*| rather than viscosity. To generate a master curve as described in the MEPDG appendix (ARA 2004(a)) would require |G*| to be converted to viscosity. To minimize errors, it was elected to use laboratory measured results directly, when possible. Therefore the PP 61 and TP 62 methods for generating master curves were preferable over the MEPDG method.

$$\log\log\eta = A + VTS\log\log T \quad (3.11)$$

where:

A, VTS = regression terms (slope and intercept, respectively)

η = viscosity (cP)

T = Temperature (°R)

In developing master curves for use in this study, it was elected to utilize the procedure laid out in AASHTO PP 61-09. With the advent of the MEPDG and need for |E*| testing, it is likely that TP 79-09 will become the state of the practice. This testing protocol reduces the number of testing frequencies and removes the low temperature requirement of its predecessor, resulting in reduced testing time. Also, when used in conjunction with AASHTO PP 61-09, a complete master curve is created using a minimum number of temperatures and frequency; a total of 10 |E*| values result for each specimen in comparison to 30 values for the previous AASHTO TP 62-07. The other advantage is the MasterSolver Excel spreadsheet that has been developed for PP 61-09 uses the |E*| testing results to not only solve for the fitting parameters described previously, but to also generate |E*| values at temperatures and frequencies required by the MEPDG. This allows those estimates to be input directly into a level 1 design. This circumvents the need to test at the extreme low and high temperatures while still conducting a level 1 design using measured results. By doing so however, the AASHTO TP79-09 and PP 61-09 relies on the functional form of the master curve (Equation 3.8) and an analytical method to predict the moduli at the extreme temperatures. As discussed, the modified Hirsch model is used to predict the maximum |E*| which would be measured under the TP 62-07 method at the extreme low temperature, -10 °C.

In a study comparing AASHTO TP 62-07 and PP 61-09 (Underwood 2011), it was found that by estimating the limiting maximum modulus from the Hirsch model, as is done in PP 61, differences from the measured modulus at -10 °C from TP 62 may be

in the range of 7-34%. Differences at the extreme high temperature, 54 °C were found to be near 5%. When moduli from the different protocols were applied to the MEPDG, it was found that the relative differences in pavement performance were small. Given these findings and the gaining popularity of the current protocol, AASHTO TP 79-09, AASHTO PP 61-09 was selected for use in this analysis.

Regardless of the testing protocol that was followed, PP 61-09 was used to generate a master curve for each unique mix from the 2006 and 2009 structural studies. Due to the difference in test temperatures, a single reference temperature was selected for the Arrhenius shift factor. A temperature of 71.6 °F (22°C or 295.2°K) was selected because it fell within the range of test temperatures from both test cycles, as well as the range of test temperatures for dynamic shear modulus testing in both test cycles. This is also close to the reference temperature of 70 °F that is used for the creation of the master curve in the MEPDG. The initial estimates utilized in the MasterSolver spreadsheet developed by Bonaquist (2009) for the fitting parameters, log $(|E^*|_{min})$, β, γ, and ΔE_a were utilized and were as follows: 0.5, -1, -0.5, 200,000, respectively. The final fitting parameters are listed in Appendix B for each AC lift.

3.5.2 Dynamic Shear Modulus Testing

For those mixtures placed in the 2006 Test Track structural study, dynamic shear modulus, |G*|, testing, in accordance with AASHTO T 315-06, was conducted on rolling thin film oven (RTFO)-aged binders using a Dynamic Shear Rheometer (DSR) to determine |G*| and associated phase angle, δ_b, at a variety of temperatures and frequencies. Testing was conducted at four temperatures, 40, 70, 100, and 130°F (4.4,

21, 37.8, and 54.4°C). A frequency sweep, in which thirteen frequencies (0.1, 0.2, 0.3, 0.4, 0.6, 1.0, 1.6, 2.5, 4.0, 6.3, 10.0, 15.9, and 25 Hz) were applied, was completed at each temperature.

Similarly, frequency sweeps were conducted on those binders that were part of the mixtures placed in the 2009 Test Track structural study, following the updated protocol, AASHTO 315-09. $|G^*|$ and δ_b were determined at three temperatures, 70, 100 and 130°F (21.1, 37.7, and 54.4°C) and thirteen frequencies (0.01, 0.0116, 0.025, 0.05386, 0.116, 0.25, 0.5386, 1.16, 2.5, 5.386, 11.6 and 25 Hz). It should be noted that due to the modified binders and unique technologies utilized during the 2009 structural study several of the binders were extracted from plant-produced mixtures following ASTM D2172-05 and were recovered in accordance with ASTM D5404-03. All lifts from the high RAP sections, (N10 and N11), the WMA sections (S10 and S11), the TLA section (S12) and the control section (S9) had frequency sweeps performed on recovered binder. The remaining Thiopave sections and the Kraton section (N5, N6 and N7, respectively) had frequency sweeps conducted on virgin binder sampled from the tank which was RTFO-aged prior to DSR testing. Due to the complicated technologies that were used in the 2009 Test Track structural study, the technique for sampling the binders (and aging of the binders) varied based on the type of technology used in each section. Despite these variations in sampling and the aging associated with the sampling techniques, this was the most reasonable method to determine dynamic shear modulus for the unique technologies and modified binders.

3.5.2.1 Dynamic Shear Modulus Master Curve

A master curve was constructed by fitting the CAM model to the |G*| results for each of the binders. The CAM model, refined by Marasteanu and Anderson (1999), is a widely adopted method for fitting dynamic shear modulus master curves and was developed with both modified and unmodified binders. Shown in Equation 3.12, it is a function of the glassy modulus of the binder, G_g, and three fitting parameters: the cross-over frequency, f_c; and shape parameters, k and m_e. For this investigation the G_g was held constant to a common value of 1 GPa, which is also consistent with the G_g utilized in constructing the |E*| master curves. Initial estimates of the fitting parameters, f_c, k and m_e were 0.1 Hz, 0.1 and 1, respectively. The reduced frequency was determined through the commonly-used Williams-Landel-Ferry (WLF) time-temperature shift factor (Ferry 1980), shown in Equation 3.13. A reference temperature of 71.6°F (22°C or 295.2°K) was selected and is consistent with the reference temperature used for the construction of the dynamic modulus master curves. Excel Solver was utilized to determine the fitting parameters through non-linear optimization with initial estimates for C_1 and C_2 consistent with the universal constants of 17.44 and 51.60, respectively. The final fitting parameters associated are listed in Appendix C for each AC lift in each test section.

$$|G*| = \frac{G_g}{\left(1+\left(\frac{f_c}{f_R}\right)^k\right)^{\frac{m_e}{k}}} \tag{3.12}$$

where:

G_g = glassy modulus (Pa)

f_c, k, m_e = fitting parameters

f_R = reduced frequency (Hz)

$f_R = f^*a(T)$

$$\log a(T) = \frac{-C_1(T-T_R)}{C_2+T-T_R} \quad (3.13)$$

where:

C_1, C_2 = fitting parameters

T = temperature (°K)

T_R = reference temperature

3.6 SUMMARY

This chapter served to describe the overall method utilized to develop a comprehensive model for predicting tensile strains at the bottom of the AC layers through the use of laboratory measured AC and binder properties as well as in-place properties of the AC layers and unbound materials. Pavement strains were measured at the NCAT Test Track during the 2006 and 2009 structural studies. Those sections included in the 2006 and 2009 studies were described as well as the traffic applied and embedded instrumentation necessary for measuring the strains and temperatures used for this investigation. Utilizing undamaged sections was necessary in this investigation; therefore the methods used for weekly performance measurements made during these studies were also described. Additionally, the FWD testing procedure and determination of backcalculated moduli were discussed.

The AC mixtures were characterized in the laboratory though dynamic modulus and resulting phase angle. From the |E*| results measured in the laboratory, a master curve was constructed for each AC mix at a reference temperature of 71.6°F (22°C or 295.2°K) using the method described in AASHTO PP 61-09 and the initial estimates for

the fitting parameters as used in the MasterSolver spreadsheet (Bonaquist 2009). The Arrhenius time-temperature shift factor was applied to the |E*| data for construction of each master curve. Dynamic shear modulus was used to characterize the asphalt binders. A master curve was fitted to the |G*| results for each unique binder using the CAM model (Marasteanu and Anderson 1999) and the WLF time-temperature shift factor (Ferry 1980).

CHAPTER 4

MODULUS-STRAIN RELATIONSHIPS

4.1 INTRODUCTION

To improve the prediction of tensile strains at the bottom of the AC layers, a model was developed to estimate the in-place modulus for a given vehicle speed and mid-depth pavement temperature. When used in conjunction with a layered elastic analysis program, the tensile strain predictions more closely matched those in the field. The first step in developing this model was to use a LEA program to determine the relationship between the composite AC modulus and the resulting tensile strain at the bottom of the AC layers. Once known, the relationship could then be applied to the strain measured in the field for each structural section to backcalculate the required modulus to achieve that strain.

4.2 MEASURED PAVEMENT RESPONSE

The first step in developing the modulus-strain relationship was to determine strain from measured pavement responses. Tensile strains were measured at the NCAT Test Track through the use of embedded strain gauges at the bottom of the AC layers, as discussed in the previous chapter. Tensile strain was measured in both the longitudinal and transverse directions as part of 2006 and 2009 structural studies. For this investigation, the maximum tensile strains were desired, as these are the primary cause of bottom up

fatigue cracking. Previous studies at the track have found that maximum tensile strains were in the longitudinal direction and induced by the trailing single axles (Timm and Priest 2008, Robbins 2009). Therefore, only tensile strains measured in the longitudinal direction under single axles were utilized for this investigation. To be consistent with the LEA program that was selected for this investigation, WESLEA version 3.0, strain was defined as the peak strain. Peak strain, as shown in Figure 4.1, is the difference between the peak value and baseline value on the strain trace. The best-hit was used in selecting strain, such that on a given date, the maximum peak strain was retrieved by surveying data from each of the working longitudinal strain gauges and selecting the maximum peak strain measured from all the passes of a given axle type. Therefore, on a given date, the maximum singular strain was selected from at most 450 strain measurements (5 trucks x 3 passes x 5 single axles x 6 longitudinal gauges) in the longitudinal direction under a single axle. The best-hit approach ensured that the most representative strain measurement was used for the analysis.

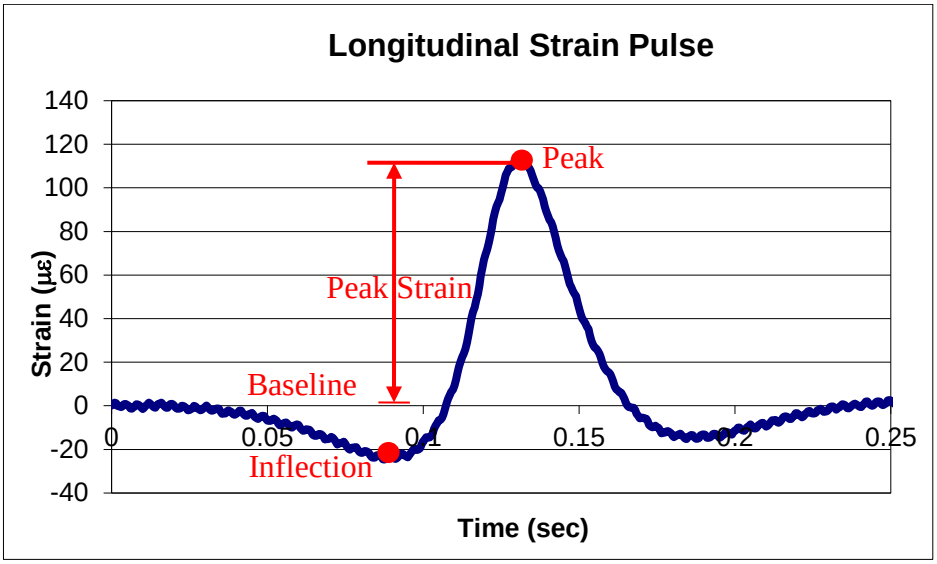

Figure 4.1: Illustration of peak tensile strain used for investigation.

4.3 STRAIN ASSOCIATED WITH DAMAGE

The goal of this investigation was to improve tensile strain predictions thereby improving the ability to predict fatigue cracking. Therefore, it was necessary to select only those strains that were induced in well-performing, undamaged sections. The weekly performance monitoring was utilized to identify rutting and cracking in the structural sections.

As noted in Chapter 3, a third party completed the |E*| testing on mixtures placed in 2003, therefore, only structural sections newly constructed in 2006 and sections part of the 2009 structural study were evaluated. During the 2006 structural study, distresses were observed in five of the six newly constructed sections: N1, N2, N8, N10 and S11. Evident by crack maps, shown in Figure 4.2, cracking was first observed in section N1 on 4/9/2007 and had progressed to 100% of the lane cracked by 1/28/2008. Cracking in N2 was first observed shortly after N1, on 4/23/2007. Although cores taken from each section revealed that the cracking was top-down rather than bottom-up cracking (Timm et al. 2009), strain from these sections was limited to the data collection date one week prior to the observed cracking: 4/4/2007 for N1 and 4/19/2007 for N2. Through crack maps, similar to the one shown in Figure 4.2, generated for each section, the dates that initial cracking was observed were established as well as the extent of the cracking over time. However, the date corresponding to initial cracking was of primary concern for this investigation. Cracking was first observed in section N8 on 4/28/2008 and it was later confirmed that it was in fact fatigue cracking (Willis and Timm 2009). As a result, only strain measured through data collection the week prior, 4/24/2008, was utilized. Fatigue cracking was also confirmed

in sections N10 and S11 with cracking first observed on 6/23/2008 and 1/28/2008, respectively (Willis and Timm 2009). Sections N10 and S11 were removed from this evaluation, however, due to the lack of |E*| testing for all mixtures in these cross-sections. Section N9 was in excellent condition at the conclusion of the 2006 test cycle, with only 5 mm of rutting, IRI of approximately 140 in/mile and no cracking observed.

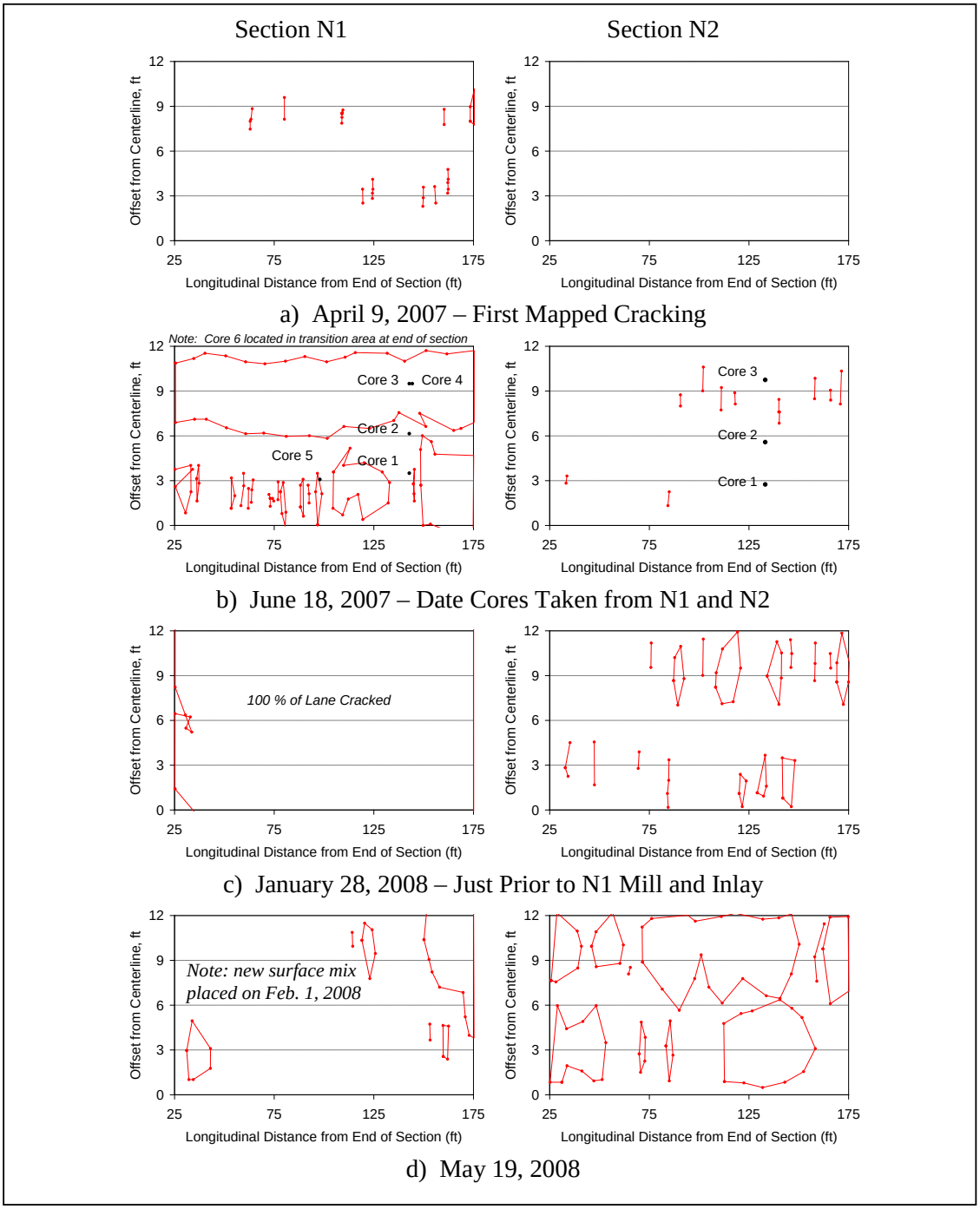

Figure 4.2: Crack maps for sections N1 and N2 (Timm et al. 2009).

In general, the 2009 structural sections performed very well over the course of the 2 year testing period. Performance (rutting, cracking and IRI) for these sections at the conclusion of the 2009 test cycle is summarized in Table 4.1. The values reported in

Table 4.1 reflect measurements obtained from the Roadware ARAN van. Only one section, S11 was observed to have rutting that approached the distress threshold of 12.5mm. In Figure 4.3 rut depth is plotted as a function of applied ESALs for section S11. From this plot it is evident that for the majority of the 2009 test cycle, the rut depths were well below this threshold. Therefore, strain measurements made throughout the test cycle were utilized in this investigation. As shown in Table 4.1, all of the sections had excellent roughness readings, with IRI measurements well below the typical 172 in/mile threshold. Minor cracking was observed in section N9, shown in Figure 4.4, near the conclusion of the 2009 test cycle on 9/30/2011. Presented in Figure 4.4, cracking is shown relative to the transverse offset from the centerline of the lane, such that 12 ft. represents the outside edge of the lane; and relative to the longitudinal offset from the transverse joint at the start of the test section. From this plot it is evident that minor cracking was observed, however, it was near the centerline of the lane, a suitable distance from the outside wheel path where strains were measured. It should be noted that section S8 was constructed with an OGFC surface course which was unable to be tested for |E*|, therefore the entire section was removed from this investigation. Based on the good performance of the sections listed in Table 4.1 there was no need to limit the strain measurements used in this evaluation based on distress.

Table 4.1: Performance summaries for 2009 structural sections

Section	Rut depth (mm)	Cracking observed	IRI (in/mile)
N5	7	No	85
N6	9	No	62
N7	3	No	120
N9	5	Yes near centerline	110
N10	2	No	80
N11	4	No	40
S9	7	No	61
S10	9	No	65
S11	11	No	100
S12	5	No	95

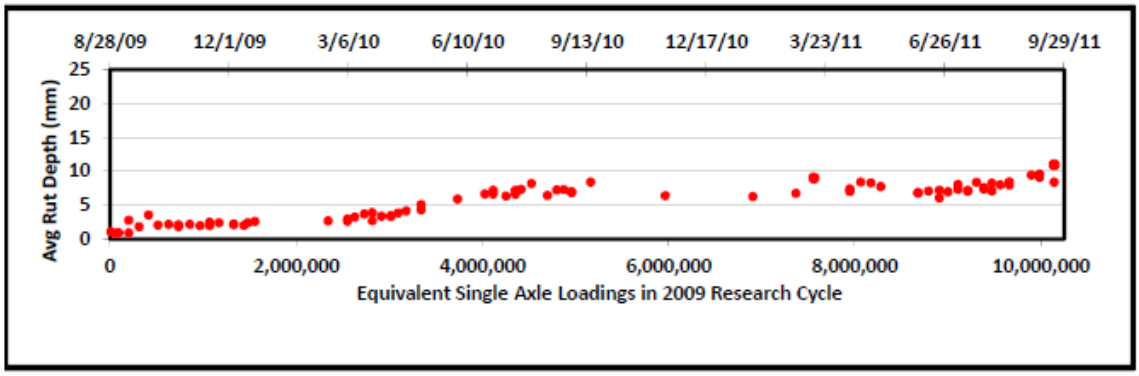

Figure 4.3: Rut depths for section S11.

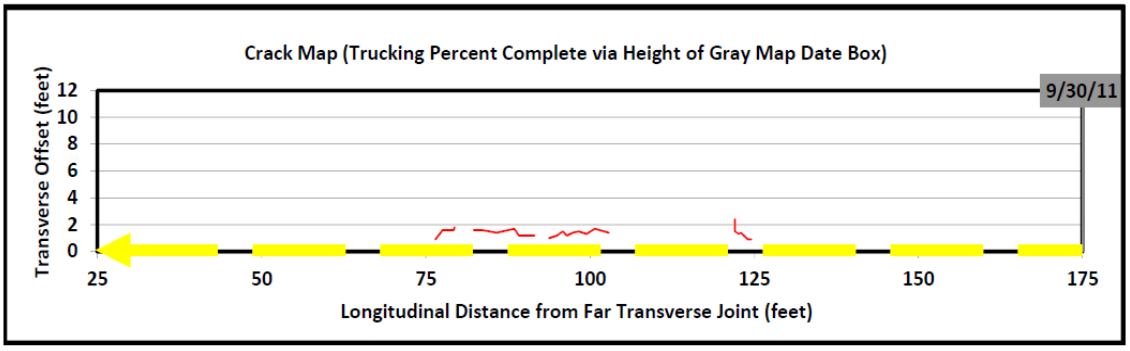

Figure 4.4: Crack map for N9 for 2009 test cycle.

4.4 NON-ELASTIC STRAIN

Since a LEA program had been selected, it was necessary to remove those strains that were not elastic in nature. An elastic strain would imply that, as shown in Figure 4.1 above, the strain trace begins at the baseline strain and as an axle applies loading, the

induced strain reaches a peak value and returns to the original baseline as the axle has completely passed the strain gauge, thereby no longer applying a load. Several methods were employed to identify possible non-elastic strain. Strain as a function of time and temperature and the RMSE associated with backcalculated AC moduli were utilized to identify possible non-elastic strain responses. Additionally, the difference between the maximum strain on a given date and the 95th percentile strain was used as a possible indicator of non-elastic behavior. The 95th percentile strain was selected for this metric based on previous work at the NCAT Test Track which found that the 95th percentile strain eliminated processing errors but represented values close to the maximum value (Willis and Timm 2009). By using the difference between the maximum and 95th percentile strain, possible errors whether due to processing or erratic strain data could be revealed.

4.4.1 Strain as a Function of Time and Temperature

For each section, strain (from the best-hit) was plotted with time and temperature. This helped identify strain measurements that did not reflect typical behavior based on the measured mid-depth pavement temperature. Mid-depth pavement temperatures were utilized for this investigation based on previous studies at the Test Track that found mid-depth temperature provided the best correlations between strain and temperature (Timm and Priest 2008). Temperatures measured from probe T2, as shown in Table 3.1, in each section were used to represent mid-depth temperatures. Figure 4.5 is an example of the plots generated for each section to identify possible plastic strain measurements. In this plot, strain and temperature are plotted against time such that strain is on the primary y-axis and mid-depth pavement temperature is on the secondary y-axis. As temperatures

increase over the spring and summer months, the strain increases as to be expected and likewise, as temperature decreases over the fall and winter months, strain also decreases. Strains that do not follow this trend may indicate non-elastic behavior and should be further investigated. An example of a strain value that seems to deviate from this trend is in Figure 4.5 on June 17, 2010 in section N6 with a measured value of 2,018 με. This value is significantly higher than the other strain values measured during the summer of 2010 and is higher than strain values measured at similar temperatures.

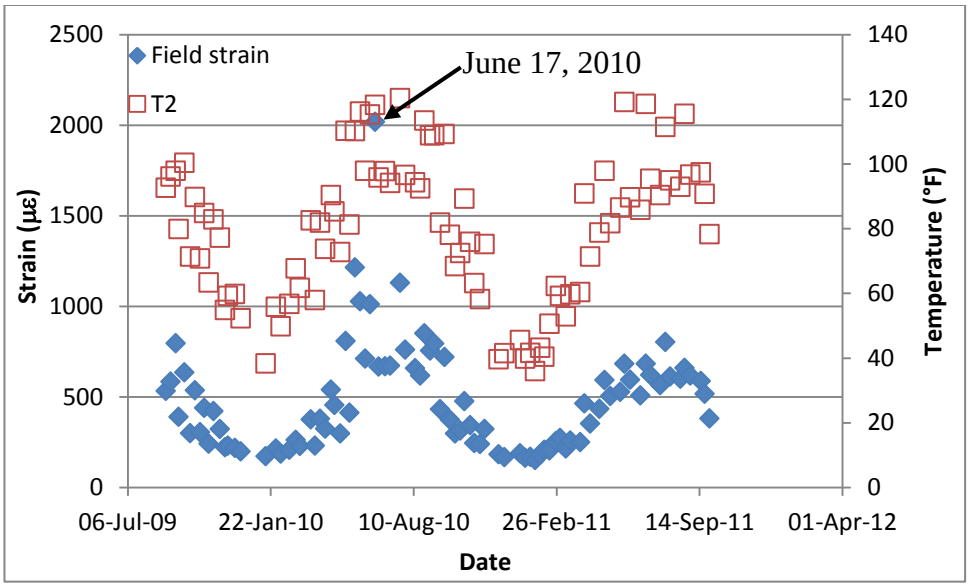

Figure 4.5: Strain and mid-depth temperature with time, section N6.

Strain values that begin to diverge from the apparent strain-temperature relationship may indicate possible non-elastic behavior. Although Figure 4.5 helps to identify strain values that do not follow typical temperature trends over time, strain values that did not represent the strain-temperature relationship were more easily identifiable by plotting strain against mid-depth pavement temperature as in Figure 4.6. This plot is also for strains measured in section N6. By applying a trendline, the relationship was visually more apparent, making it easier to identify those strain values

that needed to be further investigated. From Figure 4.6, additional strain values to be investigated were identified by the departure of data from the trendline beyond mid-depth pavement temperatures of 100°F. In addition to the strain value identified from Figure 4.5, there were two strain values measured at a mid-depth pavement temperature near 120°F that were of the same magnitude of strain values measured at temperatures 25°F cooler and another very high strain value (1200 με) that was nearly 400 με higher than others measured at similar temperatures.

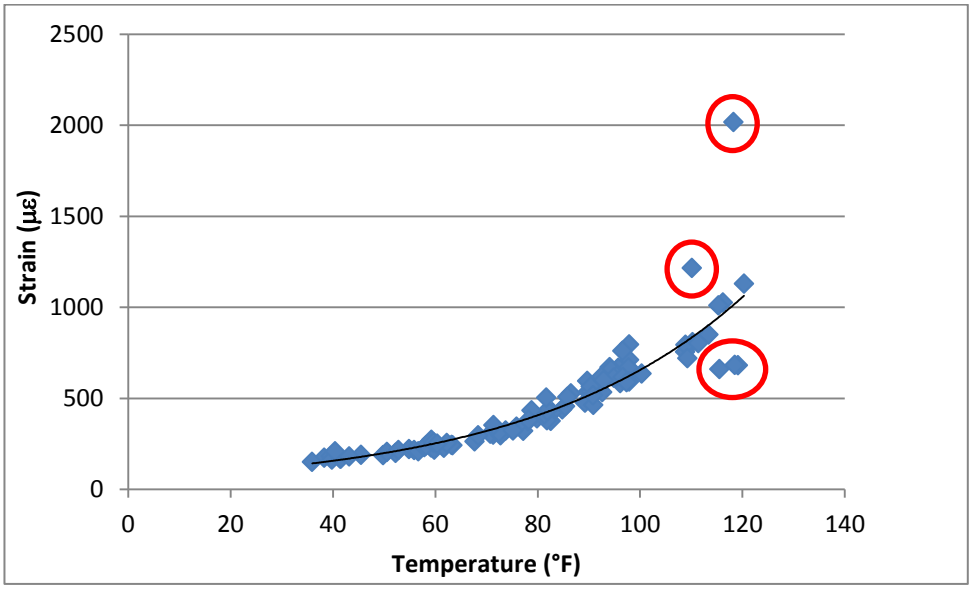

Figure 4.6: Strain with mid-depth temperature, section N6.

To investigate possible non-elastic strain, the date, strain gauge, truck, pass and axle from which the strain was measured was identified and the raw, unprocessed strain data was visually inspected. Traces were inspected for responses that did not return to the baseline when in the unloaded state, erratic strain traces or strain traces that exceeded the limitations of the gauge and therefore induced errors in processing the data into strain values. Further investigation of the four strain values highlighted in Figure 4.6 revealed that there was full return of the trace to the baseline. Also, there was no

erratic behavior nor did these strain values exceed the capacity of the strain gauges. Therefore these values were included in the analysis. An example of a strain trace that was removed is in Figure 4.7. This trace was the maximum best-hit strain on a given date and was identified as exhibiting possible non-elastic behavior based on a high strain value that deviated from the observed trend on a strain-temperature plot similar to Figure 4.6. It was removed because the last axle was the maximum best-hit strain value and as shown in Figure 4.7, it did not return to the original baseline. Although it is difficult to discern whether the failure of the strain trace to return to the baseline after the final axle pass was due to non-elastic behavior or due to functionality issues with the electrical signal from the gauge, the trace was removed. Those strain traces that exhibited behavior similar to that shown in Figure 4.7 were removed for all sections as well as those strains that exceeded the ± 5V capacity of the strain gauges.

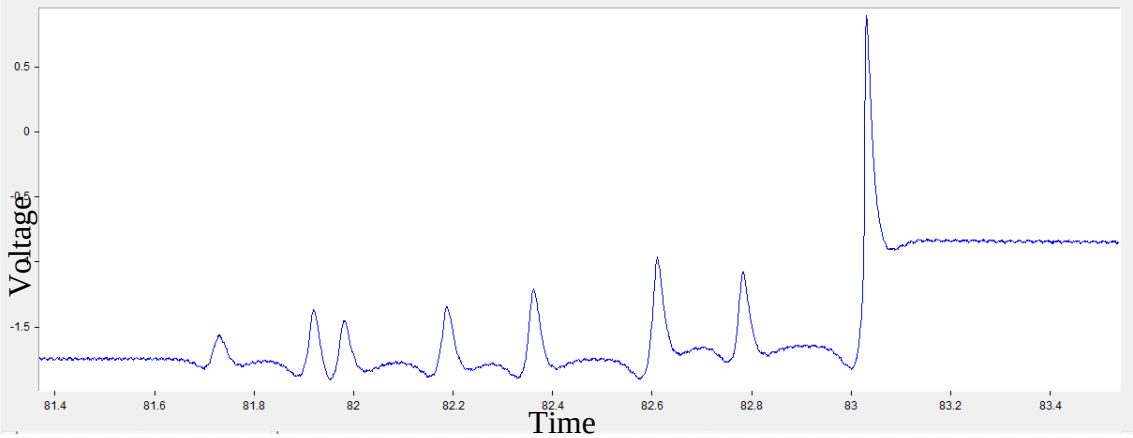

Figure 4.7: Example of strain trace removed.

4.4.2 RMSE as an Indicator of Non-elastic Behavior

The typical tolerance used at the NCAT Test Track for RMSE for backcalculated moduli is 3%. In a forensic investigation of sections N1 and N2 of the 2006 Test Track, it was found that RMSE tended to surpass this tolerance as cracking progressed through

these sections; an example of this is in Figure 4.8. In this figure, RMSE is plotted with time for the dates that FWD testing was conducted and backcalculation performed for station 12 in the gauge array under the 9-kip load level. As mentioned previously, cracking in section N1 was first observed on 4/9/2007. Shown in Figure 4.8, there is a distinct increase in RMSE after 4/9/2007 and the RMSE remained above 3% as cracking progressed throughout the section. Based on this it was believed that high RMSE values could serve as a possible indicator of damage occurring within the pavement structure. FWD testing was conducted regularly at the Test Track during the 2006 and 2009 test cycles for the structural sections from which backcalculation was performed. The results of the backcalculation for each section and date tested were compiled in a database for both test cycles. This backcalculation database was employed to identify RMSE that were outside of the typical 3% tolerance for backcalculated layer moduli for each of the sections.

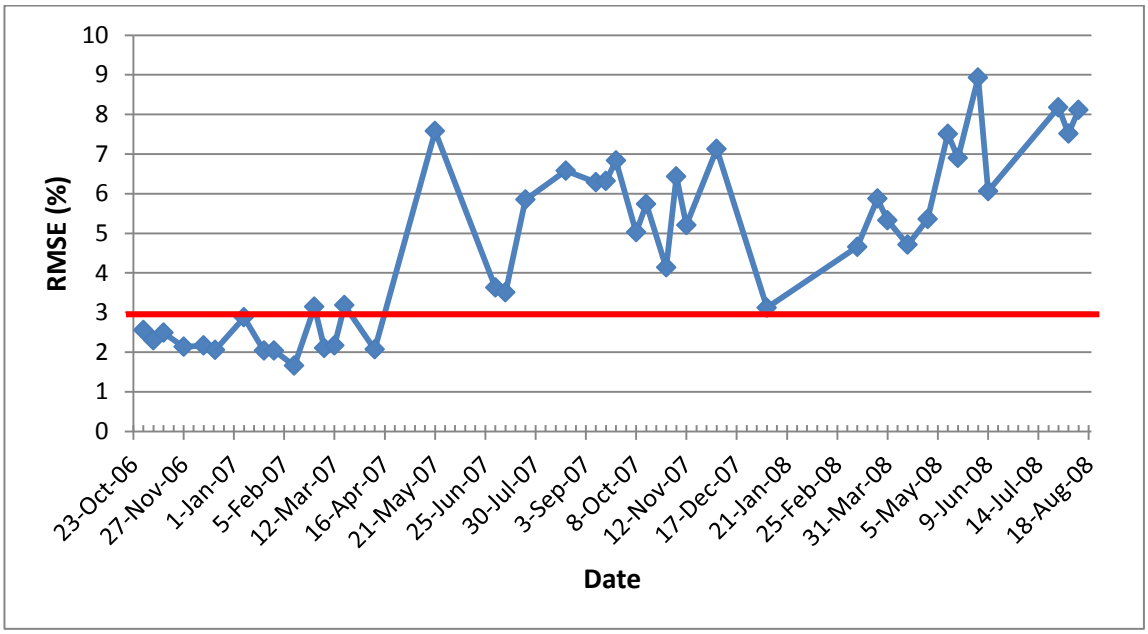

Figure 4.8: RMSE over time for section N1.

Plots similar to Figure 4.9, where mid-depth pavement temperature is plotted on the primary y-axis and RMSE on the secondary axis, were generated for each section. These plots were developed to identify time periods where RMSE were at and remained over 3%. Test section N6 was an uncracked section that saw moderate rutting and low IRI. Consistent with the good performance in this section, shown in Figure 4.9, the majority of the RMSE values were below the 3% threshold. The RMSE tended to follow the trends in mid-depth pavement temperature, such that as temperature increased, so did the RMSE. Shown in Figure 4.9, three dates had RMSE values above 3%; however they were also on days that saw high mid-depth pavement temperatures. In all of the undamaged sections, including section N9 (for backcalculation from station 12 in the OWP of the gauge array) from the 2009 Test Track, the RMSE tended to remain at or below 3%. Similar to Figure 4.9, RMSE values that exceeded the 3% threshold tended to be associated to high temperatures. This was also the case in the sections with confirmed fatigue cracking from the 2006 Test Track: RMSE values above 3% existed prior to and after observed cracking. This was the case for section N8, in which RMSE values above 4% existed during most of the summer months in 2007. However, when maximum (best-hit) strain traces were examined for dates prior to the observed cracking, particularly in the summer of 2007, the strain traces appeared elastic with complete return to the baseline when unloaded. Therefore, this approach was inconclusive in identifying damage, but did confirm the significant influence of pavement temperature on behavior.

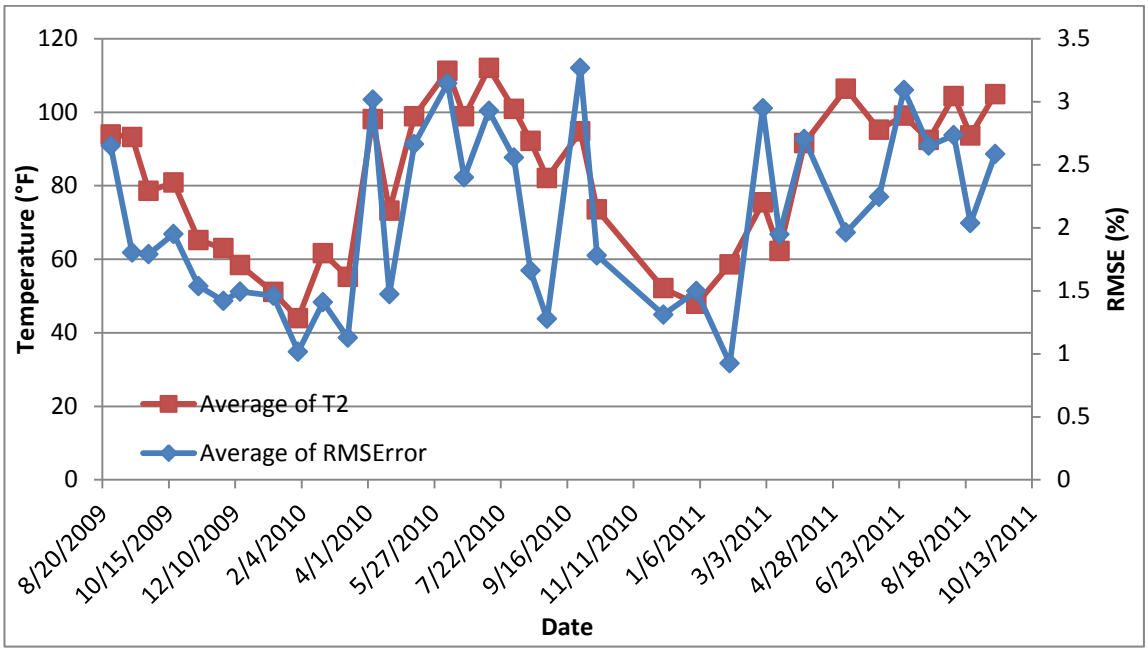

Figure 4.9: Plot of temperature and RMSE with time, section N6.

4.4.3 Difference between Maximum and 95th Percentile Strain

For normal operations during the 2009 Test Track, strain was calculated from Figure 4.1 as the difference between the peak and inflection points. Additionally, the strain distribution for each section was also determined for each data collection date using this definition of strain. The difference between the 100th and 95th percentile strains was calculated and used to identify dates that had differences exceeding 20% of the maximum strain. It was expected that a value of 20% would be large enough to capture errors in processing, erratic strain data and potential non-elastic strain without also capturing differences that are related to typical strain distributions. Although these differences were based on a different definition of strain, they indicated large variation in pavement responses that could be a result of non-elastic behavior for the strain definition used in this investigation. For each section, dates corresponding to differences

of more than 20% of the maximum strain were identified. Once identified, the raw strain traces were investigated, again looking for erratic behavior, traces that exceeded the limitations of the gauges and traces that did not return to the original baseline. This process helped identify additional strain traces that were non-elastic or erratic and thereby were removed from this investigation.

4.4.4 Gauge Functionality

Lastly, the best-hit strain was utilized to achieve the best representation of maximum strain induced in a section given the known loading condition. Thus, the number of working gauges in each section was also a factor in selecting representative strain traces. After the removal of the non-elastic strains following the previously described procedures, there were four sections from the 2009 Test Track that exhibited uncharacteristically low strains or strains that appeared to be somewhat erratic relative to the mid-depth pavement temperatures and observed strain-temperature relationships: N7 (Kraton), N9 (Oklahoma 14-inch section) , N10 (High RAP) and S12 (TLA). After further investigation of these sections, it was apparent that at some point during the testing cycle, some or most of the longitudinal strain gauges were no longer functioning.

For section N9, shown in Figure 4.10, longitudinal strain was unable to be captured during the summer of 2010 due to non-functioning gauges. It should be noted that the strain shown in Figure 4.10 as well as Figures 4.11-13 represent only elastic behavior. Although some of the gauges were able to be brought back online in the fall of 2010, several were still not functioning. For several dates beyond 6/3/2010, only one of the six longitudinal gauges was working and for most of the other dates, only two were working. This significantly reduces the chance that the longitudinal strain that was

captured accurately represented the maximum strain induced under loading. It is likely that the uncharacteristically low strain values observed in the latter part of the testing cycle and the strain values that seem to be somewhat erratic are due to the inability to capture representative strains rather than plastic strain or erratic behavior in the section. Therefore, only longitudinal strain data recorded through 6/3/2010 were utilized.

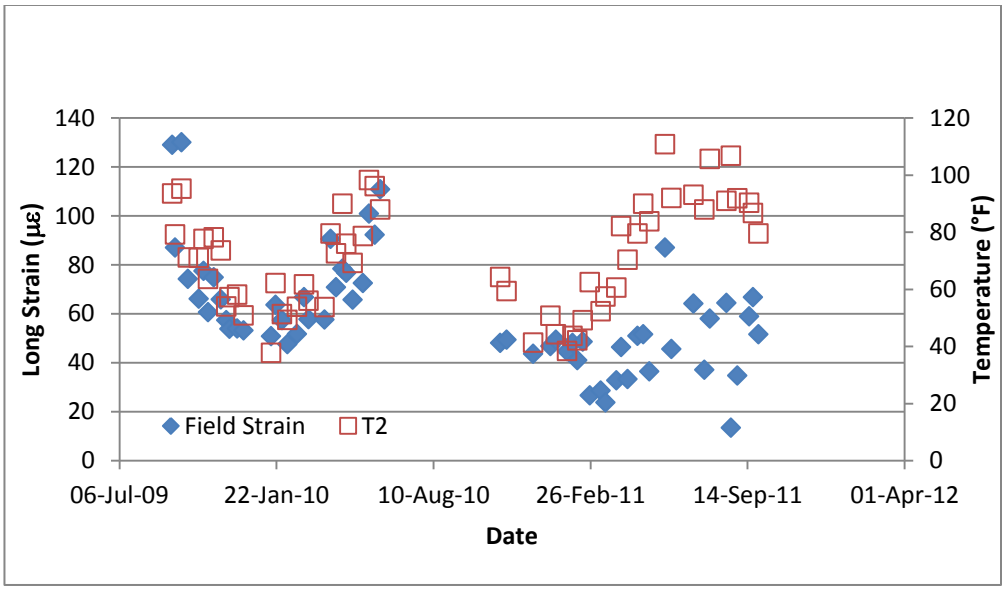

Figure 4.10: Strain and mid-depth temperature with time, N9 (2009).

Similar to N9, section N7 also had gauge failures, evident in Figure 4.11 as the strain appeared to be much lower and more erratic in the latter part of the testing cycle. Prior to 4/21/2010 the majority of the longitudinal gauges were functioning. However, beyond this date the number of gauges working fluctuated from 1to3 and often times neither of the center gauges (gauge 2 nor 11) were working. Based on previous studies at the track, wheel wander has been shown to be represented by a normal distribution (Timm and Priest 2005). Therefore, it would be expected that the majority of the maximum strains would be captured by the gauges centered in the OWP. Due to the limited functionality of these gauges, the chance of capturing the most representative

maximum strains was severely reduced. Therefore, only strain data recorded through 4/21/2010 were utilized for this analysis.

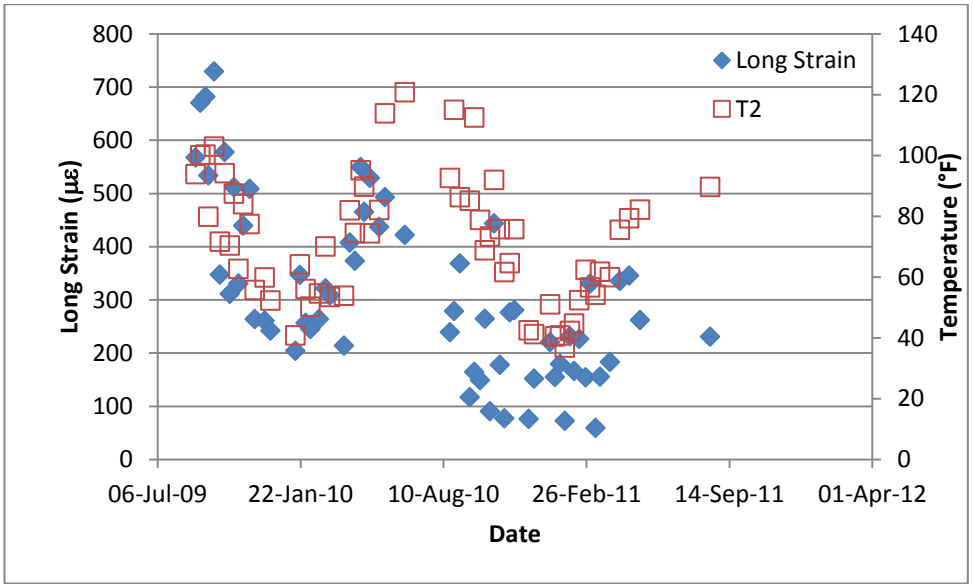

Figure 4.11: Strain and mid-depth temperature with time, N7.

Section S12, shown in Figure 4.12 with strain and mid-depth temperature plotted against time, also exhibited similar reductions in strain values despite exhibiting elastic behavior, although not as pronounced as sections N7 and N9. Gauge 11, centered along the OWP, did not survive construction, and therefore was not functioning at any point in time during the test cycle. After 5/20/2010 the other gauge centered along the OWP, gauge 2, also stopped working. The remaining longitudinal gauges did not function consistently for the remainder of the test cycle. As a result, a cut-off date of 5/20/2010 was used such that data collected after that date was excluded from analysis.

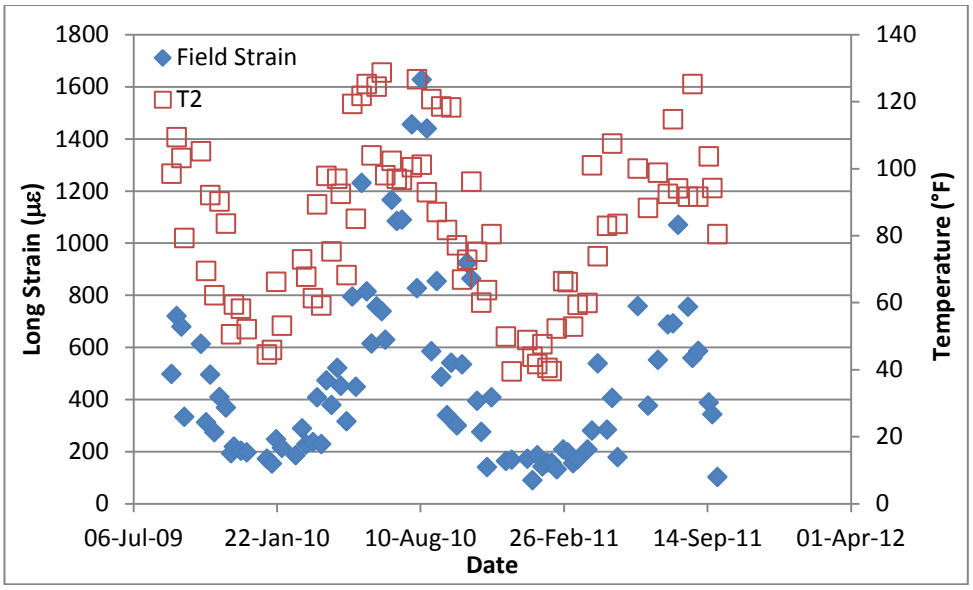

Figure 4.12: Strain and mid-depth temperature with time, S12.

Lastly, section N10 also had what appeared to be erratic strain data when strain and mid-depth temperature were plotted over time, shown in Figure 4.13. Upon further investigation, only two strain gauges functioned after 6/17/2010, and as evident by the plot below, they only functioned three dates for the remainder of the test cycle. Nor were these gauges working at the same time after 6/17/2010. Therefore, 6/17/2010 was used as the cut-off date for section N10 to accurately represent maximum longitudinal strain. Table 4.2 summarizes the cut-off dates through which strain measurements were utilized for this investigation.

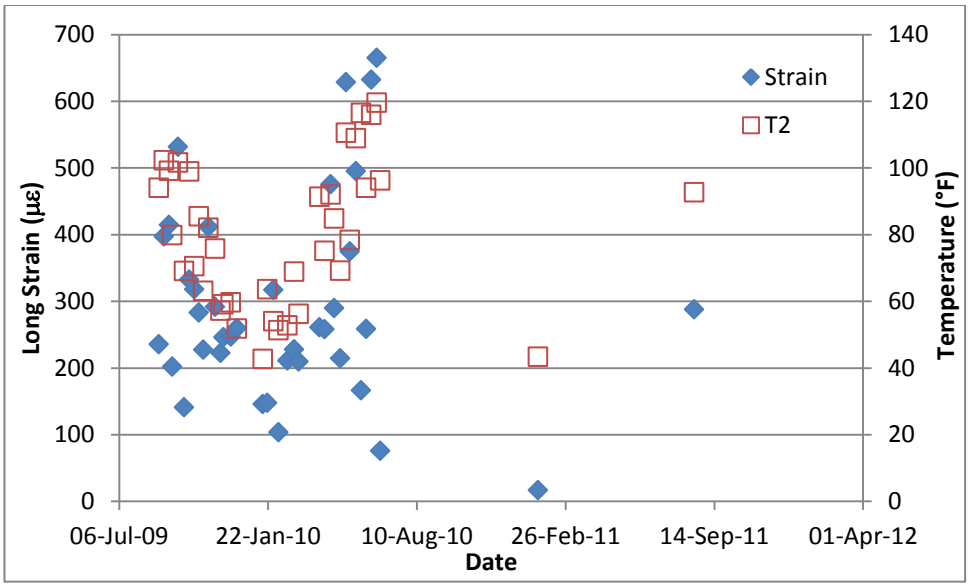

Figure 4.13: Strain and mid-depth temperature with time, N10.

Table 4.2: Summary of cut-off dates for strain

Year	Section	Cut-off date
2006	N1	4/4/2007
2006	N2	4/19/2007
2006	N8	4/24/2008
2006	N9	N/A
2009	N5	N/A
2009	N6	N/A
2009	N7	4/21/2010
2009	N9	6/3/2010
2009	N10	6/17/2010
2009	N11	N/A
2009	S9	N/A
2009	S10	N/A
2009	S11	N/A
2009	S12	5/20/2010

4.5 MODULUS-STRAIN RELATIONSHIP

A LEA program, WESLEA version 3.0, was utilized to develop modulus-strain relationships for each of the four sections from the 2006 structural study and the ten sections from the 2009 structural study. Due to the limited number of layers (5) that can

be simulated in WESLEA the AC layers were simulated as composite AC layers. WESLEA was utilized to predict tensile strain at the bottom of the AC layer for the known in-place properties of each cross-section and loading. Although the in-place moduli of the AC layers were not known, they were manually input into WESLEA and then varied across a wide range to develop modulus-strain relationships.

4.5.1 Structure

Simulations were completed such that the AC layer was atop a granular base material on top of a subgrade material. The composite AC modulus was varied to determine the relationship between AC modulus and resulting tensile strains at the bottom of the AC layer. The surveyed lift thicknesses for the composite AC layers, listed in Table 3.3, were used in conjunction with the varied AC moduli. The surveyed lift thicknesses for each individual AC lift are listed in Appendix A. For the granular base layer and subgrade layers, the surveyed lift thickness and backcalculated modulus specific to each section from Tables 3.3 and 3.4 were used. A Poisson's ratio of 0.35, 0.4 and 0.45 were assumed for the AC, base and subgrade materials, respectively.

4.5.2 Loading

To simulate the single axles at the Test Track, a single axle was selected for the WESLEA evaluation. For each tire, the load was specified at 5,250 lb with a tire pressure of 100 psi. This was consistent with the average of the single axles at the Test Track (21,000 lb).

4.5.3 Evaluation

Tensile strain was predicted at two locations at the bottom of the AC layer. The first was directly below the center of the outside tire. The second location was 6.75 inches away from the center of the tire, which represents the center space between the two tires in a single axle. The maximum strain was selected from these two locations in the longitudinal (y-direction) direction.

4.5.4 Slip Condition

To determine the appropriate slip condition to utilize for this investigation, a minimum of four slip conditions were evaluated, as illustrated in Figure 4.14. In WESLEA, a bonded condition is selected by using the number "1" and alternatively, a slipped condition is simulated by using the number "0". A full-bond condition was evaluated such that all of the AC layers were combined into one layer which therefore assumes a full bond between those individual layers. Additionally, the interface between the dense graded aggregate base (DGAB) and the AC layers was simulated as a fully bonded interface as was the interface between the DGAB and subgrade layers. In addition to the full bond condition shown, another full bond condition was simulated such that all of the AC layers were fully bonded, as shown in slip condition 1. The interface between AC layers and DGAB, and DGAB and subgrade layers, however, were considered to be in a slipped condition. Full and partial slip conditions were simulated by considering each AC lift to be identical with the same modulus input for each and using the surveyed lift thicknesses for each AC lift. Each interface between the AC layers and between the DGAB and AC, and DGAB and subgrade were assigned "0" for slip. For those sections that had more than 3 AC lifts, a "full slip" condition could not be simulated. However,

additional partial slip conditions were simulated to combine the AC lifts to create every possible combination.

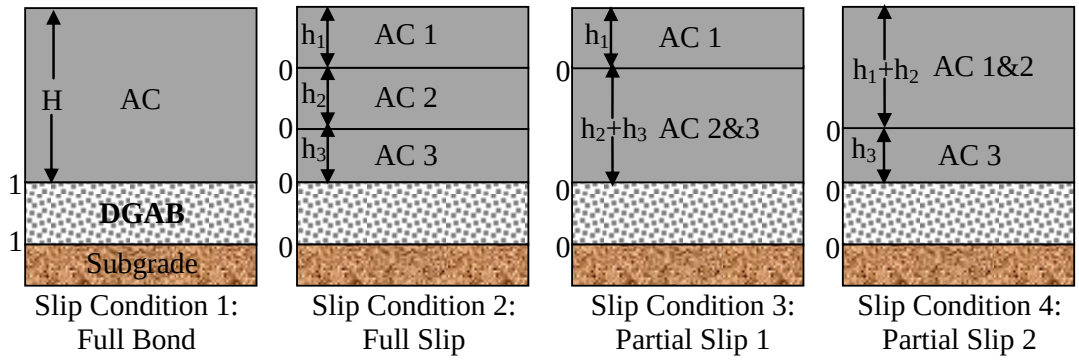

Figure 4.14: Slip conditions investigated.

4.5.5 Modulus-strain Relationship

As mentioned previously, the modulus for the AC layer(s) was varied while keeping the DGAB and subgrade moduli constant at their respective backcalculated modulus values. The ranges of AC moduli were selected to achieve predicted tensile strains that were within the range of the maximum and minimum peak strain measured in the field for each section. An example of the modulus-strain relationships that were developed for each section is shown in Figure 4.15 for section S9 in a full bond (slip condition 1) scenario. A power model was fitted to each curve and as shown in Figure 4.15 this form of the equation (Equation 4.1) fit the relationship very well with all of the 14 sections having a coefficient of determination, R^2, of 0.96 or higher.

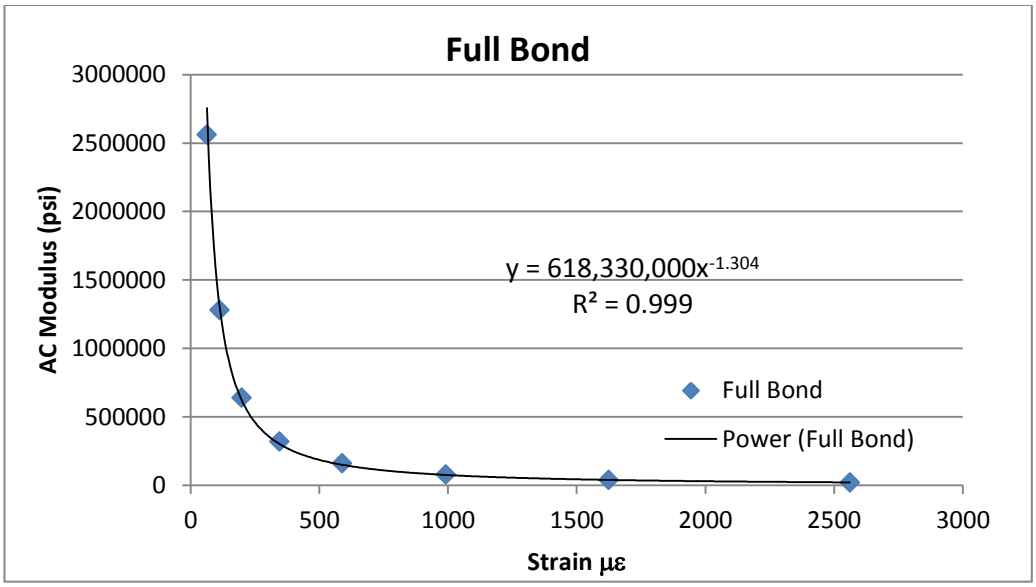

Figure 4.15: Modulus-strain relationship, S9, full bond condition.

$$E_{comp} = c\varepsilon^{d} \quad (4.1)$$

where:

E_{comp} = composite AC modulus (psi)

c,d = regression terms

ε = tensile strain at the bottom of the AC layer, με

To determine the appropriate slip condition to use for this investigation, the relationships that were developed for each condition were applied to the peak strain measured in the field to estimate the required composite modulus. For comparison, the backcalculated AC moduli (averaged for the three replicate drops for FWD testing) at the 9-kip load level were plotted with the estimated composite AC moduli from the developed relationships against mid-depth pavement temperature. Figure 4.16 is a plot developed for section S9 for the fully bonded condition and the additional full bond scenario with simulated slipped interfaces at the unbound layers ("E Full Bond_a"). Figure 4.17 is also for section S9, displaying the full slip and partial slip simulations.

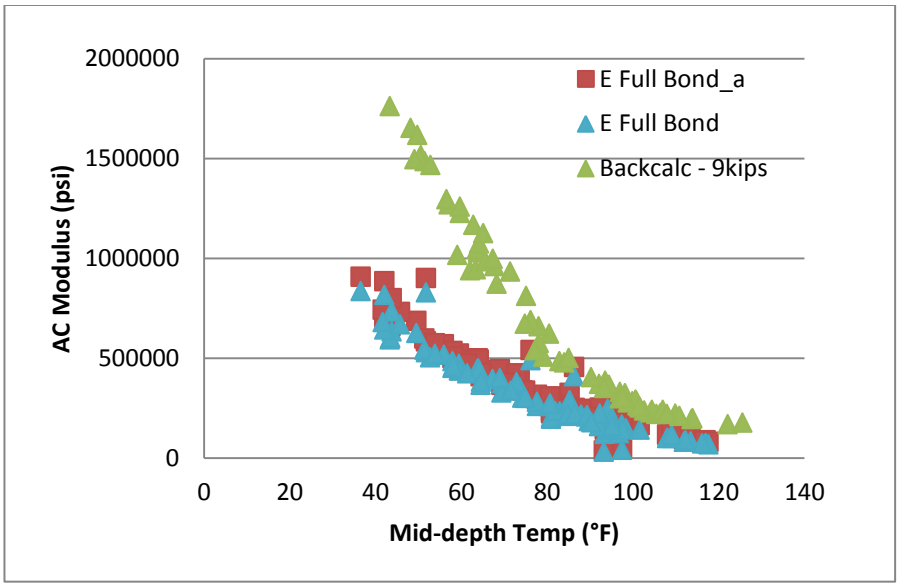

Figure 4.16: AC moduli for full bond condition, S9.

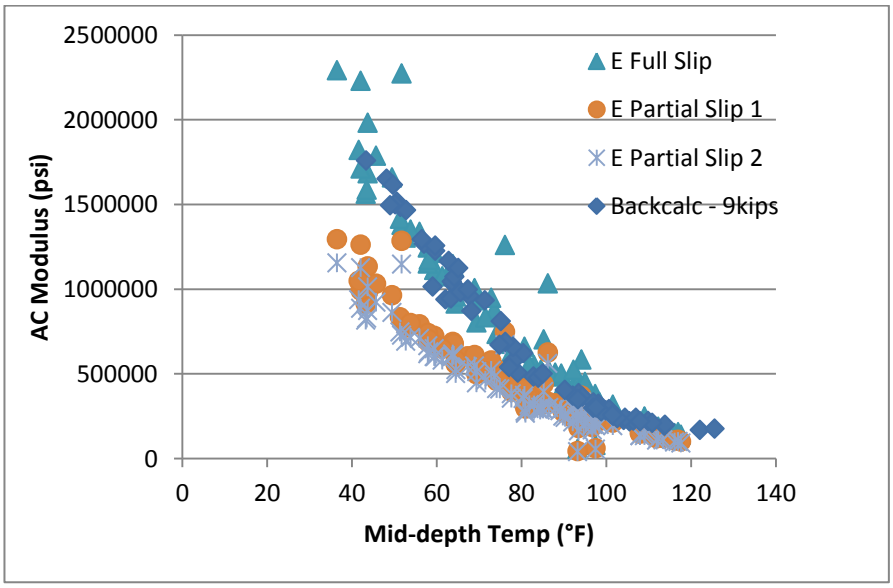

Figure 4.17: AC moduli for slip and partial slip conditions, S9.

It is interesting to note that in Figure 4.17, the backcalculated AC moduli tend to align very well with the AC moduli estimated by the full slip relationships calculated for measured peak strain. When these two series are plotted by themselves in Figure 4.18 with the tensile strain used to calculate AC moduli on the secondary axis, it is evident that the relationship for a fully slipped cross-section best matches the backcalculated

moduli in section S9. Although this was also the case for other sections (N6, N7, N11 and S12) it was not consistent for all of the fourteen sections in this investigation. This was unexpected as this would suggest that de-bonding occurred within the cross-section. However, all of these sections performed very well with no observed distresses, little-to-moderate rutting and low IRI values, as shown in Table 4.1. Additionally, trenching of section N6 (Thiopave) following the completion of the 2009 structural study revealed that debonding had not occurred in the cross-section. Therefore, backcalculated moduli may not be the best parameter to characterize the AC layers, as FWD testing is completed with an impact load rather than a dynamic load that more closely simulates a truck traveling at highway speeds. In fact, research at the Test Track has shown that the impact load applied during FWD testing is more representative of a truck traveling at 120 mph (Leiva-Villacorta 2012). The goal of this dissertation was to create a model that could be used to improve tensile strain predictions, particularly from a design standpoint, therefore to meet that goal it makes sense to select the fully bonded condition as this is likely the scenario that would be selected for design. The final model will then be calibrated to the moduli determined through a LEA for a fully bonded cross-section. The regression coefficients for each section in a fully-bonded condition are listed in Table 4.3.

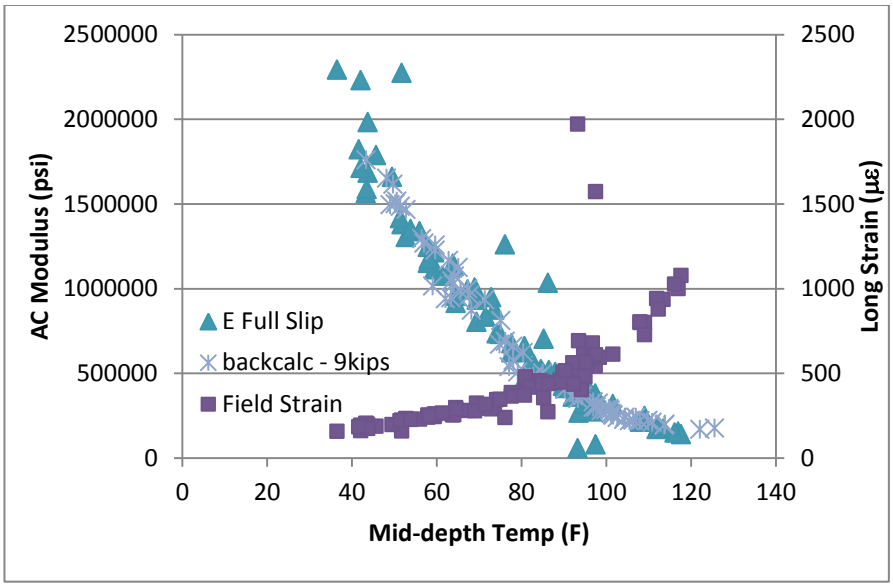

Figure 4.18: Backcalculated AC moduli and AC moduli for full-slip condition, S9.

Table 4.3: Coefficients for modulus-strain relationships in a full-bond condition

Year	Section	c	d	R^2
2006	N1	6.37E+08	-1.389	0.96
2006	N2	1.5E+09	-1.511	0.97
2006	N8	2.7E+08	-1.256	0.99
2006	N9	9.9E+07	-1.213	0.99
2009	N5	3E+08	-1.257	0.99
2009	N6	7.52E+08	-1.376	0.97
2009	N7	1E+09	-1.302	0.99
2009	N9	7.8E+07	-1.184	0.99
2009	N10	3.43E+08	-1.245	0.99
2009	N11	5.29E+08	-1.316	0.99
2009	S9	6.18E+08	-1.304	0.99
2009	S10	5.89E+08	-1.281	0.99
2009	S11	5.54E+08	-1.270	0.99
2009	S12	5.95E+08	-1.277	0.99

4.6 SUMMARY

This chapter documented the steps necessary to develop modulus-strain relationships for use in developing a model to estimate the in-place modulus required to achieve tensile strains measured at the bottom of the AC layers, thereby improving the predictions of

tensile strains when used in a LEA program. To develop modulus-strain relationships for each section, strains were selected from undamaged sections and were representative of maximum tensile elastic strains. Strains associated with damage were identified through the use of crack maps, rut depth and IRI measurements made weekly during the 2006 and 2009 structural studies. Non-elastic strains were identified by deviation from observed temperature-strain trends and through large variations of strain measurements identified by the difference between the maximum and 95^{th} percentile strain values. Modulus-strain relationships were developed through the use of WESLEA, a LEA program using the backcalculated moduli for the unbound layers and by varying the composite AC modulus to predict tensile strain at the bottom of the AC layer for a variety of AC moduli. Several slip conditions were investigated using the measured strain to estimate the required composite modulus from the developed relationships. From this investigation, it was elected to use the modulus-strain relationships for the fully bonded condition. Therefore, the model for in-place AC modulus will be calibrated to field strains using a LEA program in a fully bonded condition.

CHAPTER 5

FIELD-CALIBRATED MASTER CURVES

5.1 INTRODUCTION

The objective of this dissertation was to develop a method to improve the prediction of tensile strains at the bottom of the AC layers for use in pavement design. To meet this objective, a model that estimates the in-place composite modulus of the AC layer as a function of field conditions and known material properties was developed. The previous chapter discussed the development of modulus-strain relationships specific to each section. These relationships enable the prediction of in-place composite modulus required to achieve the induced strain measured in the field under single axle loadings at the NCAT Test Track. The developed relationships are only a function of measured strain. By varying the AC modulus over a wide range of moduli, the effects of temperature and speed were inherently considered. However, it is necessary to express the in-place composite AC modulus in terms of pavement temperature and vehicle speed. The next step in creating a model to estimate composite AC modulus for use in a LEA program was to select a form of the model and to relate the modulus to loading rate and temperature. It was decided to adapt the dynamic modulus master curve procedure discussed in Chapter 3 to field modulus (that has been calibrated to field strain) using loading rates and temperatures from the field.

5.2 MASTER CURVE CONSTRUCTION

Master curves were developed for estimating composite AC modulus based on the developed modulus-strain relationships discussed in Chapter 4. For each test section, the in-place composite moduli were calculated for each strain measurement using the modulus-strain relationships and coefficients listed in Table 4.2. The procedure outlined in AASHTO PP 61-09 for constructing dynamic modulus master curves, discussed in more detail in Chapter 3, was utilized for the development of field-calibrated master curves for the prediction of composite AC modulus for each section. However, rather than using loading rate (frequency in Hz) and temperatures as applied in dynamic modulus testing, it was elected to utilize loading rates and temperatures associated with the measured tensile strains (from which composite modulus was determined).

As discussed previously, pavement temperatures were measured from embedded temperature probes at various depths in the pavement structure and pavement temperatures were recorded at the time of strain data collection. Based on previous studies at the Test Track (Timm and Priest 2008), mid-depth pavement temperatures were utilized for use in the field-calibrated master curves. As discussed in Chapter 2, frequency is difficult if not impossible to measure in the field. Although loading time can be measured in the field, there is dissention on the most appropriate method of measuring time. Furthermore, measuring time from either stress or strain pulses requires the conversion of time to frequency, and at present, no research has been found to corroborate time-frequency relationships under field conditions. Therefore, the vehicle speed in mph was utilized for loading rate. As a result the equations for the field-

calibrated master curves were of the form of a sigmoidal fit function, as shown in Equations 5.1 and 5.2.

Just as is done in the MasterSolver spreadsheet (Bonaquist 2009) and AASHTO PP 61-09, the Arrhenius shift factor was utilized. A reference temperature of 22°C, consistent with the reference temperatures used to construct both the |E*| and |G*| master curves was used. As applied here, the activation energy represents the activation energy of the composite AC layer, $\Delta E_{a,comp}$. However, it was used to shift vehicle speed rather than loading frequency, as shown in Equation 5.2. In addition to the Arrhenius shift factor being used, the regression terms, β_{comp}, γ_{comp} and log $E_{comp,min}$, were also determined using non-linear optimization as is done in the MasterSolver spreadsheet and recommended in AASHTO 61-09. The Generalized Reduced Gradient (GRG) non-linear method was used in Excel solver to complete the non-linear optimization with the solver options identical to those used in MasterSolver as it also relies on Excel Solver. Rather than continuing to alter the fitting parameters to converge on a solution for each, the first set of solutions was utilized during the non-linear optimization. This is consistent with MasterSolver and if allowed to continue through several iterations the predictions worsen, in some cases resulting in a negative coefficient of determination. The initial values used for constructing |E*| master curves, as discussed in Chapter 3 were also utilized here for the field-calibrated master curves. Because the number of iterations that would be required to model all of the different AC lifts in each cross-section would be unmanageable and because the LEA program utilized for this analysis was limited to a maximum of 3 AC lifts, a composite modulus was determined. Therefore, the parameters utilized in developing the field-calibrated master curve must

also be composite parameters. The limiting maximum composite modulus shown in Equation 5.1 was determined just as in the AASHTO PP 61 procedure for limiting maximum dynamic modulus, utilizing the Hirsch model (Christensen et al. 2003) with a fixed |G*| value of 145,000 psi. However, the VMA and VFA used to calculate the limiting maximum composite modulus represent the VMA and VFA of the composite AC layer rather than VMA and VFA for one AC mixture.

$$\log(E_{comp}) = \log E_{comp,min} + \frac{\log E_{comp,max} - \log E_{comp,min}}{1+e^{\beta_{comp}+\gamma_{comp}(\log v_r)}} \quad (5.1)$$

where:

E_{comp} = composite modulus (ksi)

$E_{comp,min}$ = limiting minimum composite modulus (ksi)

β_{comp}, γ_{comp} = fitting parameters

$E_{comp,max}$ = limiting maximum composite modulus (ksi), see Equation 3.9

$$\log(v_r) = \log(v) + \log[a(T)] \quad (5.2)$$

where:

v_r = reduced vehicle speed (mph)

v = vehicle speed (mph)

log [$a(T)$] = Arrhenius shift factor, see Equation 3.10

5.2.1 Calculated Speed

Traffic at the NCAT Test Track operates at a target vehicle speed of 45 mph. However, the heavy triple-trailer trucks are manually operated, therefore, the speed is somewhat variable. During the 2009 structural study, vehicle speed was automatically calculated during the processing of the raw strain traces to determine the actual vehicle speed

associated to measured strain values. The vehicle speed was calculated by determining the change in time between when a given axle passed the first pressure plate (on top of the base material, gauge 13 in Figure 3.6) and when that same axle passed the second pressure plate (on top of the subgrade material, gauge 14 in Figure 3.6). Figure 5.1 illustrates time, t_1 and t_2, at which the steer axle passes over gauge 13 and gauge 14, respectively. The distance between these two pressure plates was known, allowing for the velocity to be determined by taking the ratio of distance to change in time and converting ft/sec to mph. Although the calculated vehicle speeds associated with the measured tensile strains ranged between 33 and 62 mph, the majority (95.8%) of the vehicle speeds were between 42 and 52 mph for all of the ten sections combined, shown in Figure 5.2.

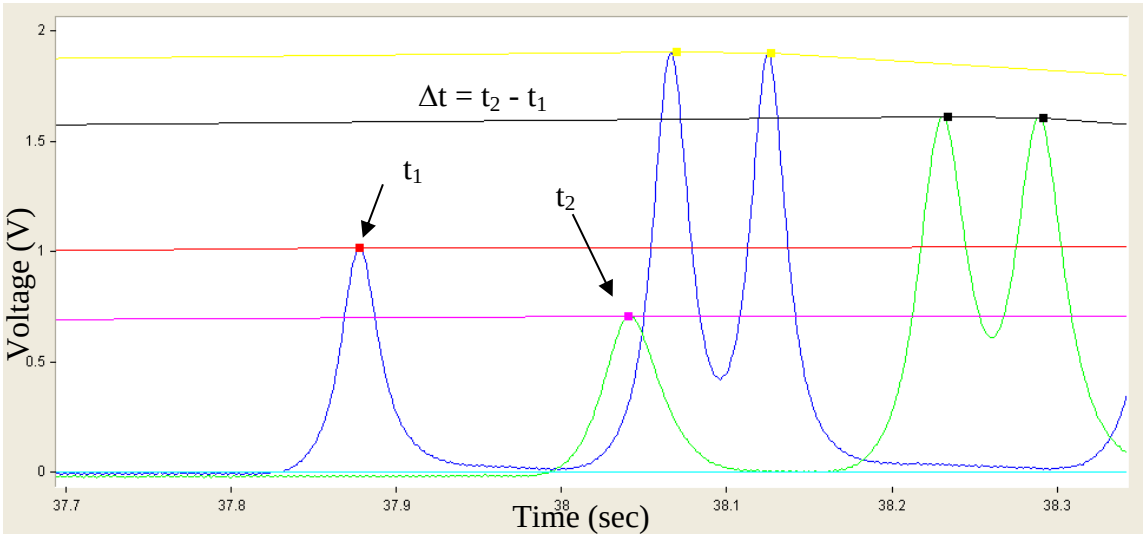

Figure 5.1: Time between steer axle at pressure plate 13 and pressure plate 14.

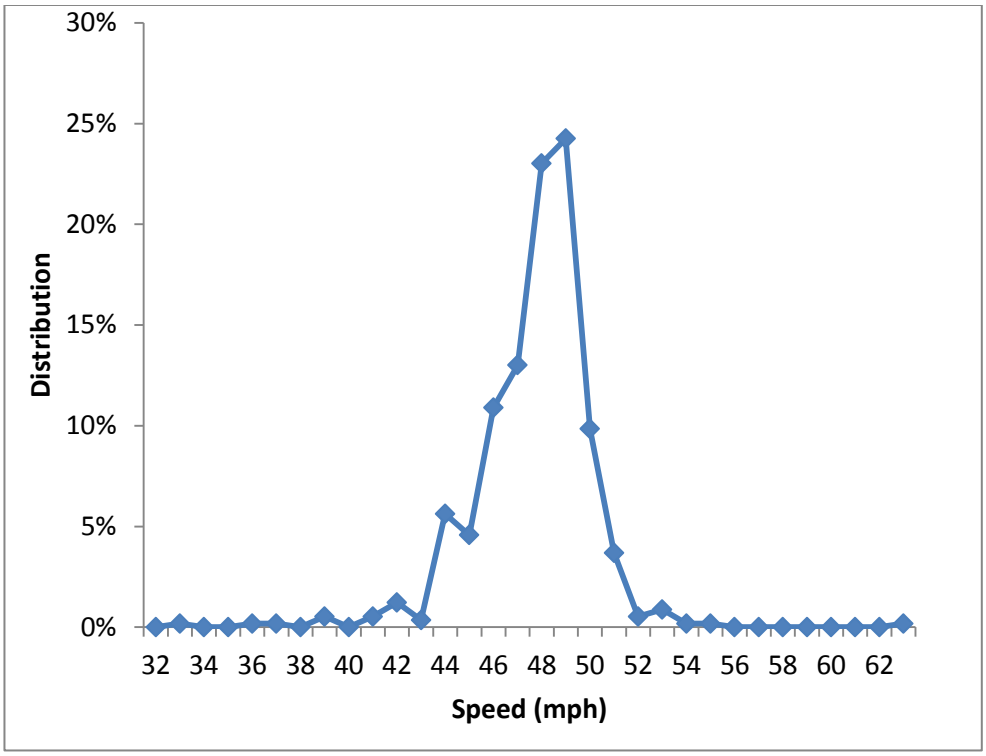

Figure 5.2: Distribution of speed for 2009 test sections.

Vehicle speed was not automatically calculated as part of data processing during the 2006 structural study. The post-processing required to determine the vehicle speed associated to every strain measurement would be extremely time-consuming. Therefore, ten representative strain values were selected for each section that covered the entire range of mid-depth pavement temperatures. Speed was then manually calculated for each of the ten strain values selected in each section. Ten strain values correspond to ten moduli for each section. This is consistent with the number of moduli required for constructing a dynamic modulus master curve following AASHTO PP 61-09. The vehicle speed was then manually calculated for each of the ten peak strain values using the strain trace for the entire truck. The distance between the steer axle and the front tandem axle, as shown in Table 3.2 is 13.6 feet for all of the trucks operated at the NCAT Test Track. Therefore, by selecting the times associated to the peak strain under

the steer axle and front tandem axle from the raw strain trace, the vehicle speed was determined by dividing 13.6 ft by the change in time and converting to mph. Due to the selection of ten strain values, the range of vehicle speeds was much narrower than that measured in the 2009 sections.

5.2.2 Composite Parameters

There are several methods that could be employed to combine the parameters of several lifts into parameters of one composite layer. For this study, three transformation methods were investigated: geometric mean, weighted average and the method used to determine the blended aggregate specific gravity (G_{sb}), shown in Equations 5.3, 5.4, and 5.5, respectively. For the percentage of the composite layer of each lift required in Equation 5.5, the ratio of lift thickness to total AC thickness (h_i/H), multiplied by 100, was used.

$$X = \sqrt[n]{X_1 \times X_2 \times ... \times X_n} \tag{5.3}$$

where:

X = composite parameter

X_i = parameter for ith lift

n = number of lifts

$$X = \frac{h_1}{H}X_1 + \frac{h_2}{H}X_2 + \cdots + \frac{h_n}{H}X_n \tag{5.4}$$

where:

h_i = the thickness of ith lift

H = total thickness of the n lifts

$$X = \frac{P_1 + P_2 + \cdots + P_n}{\frac{P_1}{X_1} + \frac{P_2}{X_2} + \cdots + \frac{P_n}{X_n}} \tag{5.5}$$

where:

P_i = Percentage of i^{th} lift of the composite layer

To determine which method was appropriate, ten strain values were selected for the control section from the 2009 structural study, section S9. These ten strain values were selected such that they were measured at mid-depth pavement temperatures similar to the temperatures at which |E*| testing is conducted following AASHTO TP 79-09: 4, 20, 45°C. The coefficients for modulus-strain relationship for S9 were then applied to the measured strains to estimate the in-place composite moduli. The mid-depth pavement temperatures, calculated vehicle speed and moduli are listed in Table 5.1. Equations 5.3-5.5 were then utilized to calculate composite VMA and VFA from in-place VMA and VFA of each AC lift in S9. The thicknesses from each lift and corresponding in-place VMA and VFA (calculated from the known density at construction, as discussed in Chapter 3) are listed in Table 5.2. Finally, the resulting composite VMA and VFA from each of the three transformation methods described above are listed in Table 5.3. Evident from Table 5.3, the resulting composite VMA and VFA are not drastically different from one another, with the largest differences between the geometric mean and the method for determining blended G_{sb}.

Table 5.1: Field-calibrated master curve inputs for S9 trial

Mid-Depth Temp (°C)	Vehicle Speed (mph)	Composite Modulus (ksi)
5.35	45.4	680.1
5.57	46.5	643.4
5.58	44.0	815.6
19.6	51.8	395.3
20.53	48.7	399.8
20.77	47.3	327.1
44.4	45.7	81.6
44.59	44.2	89.2
45.23	40.5	82.3
46.73	43.7	73.0

Table 5.2: In-place VMA and VFA for each lift, S9

Lift	Lift Thickness (in)	Total AC Thickness (in)	VMA (%)	VFA (%)
1	1.128	6.828	19.63	61.54
2	2.724	6.828	16.72	52.35
3	2.976	6.828	17.14	55.58

Table 5.3: Composite VMA and VFA, S9

Method	Composite VMA (%)	Composite VFA (%)
Geometric Mean	17.78	56.36
Weighted Avg.	17.38	55.27
Method for blended G_{sb}	17.33	55.10

Following the procedure described above and the adapted equations shown in Equations 5.1 and 5.2, three field master curves were constructed, one for each transformation method, using the inputs listed in Table 5.1. The resulting fitting parameters and fit statistics for each field-calibrated master curve are listed in Table 5.4. The composite VMA and VFA in Table 5.3 were input directly into Equation 3.9 to determine the limiting maximum composite modulus. As seen in Table 5.4, the largest $E_{comp,max}$ is due to the method for determining blended Gsb, which corresponds to the lowest composite VMA and VFA evaluated. Overall, the method for determining

blended G_{sb} proved to have the best fit, resulting in the highest R^2, albeit a very small increase over the other two transformation methods, and the lowest S_e/S_y ratio, where R^2 and S_e were calculated following Equations 5.6 and 5.7 respectively. S_y represents the standard deviation (sample) of the measured values and low S_e/S_y ratios indicate a good fit.

$$R^2 = 1 - \frac{\sum_i^n (E_{mi} - E_{pi})^2}{\sum_i^n (E_{mi} - E_{mavg})^2} \quad (5.6)$$

where:

E_{mi} = i^{th} Measured E_{comp} (ksi)

E_{pi} = i^{th} Predicted E_{comp} (ksi)

E_{mavg} = Average measured E_{comp} (ksi)

$$S_e = \sqrt{\frac{SSE}{n-1}} \quad (5.7)$$

where:

S_e = standard error of the prediction

SSE = sum of squared error = $\sum(E_{mi}\text{-}E_{pi})^2$

n = number of samples

Table 5.4: Fitting parameters and fit statistics for field-calibrated master curve, S9

Method	$E_{comp,\ max}$ (ksi)	$E_{comp,\ min}$ (ksi)	β_{comp}	γ_{comp}	$\Delta E_{a,comp}$	R^2	S_e/S_y
Geo Mean	3131.41	0.9972	-0.5084	-0.2527	224937	0.9766	0.1082
Wt Avg	3144.13	1.0156	-0.5062	-0.2508	226021	0.9766	0.1083
Blended G_{sb}	3146.45	0.7071	-0.5580	-0.2559	214182	0.9769	0.1073

To further evaluate these transformation methods, field master curves were constructed using field measured strains for section S9, from a speed study conducted during the 2009 test cycle on the structural sections. It should be noted that this speed

study was a limited investigation conducted on only four test dates and for only the 2009 structural sections, therefore it was not broad enough to accommodate the scope of this dissertation. The speed study is applicable, however, in first, identifying the appropriate transformation method to determine parameters of the composite AC layers, and second, to validate the application of the field-calibrated master curves to speeds beyond the narrow range at which they were developed. The speed study was conducted on four different test dates throughout the course of the 2009 test cycle, to capture tensile strains at a variety of mid-depth pavement temperatures and vehicle speeds. On each test date four speeds were tested: 15, 25, 35 and 45 mph. For this evaluation, however, only the first three speeds were used, as the strains at 45 mph were already incorporated into this study. The previously developed modulus-strain relationship for S9 was then applied to the measured tensile strains that resulted from the speed study. Table 5.5 summarizes the strains, resulting composite modulus, mid-depth pavement temperatures and vehicle speeds generated by the speed study for section S9.

Table 5.5: Results from speed study and resulting composite moduli, S9

Date	Mid-depth Temp (°F)	Target Speed (mph)	Actual Speed (mph)	Peak strain (με)	Composite Modulus (ksi)
16-Dec-09	48.43	15	14.48	209.3	580.8
16-Dec-09	48.85	25	23.31	214.4	562.6
16-Dec-09	48.85	35	32.59	218.6	548.7
19-Feb-10	67.10	15	14.40	363.5	282.6
19-Feb-10	67.15	25	23.11	314.1	341.9
19-Feb-10	67.16	35	33.66	331.0	319.4
16-Apr-10	82.34	15	13.41	651.5	132.0
16-Apr-10	83.84	25	24.06	566.3	158.5
16-Apr-10	84.43	35	33.25	482.6	195.3
27-May-10	112.28	15	16.07	1079.0	68.4
27-May-10	112.80	25	24.49	1003.9	75.1
27-May-10	113.09	35	33.25	971.7	78.4

The fitting parameters listed in Table 5.4 were then applied to Equations 5.1 and 5.2 to predict composite moduli for the mid-depth pavement temperatures and vehicle speeds from the speed study, shown in Table 5.5, for each transformation method. In Figures 5.2 through 5.4 the predicted moduli for each transformation method were plotted against the composite "measured" moduli computed by the modulus-strain relationship for the corresponding tensile strains. For this evaluation, the composite moduli computed from the modulus-strain relationship were considered "measured" values as they are based on tensile strains measured in the field. As illustrated in the these figures, the master curves applied to speeds outside of the range for which they were developed predict the moduli very well, with the data following the line of equality in all three plots. Four groupings are seen on each plot that represent the four test dates and within these groups are the three different speeds tested. Certainly some testing variability exists and can account for some of the deviation of the moduli due to different speeds on a given date from the line of equality, but it appears that at the high and low ends of the spectrum, the modulus differences between speeds are relatively small, possibly indicating that the moduli is more temperature susceptible than time (speed) susceptible at extreme temperatures.

The coefficient of determination, R^2, was calculated following Equation 5.6 to quantify the ability of each master curve, based on the three transformation methods, to predict composite moduli for speeds much slower than those used to develop the master curves. The R^2 values for the master curve from the geometric mean, weighted average and method to blend G_{sb} were 0.9786, 0.9785 and 0.9775, respectively; confirming the excellent fits illustrated in Figures 5.3 to5.5. By attaching a linear trendline through the

origin, the magnitude that the master curves for each transformation method overpredict or underpredict the measured composite moduli can be quantified by the slope of the line. All three methods have slopes close to one with the geometric mean and weighted average methods overpredicting the measured composite moduli by about 0.8%, whereas the method for blended G_{sb} slightly underpredicts by approximately 0.5%.

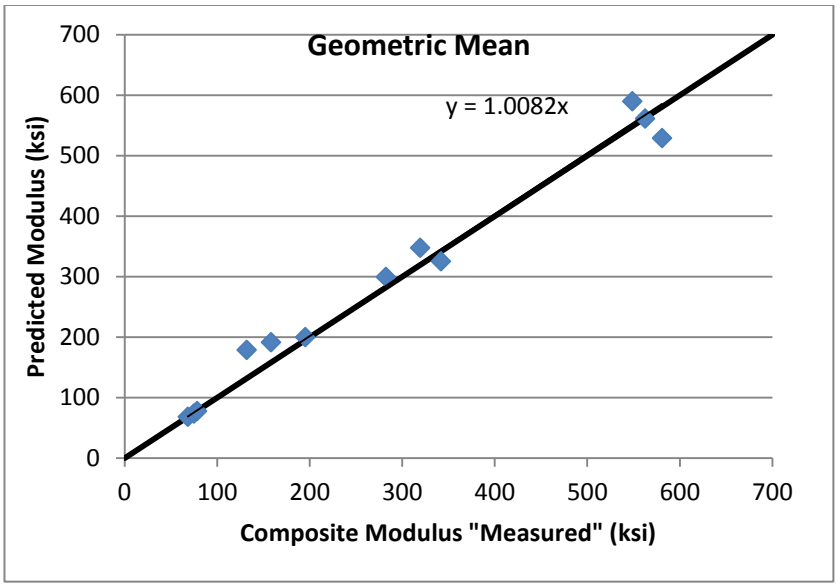

Figure 5.3: Comparison of composite moduli for geometric mean method, applied to speed study.

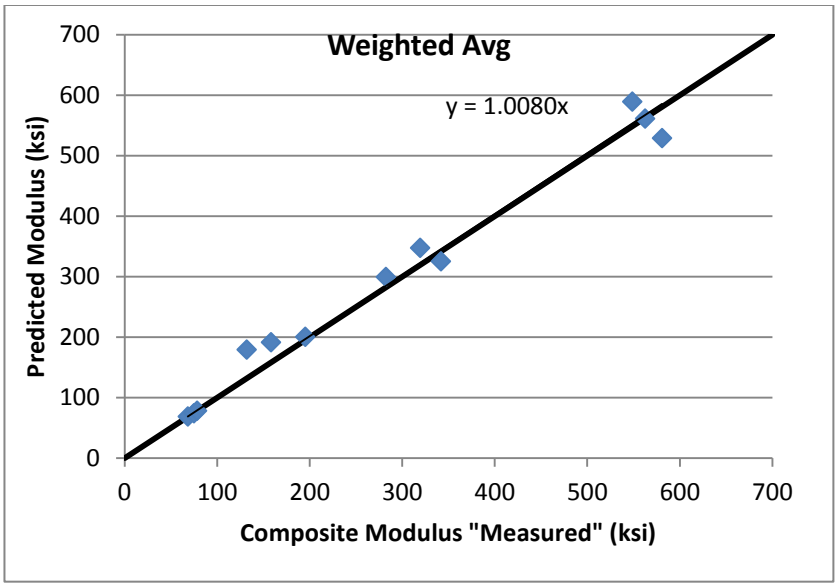

Figure 5.4: Comparison of composite moduli for weighted average method, applied to speed study.

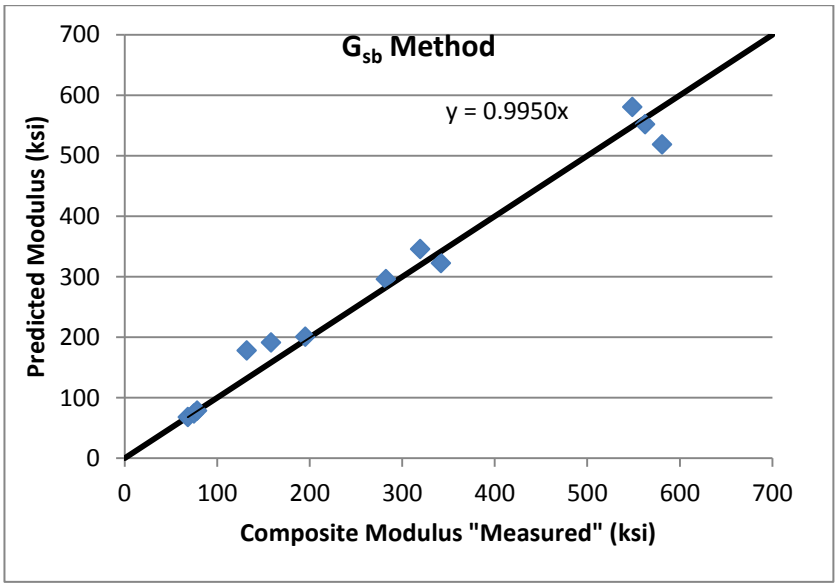

Figure 5.5: Comparison of composite moduli for method to blend G_{sb}, applied to speed study.

As a result of this evaluation, it is evident that the field-calibrated master curves can be applied to a wider range of speeds, particularly, speeds slower than the narrow range of intermediate speeds used for development. There seems to be little difference in

the performance of these master curves, indicating that any of the three transformation methods would be appropriate. It could be argued, however, that in the development of the master curves the third method, the method for blended G_{sb}, had the highest R^2 and also had the smallest deviation from the line of equality when applied to the speed study based on the slope of the linear trendline. Furthermore, this last method, the method that is used to determine the blended G_{sb} for aggregate is familiar to pavement designers. For these reasons, this method was selected for use in combining each necessary parameter (volumetrics and gravimetric properties, and fitting parameters for mix and binder master curves) from the individual AC lifts into composite parameters for the composite AC layer.

5.3 RESULTS

Field-calibrated master curves were constructed for each of the fourteen sections included in this study. The modulus-strain relationships that were developed and discussed in Chapter 4 were applied to all of the peak tensile strains measured in each section. Through non-linear optimization using Excel Solver, the resulting composite moduli, mid-depth pavement temperatures and calculated speeds associated to the measured peak strains were then used to determine the fitting parameters necessary for the master curve, described by Equations 5.1 and 5.2. The limiting maximum composite modulus was computed using VMA and VFA of the composite AC layer. To determine the composite VMA and VFA, the in-place VMA and VFA from each AC lift was combined following the same method that is used to determine the G_{sb} of blended aggregate, described by Equation 5.5.

The tensile strains used to compute composite moduli were associated to elastic behavior and undamaged sections. For the 2009 sections, all of the tensile strains deemed elastic and in an undamaged section were used for the development of each master curve and the cut-off dates identified in Chapter 4 for sections N7, N9 and S12 were applied. Although a cut-off date had been determined for section N10, the strain data did not always follow the temperature trends with strain values much lower than expected. The several methods discussed in Chapter 4 ruled out damage or non-elastic behavior in the remaining strain values and identified that the cause of the lower-than-expected strain was the lack of functioning gauges. This resulted in strains that were not representative of the maximum tensile strain induced in the section, simply because the gauge that would have recorded that strain was not functioning. Because many of the strain values did appear to follow the temperature trends, it was decided to hand select 10 strain values that followed the expected trend and that covered a wide range of mid-depth pavement temperatures to use for constructing the master curve. Similarly, as discussed earlier in this chapter, only 10 strain values were used for each section from the 2006 structural study due to the cumbersome and timely manual calculation of vehicle speeds. The 10 strain values were selected after the strain values associated to damage and non-elastic behavior had been removed from the database.

An example of a field-calibrated master curve for composite modulus is shown in Figure 5.5 for section N5(9-inch Thiopave). Field-calibrated master curves are shown in Appendix D for each section. The fitting parameters and fit statistics for the field-calibrated master curves are listed in Table 5.6 for all the sections. It should be noted that the values in Table 5.6 are for $E_{comp,max}$ and $E_{comp,min}$ in units of ksi. Overall, the

master curves fit the data very well. Only three of the fourteen sections had R^2 values less than 0.9. The field-calibrated master curves for each of these three sections, N1 (Florida, 2006), N9 from 2009 (Oklahoma) and N10 (High RAP), accounted for more than 82% of the variability in the data.

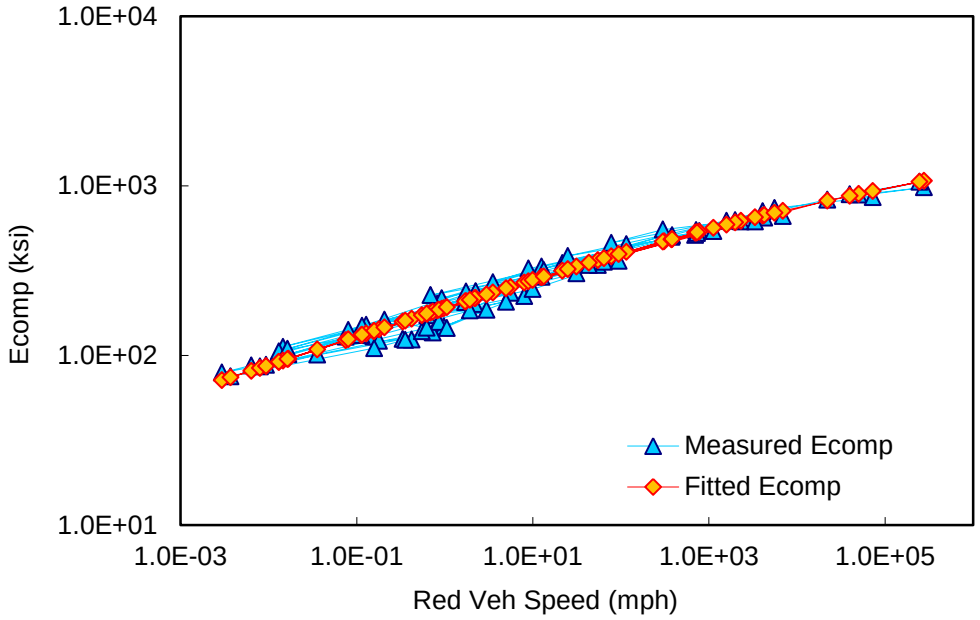

Figure 5.5: Field-calibrated master curve, N5.

Table 5.6: Summary of field master curve fitting parameters and fit statistics

Section	log $E_{comp\ max}$	log $E_{comp,\ min}$	β_{comp}	γ_{comp}	$\Delta E_{a\ comp}$	R^2	S_e/S_y
N1	3.502	0.079	-0.403	-0.217	292758	0.8246	0.4188
N2	3.511	0.722	0.110	-0.401	174524	0.9508	0.2218
N8	3.519	-0.897	-0.721	-0.248	261163	0.9293	0.2659
N9 (2006)	3.522	-0.069	-0.634	-0.210	314759	0.9546	0.2130
N5	3.497	0.776	-0.212	-0.250	285057	0.9823	0.1329
N6	3.497	0.400	-0.283	-0.199	311684	0.9566	0.2083
N7	3.502	0.511	-0.534	-0.251	228390	0.9143	0.2927
N9 (2009)	3.523	0.467	-0.711	-0.167	239440	0.8517	0.3851
N10	3.513	1.844	1.222	-0.283	318494	0.8699	0.3607
N11	3.509	0.259	-0.660	-0.182	251839	0.9599	0.1946
S9	3.498	0.044	-0.527	-0.237	242057	0.9106	0.2990
S10	3.499	0.664	-0.458	-0.225	291183	0.9338	0.2573
S11	3.497	1.817	0.528	-0.259	383847	0.9571	0.2072
S12	3.518	0.317	-0.595	-0.210	274946	0.9561	0.2094

5.4 SUMMARY

This chapter documented the steps taken to construct master curves, calibrated to field measured tensile strains through the use of the modulus-strain relationships created in Chapter 4 of this dissertation. The same process described for constructing dynamic modulus master curves was used to construct field-calibrated master curves for composite modulus with the adaption of vehicle speed in mph replacing loading frequency in Hz. The temperatures used in the creation of the field-calibrated master curves were the mid-depth pavement temperatures recorded at the time of tensile strain measurements. To follow this procedure for master curve construction, the limiting maximum composite modulus was determined by the Hirsch model with a fixed |G*| term, as is described in the AASHTO PP 61-09 and MasterSolver spreadsheet. One important difference however was the use of VMA and VFA for the composite AC layer rather than VMA and VFA from |E*| specimens.

An evaluation was completed to determine the most appropriate method to transform the values for a specific parameter associated with each lift into a singular parameter representative of a composite AC layer. Despite little difference among the fit of each master curve developed using three different transformation methods, the method used to determine G_{sb} for blended aggregate was selected. It was selected for its common use in pavement design, its slightly higher R^2 value in constructing the master curve and it had the smallest deviation from the line of equality when applied to a 2009 speed study. The evaluation of the transformation methods also showed that the field-calibrated master curve for section S9 predicted composite moduli very well when applied to speeds of 15-35 mph, which were outside of the range used for construction

of the master curves. Field-calibrated master curves were constructed for each of the fourteen test sections included in this investigation. Overall the developed master curves fit the data very well, allowing for the estimate of composite modulus specific to a test section, at a given mid-depth pavement temperature and vehicle speed.

CHAPTER 6

MODEL DEVELOPMENT AND PERFORMANCE

6.1 INTRODUCTION

Once the field-calibrated master curves had been constructed for each test section using known field conditions (vehicle speed and pavement temperature), the next step was to relate the master curves to known in-place material properties and laboratory-derived properties. This provides a model that allows for the prediction of the composite modulus for any cross-section and given vehicle speeds and mid-depth pavement temperature. Because the composite modulus was computed based on the measured tensile strain in the field using a LEA program that incorporated layer thickness and unbound layer moduli specific to each section, this developed model should improve tensile strain predictions when used in conjunction with a LEA program. The field-calibrated master curves are of the form of a sigmoidal fit function, shown in Equations 5.1 and 5.2. There are five fitting parameters that help define the shape of the master curve. One of the five is the limiting maximum composite modulus, which defines the upper boundary or asymptote for the curve. As discussed in Chapter 5, this was calculated as it is done for dynamic modulus, by using the known VMA and VFA of the mix, or rather here, the composite VMA and VFA for the asphalt concrete cross-section. The composite VMA and VFA were then entered into the Hirsch model, modified to

estimate the maximum modulus by fixing the dynamic shear modulus at the commonly accepted value for glassy modulus, 1 GPa or 145,000 psi. The other four fitting parameters were determined by non-linear optimization. To relate the composite modulus to known in-place material properties and known mix and binder properties determined in the laboratory, a model was created for each of these four fitting terms, Log $E_{comp,min}$, β_{comp}, γ_{comp}, and $\Delta E_{a,comp}$ as a function of these known properties.

Originally, the goal was to divide the dataset into calibration and validation datasets, such that the models would be developed from the calibration dataset and tested on the validation dataset. However, due to the lack of |E*| testing and other limitations, the number of available test sections was limited to fourteen. Although the fitting parameters that were determined in Chapter 5 were developed from hundreds of strain measurements, only fourteen values were determined for each fitting parameter. This is a relatively small number on which to calibrate and validate the models. A best effort was put forth to calibrate and validate on this limited data set by varying the number of test sections used to calibrate (8-12) and those left for validation (2-6), selected at random. It was found that when these models were applied to the small validation dataset the models performed very well for some and very poorly for others. These fourteen sections included a wide variety of mixtures and technologies, therefore applying models that had been developed for very unique technologies (i.e. WMA with foam, WMA with additive, and sulfur-modified WMA, etc.) to other very unique technologies was inappropriate (i.e. RAP, RAP and WMA, high polymer, etc.). Rather, it was decided to utilize all fourteen sections since they represented a very robust set of

mixtures and technologies for calibration only. Future research should focus on the validation of the models calibrated here.

6.2 PARAMETER SELECTION

Prior to developing the models for each of the four fitting parameters, parameters to represent mixture and binder properties and the in-place material properties of the composite AC layer first had to be selected. A wide variety of parameters were selected to determine the most significant parameters to be used in the models, shown in Tables 6.1 through 6.4, although not all of the parameters selected were used in the models.

Several in-place material properties of the composite AC layer were considered for use in the models, listed in Table 6.1 for each section. The in-place material properties included volumetrics utilized for design, common Superpave parameters and a gravimetric property. In-place volumetrics representative of the composite AC layer that were considered included air voids (V_a) and volume of effective binder (V_{be}), taken as the difference between in-place VMA and in-place V_a. These volumetrics, although representative of a singular mixture, are also utilized in the Witczak predictive equations (Andrei et al. 1999, Bari and Witczak 2006); although, the capability of these equations has been shown to be limited, these predictive equations suggest that there is a strong influence of these volumetrics on dynamic modulus and thus is applicable to the composite modulus. Dust proportion (DP) is a requirement of Superpave design, and as described in Chapter 3, is the ratio of dust (percent passing the #200 sieve) to percent of effective binder content. Based on several studies (Bonnaure et al. 1977, Huang et al. 2008, Flintsch et al. 2007) that found binder content influenced dynamic modulus, percent binder by weight (P_b) was also included in the pool of possible parameters.

Additionally, the maximum specific gravity of the mix (G_{mm}) was considered. A range of gradation parameters representative of the composite AC layer was also selected, shown in Table 6.2, percent by weight passing the 3/8" sieve, and the numbers 4, 8, 16 and 200 sieves ($\rho_{3/8}$, ρ_4, ρ_8, ρ_{16}, ρ_{200}) were considered, to account for the differences in gradation of the mixtures.

Table 6.1: Volumetric and gravimetric properties of composite AC layer

Section	V_a (%)	V_{be} (%)	DP	P_b (%)	G_{mm}
N1	6.90	10.02	1.57	4.67	2.526
N2	5.27	10.38	1.49	4.71	2.521
N8	5.41	8.07	2.23	5.06	2.461
N9 (2006)	6.04	7.85	2.27	4.95	2.468
N5	6.19	12.48	0.91	5.88	2.531
N6	6.17	12.52	0.88	5.93	2.527
N7	7.02	9.94	1.15	4.79	2.535
N9 (2009)	6.01	7.73	2.28	4.88	2.472
N10	6.06	9.56	1.29	4.78	2.525
N11	6.43	9.83	1.23	4.88	2.523
S9	7.74	9.52	1.25	4.75	2.533
S10	7.31	9.94	1.24	4.92	2.536
S11	7.33	10.34	1.17	5.11	2.520
S12	4.80	11.14	1.06	5.07	2.518

Table 6.2: Aggregate gradation properties for composite AC layer

Section	$\rho_{3/8}$ (%)	ρ_4 (%)	ρ_8 (%)	ρ_{16} (%)	ρ_{200} (%)
N1	78.98	56.71	46.68	37.39	6.86
N2	79.75	58.23	47.59	38.41	6.69
N8	78.76	51.67	35.15	25.51	8.04
N9 (2006)	79.68	54.91	37.40	27.05	7.92
N5	75.30	58.08	46.28	36.20	4.95
N6	77.29	58.60	46.63	36.58	5.02
N7	75.55	58.26	47.41	37.79	5.04
N9 (2009)	79.66	55.86	38.18	27.45	7.79
N10	82.99	58.72	46.80	38.22	5.48
N11	80.06	58.20	46.51	38.57	5.34
S9	79.61	59.45	48.16	38.66	5.31
S10	81.38	61.76	49.48	39.88	5.43
S11	84.24	64.91	51.51	40.70	5.31
S12	79.05	61.75	48.49	38.19	4.94

As discussed in the literature review of this dissertation, it has been found that |E*| alone cannot accurately predict tensile strains in the field. However, |E*| is an important parameter, required by M-E design frameworks, and it describes the unique viscoelastic behavior of each AC mixture. Furthermore, it is believed that the errors in predicting tensile strain are due in part to the time-frequency relationship that must be used to apply |E*| values. Thus, the fitting parameters of each AC master curve were used in the model development, rather than one or more |E*| at a given frequency and temperature. These fitting parameters should be unique to the mixture and when combined with temperature and loading rates, account for the viscoelastic properties of the mixture without relying on a frequency-to-time and ultimately, speed conversion. The transformation method discussed in Chapter 5 was applied to the fitting parameters of each mixture in the cross-section. The dynamic modulus master curve fitting parameters for the composite AC layer are listed below in Table 6.3 for each section. Log $|E^*|_{max}$ was for calculated from the modified Hirsch model using VMA and VFA of the |E*| specimens for each mixture tested while the remaining parameters were determined through non-linear optimization as described in Chapter 3.

Table 6.3: Dynamic modulus master curve fitting parameters for composite AC layer

Section	$\log \lvert E^* \rvert_{max}$	$\log \lvert E^* \rvert_{min}$	$\beta_{\lvert E^* \rvert}$	$\gamma_{\lvert E^* \rvert}$	$\Delta E_{a,\lvert E^* \rvert}$
N1	3.496	1.146	-0.468	-0.533	177766
N2	3.496	0.949	-0.555	-0.496	186992
N8	3.513	0.742	-0.455	-0.524	181165
N9 (2006)	3.514	0.735	-0.506	-0.520	181508
N5	3.490	1.116	-0.995	-0.532	195182
N6	3.489	1.080	-0.962	-0.527	195272
N7	3.499	0.900	-0.976	-0.488	201632
N9 (2009)	3.514	0.763	-0.523	-0.521	181852
N10	3.504	0.832	-1.554	-0.478	201964
N11	3.503	0.742	-1.413	-0.499	195727
S9	3.500	0.858	-0.960	-0.495	189286
S10	3.504	0.892	-0.811	-0.531	184166
S11	3.500	0.938	-0.611	-0.543	190724
S12	3.496	0.984	-0.994	-0.559	190698

Lastly, it has long been known that the stiffness of the binder affects the dynamic modulus of the mix (Bonnaure et al. 1977). Therefore, dynamic shear modulus, or |G*| was used to account for the influence of asphalt binder on the composite AC modulus. The frequency-time relationship is further complicated in the application of |G*| due to the use of angular frequency in |G*| testing. Because of this, the frequency required in the Witczak 1-40D predictive model (Bari and Witczak 2006) is different than that required for the Hirsch model to predict |E*| (Christensen et al. 2003). To alleviate this problem, as was done with |E*|, the fitting parameters associated to the |G*| master curves were considered in the model development to account for the binder effects. The dynamic shear modulus master curve fitting parameters for the composite AC layer are listed in Table 6.4 for each section.

Table 6.4: Dynamic shear modulus master curve fitting parameters for composite AC layer

Section	f_c	k	m_e	C_1	C_2
N1	1.3092E-07	1.870	0.086	15.16	129.74
N2	0.0009	1.239	0.087	12.79	94.10
N8	3.3093E-07	1.225	0.095	14.74	131.77
N9 (2006)	3.9052E-07	1.135	0.098	14.94	134.26
N5	0.4525	0.127	1.122	15.18	128.78
N6	0.5483	0.129	1.107	15.38	131.11
N7	287619	1.311	0.500	8.41	45.61
N9 (2009)	4.0855E-07	1.104	0.099	15.42	138.42
N10	0.0684	0.115	0.898	74.72	609.62
N11	0.0178	0.111	1.025	36.99	297.81
S9	0.1475	0.132	0.924	18.35	152.15
S10	0.8415	0.135	0.891	20.17	165.47
S11	0.2724	0.137	0.915	16.78	138.12
S12	8.6759	0.141	0.895	18.45	152.30

6.3 MODEL CALIBRATION

To calibrate the models, DataFit version 9.0.59, a tool for linear multivariate regression, was used to linearly combine variables based on their level of significance. This was done using a stepwise regression procedure that selected variables to be entered into the model based on the level of significance of the associated coefficients. The level of significance was defined as the t-test probability of the estimated coefficients (p-value). To enter the model, the variable must have a p-value less than or equal to the value specified for entrance to the model, p_{enter}. As new variables are entered into the model, the significance of each of the existing coefficients is checked against a pre-defined level of significance, or p_{remove}, and if a coefficient is found to be no-longer significant (greater than or equal to p_{remove}), that variable is removed from the model. The p-values used to define the level of significance to be entered and removed from the model were determined through trial and error by first selecting the default values, $p_{enter} = 0.1$ and

p_{remove} = 0.2, and increasing each incrementally while maintaining a 0.1 difference between the two until reasonable R^2 values were achieved. DataFit requires that p_{enter} be less than p_{remove}. By doing so, this method makes it difficult for a variable to be entered into the model due to the high level of significance required, however once entered, the level of significance required for the variable to remain in the model is lower, and thus more difficult to be removed. This results in a model that has only variables which have coefficients of the highest level of significance. Interaction between variables was considered by including cross-products of the variables (including the squares of each variable) in addition to the individual variables to calibrate each of the models. As was discussed in the literature review, there are a number of parameters that influence AC dynamic modulus. It is also well known that many of these parameters influence one another. By including interaction variables, the interaction of these parameters can be accounted for. The variables selected for the models are selected based on the level of significance of their estimated coefficient, therefore, the use of interaction variables is driven by the statistical fitting of the model rather than assumed relationships. Although the inclusion of interaction variables results in a more complicated model that is not as direct as simply using the individual parameters, it accounts for the interaction of variables that may otherwise have been missed. By using this method, the models took the form shown in Equation 6.1, where X_1 through X_n are the independent variables which may represent a single parameter, a cross-product of two parameters or the square of one parameter, a_1 through a_n are coefficients of the independent variables and b is the intercept.

$$y = a_1X_1 + a_2X_2 + \cdots + a_nX_n + b \quad (6.1)$$

The twenty parameters shown in Tables 6.1through 6.4 were entered into DataFit as possible independent variables for each of the dependent variables (Log $E_{comp,min}$, β_{comp}, γ_{comp}, and $\Delta E_{a,comp}$). The step-wise regression was then applied, allowing for cross-products and squares of each of those twenty parameters. From the results of the step-wise regression procedure each model was selected based on the R^2 and the number of independent variables. Although high R^2 values are desirable, it was necessary to also look at the number of independent variables to avoid over-fitting the model. The goal was to achieve models in calibration that had high R^2 values while maintaining as few independent variables as possible. For instance if the results of the stepwise regression procedure returned models with R^2 values of 0.90, 0.95 and 0.99; the model that had the fewest variables was selected. Not all of the models were able to achieve such a high R^2 value, however, and in that case the model with the highest R^2 value was selected.

In addition to overfitting a model, multicollinearity in a model can also negatively affect its predictive capability. Therefore, to reduce multicollinearity, the correlation coefficients, |r|, among the variables included in each model were evaluated. Variables associated with high correlation coefficients were removed from the pool of variables and the step-wise regression was repeated. Due to the nature of step-wise regression, this resulted in the addition of new variables and new models from which to choose. The logic described previously, in which models were sought with high R^2 values and few variables, was applied. The correlation coefficients among all of the variables included in each additional model were again checked, looking for the absolute value of the coefficients of 0.70 or higher. Highly correlated variables were again removed and the process was repeated until the variables included in the models were

not highly correlated to one another and a high R^2 value was achieved. It can be difficult to choose which of the two variables should be removed when a high correlation coefficient exists. A variable was removed if it was highly correlated to more than one variable in the model. If neither of the two variables involved were highly correlated to other variables in the model, the impact of removing one over the other was evaluated. First, the variable that was least correlated to the dependent variable was removed from the variable pool and the resulting models were evaluated. Next, the other variable was removed from the variable pool and the one that was least correlated with the dependent variable remained and the step-wise regression was again completed. At which time, the resulting models were again evaluated for goodness of fit based on R^2 values and correlation coefficients between the variables in the model. The models that were eventually selected resulted in the highest R^2 values possible while still maintaining little to moderate linear dependency among the included variables.

The final models selected for log $E_{comp,min}$, β_{comp}, γ_{comp}, and $\Delta E_{a,comp}$ are shown below in Equations 6.2, 6.3, 6.4, and 6.5, respectively. The fit statistics for each model are listed in Table 6.5. The correlation matrix for each model is shown in Table 6.6 through 6.9. It should be noted that as shown in Table 6.7, the correlation coefficient between the two variables selected for the β_{comp} model is near 0.70. Although this was the lower bound used for identifying linear dependency between variables, it was found that other variables selected by the step-wise selection regression procedure had much higher (absolute value) correlation coefficients. Furthermore, to achieve the high level of significance (p_{enter} = 0.1 and p_{remove} = 0.2) used in the step-wise regression only a few variables were eligible for entrance to the model and of the few variables, these two

variables had the lowest correlation coefficient and thus the model was selected that included these variables and maintained a relatively high coefficient of determination.

$$\log E_{comp,min} = -18.3237 + 0.035202(\rho_{3/8} \times \log|E*|_{min}) + 9.7120 \times 10^{-7}(\rho_{3/8} \times \Delta E_{a,|E*|}) + 0.004785(\rho_4 \times \rho_{200}) \quad (6.2)$$

$$\beta_{comp} = -17.8665 + 1.0087 \times 10^{-6}\left(\rho_{3/8} \times \Delta E_{a,|E*|}\right) + 0.44681(\rho_{200} \times \log|E*|_{min}) \quad (6.3)$$

$$\gamma_{comp} = -1.3893 + 0.007889(V_a \times \rho_{200}) - 0.789732\left(G_{mm} \times \gamma_{|E*|}\right) - 0.001451(\rho_{16} \times \rho_{200}) - 0.02721\left(\rho_{200} \times \beta_{|E*|}\right) \quad (6.4)$$

$$\Delta E_{a,comp} = -157028 + 6659.79(V_a \times P_b) - 3355.34\left(G_{mm} \times \rho_{3/8}\right) - 21256.4\left(\rho_{3/8} \times \gamma_{|e*|}\right) + 3.06369(C_1 \times C_2) \quad (6.5)$$

where:

$\rho_{3/8}$ = percent by weight passing 3/8" sieve

$\log|E*|_{min}$ = limiting minimum |E*| for |E*| master curve (fitting parameter)

$\Delta E_{a,|E*|}$ = activation energy for |E*| master curve (fitting parameter)

ρ_4 = percent by weight passing #4 sieve

ρ_{200} = percent by weight passing the #200 sieve

V_a = percent air voids by volume

G_{mm} = maximum specific gravity of the mix

$\gamma_{|E^*|}$ = fitting parameter for |E*| master curve

ρ_{16} = percent by weight passing the #16 sieve

$\beta_{|E^*|}$ = fitting parameter for |E*| master curve

P_b = percent by weight of asphalt binder

C_1 = fitting parameter for |G*| master curve

C_2 = fitting parameter for |G*| master curve

Table 6.5: Fit statistics for fitting parameter models

Model	R^2	S_e/S_y
$\log E_{comp,min}$	0.8220	0.4219
β_{comp}	0.8968	0.3213
γ_{comp}	0.7642	0.4856
$\Delta E_{a,comp}$	0.8364	0.4045

Table 6.6: Correlation matrix for *log* $E_{comp, min}$

	$\rho_{3/8} \times \log \lvert E^* \rvert_{min}$	$\rho_{3/8} \times \Delta E_{a,\lvert E^* \rvert}$	$\rho_4 \times \rho_{200}$
$\rho_{3/8} \times \log \lvert E^* \rvert_{min}$	1	-0.0465	-0.3970
$\rho_{3/8} \times \Delta E_{a,\lvert E^* \rvert}$		1	-0.5185
$\rho_4 \times \rho_{200}$			1

Table 6.7: Correlation matrix for β_{comp}

	$\rho_{3/8} \times \Delta E_{a,\lvert E^* \rvert}$	$\rho_{200} \times \log \lvert E^* \rvert_{min}$
$\rho_{3/8} \times \Delta E_{a,\lvert E^* \rvert}$	1	-0.7031
$\rho_{200} \times \log \lvert E^* \rvert_{min}$		1

Table 6.8: Correlation matrix for γ_{comp}

	$V_a \times \rho_{200}$	$G_{mm} \times \gamma_{,\lvert E^* \rvert}$	$\rho_{16} \times \rho_{200}$	$\rho_{200} \times \beta_{\lvert E^* \rvert}$
$V_a \times \rho_{200}$	1	0.2052	0.5292	0.4552
$G_{mm} \times \gamma_{\lvert E^* \rvert}$		1	0.1389	-0.5006
$\rho_{16} \times \rho_{200}$			1	0.3504
$\rho_{200} \times \beta_{\lvert E^* \rvert}$				1

Table 6.9: Correlation matrix for $E_{a|E^*|}$

	$V_a \times P_b$	$G_{mm} \times \rho_{3/8}$	$\rho_{3/8} \times \gamma_{\|E^*\|}$	$C_1 \times C_2$
$V_a \times P_b$	1	0.0961	-0.0205	-0.1741
$G_{mm} \times \rho_{3/8}$		1	-0.4897	0.4872
$\rho_{3/8} \times \gamma_{\|E^*\|}$			1	0.1775
$C_1 \times C_2$				1

6.4 COMPREHENSIVE MODEL PERFORMANCE

When applied to the AC composite master curve (Equations 5.1 and 5.2), these four models (Equations 6.2 through 6.5) create a comprehensive model that predicts the composite AC modulus for any vehicle speed and mid-depth pavement temperature for a given cross-section. To assess the performance of the comprehensive model, AC moduli were predicted by using Equations 6.2 through 6.5 in conjunction with Equation 5.1 and 5.2 for the vehicle speed and mid-depth pavement temperature associated to each tensile strain measurement. The performance of this comprehensive model was assessed by R^2 and S_e/S_y values, listed in Table 6.6. In calculating these statistics, the predicted values were from this comprehensive model and the measured values represent the composite AC moduli that were calculated by applying the measured tensile strains to the modulus-strain relationships developed for each section. Also listed in Table 6.6 are the fit statistics for the original field-calibrated master curve using fitting parameters determined through non-linear optimization (also shown in Table 5.6). For over half of the sections, this comprehensive model was capable of predicting the measured composite AC moduli (from modulus-strain relationships) almost as well as the field-calibrated master curves, resulting in coefficients of determination for the comprehensive model ranging from 0.78 to 0.98. The coefficient of determination

decreased by 0.1 or more when the E_{comp} comprehensive model was applied to three of the fourteen sections: N6, N7 and S11. However, the model was still able to account for at least 75% of the variability in the measured AC composite moduli for these sections. There were three sections that saw much larger reductions in R^2 relative to the field-calibrated master curves, highlighted in bold font in Table 6.10: N8, N11and S9. As expected, the S_e/S_y ratios reported for these three sections were also three of the largest ratios reported. For these sections only 62 to 69% of the variability of the data could be accounted for by the model. One section, N9 from 2009 (also shown in bold in Table 6.10), resulted in a negative R^2 value, indicating that the average of the measured values is a better predictor than the model. As shown in Table 6.10, however, the field calibrated master curve only accounted for 85% of the variability in the data for section N9 from 2009, which represents the second lowest R^2 value among the fourteen sections.

Table 6.10: Fit statistics for field-calibrated master curve and comprehensive model for composite AC modulus

	Field-calibrated master curve		Comprehensive model	
Section	R^2	S_e/S_y	R^2	S_e/S_y
N1	0.8246	0.4188	0.7826	0.4663
N2	0.9508	0.2218	0.8858	0.3379
N8	0.9293	0.2659	**0.6778**	0.5676
N9 (2006)	0.9546	0.2130	0.9653	0.1862
N5	0.9823	0.1329	0.9766	0.1530
N6	0.9566	0.2083	0.7732	0.4762
N7	0.9143	0.2927	0.7843	0.4644
N9 (2009)	0.8517	0.3851	**-0.2293**	1.1087
N10	0.8699	0.3607	0.8045	0.4422
N11	0.9599	0.1946	**0.6859**	0.5604
S9	0.9106	0.2990	**0.6161**	0.6196
S10	0.9338	0.2573	0.9293	0.2659
S11	0.9571	0.2072	0.7542	0.4958
S12	0.9561	0.2094	0.9376	0.2498

It is difficult to assess the exact reason for the mediocre performance of the comprehensive model as applied to these three sections (N8, N11 and S9) and the poor performance of N9 from the 2009 test cycle. Section N8 was comprised of approximately ten inches of AC, the third thickest section, behind sections N9 from the 2006 and 2009 cycle. It featured an SMA surface lift and a rich bottom layer designed to have 2% air voids. Rather than being placed on the compacted track soil as were the majority (11) of the remaining sections, it was placed on top of a soft subgrade material. The unique mixtures and soft subgrade included in this section could have contributed to the inability of the model to predict the in-place composite AC modulus. Section N8 was also one of the three sections that experienced cracking. However, the cracking in section N8 was confirmed to be fatigue cracking rather than the top-down cracking experienced in the other two sections (N1 and N2). Although a cut-off date was applied, it may not have been adequate as only one week separated the cut-off date for strain measurements from the first observation of cracking at the surface.

Section S9, acted as the control section for the group experiment in the 2009 test cycle. It was constructed with a conventional cross-section such that the top two lifts utilized typical polymer modified mixtures used in Alabama and the base course was a typical unmodified mixture placed in Alabama. Of all of the fourteen sections, section S9 was the only truly conventional section, as it shared the typical track soil used for subgrade material at the Test Track with the majority of the other sections and consisted of conventional materials throughout its cross-section. It should be noted that although section S9 was a conventional section, $|G^*|$ testing was completed on binder that had been extracted and recovered from plant produced mixture.

Section N11 was constructed with 7.1 inches of asphalt concrete that was produced as a WMA using the foaming technique. It also featured 50% RAP in each AC lift. Sections N10 and N11 were identical in design but N11 was produced with WMA technologies while section N10 was produced as conventional AC. Conversely, the comprehensive model was able to predict the composite moduli for N10 relatively well, based on an R^2 of 0.804. Although the composite in-place material properties and composite fitting parameters for the |E*| master curves are very similar, the composite fitting parameters for the |G*| master curves are different in magnitude, particularly for the C_1 and C_2 terms. However, both sections N10 and N11 represent the extreme high values for C_1 and C_2. It should be kept in mind that the binder used in the |G*| testing was extracted and recovered from plant produced mixtures.

Section N9 of the 2009 structural study also required a cut-off date be applied to the strain data. It was also the thickest of all of the test sections, and had a variety of different mixtures, including an SMA surface mix and a rich bottom layer designed at 2% air voids. Despite the fact that section N9 (2009) was the same N9 section from 2006, it was treated separately, mainly due the difference in age and cumulative traffic applied. The lift thicknesses used in computing composite parameters for 2009 were different than those used for the 2006 section, as was discussed in Chapter 3. Fundamentally, the strains in these two sections were different, shown in Figure 6.1 by means of strain plotted as a function of mid-depth pavement temperatures. These differences were reflected in the different fitting parameters required for the field-calibrated master curve, shown in Table 5.6. The largest differences are in the $E_{comp,min}$ and the $\Delta E_{a,comp}$ terms. However, the in-place material properties for both the 2006 and

2009 N9 sections were based on the compaction achieved during construction and therefore the properties for N9 in 2009 do not account for compaction due to 2 years of traffic and 3 years of aging experienced during the 2006 test cycle. Furthermore, the laboratory determined mix and binder properties were nearly identical for each lift; note the subtle differences between the 2006 and 2009 N9 sections, shown in Tables 6.3 and 6.4 for the composite fitting parameters, are due to the difference in lift thicknesses. Therefore, the model is being applied to seemingly identical material, mix and binder properties for sections that had two different strain regimes.

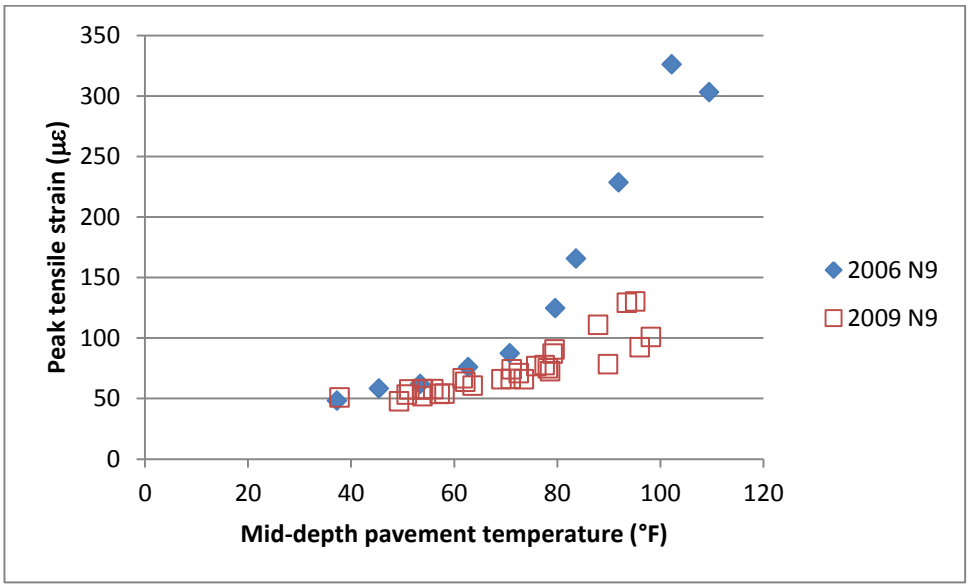

Figure 6.1: Strain-temperature relationships for section N9 from 2006 and 2009.

The composite AC moduli as predicted by the comprehensive model are plotted relative to the measured values, shown in Figures 6.2, 6.3, 6.4 and 6.5 for sections N8, N11, S9 and N9 (2009), respectively. In looking at Figure6.4, for section S9 it appears as though the predicted moduli are simply shifted above the measured moduli, which can be attributed to the β_{comp}-term or the minimum limiting modulus (log $E_{comp,\ min}$). From Equations 6.2 and 6.3, it is evident that the β_{comp} and log $E_{comp,\ min}$-terms are

functions of in-place gradation, $\rho_{3/8}$, ρ_{200}; and fitting parameters for |E*| master curve, $\Delta E_{a,|E^*|}$ and log $|E^*|_{min}$. In looking at these parameters (Tables 6.2 and 6.3) that influence the β_{comp} and log $E_{comp,\ min}$-terms, the values for section S9 do not appear to be out of the ordinary. However, as shown in Figure 6.4, there is a fair amount of scatter in the measured in-place composite AC modulus, which could have affected the mastercurve fitting parameters that were used for calibration of the models. Furthermore, the coefficient of determination is also driven down due to measured composite moduli at 42 and 31 ksi that deviate from the overall trend of the measured composite moduli.

From Figures 6.2 and 6.3, it is evident that the predicted master curves for both sections N8 and N11 are not only shifted above or below the measured moduli, as was the case with section S9, but the angles of the predicted curves are also skewed. This deviation in the predicted master curve from the measured values leads to better predictions of composite moduli from the comprehensive model at high vehicle speeds (low pavement temperatures) than at slow vehicle speeds (high pavement temperatures) for sections N8 and N11. Although the shifting of the predicted moduli values either above or below the measured values is due to the β_{comp} and log $E_{comp,\ min}$-terms, the angle of the curve is due to the γ_{comp} -term. From Equation 6.4, the γ_{comp} term is influenced by V_a, G_{mm}, $\gamma_{|E^*|}$, $\beta_{|E^*|}$ and gradation parameters. Section N8 represents the extreme low value for percent passing the #16 sieve, as well as the extreme high value for percent passing the #8 sieve among the fourteen sections. In addition to representing extreme gradation parameters, section N8 also reflects the lowest G_{mm} and highest $\beta_{|E^*|}$ among the sections. Alternatively, section N11 reflects one of smallest $\beta_{|E^*|}$ value among the

fourteen sections, second only to N10. It is likely that these extreme values associated with N8 and N11 contributed to the deviation of the predicted composite AC moduli from the measured moduli shown in Figures 6.2 and 6.3.

Section N9 from the 2009 structural study appears to be affected by both the γ_{comp} and β_{comp} terms due to some shifting on the low end and the angle of the curve. However, in looking at those parameters that influence each of these terms, the values do not appear to be out of the ordinary or represent the extreme high or low values. It is evident in Figure 6.5 that at slow speeds (or high temperatures) the comprehensive model underpredicts the measured composite AC modulus. This is consistent with the differences shown in Figure 6.1 for strain with mid-depth temperatures. The strain values were much lower at high temperatures in 2009 than in 2006, however, the composite in-place, mix and binder fitting parameters were nearly identical between the two test cycles, therefore applying the same properties would likely result in such a deviation as seen in Figure 6.5.

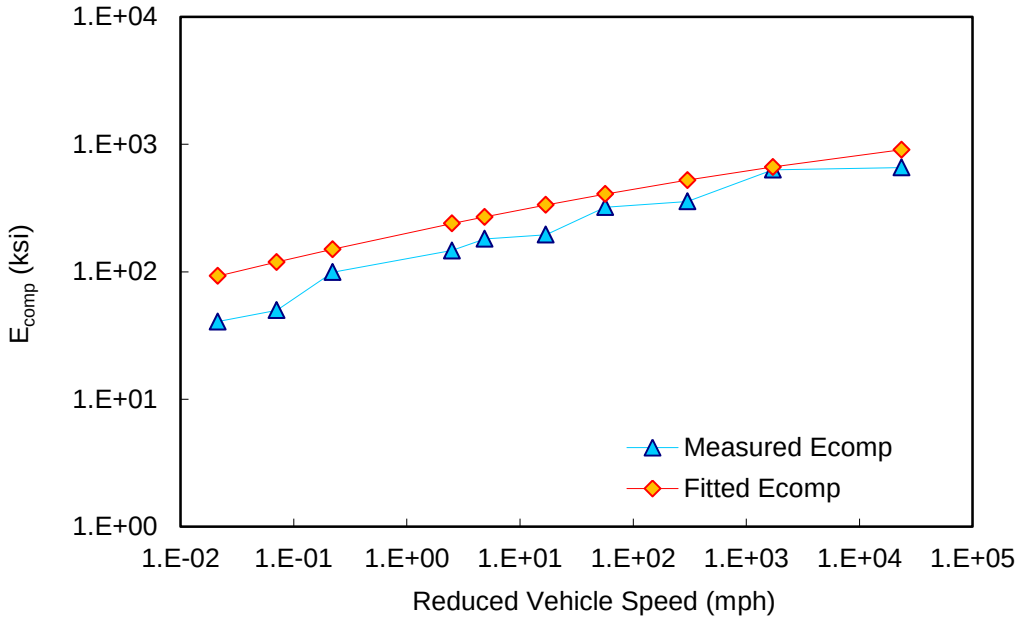

Figure 6.2: Predicted composite AC moduli from comprehensive model and measured composite AC moduli for N8.

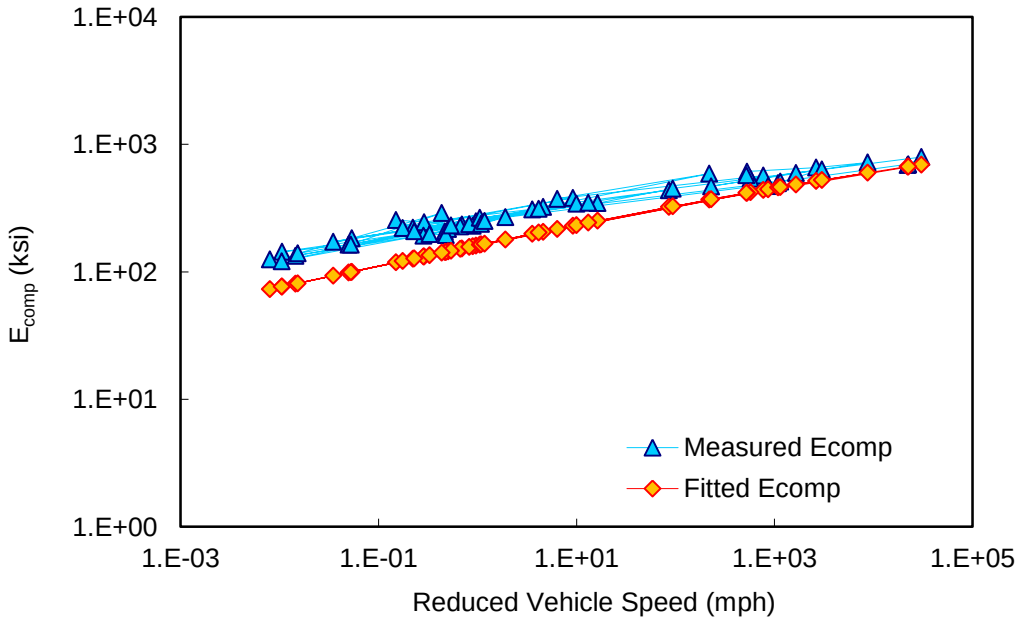

Figure 6.3: Predicted composite AC moduli from comprehensive model and measured composite AC moduli for N11.

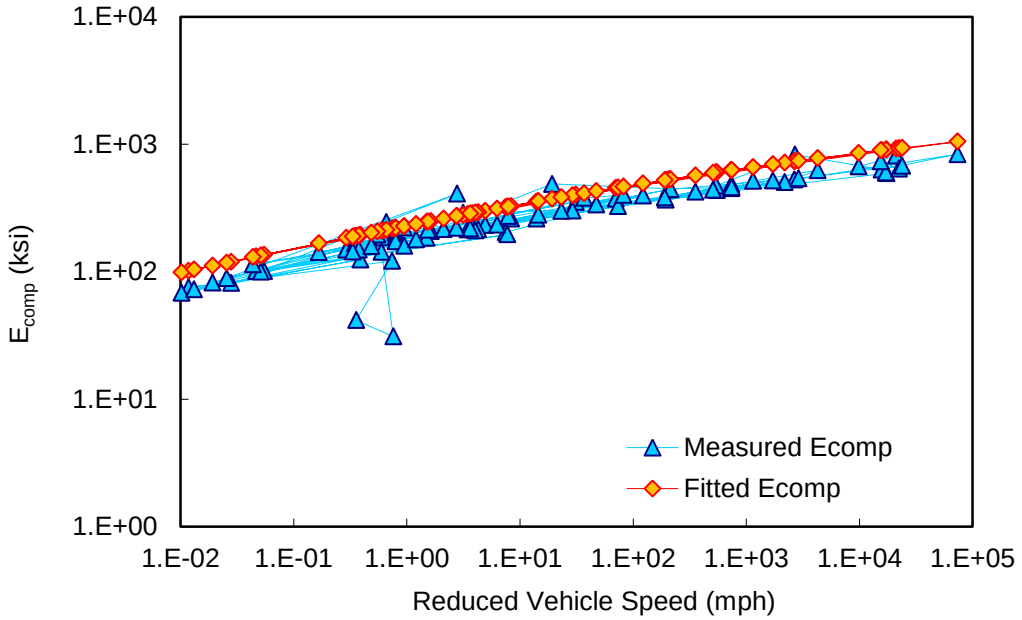

Figure 6.4: Predicted composite AC moduli from comprehensive model and measured composite AC moduli for S9.

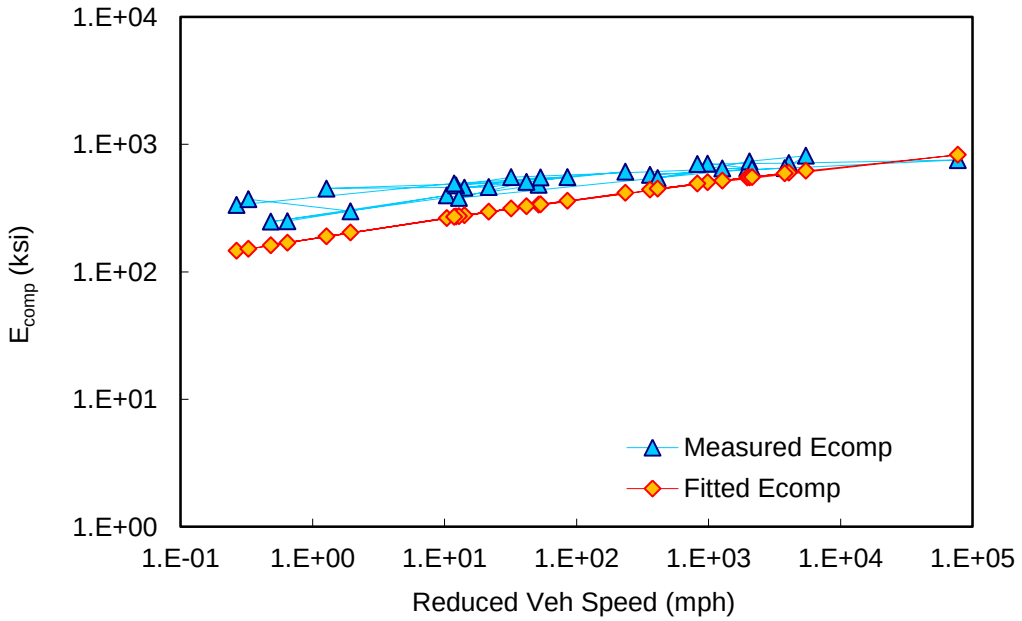

Figure 6.5: Predicted composite AC moduli from comprehensive model and measured composite AC moduli for N9 (2009 test cycle).

Although the comprehensive model for composite AC moduli did not perform well for four of the fourteen sections, looking at the performance of the model overall, it performed quite well. The R^2 and S_e/S_y ratio for the model on a global level were calculated for the predicted composite AC moduli relative to the measured moduli for all of the cross-sections, based on 610 total strain measurements and were found to be 0.8303 and 0.4120, respectively. In other words, over 83% of the variability in the measured composite AC moduli was accounted for by the comprehensive model. The standard error associated with the predicted values represented only 41% of the standard deviation of the measured values. This is quite reasonable given the variability that is associated with measured strain under live traffic, and gauge functionality. The measured composite AC moduli were plotted against the predicted composite AC moduli for all test sections in Figure 6.6. When a linear trendline was applied and forced through the origin, the slope of the line is an indication of the over or under-prediction of the model. Shown in Figure 6.6, the comprehensive model tends to under-predict the composite AC modulus by about 4%. This errs on the side of conservatism and should lead to a slight over-prediction of strain.

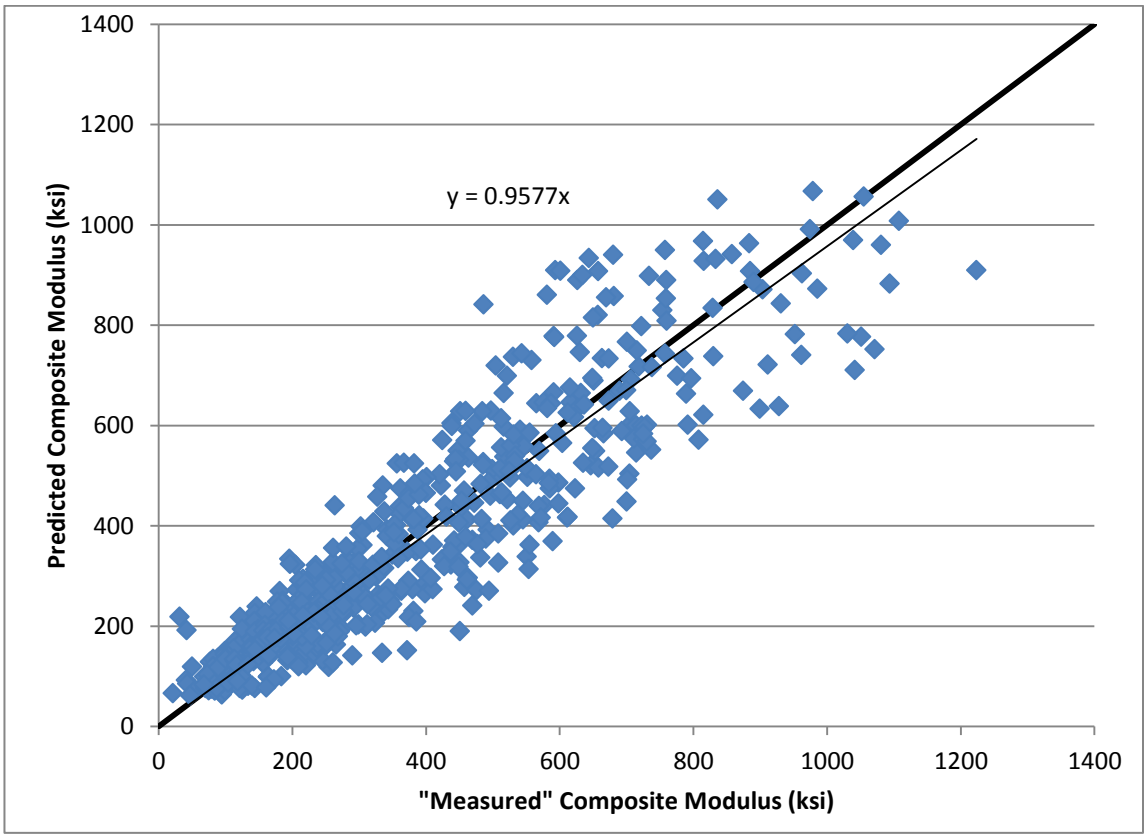

Figure 6.6: Composite modulus predicted by model with measured composite modulus.

To evaluate the effect of the modulus predictions on tensile strain, the modulus-strain relationships developed in Chapter 4 were re-arranged as to estimate strain from modulus for each section. These relationships were appropriate to use since they were developed in WESLEA specific to each test section. These relationships were then used to estimate tensile strains which were then plotted with measured tensile strain for all of the sections in Figure 6.7. Again, attaching a linear trend line with y-intercept at the origin indicates how much the model tends to overpredict or underpredict the data as shown in Figure 6.7, the slope of the linear trendline is 0.91. It appears that this is skewed due to three data points that were severely underpredicted. If these data points were removed, the slope would increase to 0.97, still reflecting a slight underprediction,

but much closer to a slope of one. The R^2 and S_e/S_y ratio calculated for the strain predictions based on the composite AC moduli predictions are 0.7100 and 0.5385, respectively. Although these values are lower than desired, there is a lot of variability in strain measurements. For instance, three data points in Figure 6.7 representing measured values greater than 1500 με were significantly underpredicted by this method. These three data points were examined prior to the development of the modulus-strain relationships and it was found that the strain traces did not reflect non-elastic behavior. However, they appear to be rare occurrences. They could very well represent, to some extent, the true strain that should be measured in the pavement under the given conditions, but due to variability in wheel wander and gauge functionality those strains are not consistently being measured. Additionally, some of the variability can be attributed to the use of the modulus-strain relationships rather than directly inputting the predicted composite AC moduli into WESLEA. Other sources of variability can be attributed to laboratory testing variability for material properties, |E*| and |G*| as well as FWD testing and backcalculation, density measurements and surveyed lift thicknesses, all of which were used for development of the comprehensive model to predict composite AC modulus.

In a previous study (Robbins 2009) at the Test Track that investigated the use of |E*| measurements and time of loading to predict tensile strains using WESLEA, it was found that strain predictions based on time of loading calculations underpredicted strain values measured in the field by approximately 42 to 62%. The absolute percent differences were calculated as the differences between measured strains and the strains predicted from the application of the composite AC modulus calculated from the

comprehensive model to the modulus-strain relationships for each section. The cumulative distribution of the absolute percent differences revealed that at the 95th percentile, the percent deviation from the measured strain values was approximately 47%. However, on average, the absolute percent difference was only 17.7%. This is a marked improvement over the strain predictions that result from the load duration calculations in the MEPDG, reflected by the 42 to 62% differences reported in the previous study at the Test Track (Robbins 2009).

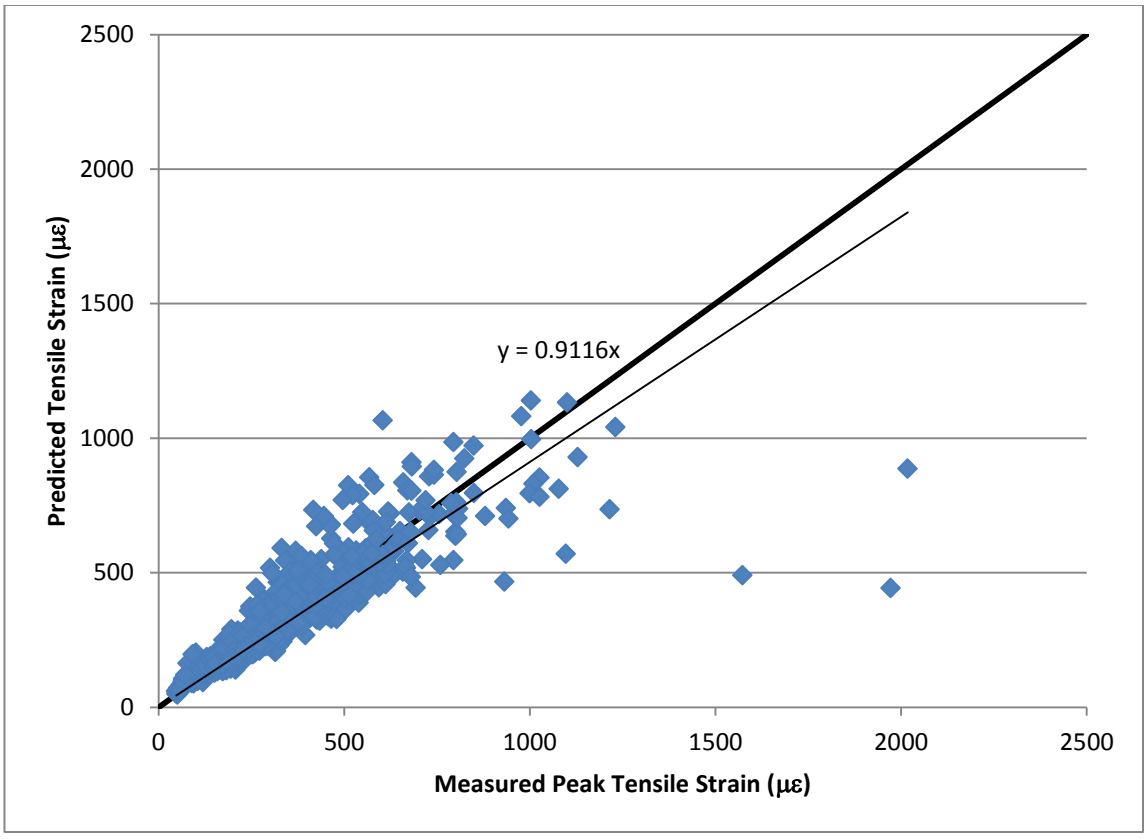

Figure 6.7: Predicted strain from predicted composite modulus against measured strain.

Delving into the strain predictions even more, it is evident that similar to the predicted composite AC moduli, they are also very dependent on the test section. The R^2 for the strain predictions found from applying the results of the comprehensive model

for composite AC modulus to the modulus-strain relationships previously developed for each section are listed in Table 6.11for each section. As to be expected, the four sections for which the comprehensive model performed the worst also had the lowest R^2 values for strain predictions, with two of the four resulting in negative values. It should be noted that two of the three measured strain values that were severely under-predicted, shown in Figure 6.7 were measured in section S9, therefore contributing to the low R^2 value reported in section S9. These two data points were also discussed in Chapter 4 and the strain traces had been visually inspected, showing no signs of non-elastic behavior.

Table 6.11: Calculated R^2 for strain predictions

Section	R^2
N1	0.8708
N2	0.8865
N8	0.4561
N9 (2006)	0.8581
N5	0.9244
N6	0.7043
N7	0.6670
N9 (2009)	-2.8764
N10	0.6987
N11	-0.6236
S9	0.4405
S10	0.8896
S11	0.7761
S12	0.9250

In addition to the four sections that did not perform well when the comprehensive model for composite AC modulus was applied, section N7 also did not perform as well as expected when the predicted moduli values were applied to the modulus-strain relationships. Section N7 was the thinnest section evaluated and due to gauge failures, a cut-off date was applied to the strain values used for the analysis. The predicted strains are plotted with the measured tensile strains in Figure 6.8 for section

N7. By applying a linear trendline through the origin, it is evident from the slope of the line that this method for predicting tensile strains resulted in an overprediction of the measured strain values by approximately 17%.

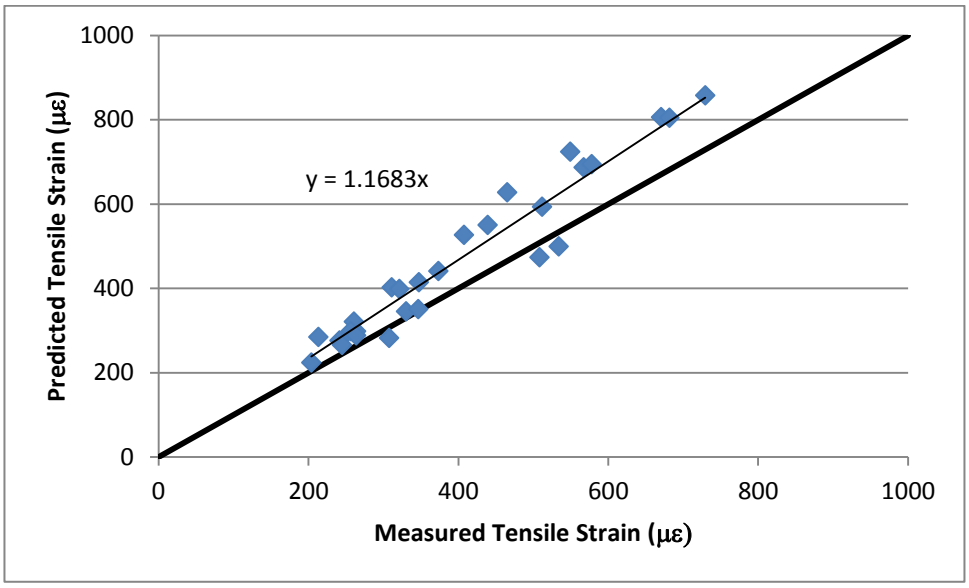

Figure 6.8: Predicted strain against measured strain, section N7.

Although the comprehensive model for composite AC modulus does not improve strain predictions for all sections, it does predict very well ($R^2 > 0.9$) for sections N5 and S12 and well ($R^2 > 0.8$) for sections N1, N2, N9 (from the 2006 test cycle) and S10. Four of the six sections were constructed with unconventional technologies or mixtures, including sulfur-modified WMA, virgin binder replaced with asphalt from Trinidad Lake Asphalt, WMA produced with foaming technology and lastly a section with an SMA surface mix and a rich bottom layer. The only conventional sections out of these six, N1 and N2, were constructed with a limerock aggregate base material rather than the granite aggregate base used in the other four sections. Therefore, the capability of the comprehensive model to predict in a LEA this well is remarkable

and is an improvement over the MEPDG which has not been calibrated for unconventional materials.

The primary objective of this dissertation was to improve critical strain predictions at the bottom of the AC layers. Looking at the 2009 NCAT Test Track study that found the MEPDG method of load duration to lead to severe underpredictions of strain (Robbins 2009), the same vehicle speeds and mid-depth pavement temperatures used for comparisons of strain were applied to the comprehensive model for the same section, N9 from 2006. The composite AC moduli were then used in the modulus-strain relationship for N9 from 2006 to predict tensile strain. The resulting strain is shown in Figure 6.9 along with the strains presented in the 2009 study (Robbins 2009). The strains that result from the comprehensive model for composite AC modulus (shown as E_{comp} in Figure 6.9) are a marked improvement over those strains that result from the current MEPDG procedure for predicting strain using a LEA analysis. The current MEPDG procedure uses |E*| values that are based on the iterative load duration calculation to predict strain in a LEA, shown in Figure 6.9 as MEPDG "t". The predicted strains from the comprehensive model are still underpredicted relative to the measured strains, with absolute percent differences of the measured values ranging from 4.1 to 28.5%. The largest differences occur at the high mid-depth pavement temperature. However, when compared with the percent differences for the MEPDG procedure, shown in Table 6.12 where negative values represent underprediction, the comprehensive model proves to result in much closer predictions than the MEPDG procedure which ranged from -41.9 to -64.8%.

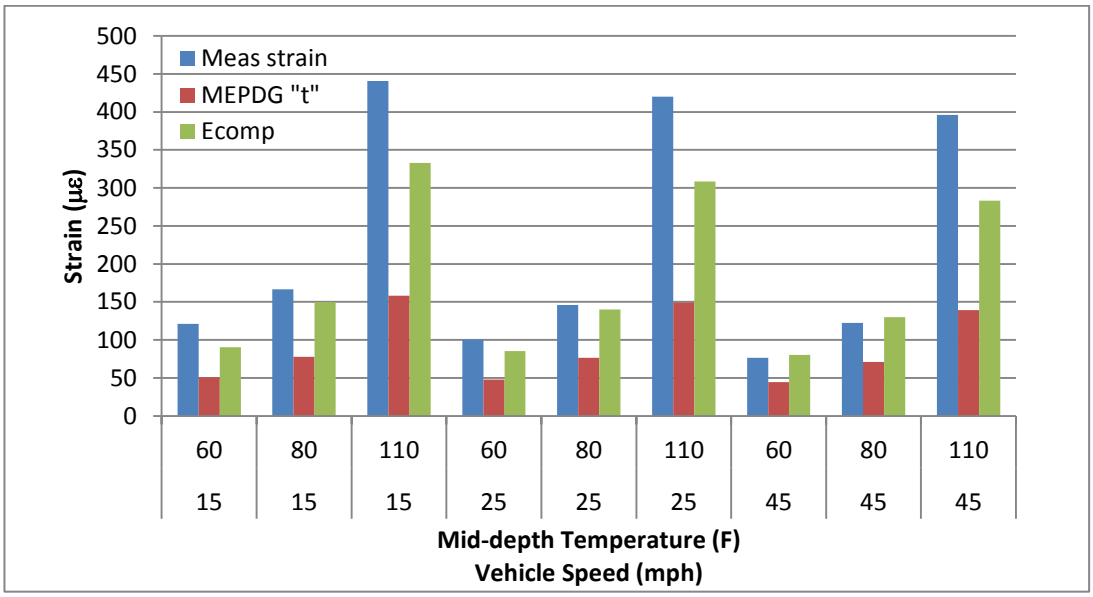

Figure 6.9: Comparison of strain values for N9 (2006 test cycle) (*after* Robbins 2009).

Table 6.12: Percent differences for strain prediction methods

Speed (mph)	Temp (ºF)	MEPDG % Difference	E_{comp} % Difference
15	60	-57.89	-25.40
15	80	-53.33	-10.31
15	110	-64.13	-24.47
25	60	-52.30	-14.93
25	80	-47.78	-4.14
25	110	-64.49	-26.50
45	60	-41.88	4.78
45	80	-41.92	6.30
45	110	-64.81	-28.51

6.5 SUMMARY

Four individual models were developed to predict the fitting parameters for the composite AC modulus master curve from known material properties. These material properties represented the composite AC layer and included in-place gradation parameters, in-place volumetrics and gravimetric values and the fitting parameters for

both |E*| and |G*| master curves. By combining these individual models with the functional form of the composite AC modulus master curve, the modulus of the composite AC layer can be predicted for a specific test section for any vehicle speed and mid-depth pavement temperature. When combined with the master curve equations for composite AC modulus, this comprehensive model was able to predict composite AC modulus as well as the field calibrated master curves that were developed in Chapter 5, for over half of the test sections investigated. When the results of the comprehensive model were entered into the modulus-strain relationships developed in Chapter 4, the strain predictions varied, with excellent predictions for two sections and good predictions for an additional four sections. Of these six sections with good or better performance, four were unconventional materials. Although some of the sections saw poor strain predictions, this should still be an improvement over the current M-E design system which has not been calibrated for unconventional or materials.

CHAPTER 7

CONCLUSIONS AND RECOMMENDATIONS

7.1 SUMMARY

Previous findings in which large discrepancies existed between predicted tensile strain at the bottom of the AC layer and the measured strain from embedded strain gauges at the NCAT Test Track led to the development of a new method for predicting critical tensile strains in a flexible pavement. This method enables the prediction of the in-place modulus of a composite AC layer for a given vehicle speed and mid-depth pavement temperature using in-place material properties and master curve fitting parameters from laboratory measured |E*| and |G*| values representative of the composite AC layer. When the moduli predicted from this comprehensive model were used in conjunction with LEA the resulting strains were found to fit the measured strains well with a calculated R^2 of 0.8 or higher for six of the fourteen sections.

To develop this new method, fourteen test sections at the NCAT Test Track, four from the 2006 structural study and 10 from the 2009 structural study were used to calibrate the comprehensive model. Due the limited amount of available test sections, validation of the resulting model was not feasible at this time. This new method for predicting critical strains was calibrated on a very robust set of data including a wide variety of unconventional materials and technologies as well as the use of 3 different granular base materials and AC layer thicknesses ranging from 5-14 inches. These test

sections were embedded with instrumentation from which strain at the bottom of the AC layers and in-situ temperatures were measured. Additionally, laboratory testing was conducted to characterize the mixture and binder properties of the mixtures in each cross-section. The general approach used to develop the new method for predicting critical tensile strains is described by Figure 7.1.

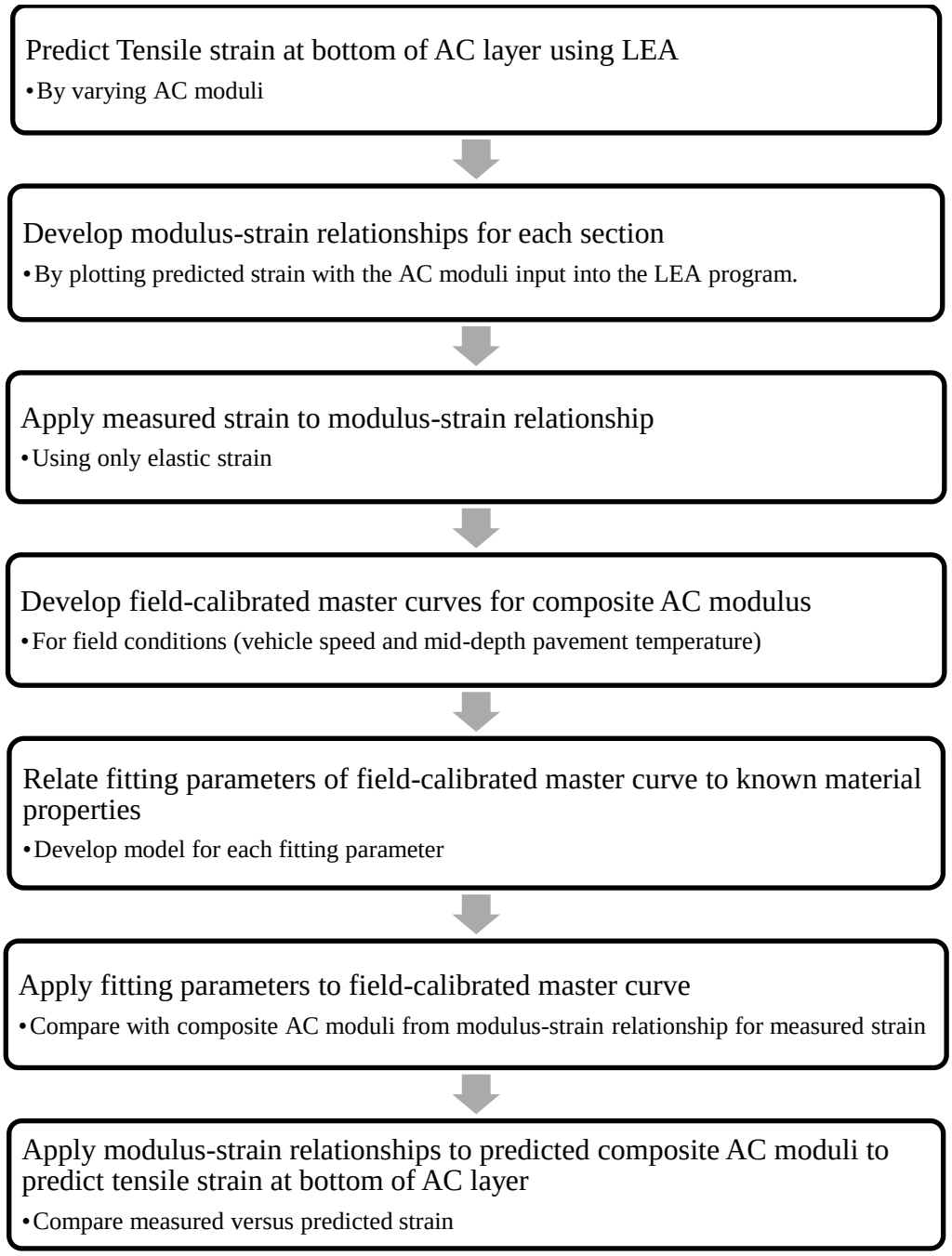

Figure 7.1: General approach to developing a new method for predicting critical tensile strains.

Field-calibrated master curves were developed by applying the measured strain to modulus-strain relationships developed in a LEA program for each section. Several

methods were employed to ensure that the measured strains used for field calibration of master curves were elastic, thereby upholding the principal assumptions in a LEA program. A sigmoidal fit function similar to the one outlined in AASHTO PP 61-09 was used to construct the field-calibrated master curves with the use of measured vehicle speed and mid-depth pavement temperature rather than loading frequency and testing temperature. This eliminated the need for time of loading and conversion to frequency using the much debated time-frequency relationship. Models were then developed to relate each of the four fitting parameters that resulted from the field-calibrated master curves with known material properties. These models are shown in Equations 7.1 through 7.4 with associated fit statistics shown in Table 7.1. These material properties included in-place volumetric, gravimetric, and gradation parameters as well as laboratory-derived mixture and binder properties. To account for mixture and binder characteristics of the composite AC layer, the fitting parameters associated to the |E*| and |G*| master curves were employed, again eliminating the need for the use of frequency. When combined with the sigmoidal fit function for the field-calibrated master curves, these models created a comprehensive model that can be used to predict composite AC modulus for a given vehicle speed and mid-depth pavement temperature and known material properties. This is a powerful tool for pavement designers as vehicle speed is an important factor in pavement design, but up to this point has been accounted for only through relationships with time of loading requiring a conversion from time to frequency, thereby introducing errors into strain predictions.

$$\log E_{comp,min} = -18.3237 + 0.035202(\rho_{3/8} \times \log|E*|_{min}) + 9.7120 \times 10^{-7}(\rho_{3/8} \times \Delta E_{a,|E*|}) + 0.004785(\rho_4 \times \rho_{200}) \quad (7.1)$$

$$\beta_{comp} = -17.8665 + 1.0087 \times 10^{-6}\left(\rho_{3/8} \times \Delta E_{a,|E*|}\right) + 0.44681(\rho_{200} \times \log|E*|_{min}) \quad (7.2)$$

$$\gamma_{comp} = -1.3893 + 0.007889(V_a \times \rho_{200}) - 0.789732\left(G_{mm} \times \gamma_{|E*|}\right) - 0.001451(\rho_{16} \times \rho_{200}) - 0.02721\left(\rho_{200} \times \beta_{|E*|}\right) \quad (7.3)$$

$$\Delta E_{a,comp} = -157028 + 6659.79(V_a \times P_b) - 3355.34\left(G_{mm} \times \rho_{3/8}\right) - 21256.4\left(\rho_{3/8} \times \gamma_{|e*|}\right) + 3.06369(C_1 \times C_2) \quad (7.4)$$

where:

$\rho_{3/8}$ = percent by weight passing 3/8" sieve

log $|E^*|_{min}$ = limiting minimum |E*| for |E*| master curve (fitting parameter)

$\Delta E_{a,|E^*|}$ = activation energy for |E*| master curve (fitting parameter)

ρ_4 = percent by weight passing #4 sieve

ρ_{200} = percent by weight passing the #200 sieve

V_a = percent air voids by volume

G_{mm} = maximum specific gravity of the mix

$\gamma_{|E^*|}$ = fitting parameter for |E*| master curve

ρ_{16} = percent by weight passing the #16 sieve

$\beta_{|E^*|}$ = fitting parameter for |E*| master curve

P_b = percent by weight of asphalt binder

C_1 = fitting parameter for |G*| master curve

C_2 = fitting parameter for |G*| master curve

Table 7.1: Fit statistics for fitting parameter models

Model	R^2	S_e/S_y
log $E_{comp,min}$	0.8220	0.4219
β_{comp}	0.8968	0.3213
γ_{comp}	0.7642	0.4856
$\Delta E_{a,comp}$	0.8364	0.4045

The comprehensive model for composite AC modulus was developed for use in a LEA program to improve tensile strain predictions. For two of the fourteen sections, this method proved to be an excellent predictor of the tensile strains used in development, and for four other sections, the model proved to be a good predictor (R^2 > 0.8). This comprehensive model which was calibrated for a variety of unconventional materials (sulfur-modified WMA, high RAP, high RAP produced with WMA technologies, high polymer modified asphalt, virgin binder replacement with Trinidad Lake Asphalt pellets) is an improvement over the current M-E design system, the MEPDG, which has yet to be calibrated for unconventional materials. Furthermore, when tensile strain was predicted from the comprehensive model for section N9 in 2006, the subject of a previous study on time of loading measurements, it was found that strain predictions were improved over predictions from the previous study based on different methods for determining time of loading. Although strain predictions did not exactly match the measured strain values, the comprehensive model significantly improved strain predictions, relative to those found in the previous study. Improvements in strain predictions through this method should also yield improvements in pavement

performance predictions, particularly for fatigue cracking, thereby resulting in more efficient and successful pavement designs.

7.2 CONCLUSIONS

Based on the findings of this investigation some important conclusions were drawn:

- The field calibrated master curve developed from the application of strain measurements to the modulus-strain relationships developed from WESLEA was found to be a good predictor of composite AC moduli when applied to slow speeds (15, 25 and 35 mph) in section S9. Therefore, it can be concluded that field calibrated master curves developed at a narrow range of speeds (96% of speeds were between 42 and 52 mph) can be applied to speeds outside the range used for model development.
- When compared with a previous study investigating the effects of time of loading on strain at varying temperatures and speed for the section N9 from 2006, improvements in strain predictions were found due to this new method of predicting critical tensile strains. Significant improvements over the current method that relies on the time of loading estimates were noted at intermediate and high mid-depth pavement temperatures (60 and 80 °F) for all speeds evaluated. Based on these findings, it can also be concluded that this new method for predicting critical strains is an improvement over current methods due to its ability to account for vehicle speed directly and its calibration to unconventional materials and technologies.

- Although this new method for predicting critical tensile strain was found to generally be a good predictor of strain when applied to the data from the previous study on section N9 from 2006, it was found that strain was predicted more accurately at intermediate temperatures than at high mid-depth pavement temperature (110°F). Underprediction of measured values ranging from 25-.4-28.5% for the speeds evaluated was found at 110°F with the highest underprediction recorded at the fastest speed evaluated (45 mph). From this it can be concluded that this comprehensive model for composite AC modulus may not entirely account for the viscoelastic effects on pavement response at high mid-depth pavement temperature and higher speeds. This is likely due to the use of a LEA program for development of the modulus-strain relationships used to develop the model.
- The comprehensive model was not able to accurately predict the moduli or strains measured during the 2009 test cycle for section N9, this is likely due to the differences in strain regimes between the two sections. Because the strain values measured in the 2009 test cycle were much lower than those measured during the 2006 test cycle and because section N9 in the 2009 test cycle had already been subjected to 10 million ESALs the differences in the strain regimes can be attributed to an increase in modulus due to aging. The in-place material properties that were used to develop and were applied to the comprehensive model were calculated based on density measurements made during construction in 2006, therefore, this model cannot account for effects of aging on in-place modulus. It can also be concluded that this model is not applicable for use in

overlay designs. However, it is possible that improvements in strain predictions could be seen if the in-place material properties associated to the aged section (2009) were to be used, this should be evaluated in future research.

7.3 RECOMMENDATIONS

Due to a limited number of test sections, the method developed in this dissertation was calibrated to a combined fourteen NCAT Test Track sections from 2006 and 2009 structural studies. Future research should be completed to validate the model using other cross-sections from future research cycles at the Test Track. Additionally, due to the differences found in sections N9 from 2006 and 2009, the use of in-place material properties for aged and in-service pavements, rather than initial in-place properties should be investigated for possible improvements in composite AC moduli predictions.

For implementation of this method it is necessary that the comprehensive model for composite AC modulus be used in conjunction with a LEA program. Therefore, this method can be used either as an alternative to the MEPDG when used with a LEA program (and appropriate transfer functions) or adopted for use in the MEPDG. As an alternative to the MEPDG, it could be used with a LEA program such as PerRoad which allows for predictions of strains based on seasonal moduli. The current MEPDG utilizes a LEA program to predict critical pavement responses from |E*| values. Therefore, to adopt this new method for predicting critical tensile strains, the comprehensive model could be used to select moduli values representative of the field conditions. This could be done by determining at what frequency the |E*| values from laboratory-derived master curves are equivalent to in-place composite moduli for design vehicle speeds with test temperatures used to represent mid-depth pavement temperature. From this, the

predicted composite AC moduli could be input at a level one design using the equivalent frequencies determined from the |E*| master curve.

Lastly, the inability to improve the fatigue cracking predictions from the MEPDG through local calibration was cited as reason to develop a new method for predicting critical tensile strains. Therefore, future research should be conducted to evaluate the effect of predicted strains from this new method on fatigue cracking performance predictions. In addition to an evaluation of the performance predictions, a calibration of the performance prediction models should also be conducted, using the strain predictions from this new method for predicting tensile strain.

REFERENCES

ARA Inc., Eres Consultants Division. Appendix CC-3, Updated Traffic Frequency Calculation for Asphalt Layers, *Guide for Mechanistic-Empirical Pavement Design of New and Rehabilitated Pavement Structures*, NCHRP 1-37A, 2003.

ARA Inc., Eres Division. Chapter 3. *Guide for Mechanistic-Empirical Pavement Design of New and Rehabilitated Pavement Structures*, NCHRP, pp. 3.3.108, March 2004.

ARA Inc., Eres Division. Part 2, Chapter 2: Material Characterization. *Guide for Mechanistic-Empirical Pavement Design of New and Rehabilitated Pavement Structures*, NCHRP, March 2004(a).

Andrei, D., M.W. Witczak, and W. Mirza. Appendix CC-4: Development of a Revised Predictive Model for the Dynamic (Complex) Modulus of Asphalt Mixtures. *Devlopment of the 2002 Guide for the Design of New and Rehabilitated Pavement Structures*, Final Document, NCHRP 1-37A, 1999.

Bari, J. and M.W. Witczak. Development of a New Revised Version of the Witczak E* Predictive Model for Hot Mix Asphalt Mixtures. *Journal of the Association of Asphalt*

Paving Technologists from the Proceedings of the Technical Sessions, Vol. 75, pp 381-423, Savannah, Ga, 2006.

Barksdale, R.D. Compressive Stress Pulse Times in Flexible Pavements for Use in Dynamic Testing. In *Highway Research Record 345*, HRB, National Research Council, Washington, D.C., 1971, pp 32-44.

Bonaquist, R.F. *MasterSovler Version 2.3*, released September 1, 2009.

Bonnaure, F., G. Gest, A. Gravois, and P. Uge. A New Method of Predicting the Stiffness of Asphalt Paving Mixtures. *Proceedings of the Association of Asphalt Paving Technologists,* Vol. 46, 1977, pp64-104.

Brown, S.F. Determination of Young's Modulus for Bituminous Materials in Pavement Design. In *Highway Research Record 431*, HRB, National Research Council, Washington, D.C., 1973, pp 38-49.

Chatti, K., H.B. Kim, K.K. Yun, J.P. Mahoney, and C.L. Monismith. Field Investigations into Effects of Vehicle Speed and Tire Pressure on Asphalt Concrete Pavement Strains. In *Transportation Research Record: Journal of the Transportation Research Board, No. 1539*, TRB, National Research Council, Washington, D.C., 1996, pp 66-71.

Christensen, Jr., D.W., T. Pellinen, and R.F. Bonaquist. Hirsch Model for Estimating the Modulus of Asphalt Concrete. *Journal of the Association of Asphalt Paving Technologists from the Proceedings of the Technical Sessions,* Vol. 72, pp 97-121, Lexington, KY, 2003.

Dongre, R., L. Myers, J. and D'Angelo. Conversion of Testing Frequency to Loading Time: Impact on Performance Predictions Obtained from The M-E Pavement Design Guide. In *Proceedings of the 85th Annual Meeting of the Transportation Research Board,* TRB, National Council, Washington D.C., 2006.

Dongre, R., L. Myers, J. D'Angelo, C. Paugh, and J. Gudimettla. Field Evaluation of Witczak and Hirsch Models for Predicting Dynamic Modulus of Hot-Mix Asphalt. *Journal of the Association of Asphalt Paving Technologists from the Proceedings of the Technical Sessions,* Vol. 74, pp 381-442, Long Beach, CA, 2005.

Ferry, J.D. *Viscoelastic Properties of Polymers,* 3rd Ed., New York, Wiley, 1980.

Flinstch, G.W., A. Loulizi, S.D. Diefenderfer, K.A. Galal, and B.K. Diefenderfer. *Asphalt Materials Characterization in Support of Implementation of the Proposed Mechanistic-Empirical Pavement Design Guide*. Virginia Department of Transportation Final Report. Report No. VTRC 07-CR10, 2007.
http://www.virginiadot.org/vtrc/main/online_reports/pdf/07-cr10.pdf

Garcia, G., and M.R. Thompson. Strain and Pulse Duration Considerations for Extended Hot Mix Asphalt Pavement Design. In *Transportation Research Record: Journal of Transportation Research Board, No. 2087*, Washington, D.C., 2008, pp. 3-12.

Hornyak, N. and J. A. Crovetti. Analysis of Load Pulse Durations for Marquette Interchange Instrumentation Project. In *Transportation Research Record: Journal of Transportation Research Board, No. 2094*, Washington, D.C., 2009, pp. 53-61.

Huang, B., X. Shu, and J. Bass. Investigation of Simple Performance Characteristics of Plant-Produced Asphalt Mixtures in Tennessee. In *Transportation Research Record: Journal of the Transportation Research Board No. 2057*, TRB, National Research Council, Washington, D.C., 2008, pp 140-148.

Leiva-Villacorta, F. Advanced Computing Techniques in Structural Evaluation of Flexible Pavement Using the Falling Weight Deflectometer. *Doctoral Dissertation*. Auburn University, 2012.

Loulizi, A., I.L. Al-Qadi, S. Lahouar, and T.E. Freeman. Measurement of Vertical Compressive Stress Pulse in Flexible Pavements: Representation for Dynamic Loading Tests. In *Transportation Research Record: Journal of the Transportation Research Board No. 1816*, Transportation Research Board of the National Academies, National Research Council, Washington D.C., 2002, pp. 125-136.

Marasteanu, M.O. and D.A. Anderson. Improved Model for Bitumen Rheological Characterization. Proceedings of *Eurobitume Workshop on Performance – Related Properties of Bituminous Binders*, 1-4, 1999.

Mateos, A. and M.B. Snyder. Validation of Flexible Pavement Structural Response Model with Data from the Minnesota Road Research Project. In *Transportation Research Record: Journal of the Transportation Research Board, No. 1806*, TRB, National Research Council, Washington, D.C., 2002, pp 19-29.

Mehta, Y.A and D.W. Christensen. Determination of the Linear Viscoelastic Limits of Asphalt Concrete at Low and Intermediate Temperatures. In *Journal of the Association of Asphalt Paving Technologists from the Proceedings of the Technical Sessions*, Vol. 69, 2001, pp. 281-312.

Mohammad, L.N., S. Saadeh, S. Obulareddy, and S. Cooper. Characterization of Louisiana Asphalt Mixtures Using Simple Performance Tests. In *Proceedings of the 86th Annual Meeting of the Transportation Research Board*, TRB, National Research Council, Washington, D.C., 2007.

Muench, S. HMA Performance Tests, *Pavement Interactive*. http://www.pavementinteractive.org/article/HMA-Performance-Tests/. Figure 5, 2003.

NCHRP, Independent Review of the Mechanistic-Empirical Pavement Design Guide and Software. In *Research Results Digest 307*. NCHRP Project 1-40A. National Cooperative Highway Research Program, National Research Council, Washington, D.C., 2006.

Papazian, H.S. The Response of Linear Viscoelastic Materials in the Frequency Domain with Emphasis on Asphaltic Concrete. In Proceedings of *1st International Conference on the Structural Design of Asphalt Pavements,* Ann Arbor, MI, 1962, pp. 454-463.

Pellinen, T.K. and M.W. Witczak. Stress Dependent Master Curve Construction for Dynamic (Complex) Modulus. In *Journal of the Association of Asphalt Paving Technologists from the Proceedings of the Technical Sessions,* Vol. 71, Colorado Springs, CO, 2002, pp. 315-344.

Ping, W.V., and Y. Xiao. Evaluation of the Dynamic Complex Modulus Test and Indirect Diametral Test for Implementing the AASHTO 2002 Design Guide for Pavement Structures in Florida. *Final Report*, Florida Department of Transportation, BC-352-12, Tallahassee, FL, 2007.

Priest, A.L. and D.H. Timm. Methodology and Calibration of Fatigue Transfer Functions for Mechanistic-Empirical Flexible Pavement Design, *Report No. 06-03,* National Center for Asphalt Technology, Auburn University, 2006.

Robbins, M.M. *An Investigation into Dynamic Modulus of Hot-Mix Asphalt and its Contributing Factors*, M.S. Thesis, Auburn University, 2009.

Tashman, L. and M. A. Elangovan. *Dynamic Modulus Test - Laboratory Investigation and Future Implementation in the State of Washington*. Washington State Department of Transportation Final Report. Final Research Report No. WA-RD 704.1, 2007. http://www.wsdot.wa.gov/research/reports/fullreports/704.1.pdf

Taylor, A. J. Mechanistic Characterization of Resilient Moduli for Unbound Pavement Layer Materials. *M.S. Thesis*, Auburn University, 2008.

Timm, D.H. and A.L. Priest. Wheel Wander at the NCAT Test Track. *Report No. 05-02*. National Center for Asphalt Technology, Auburn University, 2005.

Timm, D.H. and A.L. Priest. Flexible Pavement Fatigue Cracking and Measured Strain Response at the NCAT Test Track. *Proceedings of the 87th Annual Meeting of the Transportation Research Board*, Washington, D.C., 2008

Timm, D.H. Design, Construction and Instrumentation of the 2006 Test Track Structural Study, *Report No. 09-01*, National Center for Asphalt Technology, Auburn University, 2009.

Timm, D.H., G.A. Sholar, J. Kim and J.R. Willis. Forensic Investigation and Validation of Energy Ratio Concept, In *Transportation Research Record: Journal of the Transportation Research Board, No. 2127*. Transportation Research Board of the National Academies, Washington D.C., 2009, pp. 43-51.

Timm, D.H., N.H. Tran, A.J. Taylor, M.M. Robbins and R. Powell. Evaluation of Mixture Performance and Structural Capacity of Pavements Utilizing Shell Thiopave ®; Phase I: Mix Design, Laboratory Performance Evaluation and Structural Pavement Analysis and Design. *Report No. 09-05*, National Center for Asphalt Technology, Auburn University, 2009.

Timm, D.H., M.M. Robbins, J.R. Willis, A.J. Taylor and N.H. Tran. *Evaluation of* Mixture Performance and Structural Capacity of Pavements Utilizing Shell Thiopave ®; Phase II: Construction, Laboratory Evaluation and Full-Scale Testing of Thiopave ® Test Sections – One Year Report. *Report No. 11-03*, National Center for Asphalt Technology, Auburn University, 2011.

Timm, D.H., X. Guo, M.M. Robbins, and C. Wagner. M-E Calibration Studies at the NCAT Test Track. *Asphalt Pavement Magazine*. Volume 17, No. 5. September/October 2012, pp. 45-51.

Tran, N.H and K.D. Hall. An Examination of Strain Levels Used in the Dynamic Modulus Testing. In *Journal of the Association of Asphalt Paving Technologists from the Proceedings of the Technical Sessions,* Vol. 75, Savannah, GA, 2006, pp. 331-343.

Underwood, B.S., M. Ashouri and Y.R. Kim, Effect on Dynamic Modulus Measurement Protocol on Predicted Pavement Performance. *Journal of the Association of Asphalt Paving Technologists from the Proceedings of the Technical Sessions,* Vol. 80, pp 65-499, Tampa, FL, 2011.

Willis, J.R. and D.H. Timm. Field-based Strain Thresholds for Flexible Perpetual Pavements. *Report No. 09-09,* National Center for Asphalt Technology, Auburn University, 2009.

Witczak, M.W., K.Kaloush, T.K. Pellinen, M. El-Basyouny and H. von Quintus. *NCHRP 465: Simple Performance Test for Superpave Mix Design*. Transportation Research Board, National Research Council, Washington D.C., 2002.

APPENDIX A

AS-BUILT PROPERTIES

Table A.1: Surveyed lift thicknesses

		Lift Thickness (in.)					
Year	Section	Lift 1	Lift 2	Lift 3	Lift 4	Lift 5	Base
2006	N1	2.256	1.872	3.336			9.964
2006	N2	2.019	1.990	3.000			9.932
2006	N8	2.040	2.760	2.706	1.931		6.523
2006	N9	2.160	3.840	2.760	2.280	2.880	9.600
2009	N5	1.092	2.568	2.148	2.880		5.784
2009	N6	1.008	2.940	3.132			5.400
2009	N7	0.756	1.836	2.448			5.376
2009	N9	1.960	3.940	3.060	2.680	2.680	9.000
2009	N10	1.440	2.832	3.228			3.372
2009	N11	1.428	2.928	2.748			4.615
2009	S9	1.128	2.724	2.976			6.216
2009	S10	1.320	2.664	2.82			7.020
2009	S11	1.728	2.652	2.484			6.264
2009	S12	1.632	2.328	2.688			5.160

As Built Properties Recorded at Construction:

Quadrant: N
Section: 1
Sublot: 1

Laboratory Diary

General Desccription of Mix and Materials

Design Method:	Super
Compactive Effort:	100 gyrations
Binder Performance Grade:	67-22
Modifier Type:	NA
Aggregate Type:	Grn/Lms
Design Gradation Type:	Dense

Avg. Lab Properties of Plant Produced Mix

Sieve Size	Design	QC
1":	100	100
3/4":	100	100
1/2":	97	97
3/8":	82	82
No. 4:	60	59
No. 8:	50	49
No. 16:	38	39
No. 30:	28	30
No. 50:	19	22
No. 100:	12	14
No. 200:	7.0	8.8
Asphalt Content:	4.8	4.9
Pill Bulk Gravity:	2.413	2.431
TMD (Rice):	2.514	2.499
Avg Air Voids:	4.0	2.7
Avg VMA:	14.4	13.3

Construction Diary

Relevant Conditions for Construction

Completion Date:	September 29, 20(
24 Hour High Temperature (F):	73
24 Hour Low Temperature (F):	48
24 Hour Rainfall (in):	0.00
Planned Mill / Lift Thickness (in):	2.00
Paving Machine:	Roadtec

Plant Configuration and Placement Details

Component	% Setting
Asphalt Content (Plant Setting)	4.7
78 LaGrange Granite	45.0
M10 Columbus Granite	45.0
8910 Opelika Limestone Screenings	10.0

Approximate Length (ft):	200
Survey Mill / Lift Thickness (in):	2.1
Type of Tack Coat Utilized:	67-22
Target Tack Application Rate (gal/sy):	0.05
Avg Temperature at Plant (F):	305
Avg Section Compaction:	94.6%

General Notes:

1) Mixes are referenced by quadrant (E=East, N=North, W=West, and S=South), section number (sequential) and sublot (top=1);
2) The total research thickness of all mix performance sections ranges from 3/4 to 4 inches by design;
3) The total HMA thickness of all structural study sections (N1 through N10) ranges from 7 to 14 inches by design;
4) ARZ, TRZ and BRZ refer to gradations intended to pass above, through and below the restricted zone, respectively;
5) SMA and OGFC refer to stone matrix asphalt and open-graded friction course, respectively; and
6) VMA values computed from QC volumetrics are based on design values of Gsb (stockpile gravity testing is ongoing).

Quadrant: N
Section: 1
Sublot: 2

Laboratory Diary

General Desccription of Mix and Materials

Design Method:	Super
Compactive Effort:	100 gyrations
Binder Performance Grade:	67-22
Modifier Type:	NA
Aggregate Type:	Grn/Lms
Design Gradation Type:	Dense

Avg. Lab Properties of Plant Produced Mix

Sieve Size	Design	QC
1":	100	100
3/4":	100	100
1/2":	97	97
3/8":	82	85
No. 4:	60	61
No. 8:	50	51
No. 16:	38	39
No. 30:	28	31
No. 50:	19	22
No. 100:	12	14
No. 200:	7.0	8.7
Asphalt Content:	4.8	4.9
Pill Bulk Gravity:	2.413	2.384
TMD (Rice):	2.514	2.488
Avg Air Voids:	4.0	4.2
Avg VMA:	14.4	15.0

Construction Diary

Relevant Conditions for Construction

Completion Date:	September 28, 2006
24 Hour High Temperature (F):	84
24 Hour Low Temperature (F):	63
24 Hour Rainfall (in):	0.02
Planned Mill / Lift Thickness (in):	2.00
Paving Machine:	Roadtec

Plant Configuration and Placement Details

Component	% Setting
Asphalt Content (Plant Setting)	4.8
78 LaGrange Granite	43.0
M10 Columbus Granite	47.0
8910 Opelika Limestone Screenings	10.0
Approximate Length (ft):	200
Survey Mill / Lift Thickness (in):	1.9
Type of Tack Coat Utilized:	67-22
Target Tack Application Rate (gal/sy):	0.05
Avg Temperature at Plant (F):	300
Avg Section Compaction:	92.2%

General Notes:

1) Mixes are referenced by quadrant (E=East, N=North, W=West, and S=South), section number (sequential) and sublot (top=1);
2) The total research thickness of all mix performance sections ranges from 3/4 to 4 inches by design;
3) The total HMA thickness of all structural study sections (N1 through N10) ranges from 7 to 14 inches by design;
4) ARZ, TRZ and BRZ refer to gradations intended to pass above, through and below the restricted zone, respectively;
5) SMA and OGFC refer to stone matrix asphalt and open-graded friction course, respectively; and
6) VMA values computed from QC volumetrics are based on design values of Gsb (stockpile gravity testing is ongoing).

Quadrant: N
Section: 1
Sublot: 3

Laboratory Diary

General Desccription of Mix and Materials

Design Method:	Super
Compactive Effort:	60 gyrations
Binder Performance Grade:	67-22
Modifier Type:	NA
Aggregate Type:	Lms/Grn/Snd
Design Gradation Type:	Dense

Avg. Lab Properties of Plant Produced Mix

Sieve Size	Design	QC
1":	100	100
3/4":	94	96
1/2":	84	85
3/8":	72	74
No. 4:	53	53
No. 8:	45	43
No. 16:	36	36
No. 30:	28	26
No. 50:	15	14
No. 100:	8	8
No. 200:	5.0	5.4
Asphalt Content:	4.5	4.6
Pill Bulk Gravity:	2.468	2.415
TMD (Rice):	2.571	2.567
Avg Air Voids:	4.0	5.9
Avg VMA:	14.2	15.8

Construction Diary

Relevant Conditions for Construction

Completion Date:	September 27, 2006
24 Hour High Temperature (F):	81
24 Hour Low Temperature (F):	52
24 Hour Rainfall (in):	0.00
Planned Mill / Lift Thickness (in):	3.00
Paving Machine:	Roadtec

Plant Configuration and Placement Details

Component	% Setting
Asphalt Content (Plant Setting)	4.6
78 Opelika Limestone	33.0
57 Opelika Limestone	20.0
M10 Columbus Granite	25.0
Shorter Coarse Sand	22.0

Approximate Length (ft):	200
Survey Mill / Lift Thickness (in):	NA
Type of Tack Coat Utilized:	67-22
Target Tack Application Rate (gal/sy):	0.05
Avg Temperature at Plant (F):	315
Avg Section Compaction:	92.1%

General Notes:

1) Mixes are referenced by quadrant (E=East, N=North, W=West, and S=South), section number (sequential) and sublot (top=1);
2) The total research thickness of all mix performance sections ranges from 3/4 to 4 inches by design;
3) The total HMA thickness of all structural study sections (N1 through N10) ranges from 7 to 14 inches by design;
4) ARZ, TRZ and BRZ refer to gradations intended to pass above, through and below the restricted zone, respectively;
5) SMA and OGFC refer to stone matrix asphalt and open-graded friction course, respectively; and
6) VMA values computed from QC volumetrics are based on design values of Gsb (stockpile gravity testing is ongoing).

Quadrant: N
Section: 2
Sublot: 1

Laboratory Diary

General Desccription of Mix and Materials

Design Method:	Super
Compactive Effort:	100 gyrations
Binder Performance Grade:	76-22
Modifier Type:	SBS
Aggregate Type:	Grn/Lms
Design Gradation Type:	Dense

Avg. Lab Properties of Plant Produced Mix

Sieve Size	Design	QC
1":	100	100
3/4":	100	100
1/2":	97	97
3/8":	82	85
No. 4:	60	61
No. 8:	50	50
No. 16:	38	39
No. 30:	28	31
No. 50:	19	23
No. 100:	12	15
No. 200:	7.0	9.6
Asphalt Content:	4.8	4.8
Pill Bulk Gravity:	2.413	2.429
TMD (Rice):	2.514	2.499
Avg Air Voids:	4.0	2.8
Avg VMA:	14.4	13.3

Construction Diary

Relevant Conditions for Construction

Completion Date:	September 29, 2006
24 Hour High Temperature (F):	73
24 Hour Low Temperature (F):	48
24 Hour Rainfall (in):	0.00
Planned Mill / Lift Thickness (in):	2.00
Paving Machine:	Roadtec

Plant Configuration and Placement Details

Component	% Setting
Asphalt Content (Plant Setting)	4.7
78 LaGrange Granite	45.0
M10 Columbus Granite	45.0
8910 Opelika Limestone Screenings	10.0

Approximate Length (ft):	200
Survey Mill / Lift Thickness (in):	2.0
Type of Tack Coat Utilized:	67-22
Target Tack Application Rate (gal/sy):	0.05
Avg Temperature at Plant (F):	315
Avg Section Compaction:	95.0%

General Notes:

1) Mixes are referenced by quadrant (E=East, N=North, W=West, and S=South), section number (sequential) and sublot (top=1);
2) The total research thickness of all mix performance sections ranges from 3/4 to 4 inches by design;
3) The total HMA thickness of all structural study sections (N1 through N10) ranges from 7 to 14 inches by design;
4) ARZ, TRZ and BRZ refer to gradations intended to pass above, through and below the restricted zone, respectively;
5) SMA and OGFC refer to stone matrix asphalt and open-graded friction course, respectively; and
6) VMA values computed from QC volumetrics are based on design values of Gsb (stockpile gravity testing is ongoing).

Quadrant: N
Section: 2
Sublot: 2

Laboratory Diary

General Desccription of Mix and Materials

Design Method:	Super
Compactive Effort:	100 gyrations
Binder Performance Grade:	76-22
Modifier Type:	SBS
Aggregate Type:	Grn/Lms
Design Gradation Type:	Dense

Avg. Lab Properties of Plant Produced Mix

Sieve Size	Design	QC
1":	100	100
3/4":	100	100
1/2":	97	91
3/8":	82	82
No. 4:	60	62
No. 8:	50	50
No. 16:	38	41
No. 30:	28	29
No. 50:	19	16
No. 100:	12	10
No. 200:	7.0	6.6
Asphalt Content:	4.8	5.0
Pill Bulk Gravity:	2.413	2.384
TMD (Rice):	2.514	2.475
Avg Air Voids:	4.0	3.7
Avg VMA:	14.4	15.1

Construction Diary

Relevant Conditions for Construction

Completion Date:	September 28, 2006
24 Hour High Temperature (F):	84
24 Hour Low Temperature (F):	63
24 Hour Rainfall (in):	0.02
Planned Mill / Lift Thickness (in):	2.00
Paving Machine:	Roadtec

Plant Configuration and Placement Details

Component	% Setting
Asphalt Content (Plant Setting)	4.8
78 LaGrange Granite	43.0
M10 Columbus Granite	47.0
8910 Opelika Limestone Screenings	10.0

Approximate Length (ft):	200
Survey Mill / Lift Thickness (in):	2.0
Type of Tack Coat Utilized:	67-22
Target Tack Application Rate (gal/sy):	0.05
Avg Temperature at Plant (F):	310
Avg Section Compaction:	94.2%

General Notes:

1) Mixes are referenced by quadrant (E=East, N=North, W=West, and S=South), section number (sequential) and sublot (top=1);
2) The total research thickness of all mix performance sections ranges from 3/4 to 4 inches by design;
3) The total HMA thickness of all structural study sections (N1 through N10) ranges from 7 to 14 inches by design;
4) ARZ, TRZ and BRZ refer to gradations intended to pass above, through and below the restricted zone, respectively;
5) SMA and OGFC refer to stone matrix asphalt and open-graded friction course, respectively; and
6) VMA values computed from QC volumetrics are based on design values of Gsb (stockpile gravity testing is ongoing).

Quadrant: N
Section: 2
Sublot: 3

Laboratory Diary

General Desccription of Mix and Materials

Design Method:	Super
Compactive Effort:	60 gyrations
Binder Performance Grade:	67-22
Modifier Type:	NA
Aggregate Type:	Lms/Grn/Snd
Design Gradation Type:	Dense

Avg. Lab Properties of Plant Produced Mix

Sieve Size	Design	QC
1":	100	100
3/4":	94	96
1/2":	84	86
3/8":	72	75
No. 4:	53	54
No. 8:	45	45
No. 16:	36	36
No. 30:	28	26
No. 50:	15	14
No. 100:	8	9
No. 200:	5.0	5.6
Asphalt Content:	4.5	4.7
Pill Bulk Gravity:	2.468	2.424
TMD (Rice):	2.571	2.567
Avg Air Voids:	4.0	5.6
Avg VMA:	14.2	15.5

Construction Diary

Relevant Conditions for Construction

Completion Date:	September 27, 2006
24 Hour High Temperature (F):	81
24 Hour Low Temperature (F):	52
24 Hour Rainfall (in):	0.00
Planned Mill / Lift Thickness (in):	3.00
Paving Machine:	Roadtec

Plant Configuration and Placement Details

Component	% Setting
Asphalt Content (Plant Setting)	4.6
78 Opelika Limestone	33.0
57 Opelika Limestone	20.0
M10 Columbus Granite	25.0
Shorter Coarse Sand	22.0

Approximate Length (ft):	200
Survey Mill / Lift Thickness (in):	3.1
Type of Tack Coat Utilized:	67-22
Target Tack Application Rate (gal/sy):	0.05
Avg Temperature at Plant (F):	310
Avg Section Compaction:	94.9%

General Notes:

1) Mixes are referenced by quadrant (E=East, N=North, W=West, and S=South), section number (sequential) and sublot (top=1);
2) The total research thickness of all mix performance sections ranges from 3/4 to 4 inches by design;
3) The total HMA thickness of all structural study sections (N1 through N10) ranges from 7 to 14 inches by design;
4) ARZ, TRZ and BRZ refer to gradations intended to pass above, through and below the restricted zone, respectively;
5) SMA and OGFC refer to stone matrix asphalt and open-graded friction course, respectively; and
6) VMA values computed from QC volumetrics are based on design values of Gsb (stockpile gravity testing is ongoing).

Quadrant: N
Section: 8
Sublot: 1

Laboratory Diary

General Desccription of Mix and Materials

Design Method:	SMA
Compactive Effort:	50 gyrations
Binder Performance Grade:	76-28
Modifier Type:	SBS
Aggregate Type:	Granite
Design Gradation Type:	SMA

Avg. Lab Properties of Plant Produced Mix

Sieve Size	Design	QC
1":	100	100
3/4":	100	100
1/2":	97	93
3/8":	78	71
No. 4:	29	31
No. 8:	23	22
No. 16:	19	17
No. 30:	16	15
No. 50:	15	13
No. 100:	14	12
No. 200:	12.3	10.5
Asphalt Content:	6.8	6.9
Pill Bulk Gravity:	2.319	2.276
TMD (Rice):	2.414	2.397
Avg Air Voids:	3.9	5.0
Avg VMA:	17.9	15.6

Construction Diary

Relevant Conditions for Construction

Completion Date:	October 18, 2006
24 Hour High Temperature (F):	84
24 Hour Low Temperature (F):	70
24 Hour Rainfall (in):	0.00
Planned Mill / Lift Thickness (in):	2.00
Paving Machine:	Roadtec

Plant Configuration and Placement Details

Component	% Setting
Asphalt Content (Plant Setting)	6.1
Hanson 5/8 Chips	71.0
Hanson Screenings	14.0
GMI Sand	10.0
Flyash	5.0
Cellulose	0.3
Approximate Length (ft):	200
Survey Mill / Lift Thickness (in):	2.3
Type of Tack Coat Utilized:	67-22
Target Tack Application Rate (gal/sy):	0.05
Avg Temperature at Plant (F):	350
Avg Section Compaction:	91.8%

General Notes:

1) Mixes are referenced by quadrant (E=East, N=North, W=West, and S=South), section number (sequential) and sublot (top=1);
2) The total research thickness of all mix performance sections ranges from 3/4 to 4 inches by design;
3) The total HMA thickness of all structural study sections (N1 through N10) ranges from 7 to 14 inches by design;
4) ARZ, TRZ and BRZ refer to gradations intended to pass above, through and below the restricted zone, respectively;
5) SMA and OGFC refer to stone matrix asphalt and open-graded friction course, respectively; and
6) VMA values computed from QC volumetrics are based on design values of Gsb (stockpile gravity testing is ongoing).

Quadrant: N
Section: 8
Sublot: 2

Laboratory Diary

General Desccription of Mix and Materials

Design Method:	S3
Compactive Effort:	100 gyrations
Binder Performance Grade:	76-28
Modifier Type:	SBS
Aggregate Type:	Granite
Design Gradation Type:	Dense

Avg. Lab Properties of Plant Produced Mix

Sieve Size	Design	QC
1":	100	100
3/4":	95	95
1/2":	81	83
3/8":	72	79
No. 4:	64	64
No. 8:	44	43
No. 16:	30	31
No. 30:	22	24
No. 50:	15	17
No. 100:	8	10
No. 200:	5.4	6.7
Asphalt Content:	4.3	5.2
Pill Bulk Gravity:	2.415	2.426
TMD (Rice):	2.498	2.496
Avg Air Voids:	3.3	2.8
Avg VMA:	13.5	10.4

Construction Diary

Relevant Conditions for Construction

Completion Date:	October 18, 2006
24 Hour High Temperature (F):	84
24 Hour Low Temperature (F):	70
24 Hour Rainfall (in):	0.00
Planned Mill / Lift Thickness (in):	3.00
Paving Machine:	Roadtec

Plant Configuration and Placement Details

Component	% Setting
Asphalt Content (Plant Setting)	4.1
Hanson 1 Chips	30.0
Hanson Screenings	25.0
Dolese Screenings	8.0
Martin Marietta Stone Sand	27.0
GMI Sand	10.0
Approximate Length (ft):	200
Survey Mill / Lift Thickness (in):	3.0
Type of Tack Coat Utilized:	67-22
Target Tack Application Rate (gal/sy):	0.05
Avg Temperature at Plant (F):	340
Avg Section Compaction:	93.6%

General Notes:

1) Mixes are referenced by quadrant (E=East, N=North, W=West, and S=South), section number (sequential) and sublot (top=1);
2) The total research thickness of all mix performance sections ranges from 3/4 to 4 inches by design;
3) The total HMA thickness of all structural study sections (N1 through N10) ranges from 7 to 14 inches by design;
4) ARZ, TRZ and BRZ refer to gradations intended to pass above, through and below the restricted zone, respectively;
5) SMA and OGFC refer to stone matrix asphalt and open-graded friction course, respectively; and
6) VMA values computed from QC volumetrics are based on design values of Gsb (stockpile gravity testing is ongoing).

Quadrant: N
Section: 8
Sublot: 3

Laboratory Diary

General Desccription of Mix and Materials

Design Method:	S3
Compactive Effort:	100 gyrations
Binder Performance Grade:	64-22
Modifier Type:	NA
Aggregate Type:	Granite
Design Gradation Type:	Dense

Avg. Lab Properties of Plant Produced Mix

Sieve Size	Design	QC
1":	100	100
3/4":	95	95
1/2":	81	85
3/8":	72	80
No. 4:	64	64
No. 8:	44	43
No. 16:	30	31
No. 30:	22	24
No. 50:	15	17
No. 100:	8	10
No. 200:	5.4	7.0
Asphalt Content:	4.3	4.9
Pill Bulk Gravity:	2.415	2.393
TMD (Rice):	2.498	2.503
Avg Air Voids:	3.3	4.4
Avg VMA:	13.5	11.3

Construction Diary

Relevant Conditions for Construction

Completion Date:	October 16, 2006
24 Hour High Temperature (F):	64
24 Hour Low Temperature (F):	55
24 Hour Rainfall (in):	0.01
Planned Mill / Lift Thickness (in):	3.00
Paving Machine:	Roadtec

Plant Configuration and Placement Details

Component	% Setting
Asphalt Content (Plant Setting)	4.3
Hanson 1 Chips	30.0
Hanson Screenings	25.0
Dolese Screenings	10.0
Martin Marietta Stone Sand	25.0
GMI Sand	10.0
Approximate Length (ft):	200
Survey Mill / Lift Thickness (in):	2.9
Type of Tack Coat Utilized:	67-22
Target Tack Application Rate (gal/sy):	0.05
Avg Temperature at Plant (F):	345
Avg Section Compaction:	92.9%

General Notes:

1) Mixes are referenced by quadrant (E=East, N=North, W=West, and S=South), section number (sequential) and sublot (top=1);
2) The total research thickness of all mix performance sections ranges from 3/4 to 4 inches by design;
3) The total HMA thickness of all structural study sections (N1 through N10) ranges from 7 to 14 inches by design;
4) ARZ, TRZ and BRZ refer to gradations intended to pass above, through and below the restricted zone, respectively;
5) SMA and OGFC refer to stone matrix asphalt and open-graded friction course, respectively; and
6) VMA values computed from QC volumetrics are based on design values of Gsb (stockpile gravity testing is ongoing).

Quadrant: N
Section: 8
Sublot: 4

Laboratory Diary

General Desccription of Mix and Materials

Design Method:	RBL
Compactive Effort:	50 gyrations
Binder Performance Grade:	64-22
Modifier Type:	NA
Aggregate Type:	Granite
Design Gradation Type:	Dense

Avg. Lab Properties of Plant Produced Mix

Sieve Size	Design	QC
1":	100	100
3/4":	100	100
1/2":	99	97
3/8":	88	87
No. 4:	58	61
No. 8:	39	39
No. 16:	25	26
No. 30:	18	19
No. 50:	13	15
No. 100:	10	12
No. 200:	8.1	10.5
Asphalt Content:	6.0	7.1
Pill Bulk Gravity:	2.400	2.374
TMD (Rice):	2.452	2.424
Avg Air Voids:	2.0	2.1
Avg VMA:	14.6	12.6

Construction Diary

Relevant Conditions for Construction

Completion Date:	October 13, 2006
24 Hour High Temperature (F):	66
24 Hour Low Temperature (F):	48
24 Hour Rainfall (in):	0.00
Planned Mill / Lift Thickness (in):	2.00
Paving Machine:	Roadtec

Plant Configuration and Placement Details

Component	% Setting
Asphalt Content (Plant Setting)	6.2
Hanson 5/8 Chips	35.0
Hanson Screenings	20.0
Dolese Screenings	45.0

Approximate Length (ft):	200
Survey Mill / Lift Thickness (in):	1.9
Type of Tack Coat Utilized:	67-22
Target Tack Application Rate (gal/sy):	0.05
Avg Temperature at Plant (F):	345
Avg Section Compaction:	97.2%

General Notes:

1) Mixes are referenced by quadrant (E=East, N=North, W=West, and S=South), section number (sequential) and sublot (top=1);
2) The total research thickness of all mix performance sections ranges from 3/4 to 4 inches by design;
3) The total HMA thickness of all structural study sections (N1 through N10) ranges from 7 to 14 inches by design;
4) ARZ, TRZ and BRZ refer to gradations intended to pass above, through and below the restricted zone, respectively;
5) SMA and OGFC refer to stone matrix asphalt and open-graded friction course, respectively; and
6) VMA values computed from QC volumetrics are based on design values of Gsb (stockpile gravity testing is ongoing).

Quadrant: N
Section: 9
Sublot: 1

Laboratory Diary

General Description of Mix and Materials

Design Method:	SMA
Compactive Effort:	50 gyrations
Binder Performance Grade:	76-28
Modifier Type:	SBS
Aggregate Type:	Granite
Design Gradation Type:	SMA

Avg. Lab Properties of Plant Produced Mix

Sieve Size	Design	QC
1":	100	100
3/4":	100	100
1/2":	97	94
3/8":	78	72
No. 4:	29	32
No. 8:	23	23
No. 16:	19	18
No. 30:	16	15
No. 50:	15	13
No. 100:	14	12
No. 200:	12.3	10.9
Asphalt Content:	6.8	7.0
Pill Bulk Gravity:	2.319	2.279
TMD (Rice):	2.414	2.397
Avg Air Voids:	3.9	4.9
Avg VMA:	17.9	15.5

Construction Diary

Relevant Conditions for Construction

Completion Date:	October 18, 2006
24 Hour High Temperature (F):	84
24 Hour Low Temperature (F):	70
24 Hour Rainfall (in):	0.00
Planned Mill / Lift Thickness (in):	2.00
Paving Machine:	Roadtec

Plant Configuration and Placement Details

Component	% Setting
Asphalt Content (Plant Setting)	6.1
Hanson 5/8 Chips	71.0
Hanson Screenings	14.0
GMI Sand	10.0
Flyash	5.0
Cellulose	0.3
Approximate Length (ft):	197
Survey Mill / Lift Thickness (in):	2.0
Type of Tack Coat Utilized:	67-22
Target Tack Application Rate (gal/sy):	0.05
Avg Temperature at Plant (F):	350
Avg Section Compaction:	93.0%

General Notes:

1) Mixes are referenced by quadrant (E=East, N=North, W=West, and S=South), section number (sequential) and sublot (top=1);
2) The total research thickness of all mix performance sections ranges from 3/4 to 4 inches by design;
3) The total HMA thickness of all structural study sections (N1 through N10) ranges from 7 to 14 inches by design;
4) ARZ, TRZ and BRZ refer to gradations intended to pass above, through and below the restricted zone, respectively;
5) SMA and OGFC refer to stone matrix asphalt and open-graded friction course, respectively; and
6) VMA values computed from QC volumetrics are based on design values of Gsb (stockpile gravity testing is ongoing).

Quadrant: N
Section: 9
Sublot: 2

Laboratory Diary

General Description of Mix and Materials

Design Method:	S3
Compactive Effort:	100 gyrations
Binder Performance Grade:	76-28
Modifier Type:	SBS
Aggregate Type:	Granite
Design Gradation Type:	Dense

Avg. Lab Properties of Plant Produced Mix

Sieve Size	Design	QC
1":	100	99
3/4":	95	96
1/2":	81	86
3/8":	72	82
No. 4:	64	67
No. 8:	44	45
No. 16:	30	32
No. 30:	22	25
No. 50:	15	17
No. 100:	8	10
No. 200:	5.4	7.0
Asphalt Content:	4.3	5.1
Pill Bulk Gravity:	2.415	2.422
TMD (Rice):	2.498	2.496
Avg Air Voids:	3.3	3.0
Avg VMA:	13.5	10.5

Construction Diary

Relevant Conditions for Construction

Completion Date:	October 18, 2006
24 Hour High Temperature (F):	84
24 Hour Low Temperature (F):	70
24 Hour Rainfall (in):	0.00
Planned Mill / Lift Thickness (in):	3.00
Paving Machine:	Roadtec

Plant Configuration and Placement Details

Component	% Setting
Asphalt Content (Plant Setting)	4.1
Hanson 1 Chips	30.0
Hanson Screenings	25.0
Dolese Screenings	8.0
Martin Marietta Stone Sand	27.0
GMI Sand	10.0
Approximate Length (ft):	197
Survey Mill / Lift Thickness (in):	3.5
Type of Tack Coat Utilized:	67-22
Target Tack Application Rate (gal/sy):	0.05
Avg Temperature at Plant (F):	340
Avg Section Compaction:	92.9%

General Notes:

1) Mixes are referenced by quadrant (E=East, N=North, W=West, and S=South), section number (sequential) and sublot (top=1);
2) The total research thickness of all mix performance sections ranges from 3/4 to 4 inches by design;
3) The total HMA thickness of all structural study sections (N1 through N10) ranges from 7 to 14 inches by design;
4) ARZ, TRZ and BRZ refer to gradations intended to pass above, through and below the restricted zone, respectively;
5) SMA and OGFC refer to stone matrix asphalt and open-graded friction course, respectively; and
6) VMA values computed from QC volumetrics are based on design values of Gsb (stockpile gravity testing is ongoing).

Quadrant: N
Section: 9
Sublot: 3

Laboratory Diary

General Description of Mix and Materials

Design Method:	S3
Compactive Effort:	100 gyrations
Binder Performance Grade:	64-22
Modifier Type:	NA
Aggregate Type:	Granite
Design Gradation Type:	Dense

Avg. Lab Properties of Plant Produced Mix

Sieve Size	Design	QC
1":	100	100
3/4":	95	96
1/2":	81	84
3/8":	72	80
No. 4:	64	66
No. 8:	44	45
No. 16:	30	32
No. 30:	22	24
No. 50:	15	17
No. 100:	8	10
No. 200:	5.4	6.5
Asphalt Content:	4.3	5.0
Pill Bulk Gravity:	2.415	2.419
TMD (Rice):	2.498	2.503
Avg Air Voids:	3.3	3.4
Avg VMA:	13.5	10.4

Construction Diary

Relevant Conditions for Construction

Completion Date:	October 16, 2006
24 Hour High Temperature (F):	64
24 Hour Low Temperature (F):	55
24 Hour Rainfall (in):	0.01
Planned Mill / Lift Thickness (in):	3.00
Paving Machine:	Roadtec

Plant Configuration and Placement Details

Component	% Setting
Asphalt Content (Plant Setting)	4.3
Hanson 1 Chips	30.0
Hanson Screenings	25.0
Dolese Screenings	10.0
Martin Marietta Stone Sand	25.0
GMI Sand	10.0

Approximate Length (ft):	197
Survey Mill / Lift Thickness (in):	3.1
Type of Tack Coat Utilized:	67-22
Target Tack Application Rate (gal/sy):	0.05
Avg Temperature at Plant (F):	345
Avg Section Compaction:	95.1%

General Notes:

1) Mixes are referenced by quadrant (E=East, N=North, W=West, and S=South), section number (sequential) and sublot (top=1);
2) The total research thickness of all mix performance sections ranges from 3/4 to 4 inches by design;
3) The total HMA thickness of all structural study sections (N1 through N10) ranges from 7 to 14 inches by design;
4) ARZ, TRZ and BRZ refer to gradations intended to pass above, through and below the restricted zone, respectively;
5) SMA and OGFC refer to stone matrix asphalt and open-graded friction course, respectively; and
6) VMA values computed from QC volumetrics are based on design values of Gsb (stockpile gravity testing is ongoing).

Quadrant: N
Section: 9
Sublot: 4

Laboratory Diary

General Description of Mix and Materials

Design Method:	S3
Compactive Effort:	100 gyrations
Binder Performance Grade:	64-22
Modifier Type:	NA
Aggregate Type:	Granite
Design Gradation Type:	Dense

Avg. Lab Properties of Plant Produced Mix

Sieve Size	Design	QC
1":	100	100
3/4":	95	93
1/2":	81	81
3/8":	72	76
No. 4:	63	61
No. 8:	43	42
No. 16:	29	30
No. 30:	22	23
No. 50:	15	17
No. 100:	7	10
No. 200:	4.9	7.2
Asphalt Content:	4.3	4.6
Pill Bulk Gravity:	2.415	2.411
TMD (Rice):	2.498	2.507
Avg Air Voids:	3.3	3.8
Avg VMA:	13.5	10.4

Construction Diary

Relevant Conditions for Construction

Completion Date:	October 16, 2006
24 Hour High Temperature (F):	64
24 Hour Low Temperature (F):	55
24 Hour Rainfall (in):	0.01
Planned Mill / Lift Thickness (in):	3.00
Paving Machine:	Roadtec

Plant Configuration and Placement Details

Component	% Setting
Asphalt Content (Plant Setting)	4.0
Hanson 1 Chips	30.0
Hanson Screenings	25.0
Dolese Screenings	10.0
Martin Marietta Stone Sand	25.0
GMI Sand	10.0

Approximate Length (ft):	197
Survey Mill / Lift Thickness (in):	2.6
Type of Tack Coat Utilized:	67-22
Target Tack Application Rate (gal/sy):	0.05
Avg Temperature at Plant (F):	350
Avg Section Compaction:	93.9%

General Notes:

1) Mixes are referenced by quadrant (E=East, N=North, W=West, and S=South), section number (sequential) and sublot (top=1);
2) The total research thickness of all mix performance sections ranges from 3/4 to 4 inches by design;
3) The total HMA thickness of all structural study sections (N1 through N10) ranges from 7 to 14 inches by design;
4) ARZ, TRZ and BRZ refer to gradations intended to pass above, through and below the restricted zone, respectively;
5) SMA and OGFC refer to stone matrix asphalt and open-graded friction course, respectively; and
6) VMA values computed from QC volumetrics are based on design values of Gsb (stockpile gravity testing is ongoing).

Quadrant: N
Section: 9
Sublot: 5

Laboratory Diary

General Descoription of Mix and Materials

Design Method:	RBL
Compactive Effort:	50 gyrations
Binder Performance Grade:	64-22
Modifier Type:	NA
Aggregate Type:	Granite
Design Gradation Type:	Dense

Avg. Lab Properties of Plant Produced Mix

Sieve Size	Design	QC
1":	100	100
3/4":	100	100
1/2":	99	96
3/8":	88	85
No. 4:	58	59
No. 8:	39	38
No. 16:	25	26
No. 30:	18	19
No. 50:	13	15
No. 100:	10	13
No. 200:	8.1	10.5
Asphalt Content:	6.0	7.0
Pill Bulk Gravity:	2.400	2.384
TMD (Rice):	2.452	2.424
Avg Air Voids:	2.0	1.7
Avg VMA:	14.6	12.2

Construction Diary

Relevant Conditions for Construction

Completion Date:	October 13, 2006
24 Hour High Temperature (F):	66
24 Hour Low Temperature (F):	48
24 Hour Rainfall (in):	0.00
Planned Mill / Lift Thickness (in):	3.00
Paving Machine:	Roadtec

Plant Configuration and Placement Details

Component	% Setting
Asphalt Content (Plant Setting)	6.2
Hanson 5/8 Chips	35.0
Hanson Screenings	20.0
Dolese Screenings	45.0

Approximate Length (ft):	197
Survey Mill / Lift Thickness (in):	3.2
Type of Tack Coat Utilized:	67-22
Target Tack Application Rate (gal/sy):	0.05
Avg Temperature at Plant (F):	345
Avg Section Compaction:	94.4%

General Notes:

1) Mixes are referenced by quadrant (E=East, N=North, W=West, and S=South), section number (sequential) and sublot (top=1);
2) The total research thickness of all mix performance sections ranges from 3/4 to 4 inches by design;
3) The total HMA thickness of all structural study sections (N1 through N10) ranges from 7 to 14 inches by design;
4) ARZ, TRZ and BRZ refer to gradations intended to pass above, through and below the restricted zone, respectively;
5) SMA and OGFC refer to stone matrix asphalt and open-graded friction course, respectively; and
6) VMA values computed from QC volumetrics are based on design values of Gsb (stockpile gravity testing is ongoing).

Quadrant: N
Section: 5
Sublot: 1

Laboratory Diary

General Descciption of Mix and Materials

Design Method:	Super
Compactive Effort:	80 gyrations
Binder Performance Grade:	76-22
Modifier Type:	SBS
Aggregate Type:	Grn/Sand/Lms
Design Gradation Type:	Fine

Avg. Lab Properties of Plant Produced Mix

Sieve Size	Design	QC
25 mm (1"):	100	100
19 mm (3/4"):	100	100
12.5 mm (1/2"):	100	100
9.5 mm (3/8"):	100	100
4.75 mm (#4):	78	83
2.36 mm (#8):	60	62
1.18 mm (#16):	46	47
0.60 mm (#30):	31	33
0.30 mm (#50):	16	16
0.15 mm (#100):	10	10
0.075 mm (#200):	5.8	6.4
Binder Content (Pb):	5.8	6.1
Eff. Binder Content (Pbe):	5.1	5.4
Dust-to-Binder Ratio:	1.1	1.2
Rice Gravity (Gmm):	2.483	2.472
Avg. Bulk Gravity (Gmb):	2.384	2.380
Avg Air Voids (Va):	4.0	3.7
Agg. Bulk Gravity (Gsb):	2.667	2.671
Avg VMA:	15.8	16.3
Avg. VFA:	75	77

Construction Diary

Relevant Conditions for Construction

Completion Date:	August 3, 2009
24 Hour High Temperature (F):	91
24 Hour Low Temperature (F):	72
24 Hour Rainfall (in):	0.00
Planned Subot Lift Thickness (in):	1.3
Paving Machine:	Roadtec

Plant Configuration and Placement Details

Component	% Setting
Asphalt Content (Plant Setting)	6.2
89 Columbus Granite	36.0
8910 Opelika Limestone Screenings	23.0
M10 Columbus Granite	13.0
Shorter Coarse Sand	28.0
As-Built Sublot Lift Thickness (in):	1.3
Total Thickness of All 2009 Sublots (in):	9.0
Approx. Underlying HMA Thickness (in):	0.0
Type of Tack Coat Utilized:	PG67-22
Target Tack Application Rate (gal/sy):	0.05
Approx. Avg. Temperature at Plant (F):	340
Avg. Measured Mat Compaction:	94.1%

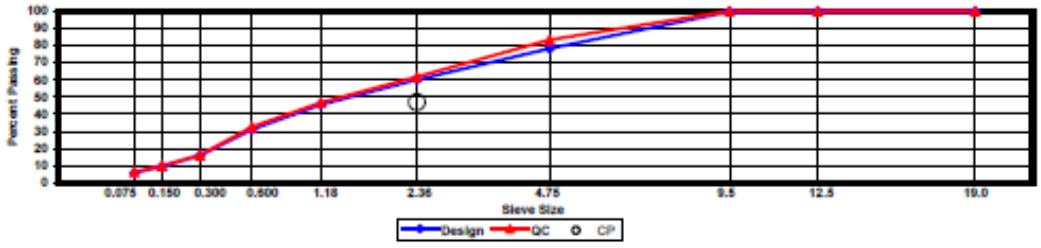

General Notes:

1) Mixes are referenced by quadrant (E=East, N=North, W=West, and S=South), section # (sequential) and sublot (top=1);
3) The total HMA thickness of all structural study sections (N1-N11 and S8-S12) ranges from 5-3/4 to 14 inches by design;
3) All non-structural sections are supprted by a uniform perpetual foundation in order to study surface mix performance;
4) SMA and OGFC refer to stone matrix asphalt and open-graded friction course, respectively; and
5) All liquid asphalt purchased for use in Track reconstruction contained LOF 6500 antistrip additive at a rate of 0.5 percent

Quadrant: N
Section: 5
Sublot: 2

Laboratory Diary

General Desccription of Mix and Materials

Design Method:	WMA-T
Compactive Effort:	60 gyrations
Binder Performance Grade:	67-22
Modifier Type:	Thiopave
Aggregate Type:	Lms/Sand/Grn
Design Gradation Type:	Fine

Avg. Lab Properties of Plant Produced Mix

Sieve Size	Design	QC
25 mm (1"):	100	100
19 mm (3/4"):	93	90
12.5 mm (1/2"):	82	81
9.5 mm (3/8"):	71	73
4.75 mm (#4):	52	58
2.36 mm (#8):	45	46
1.18 mm (#16):	35	36
0.60 mm (#30):	24	24
0.30 mm (#50):	12	12
0.15 mm (#100):	7	8
0.075 mm (#200):	3.9	4.7
Binder Content (Pb):	6.2	5.7
Eff. Binder Content (Pbe):	5.6	5.3
Dust-to-Binder Ratio:	0.7	0.9
Rice Gravity (Gmm):	2.581	2.554
Avg. Bulk Gravity (Gmb):	2.491	2.439
Avg Air Voids (Va):	3.5	4.5
Agg. Bulk Gravity (Gsb):	2.737	2.772
Avg VMA:	14.6	17.1
Avg. VFA:	76	74

Construction Diary

Relevant Conditions for Construction

Completion Date:	July 24, 2009
24 Hour High Temperature (F):	90
24 Hour Low Temperature (F):	68
24 Hour Rainfall (in):	0.00
Planned Subot Lift Thickness (in):	2.8
Paving Machine:	Roadtec

Plant Configuration and Placement Details

Component	% Setting
Asphalt Content (Plant Setting)	4.0
78 Opelika Limestone	30.0
57 Opelika Limestone	18.0
M10 Columbus Granite	25.0
Shorter Coarse Sand	27.0
Thiopave	40.0
Compaction Agent	1.0
As-Built Sublot Lift Thickness (in):	2.8
Total Thickness of All 2009 Sublots (in):	9.0
Approx. Underlying HMA Thickness (in):	0.0
Type of Tack Coat Utilized:	NTSS-1HM
Target Tack Application Rate (gal/sy):	0.05
Approx. Avg. Temperature at Plant (F):	275
Avg. Measured Mat Compaction:	93.0%

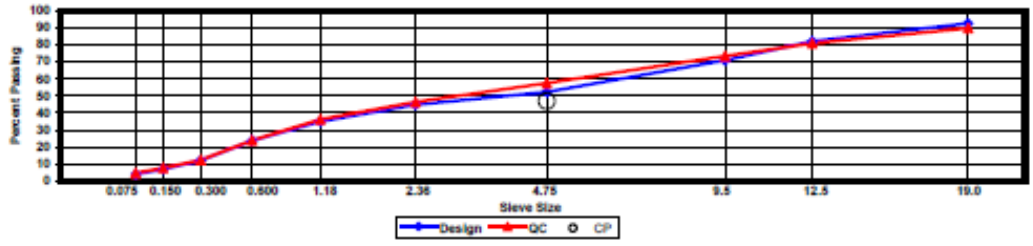

General Notes:

1) Mixes are referenced by quadrant (E=East, N=North, W=West, and S=South), section # (sequential) and sublot (top=1);
3) The total HMA thickness of all structural study sections (N1-N11 and S8-S12) ranges from 5-3/4 to 14 inches by design;
3) All non-structural sections are supprted by a uniform perpetual foundation in order to study surface mix performance;
4) SMA and OGFC refer to stone matrix asphalt and open-graded friction course, respectively; and
5) All liquid asphalt purchased for use in Track reconstruction contained LOF 6500 antistrip additive at a rate of 0.5 percent

Quadrant: N
Section: 5
Sublot: 3

Laboratory Diary

General Description of Mix and Materials

Design Method:	WMA-T
Compactive Effort:	60 gyrations
Binder Performance Grade:	67-22
Modifier Type:	Thiopave
Aggregate Type:	Lms/Sand/Gm
Design Gradation Type:	Fine

Avg. Lab Properties of Plant Produced Mix

Sieve Size	Design	QC
25 mm (1"):	100	98
19 mm (3/4"):	93	92
12.5 mm (1/2"):	82	82
9.5 mm (3/8"):	71	72
4.75 mm (#4):	52	54
2.36 mm (#8):	45	44
1.18 mm (#16):	35	34
0.60 mm (#30):	24	23
0.30 mm (#50):	12	12
0.15 mm (#100):	7	8
0.075 mm (#200):	3.9	4.9
Binder Content (Pb):	6.2	5.6
Eff. Binder Content (Pbe):	5.6	5.1
Dust-to-Binder Ratio:	0.7	1.0
Rice Gravity (Gmm):	2.581	2.553
Avg. Bulk Gravity (Gmb):	2.491	2.440
Avg Air Voids (Va):	3.5	4.4
Agg. Bulk Gravity (Gsb):	2.737	2.762
Avg VMA:	14.6	16.6
Avg. VFA:	76	73

Construction Diary

Relevant Conditions for Construction

Completion Date:	July 23, 2009
24 Hour High Temperature (F):	89
24 Hour Low Temperature (F):	74
24 Hour Rainfall (in):	0.00
Planned Subot Lift Thickness (in):	2.3
Paving Machine:	Roadtec

Plant Configuration and Placement Details

Component	% Setting
Asphalt Content (Plant Setting)	4.0
78 Opelika Limestone	30.0
57 Opelika Limestone	18.0
M10 Columbus Granite	25.0
Shorter Coarse Sand	27.0
Thiopave	40.0
Compaction Agent	1.0
As-Built Sublot Lift Thickness (in):	2.0
Total Thickness of All 2009 Sublots (in):	9.0
Approx. Underlying HMA Thickness (in):	0.0
Type of Tack Coat Utilized:	NTSS-1HM
Target Tack Application Rate (gal/sy):	0.07
Approx. Avg. Temperature at Plant (F):	275
Avg. Measured Mat Compaction:	92.9%

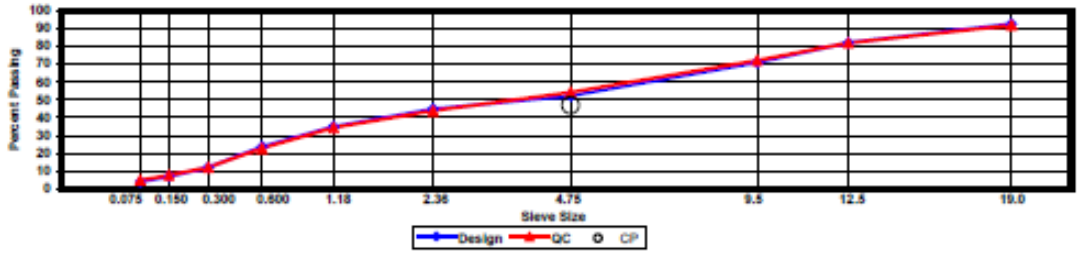

General Notes:

1) Mixes are referenced by quadrant (E=East, N=North, W=West, and S=South), section # (sequential) and sublot (top=1);
3) The total HMA thickness of all structural study sections (N1-N11 and S8-S12) ranges from 5-3/4 to 14 inches by design;
3) All non-structural sections are supprted by a uniform perpetual foundation in order to study surface mix performance;
4) SMA and OGFC refer to stone matrix asphalt and open-graded friction course, respectively; and
5) All liquid asphalt purchased for use in Track reconstruction contained LOF 6500 antistrip additive at a rate of 0.5 percent

Quadrant: N
Section: 5
Sublot: 4

Laboratory Diary

General Description of Mix and Materials

Design Method:	WMA-T
Compactive Effort:	60 gyrations
Binder Performance Grade:	67-22
Modifier Type:	Thiopave
Aggregate Type:	Lms/Sand/Grn
Design Gradation Type:	Fine

Avg. Lab Properties of Plant Produced Mix

Sieve Size	Design	QC
25 mm (1"):	100	100
19 mm (3/4"):	93	93
12.5 mm (1/2"):	82	82
9.5 mm (3/8"):	71	73
4.75 mm (#4):	52	55
2.36 mm (#8):	45	44
1.18 mm (#16):	35	35
0.60 mm (#30):	24	24
0.30 mm (#50):	12	12
0.15 mm (#100):	7	8
0.075 mm (#200):	3.9	4.8
Binder Content (Pb):	6.3	6.2
Eff. Binder Content (Pbe):	5.8	5.8
Dust-to-Binder Ratio:	0.7	0.8
Rice Gravity (Gmm):	2.558	2.518
Avg. Bulk Gravity (Gmb):	2.507	2.459
Avg Air Voids (Va):	2.0	2.3
Agg. Bulk Gravity (Gsb):	2.737	2.749
Avg VMA:	14.1	16.1
Avg. VFA:	86	85

Construction Diary

Relevant Conditions for Construction

Completion Date:	July 23, 2009
24 Hour High Temperature (F):	89
24 Hour Low Temperature (F):	74
24 Hour Rainfall (in):	0.00
Planned Subot Lift Thickness (in):	2.8
Paving Machine:	Roadtec

Plant Configuration and Placement Details

Component	% Setting
Asphalt Content (Plant Setting)	5.1
78 Opelika Limestone	30.0
57 Opelika Limestone	18.0
M10 Columbus Granite	25.0
Shorter Coarse Sand	27.0
Thiopave	30.0
Compaction Agent	1.0
As-Built Sublot Lift Thickness (in):	2.9
Total Thickness of All 2009 Sublots (in):	9.0
Approx. Underlying HMA Thickness (in):	0.0
Type of Tack Coat Utilized:	NA
Target Tack Application Rate (gal/sy):	NA
Approx. Avg. Temperature at Plant (F):	275
Avg. Measured Mat Compaction:	93.6%

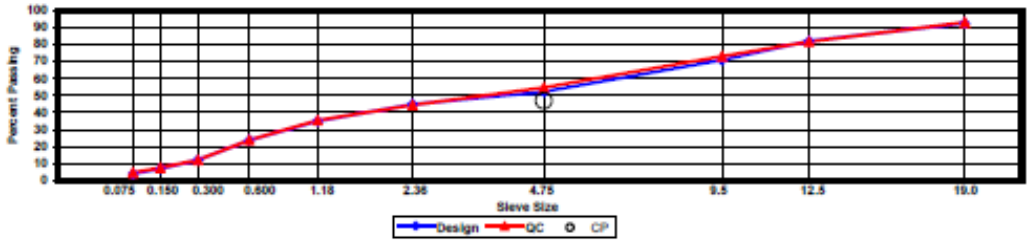

General Notes:

1) Mixes are referenced by quadrant (E=East, N=North, W=West, and S=South), section # (sequential) and sublot (top=1);
3) The total HMA thickness of all structural study sections (N1-N11 and S8-S12) ranges from 5-3/4 to 14 inches by design;
3) All non-structural sections are supprted by a uniform perpetual foundation in order to study surface mix performance;
4) SMA and OGFC refer to stone matrix asphalt and open-graded friction course, respectively; and
5) All liquid asphalt purchased for use in Track reconstruction contained LOF 6500 antistrip additive at a rate of 0.5 percent

Quadrant: N
Section: 6
Sublot: 1

Laboratory Diary

General Description of Mix and Materials

Design Method:	Super
Compactive Effort:	80 gyrations
Binder Performance Grade:	76-22
Modifier Type:	SBS
Aggregate Type:	Grn/Sand/Lms
Design Gradation Type:	Fine

Avg. Lab Properties of Plant Produced Mix

Sieve Size	Design	QC
25 mm (1"):	100	100
19 mm (3/4"):	100	100
12.5 mm (1/2"):	100	100
9.5 mm (3/8"):	100	100
4.75 mm (#4):	78	82
2.36 mm (#8):	60	55
1.18 mm (#16):	46	45
0.60 mm (#30):	31	30
0.30 mm (#50):	16	16
0.15 mm (#100):	10	10
0.075 mm (#200):	5.8	6.4
Binder Content (Pb):	5.8	6.1
Eff. Binder Content (Pbe):	5.1	5.4
Dust-to-Binder Ratio:	1.1	1.2
Rice Gravity (Gmm):	2.483	2.466
Avg. Bulk Gravity (Gmb):	2.384	2.370
Avg Air Voids (Va):	4.0	3.9
Agg. Bulk Gravity (Gsb):	2.667	2.662
Avg VMA:	15.8	16.4
Avg. VFA:	75	76

Construction Diary

Relevant Conditions for Construction

Completion Date:	August 3, 2009
24 Hour High Temperature (F):	91
24 Hour Low Temperature (F):	72
24 Hour Rainfall (in):	0.00
Planned Subot Lift Thickness (in):	1.3
Paving Machine:	Roadtec

Plant Configuration and Placement Details

Component	% Setting
Asphalt Content (Plant Setting)	6.2
89 Columbus Granite	36.0
8910 Opelika Limestone Screenings	23.0
M10 Columbus Granite	13.0
Shorter Coarse Sand	28.0
As-Built Sublot Lift Thickness (in):	1.1
Total Thickness of All 2009 Sublots (in):	6.9
Approx. Underlying HMA Thickness (in):	0.0
Type of Tack Coat Utilized:	PG67-22
Target Tack Application Rate (gal/sy):	0.05
Approx. Avg. Temperature at Plant (F):	340
Avg. Measured Mat Compaction:	93.8%

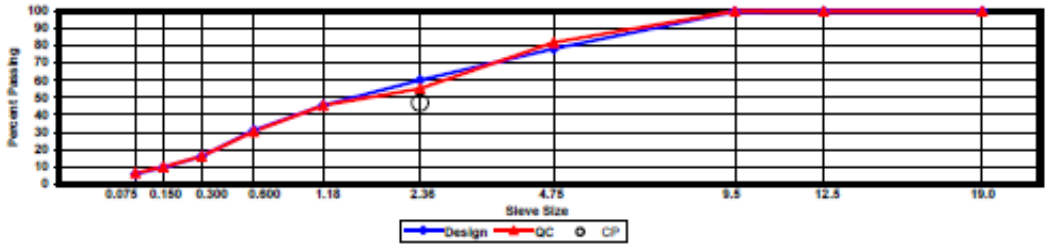

General Notes:

1) Mixes are referenced by quadrant (E=East, N=North, W=West, and S=South), section # (sequential) and sublot (top=1);
3) The total HMA thickness of all structural study sections (N1-N11 and S8-S12) ranges from 5-3/4 to 14 inches by design;
3) All non-structural sections are supprted by a uniform perpetual foundation in order to study surface mix performance;
4) SMA and OGFC refer to stone matrix asphalt and open-graded friction course, respectively; and
5) All liquid asphalt purchased for use in Track reconstruction contained LOF 6500 antistrip additive at a rate of 0.5 percent

Quadrant: N
Section: 6
Sublot: 2

Laboratory Diary

General Description of Mix and Materials

Design Method:	WMA-T
Compactive Effort:	60 gyrations
Binder Performance Grade:	67-22
Modifier Type:	Thiopave
Aggregate Type:	Lms/Sand/Grn
Design Gradation Type:	Fine

Avg. Lab Properties of Plant Produced Mix

Sieve Size	Design	QC
25 mm (1"):	100	100
19 mm (3/4"):	93	89
12.5 mm (1/2"):	82	82
9.5 mm (3/8"):	71	75
4.75 mm (#4):	52	57
2.36 mm (#8):	45	46
1.18 mm (#16):	35	36
0.60 mm (#30):	24	24
0.30 mm (#50):	12	12
0.15 mm (#100):	7	8
0.075 mm (#200):	3.9	4.9
Binder Content (Pb):	6.2	5.7
Eff. Binder Content (Pbe):	5.6	5.2
Dust-to-Binder Ratio:	0.7	0.9
Rice Gravity (Gmm):	2.581	2.554
Avg. Bulk Gravity (Gmb):	2.491	2.440
Avg Air Voids (Va):	3.5	4.5
Agg. Bulk Gravity (Gsb):	2.737	2.768
Avg VMA:	14.6	16.9
Avg. VFA:	76	74

Construction Diary

Relevant Conditions for Construction

Completion Date:	July 24, 2009
24 Hour High Temperature (F):	90
24 Hour Low Temperature (F):	68
24 Hour Rainfall (in):	0.00
Planned Subot Lift Thickness (in):	2.8
Paving Machine:	Roadtec

Plant Configuration and Placement Details

Component	% Setting
Asphalt Content (Plant Setting)	4.0
78 Opelika Limestone	30.0
57 Opelika Limestone	18.0
M10 Columbus Granite	25.0
Shorter Coarse Sand	27.0
Thiopave	40.0
Compaction Agent	1.0
As-Built Sublot Lift Thickness (in):	2.8
Total Thickness of All 2009 Sublots (in):	6.9
Approx. Underlying HMA Thickness (in):	0.0
Type of Tack Coat Utilized:	NTSS-1HM
Target Tack Application Rate (gal/sy):	0.05
Approx. Avg. Temperature at Plant (F):	275
Avg. Measured Mat Compaction:	92.9%

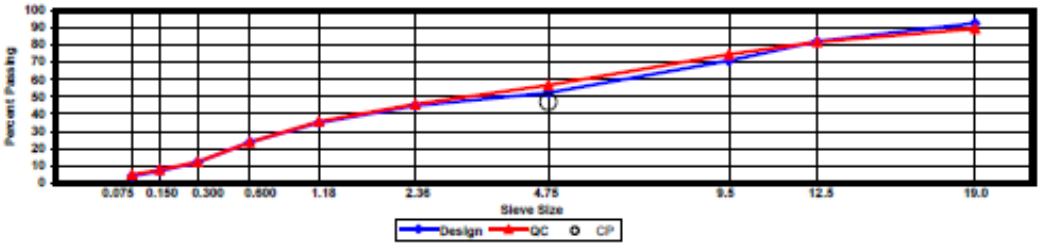

General Notes:

1) Mixes are referenced by quadrant (E=East, N=North, W=West, and S=South), section # (sequential) and sublot (top=1);
3) The total HMA thickness of all structural study sections (N1-N11 and S8-S12) ranges from 5-3/4 to 14 inches by design;
3) All non-structural sections are supprted by a uniform perpetual foundation in order to study surface mix performance;
4) SMA and OGFC refer to stone matrix asphalt and open-graded friction course, respectively; and
5) All liquid asphalt purchased for use in Track reconstruction contained LOF 6500 antistrip additive at a rate of 0.5 percent

Quadrant: N
Section: 6
Sublot: 3

Laboratory Diary

General Desccription of Mix and Materials

Design Method:	WMA-T
Compactive Effort:	60 gyrations
Binder Performance Grade:	67-22
Modifier Type:	Thiopave
Aggregate Type:	Lms/Sand/Grn
Design Gradation Type:	Fine

Avg. Lab Properties of Plant Produced Mix

Sieve Size	Design	QC
25 mm (1"):	100	100
19 mm (3/4"):	93	93
12.5 mm (1/2"):	82	82
9.5 mm (3/8"):	71	74
4.75 mm (#4):	52	55
2.36 mm (#8):	45	45
1.18 mm (#16):	35	35
0.60 mm (#30):	24	24
0.30 mm (#50):	12	12
0.15 mm (#100):	7	8
0.075 mm (#200):	3.9	4.8
Binder Content (Pb):	6.3	6.1
Eff. Binder Content (Pbe):	5.8	5.6
Dust-to-Binder Ratio:	0.7	0.8
Rice Gravity (Gmm):	2.558	2.521
Avg. Bulk Gravity (Gmb):	2.507	2.448
Avg Air Voids (Va):	2.0	2.9
Agg. Bulk Gravity (Gsb):	2.737	2.747
Avg VMA:	14.1	16.3
Avg. VFA:	86	82

Construction Diary

Relevant Conditions for Construction

Completion Date:	July 23, 2009
24 Hour High Temperature (F):	89
24 Hour Low Temperature (F):	74
24 Hour Rainfall (in):	0.00
Planned Subot Lift Thickness (in):	3.0
Paving Machine:	Roadtec

Plant Configuration and Placement Details

Component	% Setting
Asphalt Content (Plant Setting)	5.1
78 Opelika Limestone	30.0
57 Opelika Limestone	18.0
M10 Columbus Granite	25.0
Shorter Coarse Sand	27.0
Thiopave	30.0
Compaction Agent	1.0
As-Built Sublot Lift Thickness (in):	3.1
Total Thickness of All 2009 Sublots (in):	6.9
Approx. Underlying HMA Thickness (in):	0.0
Type of Tack Coat Utilized:	NA
Target Tack Application Rate (gal/sy):	NA
Approx. Avg. Temperature at Plant (F):	275
Avg. Measured Mat Compaction:	93.7%

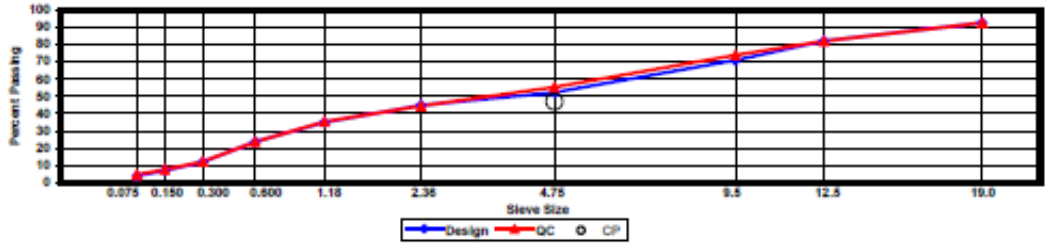

General Notes:

1) Mixes are referenced by quadrant (E=East, N=North, W=West, and S=South), section # (sequential) and sublot (top=1);
3) The total HMA thickness of all structural study sections (N1-N11 and S8-S12) ranges from 5-3/4 to 14 inches by design;
3) All non-structural sections are supprted by a uniform perpetual foundation in order to study surface mix performance;
4) SMA and OGFC refer to stone matrix asphalt and open-graded friction course, respectively; and
5) All liquid asphalt purchased for use in Track reconstruction contained LOF 6500 antistrip additive at a rate of 0.5 percent

Quadrant: N
Section: 7
Sublot: 1

Laboratory Diary

General Description of Mix and Materials

Design Method:	Super
Compactive Effort:	80 gyrations
Binder Performance Grade:	94-xx
Modifier Type:	7.5% SBS
Aggregate Type:	Grn/Sand/Lms
Design Gradation Type:	Fine

Avg. Lab Properties of Plant Produced Mix

Sieve Size	Design	QC
25 mm (1"):	100	100
19 mm (3/4"):	100	100
12.5 mm (1/2"):	100	100
9.5 mm (3/8"):	100	100
4.75 mm (#4):	77	82
2.36 mm (#8):	60	63
1.18 mm (#16):	45	48
0.60 mm (#30):	31	32
0.30 mm (#50):	16	17
0.15 mm (#100):	9	10
0.075 mm (#200):	5.7	6.6
Binder Content (Pb):	5.9	6.3
Eff. Binder Content (Pbe):	5.3	5.7
Dust-to-Binder Ratio:	1.1	1.2
Rice Gravity (Gmm):	2.474	2.468
Avg. Bulk Gravity (Gmb):	2.375	2.367
Avg Air Voids (Va):	4.0	4.1
Agg. Bulk Gravity (Gsb):	2.667	2.678
Avg VMA:	16.2	17.2
Avg. VFA:	75	76

Construction Diary

Relevant Conditions for Construction

Completion Date:	July 22, 2009
24 Hour High Temperature (F):	88
24 Hour Low Temperature (F):	60
24 Hour Rainfall (in):	0.00
Planned Subot Lift Thickness (in):	1.3
Paving Machine:	Roadtec

Plant Configuration and Placement Details

Component	% Setting
Asphalt Content (Plant Setting)	6.2
89 Columbus Granite	36.0
8910 Opelika Limestone Screenings	23.0
M10 Columbus Granite	13.0
Shorter Coarse Sand	28.0
As-Built Sublot Lift Thickness (in):	1.1
Total Thickness of All 2009 Sublots (in):	5.8
Approx. Underlying HMA Thickness (in):	0.0
Type of Tack Coat Utilized:	NTSS-1HM
Target Tack Application Rate (gal/sy):	0.07
Approx. Avg. Temperature at Plant (F):	345
Avg. Measured Mat Compaction:	93.7%

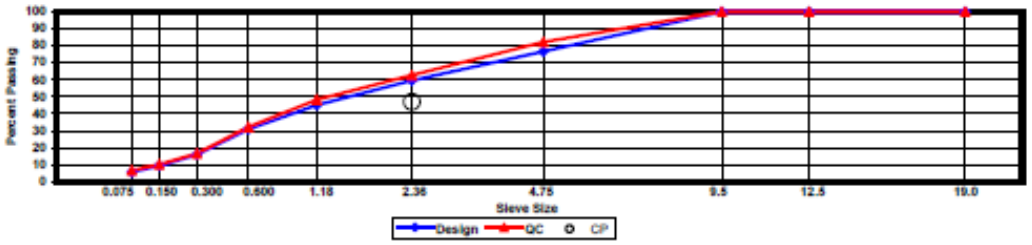

General Notes:

1) Mixes are referenced by quadrant (E=East, N=North, W=West, and S=South), section # (sequential) and sublot (top=1);
3) The total HMA thickness of all structural study sections (N1-N11 and S8-S12) ranges from 5-3/4 to 14 inches by design;
3) All non-structural sections are supprted by a uniform perpetual foundation in order to study surface mix performance;
4) SMA and OGFC refer to stone matrix asphalt and open-graded friction course, respectively; and
5) All liquid asphalt purchased for use in Track reconstruction contained LOF 6500 antistrip additive at a rate of 0.5 percent

Quadrant: N
Section: 7
Sublot: 2

Laboratory Diary

General Desccription of Mix and Materials

Design Method:	Kraton
Compactive Effort:	80 gyrations
Binder Performance Grade:	94-xx
Modifier Type:	7.5% SBS
Aggregate Type:	Lms/Sand/Grn
Design Gradation Type:	Fine

Avg. Lab Properties of Plant Produced Mix

Sieve Size	Design	QC
25 mm (1"):	100	98
19 mm (3/4"):	93	92
12.5 mm (1/2"):	82	82
9.5 mm (3/8"):	71	73
4.75 mm (#4):	52	56
2.36 mm (#8):	45	46
1.18 mm (#16):	35	37
0.60 mm (#30):	24	25
0.30 mm (#50):	12	13
0.15 mm (#100):	7	8
0.075 mm (#200):	3.9	5.2
Binder Content (Pb):	4.6	4.6
Eff. Binder Content (Pbe):	4.2	4.2
Dust-to-Binder Ratio:	0.9	1.2
Rice Gravity (Gmm):	2.570	2.549
Avg. Bulk Gravity (Gmb):	2.467	2.423
Avg Air Voids (Va):	4.0	4.9
Agg. Bulk Gravity (Gsb):	2.737	2.712
Avg VMA:	14.0	14.8
Avg. VFA:	72	67

Construction Diary

Relevant Conditions for Construction

Completion Date:	July 21, 2009
24 Hour High Temperature (F):	88
24 Hour Low Temperature (F):	60
24 Hour Rainfall (in):	0.00
Planned Subot Lift Thickness (in):	2.3
Paving Machine:	Roadtec

Plant Configuration and Placement Details

Component	% Setting
Asphalt Content (Plant Setting)	4.8
78 Opelika Limestone	30.0
57 Opelika Limestone	18.0
M10 Columbus Granite	25.0
Shorter Coarse Sand	27.0

As-Built Sublot Lift Thickness (in):	2.1
Total Thickness of All 2009 Sublots (in):	5.8
Approx. Underlying HMA Thickness (in):	0.0
Type of Tack Coat Utilized:	NTSS-1HM
Target Tack Application Rate (gal/sy):	0.07
Approx. Avg. Temperature at Plant (F):	345
Avg. Measured Mat Compaction:	92.7%

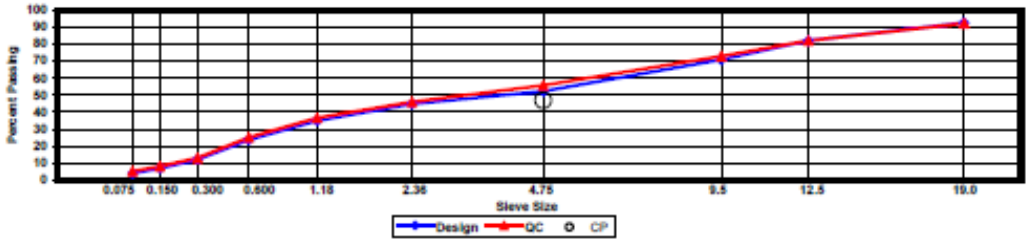

General Notes:

1) Mixes are referenced by quadrant (E=East, N=North, W=West, and S=South), section # (sequential) and sublot (top=1);
3) The total HMA thickness of all structural study sections (N1-N11 and S8-S12) ranges from 5-3/4 to 14 inches by design;
3) All non-structural sections are supprted by a uniform perpetual foundation in order to study surface mix performance;
4) SMA and OGFC refer to stone matrix asphalt and open-graded friction course, respectively; and
5) All liquid asphalt purchased for use in Track reconstruction contained LOF 6500 antistrip additive at a rate of 0.5 percent

Quadrant: N
Section: 7
Sublot: 3

Laboratory Diary

General Desccription of Mix and Materials

Design Method:	Kraton
Compactive Effort:	80 gyrations
Binder Performance Grade:	94-xx
Modifier Type:	7.5% SBS
Aggregate Type:	Lms/Sand/Grn
Design Gradation Type:	Fine

Avg. Lab Properties of Plant Produced Mix

Sieve Size	Design	QC
25 mm (1"):	100	98
19 mm (3/4"):	93	91
12.5 mm (1/2"):	82	81
9.5 mm (3/8"):	71	72
4.75 mm (#4):	52	55
2.36 mm (#8):	45	45
1.18 mm (#16):	35	36
0.60 mm (#30):	24	25
0.30 mm (#50):	12	12
0.15 mm (#100):	7	7
0.075 mm (#200):	3.9	4.6
Binder Content (Pb):	4.6	4.6
Eff. Binder Content (Pbe):	4.2	4.2
Dust-to-Binder Ratio:	0.9	1.1
Rice Gravity (Gmm):	2.570	2.545
Avg. Bulk Gravity (Gmb):	2.467	2.427
Avg Air Voids (Va):	4.0	4.6
Agg. Bulk Gravity (Gsb):	2.737	2.707
Avg VMA:	14.0	14.5
Avg. VFA:	72	68

Construction Diary

Relevant Conditions for Construction

Completion Date:	July 20, 2009
24 Hour High Temperature (F):	85
24 Hour Low Temperature (F):	60
24 Hour Rainfall (in):	0.00
Planned Subot Lift Thickness (in):	2.3
Paving Machine:	Roadtec

Plant Configuration and Placement Details

Component	% Setting
Asphalt Content (Plant Setting)	4.8
78 Opelika Limestone	30.0
57 Opelika Limestone	18.0
M10 Columbus Granite	25.0
Shorter Coarse Sand	27.0

As-Built Sublot Lift Thickness (in):	2.5
Total Thickness of All 2009 Sublots (in):	5.8
Approx. Underlying HMA Thickness (in):	0.0
Type of Tack Coat Utilized:	NA
Target Tack Application Rate (gal/sy):	NA
Approx. Avg. Temperature at Plant (F):	340
Avg. Measured Mat Compaction:	92.8%

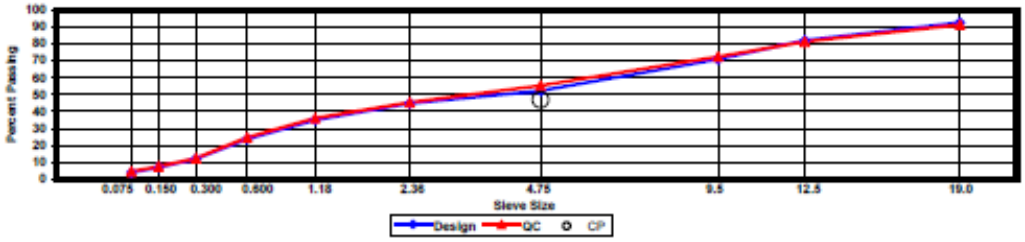

General Notes:

1) Mixes are referenced by quadrant (E=East, N=North, W=West, and S=South), section # (sequential) and sublot (top=1);
3) The total HMA thickness of all structural study sections (N1-N11 and S8-S12) ranges from 5-3/4 to 14 inches by design;
3) All non-structural sections are supprted by a uniform perpetual foundation in order to study surface mix performance;
4) SMA and OGFC refer to stone matrix asphalt and open-graded friction course, respectively; and
5) All liquid asphalt purchased for use in Track reconstruction contained LOF 6500 antistrip additive at a rate of 0.5 percent

Quadrant: N
Section: 10
Sublot: 1

Laboratory Diary

General Description of Mix and Materials

Design Method:	Super
Compactive Effort:	80 gyrations
Binder Performance Grade:	67-22
Modifier Type:	NA
Aggregate Type:	RAP/Sand/Gm
Design Gradation Type:	Fine

Avg. Lab Properties of Plant Produced Mix

Sieve Size	Design	QC
25 mm (1"):	100	100
19 mm (3/4"):	100	100
12.5 mm (1/2"):	100	100
9.5 mm (3/8"):	96	95
4.75 mm (#4):	64	67
2.36 mm (#8):	52	48
1.18 mm (#16):	42	39
0.60 mm (#30):	29	27
0.30 mm (#50):	14	12
0.15 mm (#100):	8	7
0.075 mm (#200):	5.2	4.7
Binder Content (Pb):	6.2	6.0
Eff. Binder Content (Pbe):	5.5	5.2
Dust-to-Binder Ratio:	0.9	0.9
Rice Gravity (Gmm):	2.447	2.450
Avg. Bulk Gravity (Gmb):	2.349	2.356
Avg Air Voids (Va):	4.0	3.8
Agg. Bulk Gravity (Gsb):	2.636	2.631
Avg VMA:	16.4	15.8
Avg. VFA:	76	76

Construction Diary

Relevant Conditions for Construction

Completion Date:	August 11, 2009
24 Hour High Temperature (F):	95
24 Hour Low Temperature (F):	76
24 Hour Rainfall (in):	0.00
Planned Subot Lift Thickness (in):	1.3
Paving Machine:	Roadtec

Plant Configuration and Placement Details

Component	% Setting
Asphalt Content (Plant Setting)	5.6
89 Columbus Granite	24.0
Shorter Coarse Sand	26.0
Fine Fraction Local RAP	15.0
Coarse Fraction Local RAP	35.0
As-Built Sublot Lift Thickness (in):	1.4
Total Thickness of All 2009 Sublots (in):	7.1
Approx. Underlying HMA Thickness (in):	0.0
Type of Tack Coat Utilized:	PG67-22
Target Tack Application Rate (gal/sy):	0.05
Approx. Avg. Temperature at Plant (F):	325
Avg. Measured Mat Compaction:	92.6%

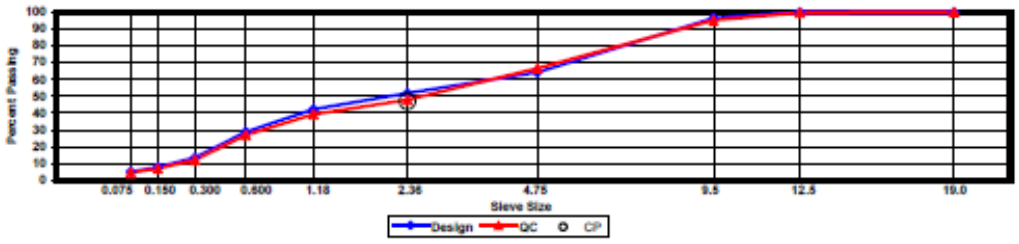

General Notes:

1) Mixes are referenced by quadrant (E=East, N=North, W=West, and S=South), section # (sequential) and sublot (top=1);
3) The total HMA thickness of all structural study sections (N1-N11 and S8-S12) ranges from 5-3/4 to 14 inches by design;
3) All non-structural sections are supprted by a uniform perpetual foundation in order to study surface mix performance;
4) SMA and OGFC refer to stone matrix asphalt and open-graded friction course, respectively; and
5) All liquid asphalt purchased for use in Track reconstruction contained LOF 6500 antistrip additive at a rate of 0.5 percent

Quadrant: N
Section: 10
Sublot: 2

Laboratory Diary

General Description of Mix and Materials

Design Method:	Super
Compactive Effort:	80 gyrations
Binder Performance Grade:	67-22
Modifier Type:	NA
Aggregate Type:	RAP/Lms/Sand
Design Gradation Type:	Fine

Avg. Lab Properties of Plant Produced Mix

Sieve Size	Design	QC
25 mm (1"):	100	98
19 mm (3/4"):	94	93
12.5 mm (1/2"):	87	86
9.5 mm (3/8"):	78	79
4.75 mm (#4):	54	56
2.36 mm (#8):	46	46
1.18 mm (#16):	37	37
0.60 mm (#30):	26	26
0.30 mm (#50):	14	13
0.15 mm (#100):	8	8
0.075 mm (#200):	5.1	5.6
Binder Content (Pb):	4.8	4.4
Eff. Binder Content (Pbe):	4.2	3.8
Dust-to-Binder Ratio:	1.2	1.5
Rice Gravity (Gmm):	2.542	2.552
Avg. Bulk Gravity (Gmb):	2.440	2.436
Avg Air Voids (Va):	4.0	4.5
Agg. Bulk Gravity (Gsb):	2.698	2.695
Avg VMA:	13.9	13.6
Avg. VFA:	72	67

Construction Diary

Relevant Conditions for Construction

Completion Date:	August 4, 2009
24 Hour High Temperature (F):	94
24 Hour Low Temperature (F):	73
24 Hour Rainfall (in):	0.00
Planned Subot Lift Thickness (in):	2.8
Paving Machine:	Roadtec

Plant Configuration and Placement Details

Component	% Setting
Asphalt Content (Plant Setting)	5.8
78 Opelika Limestone	15.0
57 Opelika Limestone	15.0
Shorter Coarse Sand	20.0
Fine Fraction Local RAP	20.0
Coarse Fraction Local RAP	30.0
As-Built Sublot Lift Thickness (in):	2.7
Total Thickness of All 2009 Sublots (in):	7.1
Approx. Underlying HMA Thickness (in):	0.0
Type of Tack Coat Utilized:	NTSS-1HM
Target Tack Application Rate (gal/sy):	0.05
Approx. Avg. Temperature at Plant (F):	325
Avg. Measured Mat Compaction:	92.9%

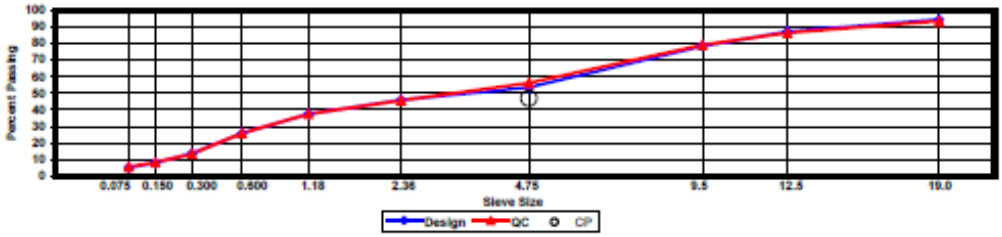

General Notes:

1) Mixes are referenced by quadrant (E=East, N=North, W=West, and S=South), section # (sequential) and sublot (top=1);
3) The total HMA thickness of all structural study sections (N1-N11 and S8-S12) ranges from 5-3/4 to 14 inches by design;
3) All non-structural sections are supprted by a uniform perpetual foundation in order to study surface mix performance;
4) SMA and OGFC refer to stone matrix asphalt and open-graded friction course, respectively; and
5) All liquid asphalt purchased for use in Track reconstruction contained LOF 6500 antistrip additive at a rate of 0.5 percent

Quadrant: N
Section: 10
Sublot: 3

Laboratory Diary

General Description of Mix and Materials

Design Method:	Super
Compactive Effort:	80 gyrations
Binder Performance Grade:	67-22
Modifier Type:	NA
Aggregate Type:	RAP/Lms/Sand
Design Gradation Type:	Fine

Avg. Lab Properties of Plant Produced Mix

Sieve Size	Design	QC
25 mm (1"):	100	99
19 mm (3/4"):	94	95
12.5 mm (1/2"):	87	89
9.5 mm (3/8"):	78	82
4.75 mm (#4):	54	58
2.36 mm (#8):	46	47
1.18 mm (#16):	37	39
0.60 mm (#30):	26	27
0.30 mm (#50):	14	14
0.15 mm (#100):	8	9
0.075 mm (#200):	5.1	5.8
Binder Content (Pb):	4.8	4.7
Eff. Binder Content (Pbe):	4.2	4.1
Dust-to-Binder Ratio:	1.2	1.4
Rice Gravity (Gmm):	2.542	2.537
Avg. Bulk Gravity (Gmb):	2.440	2.431
Avg Air Voids (Va):	4.0	4.2
Agg. Bulk Gravity (Gsb):	2.698	2.688
Avg VMA:	13.9	13.8
Avg. VFA:	72	70

Construction Diary

Relevant Conditions for Construction

Completion Date:	August 4, 2009
24 Hour High Temperature (F):	94
24 Hour Low Temperature (F):	73
24 Hour Rainfall (in):	0.00
Planned Subot Lift Thickness (in):	3.0
Paving Machine:	Roadtec

Plant Configuration and Placement Details

Component	% Setting
Asphalt Content (Plant Setting)	5.8
78 Opelika Limestone	15.0
57 Opelika Limestone	15.0
Shorter Coarse Sand	20.0
Fine Fraction Local RAP	20.0
Coarse Fraction Local RAP	30.0
As-Built Sublot Lift Thickness (in):	3.0
Total Thickness of All 2009 Sublots (in):	7.1
Approx. Underlying HMA Thickness (in):	0.0
Type of Tack Coat Utilized:	NA
Target Tack Application Rate (gal/sy):	NA
Approx. Avg. Temperature at Plant (F):	325
Avg. Measured Mat Compaction:	95.0%

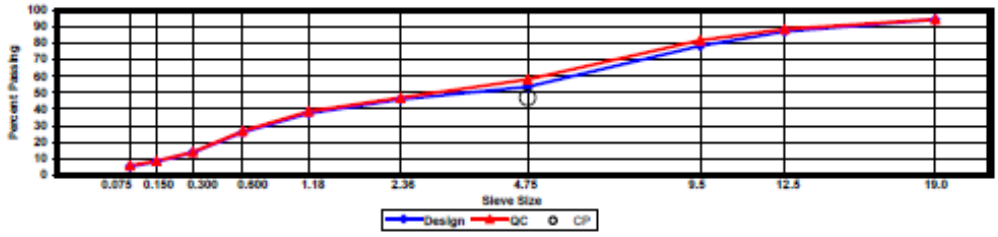

General Notes:

1) Mixes are referenced by quadrant (E=East, N=North, W=West, and S=South), section # (sequential) and sublot (top=1);
3) The total HMA thickness of all structural study sections (N1-N11 and S8-S12) ranges from 5-3/4 to 14 inches by design;
3) All non-structural sections are supprted by a uniform perpetual foundation in order to study surface mix performance;
4) SMA and OGFC refer to stone matrix asphalt and open-graded friction course, respectively; and
5) All liquid asphalt purchased for use in Track reconstruction contained LOF 6500 antistrip additive at a rate of 0.5 percent

Quadrant: N
Section: 11
Sublot: 1

Laboratory Diary

General Description of Mix and Materials

Design Method:	Super
Compactive Effort:	80 gyrations
Binder Performance Grade:	67-22
Modifier Type:	NA
Aggregate Type:	RAP/Sand/Gm
Design Gradation Type:	Fine

Avg. Lab Properties of Plant Produced Mix

Sieve Size	Design	QC
25 mm (1"):	100	100
19 mm (3/4"):	100	100
12.5 mm (1/2"):	100	99
9.5 mm (3/8"):	96	95
4.75 mm (#4):	64	69
2.36 mm (#8):	52	51
1.18 mm (#16):	42	41
0.60 mm (#30):	29	27
0.30 mm (#50):	14	12
0.15 mm (#100):	8	7
0.075 mm (#200):	5.2	4.8
Binder Content (Pb):	6.2	6.1
Eff. Binder Content (Pbe):	5.5	5.3
Dust-to-Binder Ratio:	0.9	0.9
Rice Gravity (Gmm):	2.447	2.449
Avg. Bulk Gravity (Gmb):	2.349	2.371
Avg Air Voids (Va):	4.0	3.2
Agg. Bulk Gravity (Gsb):	2.636	2.633
Avg VMA:	16.4	15.5
Avg. VFA:	76	79

Construction Diary

Relevant Conditions for Construction

Completion Date:	August 11, 2009
24 Hour High Temperature (F):	95
24 Hour Low Temperature (F):	76
24 Hour Rainfall (in):	0.00
Planned Subot Lift Thickness (in):	1.3
Paving Machine:	Roadtec

Plant Configuration and Placement Details

Component	% Setting
Asphalt Content (Plant Setting)	5.6
89 Columbus Granite	24.0
Shorter Coarse Sand	26.0
Fine Fraction Local RAP	15.0
Coarse Fraction Local RAP	35.0
As-Built Sublot Lift Thickness (in):	1.2
Total Thickness of All 2009 Sublots (in):	7.1
Approx. Underlying HMA Thickness (in):	0.0
Type of Tack Coat Utilized:	PG67-22
Target Tack Application Rate (gal/sy):	0.05
Approx. Avg. Temperature at Plant (F):	275
Avg. Measured Mat Compaction:	92.1%

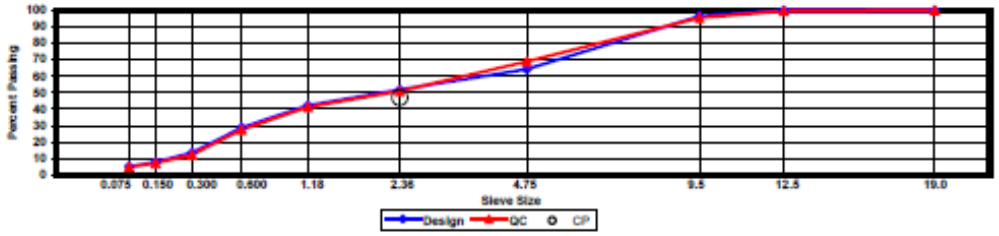

General Notes:

1) Mixes are referenced by quadrant (E=East, N=North, W=West, and S=South), section # (sequential) and sublot (top=1);
3) The total HMA thickness of all structural study sections (N1-N11 and S8-S12) ranges from 5-3/4 to 14 inches by design;
3) All non-structural sections are supprted by a uniform perpetual foundation in order to study surface mix performance;
4) SMA and OGFC refer to stone matrix asphalt and open-graded friction course, respectively; and
5) All liquid asphalt purchased for use in Track reconstruction contained LOF 6500 antistrip additive at a rate of 0.5 percent

Quadrant: N
Section: 11
Sublot: 2

Laboratory Diary

General Description of Mix and Materials

Design Method:	Super
Compactive Effort:	80 gyrations
Binder Performance Grade:	67-22
Modifier Type:	NA
Aggregate Type:	RAP/Lms/Sand
Design Gradation Type:	Fine

Avg. Lab Properties of Plant Produced Mix

Sieve Size	Design	QC
25 mm (1"):	100	99
19 mm (3/4"):	94	93
12.5 mm (1/2"):	87	86
9.5 mm (3/8"):	78	79
4.75 mm (#4):	54	58
2.36 mm (#8):	46	47
1.18 mm (#16):	37	39
0.60 mm (#30):	26	27
0.30 mm (#50):	14	14
0.15 mm (#100):	8	8
0.075 mm (#200):	5.1	5.7
Binder Content (Pb):	4.8	4.7
Eff. Binder Content (Pbe):	4.2	4.1
Dust-to-Binder Ratio:	1.2	1.4
Rice Gravity (Gmm):	2.542	2.541
Avg. Bulk Gravity (Gmb):	2.440	2.446
Avg Air Voids (Va):	4.0	3.7
Agg. Bulk Gravity (Gsb):	2.698	2.697
Avg VMA:	13.9	13.6
Avg. VFA:	72	72

Construction Diary

Relevant Conditions for Construction

Completion Date:	August 4, 2009
24 Hour High Temperature (F):	94
24 Hour Low Temperature (F):	73
24 Hour Rainfall (in):	0.00
Planned Subot Lift Thickness (in):	2.8
Paving Machine:	Roadtec

Plant Configuration and Placement Details

Component	% Setting
Asphalt Content (Plant Setting)	5.8
78 Opelika Limestone	15.0
57 Opelika Limestone	15.0
Shorter Coarse Sand	20.0
Fine Fraction Local RAP	20.0
Coarse Fraction Local RAP	30.0
As-Built Sublot Lift Thickness (in):	3.0
Total Thickness of All 2009 Sublots (in):	7.1
Approx. Underlying HMA Thickness (in):	0.0
Type of Tack Coat Utilized:	NTSS-1HM
Target Tack Application Rate (gal/sy):	0.05
Approx. Avg. Temperature at Plant (F):	275
Avg. Measured Mat Compaction:	93.1%

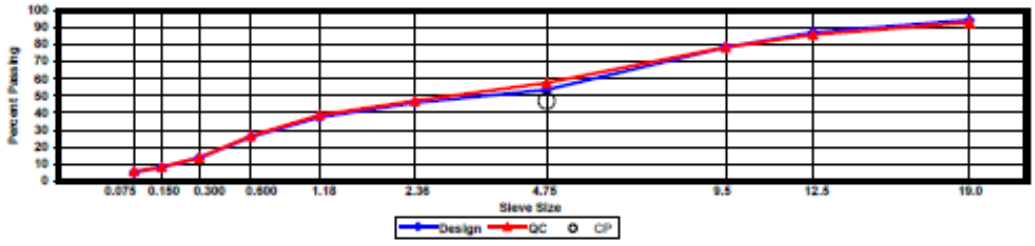

General Notes:

1) Mixes are referenced by quadrant (E=East, N=North, W=West, and S=South), section # (sequential) and sublot (top=1);
3) The total HMA thickness of all structural study sections (N1-N11 and S8-S12) ranges from 5-3/4 to 14 inches by design;
3) All non-structural sections are supprted by a uniform perpetual foundation in order to study surface mix performance;
4) SMA and OGFC refer to stone matrix asphalt and open-graded friction course, respectively; and
5) All liquid asphalt purchased for use in Track reconstruction contained LOF 6500 antistrip additive at a rate of 0.5 percent

Quadrant: N
Section: 11
Sublot: 3

Laboratory Diary

General Description of Mix and Materials

Design Method:	Superpave
Compactive Effort:	80 gyrations
Binder Performance Grade:	67-22
Modifier Type:	NA
Aggregate Type:	RAP/Lms/Sand
Design Gradation Type:	Fine

Avg. Lab Properties of Plant Produced Mix

Sieve Size	Design	QC
25 mm (1"):	100	97
19 mm (3/4"):	94	89
12.5 mm (1/2"):	87	83
9.5 mm (3/8"):	78	75
4.75 mm (#4):	54	54
2.36 mm (#8):	46	44
1.18 mm (#16):	37	37
0.60 mm (#30):	26	25
0.30 mm (#50):	14	13
0.15 mm (#100):	8	8
0.075 mm (#200):	5.1	5.3
Binder Content (Pb):	4.8	4.6
Eff. Binder Content (Pbe):	4.2	4.0
Dust-to-Binder Ratio:	1.2	1.3
Rice Gravity (Gmm):	2.542	2.544
Avg. Bulk Gravity (Gmb):	2.440	2.439
Avg Air Voids (Va):	4.0	4.1
Agg. Bulk Gravity (Gsb):	2.698	2.695
Avg VMA:	13.9	13.7
Avg. VFA:	72	70

Construction Diary

Relevant Conditions for Construction

Completion Date:	August 4, 2009
24 Hour High Temperature (F):	94
24 Hour Low Temperature (F):	73
24 Hour Rainfall (in):	0.00
Planned Subot Lift Thickness (in):	3.0
Paving Machine:	Roadtec

Plant Configuration and Placement Details

Component	% Setting
Asphalt Content (Plant Setting)	5.8
78 Opelika Limestone	15.0
57 Opelika Limestone	15.0
Shorter Coarse Sand	20.0
Fine Fraction Local RAP	20.0
Coarse Fraction Local RAP	30.0
As-Built Sublot Lift Thickness (in):	2.9
Total Thickness of All 2009 Sublots (in):	7.1
Approx. Underlying HMA Thickness (in):	0.0
Type of Tack Coat Utilized:	NA
Target Tack Application Rate (gal/sy):	NA
Approx. Avg. Temperature at Plant (F):	275
Avg. Measured Mat Compaction:	94.2%

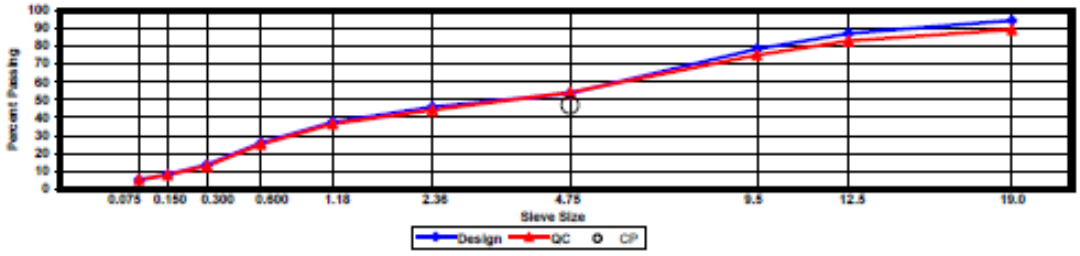

General Notes:

1) Mixes are referenced by quadrant (E=East, N=North, W=West, and S=South), section # (sequential) and sublot (top=1);
3) The total HMA thickness of all structural study sections (N1-N11 and S8-S12) ranges from 5-3/4 to 14 inches by design;
3) All non-structural sections are supprted by a uniform perpetual foundation in order to study surface mix performance;
4) SMA and OGFC refer to stone matrix asphalt and open-graded friction course, respectively; and
5) All liquid asphalt purchased for use in Track reconstruction contained LOF 6500 antistrip additive at a rate of 0.5 percent

Quadrant: S
Section: 9
Sublot: 1

Laboratory Diary

General Descciption of Mix and Materials

Design Method:	Super
Compactive Effort:	80 gyrations
Binder Performance Grade:	76-22
Modifier Type:	SBS
Aggregate Type:	Grn/Sand/Lms
Design Gradation Type:	Fine

Avg. Lab Properties of Plant Produced Mix

Sieve Size	Design	QC
25 mm (1"):	100	100
19 mm (3/4"):	100	100
12.5 mm (1/2"):	100	100
9.5 mm (3/8"):	100	100
4.75 mm (#4):	78	81
2.36 mm (#8):	60	59
1.18 mm (#16):	46	46
0.60 mm (#30):	31	31
0.30 mm (#50):	16	16
0.15 mm (#100):	10	9
0.075 mm (#200):	5.8	6.0
Binder Content (Pb):	5.8	6.1
Eff. Binder Content (Pbe):	5.1	5.4
Dust-to-Binder Ratio:	1.1	1.1
Rice Gravity (Gmm):	2.483	2.472
Avg. Bulk Gravity (Gmb):	2.384	2.374
Avg Air Voids (Va):	4.0	4.0
Agg. Bulk Gravity (Gsb):	2.667	2.670
Avg VMA:	15.8	16.5
Avg. VFA:	75	76

Construction Diary

Relevant Conditions for Construction

Completion Date:	July 16, 2009
24 Hour High Temperature (F):	92
24 Hour Low Temperature (F):	74
24 Hour Rainfall (in):	0.00
Planned Subot Lift Thickness (in):	1.3
Paving Machine:	Roadtec

Plant Configuration and Placement Details

Component	% Setting
Asphalt Content (Plant Setting)	6.5
89 Columbus Granite	36.0
8910 Opelika Limestone Screenings	23.0
M10 Columbus Granite	13.0
Shorter Coarse Sand	28.0
As-Built Sublot Lift Thickness (in):	1.2
Total Thickness of All 2009 Sublots (in):	7.0
Approx. Underlying HMA Thickness (in):	0.0
Type of Tack Coat Utilized:	NTSS-1HM
Target Tack Application Rate (gal/sy):	0.04
Approx. Avg. Temperature at Plant (F):	335
Avg. Measured Mat Compaction:	93.1%

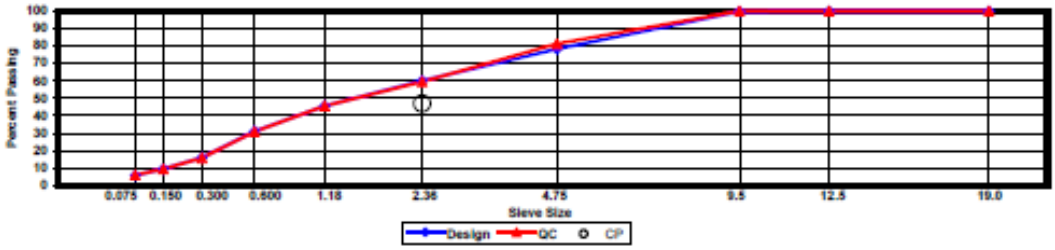

General Notes:

1) Mixes are referenced by quadrant (E=East, N=North, W=West, and S=South), section # (sequential) and sublot (top=1);
3) The total HMA thickness of all structural study sections (N1-N11 and S8-S12) ranges from 5-3/4 to 14 inches by design;
3) All non-structural sections are supprted by a uniform perpetual foundation in order to study surface mix performance;
4) SMA and OGFC refer to stone matrix asphalt and open-graded friction course, respectively; and
5) All liquid asphalt purchased for use in Track reconstruction contained LOF 6500 antistrip additive at a rate of 0.5 percent

Quadrant: S
Section: 9
Sublot: 2

Laboratory Diary

General Description of Mix and Materials

Design Method:	Super
Compactive Effort:	80 gyrations
Binder Performance Grade:	76-22
Modifier Type:	SBS
Aggregate Type:	Lms/Sand/Grn
Design Gradation Type:	Fine

Avg. Lab Properties of Plant Produced Mix

Sieve Size	Design	QC
25 mm (1"):	100	99
19 mm (3/4"):	93	92
12.5 mm (1/2"):	82	84
9.5 mm (3/8"):	71	76
4.75 mm (#4):	52	57
2.36 mm (#8):	45	47
1.18 mm (#16):	35	38
0.60 mm (#30):	24	26
0.30 mm (#50):	12	15
0.15 mm (#100):	7	9
0.075 mm (#200):	3.9	5.3
Binder Content (Pb):	4.7	4.4
Eff. Binder Content (Pbe):	4.1	3.9
Dust-to-Binder Ratio:	0.9	1.4
Rice Gravity (Gmm):	2.575	2.551
Avg. Bulk Gravity (Gmb):	2.472	2.439
Avg Air Voids (Va):	4.0	4.4
Agg. Bulk Gravity (Gsb):	2.737	2.695
Avg VMA:	13.9	13.5
Avg. VFA:	71	68

Construction Diary

Relevant Conditions for Construction

Completion Date:	July 14, 2009
24 Hour High Temperature (F):	93
24 Hour Low Temperature (F):	72
24 Hour Rainfall (in):	0.00
Planned Subot Lift Thickness (in):	2.8
Paving Machine:	Roadtec

Plant Configuration and Placement Details

Component	% Setting
Asphalt Content (Plant Setting)	4.7
78 Opelika Limestone	30.0
57 Opelika Limestone	18.0
M10 Columbus Granite	25.0
Shorter Coarse Sand	27.0

As-Built Sublot Lift Thickness (in):	2.8
Total Thickness of All 2009 Sublots (in):	7.0
Approx. Underlying HMA Thickness (in):	0.0
Type of Tack Coat Utilized:	NTSS-1HM
Target Tack Application Rate (gal/sy):	0.07
Approx. Avg. Temperature at Plant (F):	335
Avg. Measured Mat Compaction:	92.8%

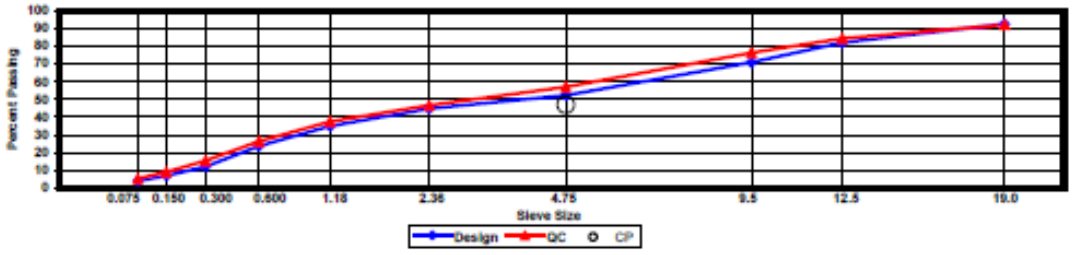

General Notes:

1) Mixes are referenced by quadrant (E=East, N=North, W=West, and S=South), section # (sequential) and sublot (top=1);
3) The total HMA thickness of all structural study sections (N1-N11 and S8-S12) ranges from 5-3/4 to 14 inches by design;
3) All non-structural sections are supprted by a uniform perpetual foundation in order to study surface mix performance;
4) SMA and OGFC refer to stone matrix asphalt and open-graded friction course, respectively; and
5) All liquid asphalt purchased for use in Track reconstruction contained LOF 6500 antistrip additive at a rate of 0.5 percent

Quadrant: S
Section: 9
Sublot: 3

Laboratory Diary

General Desccription of Mix and Materials

Design Method:	Super
Compactive Effort:	80 gyrations
Binder Performance Grade:	67-22
Modifier Type:	NA
Aggregate Type:	Lms/Sand/Gm
Design Gradation Type:	Fine

Avg. Lab Properties of Plant Produced Mix

Sieve Size	Design	QC
25 mm (1"):	100	99
19 mm (3/4"):	93	95
12.5 mm (1/2"):	84	87
9.5 mm (3/8"):	73	77
4.75 mm (#4):	55	56
2.36 mm (#8):	47	46
1.18 mm (#16):	36	37
0.60 mm (#30):	25	26
0.30 mm (#50):	14	15
0.15 mm (#100):	8	9
0.075 mm (#200):	4.6	5.1
Binder Content (Pb):	4.6	4.7
Eff. Binder Content (Pbe):	4.1	4.2
Dust-to-Binder Ratio:	1.1	1.2
Rice Gravity (Gmm):	2.574	2.540
Avg. Bulk Gravity (Gmb):	2.471	2.439
Avg Air Voids (Va):	4.0	4.0
Agg. Bulk Gravity (Gsb):	2.738	2.699
Avg VMA:	13.9	13.9
Avg. VFA:	71	71

Construction Diary

Relevant Conditions for Construction

Completion Date:	July 3, 2009
24 Hour High Temperature (F):	92
24 Hour Low Temperature (F):	69
24 Hour Rainfall (in):	0.00
Planned Subot Lift Thickness (in):	3.0
Paving Machine:	Roadtec

Plant Configuration and Placement Details

Component	% Setting
Asphalt Content (Plant Setting)	4.9
78 Opelika Limestone	30.0
57 Opelika Limestone	18.0
M10 Columbus Granite	25.0
Shorter Coarse Sand	27.0

As-Built Sublot Lift Thickness (in):	3.0
Total Thickness of All 2009 Sublots (in):	7.0
Approx. Underlying HMA Thickness (in):	0.0
Type of Tack Coat Utilized:	NA
Target Tack Application Rate (gal/sy):	NA
Approx. Avg. Temperature at Plant (F):	325
Avg. Measured Mat Compaction:	92.6%

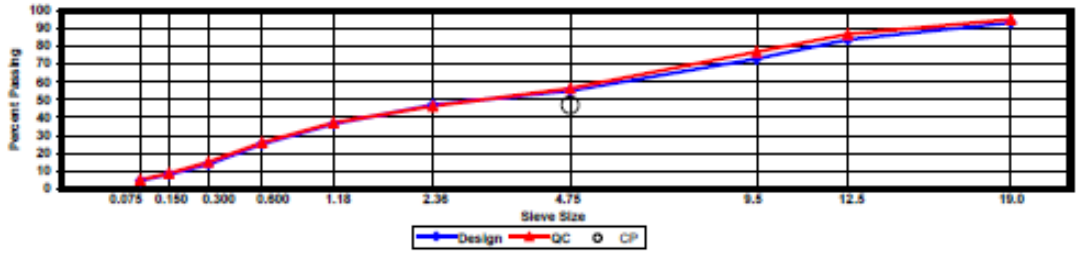

General Notes:

1) Mixes are referenced by quadrant (E=East, N=North, W=West, and S=South), section # (sequential) and sublot (top=1);
3) The total HMA thickness of all structural study sections (N1-N11 and S8-S12) ranges from 5-3/4 to 14 inches by design;
3) All non-structural sections are supprted by a uniform perpetual foundation in order to study surface mix performance;
4) SMA and OGFC refer to stone matrix asphalt and open-graded friction course, respectively; and
5) All liquid asphalt purchased for use in Track reconstruction contained LOF 6500 antistrip additive at a rate of 0.5 percent

Quadrant: S
Section: 10
Sublot: 1

Laboratory Diary

General Description of Mix and Materials

Design Method:	WMA
Compactive Effort:	80 gyrations
Binder Performance Grade:	76-22
Modifier Type:	Foam
Aggregate Type:	Grn/Sand/Lms
Design Gradation Type:	Fine

Avg. Lab Properties of Plant Produced Mix

Sieve Size	Design	QC
25 mm (1"):	100	100
19 mm (3/4"):	100	100
12.5 mm (1/2"):	100	100
9.5 mm (3/8"):	100	100
4.75 mm (#4):	78	81
2.36 mm (#8):	60	60
1.18 mm (#16):	46	47
0.60 mm (#30):	31	32
0.30 mm (#50):	16	17
0.15 mm (#100):	10	10
0.075 mm (#200):	5.8	6.7
Binder Content (Pb):	5.8	6.1
Eff. Binder Content (Pbe):	5.1	5.5
Dust-to-Binder Ratio:	1.1	1.2
Rice Gravity (Gmm):	2.483	2.471
Avg. Bulk Gravity (Gmb):	2.384	2.390
Avg Air Voids (Va):	4.0	3.3
Agg. Bulk Gravity (Gsb):	2.667	2.671
Avg VMA:	15.8	16.0
Avg. VFA:	75	80

Construction Diary

Relevant Conditions for Construction

Completion Date:	July 16, 2009
24 Hour High Temperature (F):	92
24 Hour Low Temperature (F):	74
24 Hour Rainfall (in):	0.00
Planned Subot Lift Thickness (in):	1.3
Paving Machine:	Roadtec

Plant Configuration and Placement Details

Component	% Setting
Asphalt Content (Plant Setting)	6.5
89 Columbus Granite	36.0
8910 Opelika Limestone Screenings	23.0
M10 Columbus Granite	13.0
Shorter Coarse Sand	28.0

As-Built Sublot Lift Thickness (in):	1.3
Total Thickness of All 2009 Sublots (in):	7.0
Approx. Underlying HMA Thickness (in):	0.0
Type of Tack Coat Utilized:	NTSS-1HM
Target Tack Application Rate (gal/sy):	0.04
Approx. Avg. Temperature at Plant (F):	275
Avg. Measured Mat Compaction:	92.3%

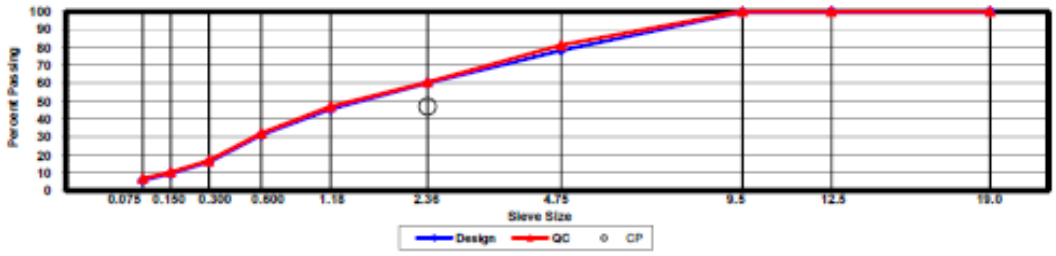

General Notes:

1) Mixes are referenced by quadrant (E=East, N=North, W=West, and S=South), section # (sequential) and sublot (top=1);
3) The total HMA thickness of all structural study sections (N1-N11 and S8-S12) ranges from 5-3/4 to 14 inches by design;
3) All non-structural sections are supprted by a uniform perpetual foundation in order to study surface mix performance;
4) SMA and OGFC refer to stone matrix asphalt and open-graded friction course, respectively; and
5) All liquid asphalt purchased for use in Track reconstruction contained LOF 6500 antistrip additive at a rate of 0.5 percent

Quadrant: S
Section: 10
Sublot: 2

Laboratory Diary

General Description of Mix and Materials

Design Method:	WMA
Compactive Effort:	80 gyrations
Binder Performance Grade:	76-22
Modifier Type:	Foam
Aggregate Type:	Lms/Sand/Grn
Design Gradation Type:	Fine

Avg. Lab Properties of Plant Produced Mix

Sieve Size	Design	QC
25 mm (1"):	100	99
19 mm (3/4"):	93	96
12.5 mm (1/2"):	82	89
9.5 mm (3/8"):	71	80
4.75 mm (#4):	52	60
2.36 mm (#8):	45	48
1.18 mm (#16):	35	39
0.60 mm (#30):	24	27
0.30 mm (#50):	12	14
0.15 mm (#100):	7	9
0.075 mm (#200):	3.9	5.3
Binder Content (Pb):	4.7	4.7
Eff. Binder Content (Pbe):	**4.1**	**4.1**
Dust-to-Binder Ratio:	0.9	1.3
Rice Gravity (Gmm):	2.575	2.550
Avg. Bulk Gravity (Gmb):	2.472	2.433
Avg Air Voids (Va):	4.0	4.6
Agg. Bulk Gravity (Gsb):	2.737	2.706
Avg VMA:	13.9	14.3
Avg. VFA:	71	68

Construction Diary

Relevant Conditions for Construction

Completion Date:	July 14, 2009
24 Hour High Temperature (F):	93
24 Hour Low Temperature (F):	72
24 Hour Rainfall (in):	0.00
Planned Subot Lift Thickness (in):	2.8
Paving Machine:	Roadtec

Plant Configuration and Placement Details

Component	% Setting
Asphalt Content (Plant Setting)	4.7
78 Opelika Limestone	30.0
57 Opelika Limestone	18.0
M10 Columbus Granite	25.0
Shorter Coarse Sand	27.0

As-Built Sublot Lift Thickness (in):	2.7
Total Thickness of All 2009 Sublots (in):	7.0
Approx. Underlying HMA Thickness (in):	0.0
Type of Tack Coat Utilized:	NTSS-1HM
Target Tack Application Rate (gal/sy):	0.07
Approx. Avg. Temperature at Plant (F):	275
Avg. Measured Mat Compaction:	92.9%

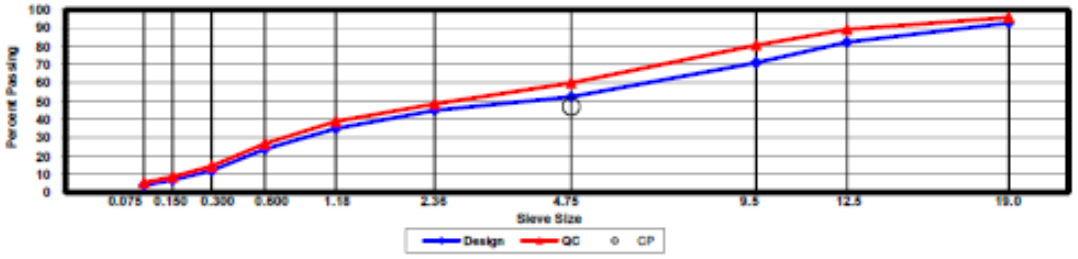

General Notes:

1) Mixes are referenced by quadrant (E=East, N=North, W=West, and S=South), section # (sequential) and sublot (top=1);
3) The total HMA thickness of all structural study sections (N1-N11 and S8-S12) ranges from 5-3/4 to 14 inches by design;
3) All non-structural sections are supprted by a uniform perpetual foundation in order to study surface mix performance;
4) SMA and OGFC refer to stone matrix asphalt and open-graded friction course, respectively; and
5) All liquid asphalt purchased for use in Track reconstruction contained LOF 6500 antistrip additive at a rate of 0.5 percent

Quadrant: S
Section: 10
Sublot: 3

Laboratory Diary

General Description of Mix and Materials

Design Method:	WMA
Compactive Effort:	80 gyrations
Binder Performance Grade:	67-22
Modifier Type:	Foam
Aggregate Type:	Lms/Sand/Grn
Design Gradation Type:	Fine

Avg. Lab Properties of Plant Produced Mix

Sieve Size	Design	QC
25 mm (1"):	100	99
19 mm (3/4"):	93	94
12.5 mm (1/2"):	84	85
9.5 mm (3/8"):	73	76
4.75 mm (#4):	55	57
2.36 mm (#8):	47	47
1.18 mm (#16):	36	38
0.60 mm (#30):	25	21
0.30 mm (#50):	14	12
0.15 mm (#100):	8	7
0.075 mm (#200):	4.6	5.1
Binder Content (Pb):	4.6	4.7
Eff. Binder Content (Pbe):	**4.1**	**4.2**
Dust-to-Binder Ratio:	1.1	1.2
Rice Gravity (Gmm):	2.574	2.553
Avg. Bulk Gravity (Gmb):	2.471	2.448
Avg Air Voids (Va):	4.0	4.1
Agg. Bulk Gravity (Gsb):	2.738	2.715
Avg VMA:	13.9	14.0
Avg. VFA:	71	71

Construction Diary

Relevant Conditions for Construction

Completion Date:	July 3, 2009
24 Hour High Temperature (F):	92
24 Hour Low Temperature (F):	69
24 Hour Rainfall (in):	0.00
Planned Subot Lift Thickness (in):	3.0
Paving Machine:	Roadtec

Plant Configuration and Placement Details

Component	% Setting
Asphalt Content (Plant Setting)	4.9
78 Opelika Limestone	30.0
57 Opelika Limestone	18.0
M10 Columbus Granite	25.0
Shorter Coarse Sand	27.0

As-Built Sublot Lift Thickness (in):	3.0
Total Thickness of All 2009 Sublots (in):	7.0
Approx. Underlying HMA Thickness (in):	0.0
Type of Tack Coat Utilized:	NA
Target Tack Application Rate (gal/sy):	NA
Approx. Avg. Temperature at Plant (F):	275
Avg. Measured Mat Compaction:	92.3%

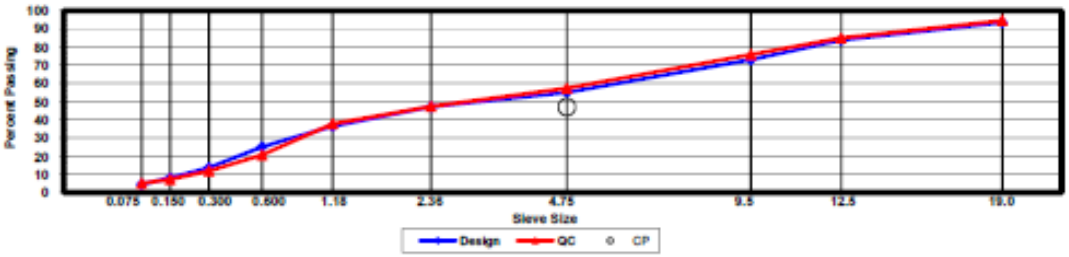

General Notes:

1) Mixes are referenced by quadrant (E=East, N=North, W=West, and S=South), section # (sequential) and sublot (top=1);
3) The total HMA thickness of all structural study sections (N1-N11 and S8-S12) ranges from 5-3/4 to 14 inches by design;
3) All non-structural sections are supprted by a uniform perpetual foundation in order to study surface mix performance;
4) SMA and OGFC refer to stone matrix asphalt and open-graded friction course, respectively; and
5) All liquid asphalt purchased for use in Track reconstruction contained LOF 6500 antistrip additive at a rate of 0.5 percent

Quadrant: S
Section: 11
Sublot: 1

Laboratory Diary

General Description of Mix and Materials

Design Method:	WMA
Compactive Effort:	80 gyrations
Binder Performance Grade:	76-22+
Modifier Type:	Additive
Aggregate Type:	Grn/Sand/Lms
Design Gradation Type:	Fine

Avg. Lab Properties of Plant Produced Mix

Sieve Size	Design	QC
25 mm (1"):	100	100
19 mm (3/4"):	100	100
12.5 mm (1/2"):	100	100
9.5 mm (3/8"):	100	100
4.75 mm (#4):	78	83
2.36 mm (#8):	60	61
1.18 mm (#16):	46	47
0.60 mm (#30):	31	31
0.30 mm (#50):	16	16
0.15 mm (#100):	10	9
0.075 mm (#200):	5.8	6.1
Binder Content (Pb):	5.8	6.4
Eff. Binder Content (Pbe):	5.1	5.7
Dust-to-Binder Ratio:	1.1	1.1
Rice Gravity (Gmm):	2.483	2.464
Avg. Bulk Gravity (Gmb):	2.384	2.380
Avg Air Voids (Va):	4.0	3.4
Agg. Bulk Gravity (Gsb):	2.667	2.675
Avg VMA:	15.8	16.7
Avg. VFA:	75	80

Construction Diary

Relevant Conditions for Construction

Completion Date:	July 16, 2009
24 Hour High Temperature (F):	92
24 Hour Low Temperature (F):	74
24 Hour Rainfall (in):	0.00
Planned Subot Lift Thickness (in):	1.3
Paving Machine:	Roadtec

Plant Configuration and Placement Details

Component	% Setting
Asphalt Content (Plant Setting)	6.5
89 Columbus Granite	36.0
8910 Opelika Limestone Screenings	23.0
M10 Columbus Granite	13.0
Shorter Coarse Sand	28.0

As-Built Sublot Lift Thickness (in):	1.5
Total Thickness of All 2009 Sublots (in):	6.9
Approx. Underlying HMA Thickness (in):	0.0
Type of Tack Coat Utilized:	NTSS-1HM
Target Tack Application Rate (gal/sy):	0.04
Approx. Avg. Temperature at Plant (F):	250
Avg. Measured Mat Compaction:	93.7%

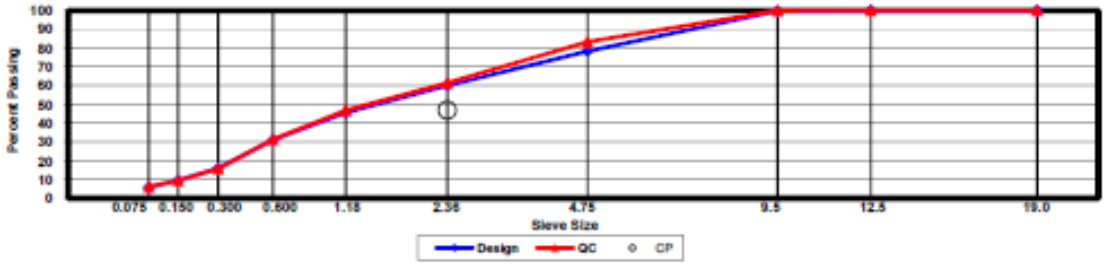

General Notes:

1) Mixes are referenced by quadrant (E=East, N=North, W=West, and S=South), section # (sequential) and sublot (top=1);
3) The total HMA thickness of all structural study sections (N1-N11 and S8-S12) ranges from 5-3/4 to 14 inches by design;
3) All non-structural sections are supprted by a uniform perpetual foundation in order to study surface mix performance;
4) SMA and OGFC refer to stone matrix asphalt and open-graded friction course, respectively; and
5) All liquid asphalt purchased for use in Track reconstruction contained LOF 6500 antistrip additive at a rate of 0.5 percent

Quadrant: S
Section: 11
Sublot: 2

Laboratory Diary

General Description of Mix and Materials

Design Method:	WMA
Compactive Effort:	80 gyrations
Binder Performance Grade:	76-22+
Modifier Type:	Additive
Aggregate Type:	Lms/Sand/Grn
Design Gradation Type:	Fine

Avg. Lab Properties of Plant Produced Mix

Sieve Size	Design	QC
25 mm (1"):	100	98
19 mm (3/4"):	93	94
12.5 mm (1/2"):	82	87
9.5 mm (3/8"):	71	80
4.75 mm (#4):	52	60
2.36 mm (#8):	45	48
1.18 mm (#16):	35	38
0.60 mm (#30):	24	25
0.30 mm (#50):	12	13
0.15 mm (#100):	7	8
0.075 mm (#200):	3.9	4.9
Binder Content (Pb):	4.7	4.6
Eff. Binder Content (Pbe):	**4.1**	**4.0**
Dust-to-Binder Ratio:	0.9	1.2
Rice Gravity (Gmm):	2.575	2.555
Avg. Bulk Gravity (Gmb):	2.472	2.429
Avg Air Voids (Va):	4.0	4.9
Agg. Bulk Gravity (Gsb):	2.737	2.709
Avg VMA:	13.9	14.5
Avg. VFA:	71	66

Construction Diary

Relevant Conditions for Construction

Completion Date:	July 14, 2009
24 Hour High Temperature (F):	93
24 Hour Low Temperature (F):	72
24 Hour Rainfall (in):	0.00
Planned Subot Lift Thickness (in):	2.8
Paving Machine:	Roadtec

Plant Configuration and Placement Details

Component	% Setting
Asphalt Content (Plant Setting)	4.7
78 Opelika Limestone	30.0
57 Opelika Limestone	18.0
M10 Columbus Granite	25.0
Shorter Coarse Sand	27.0

As-Built Sublot Lift Thickness (in):	2.8
Total Thickness of All 2009 Sublots (in):	6.9
Approx. Underlying HMA Thickness (in):	0.0
Type of Tack Coat Utilized:	NTSS-1HM
Target Tack Application Rate (gal/sy):	0.07
Approx. Avg. Temperature at Plant (F):	250
Avg. Measured Mat Compaction:	92.9%

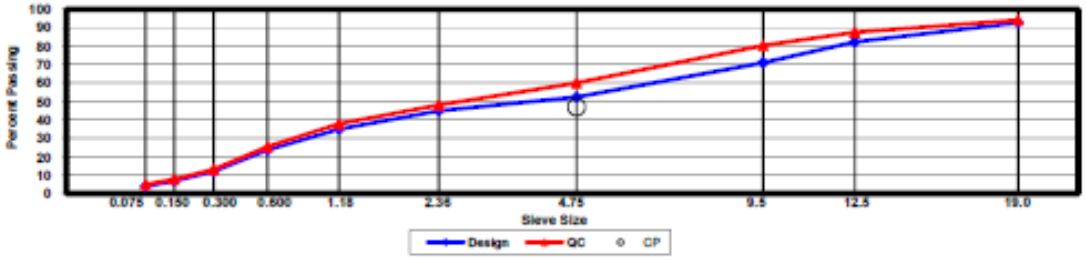

General Notes:

1) Mixes are referenced by quadrant (E=East, N=North, W=West, and S=South), section # (sequential) and sublot (top=1);
3) The total HMA thickness of all structural study sections (N1-N11 and S8-S12) ranges from 5-3/4 to 14 inches by design;
3) All non-structural sections are supprted by a uniform perpetual foundation in order to study surface mix performance;
4) SMA and OGFC refer to stone matrix asphalt and open-graded friction course, respectively; and
5) All liquid asphalt purchased for use in Track reconstruction contained LOF 6500 antistrip additive at a rate of 0.5 percent

Quadrant: S
Section: 11
Sublot: 3

Laboratory Diary

General Description of Mix and Materials

Design Method:	WMA
Compactive Effort:	80 gyrations
Binder Performance Grade:	67-22+
Modifier Type:	Additive
Aggregate Type:	Lms/Sand/Grn
Design Gradation Type:	Fine

Avg. Lab Properties of Plant Produced Mix

Sieve Size	Design	QC
25 mm (1"):	100	99
19 mm (3/4"):	93	95
12.5 mm (1/2"):	84	87
9.5 mm (3/8"):	73	80
4.75 mm (#4):	55	61
2.36 mm (#8):	47	50
1.18 mm (#16):	36	40
0.60 mm (#30):	25	28
0.30 mm (#50):	14	16
0.15 mm (#100):	8	9
0.075 mm (#200):	4.6	5.3
Binder Content (Pb):	4.6	5.0
Eff. Binder Content (Pbe):	**4.1**	**4.5**
Dust-to-Binder Ratio:	1.1	1.2
Rice Gravity (Gmm):	2.574	2.522
Avg. Bulk Gravity (Gmb):	2.471	2.447
Avg Air Voids (Va):	4.0	3.0
Agg. Bulk Gravity (Gsb):	2.738	2.693
Avg VMA:	13.9	13.7
Avg. VFA:	71	78

Construction Diary

Relevant Conditions for Construction

Completion Date:	July 3, 2009
24 Hour High Temperature (F):	92
24 Hour Low Temperature (F):	69
24 Hour Rainfall (in):	0.00
Planned Subot Lift Thickness (in):	3.0
Paving Machine:	Roadtec

Plant Configuration and Placement Details

Component	% Setting
Asphalt Content (Plant Setting)	4.9
78 Opelika Limestone	30.0
57 Opelika Limestone	18.0
M10 Columbus Granite	25.0
Shorter Coarse Sand	27.0

As-Built Sublot Lift Thickness (in):	2.6
Total Thickness of All 2009 Sublots (in):	6.9
Approx. Underlying HMA Thickness (in):	0.0
Type of Tack Coat Utilized:	NA
Target Tack Application Rate (gal/sy):	NA
Approx. Avg. Temperature at Plant (F):	250
Avg. Measured Mat Compaction:	93.9%

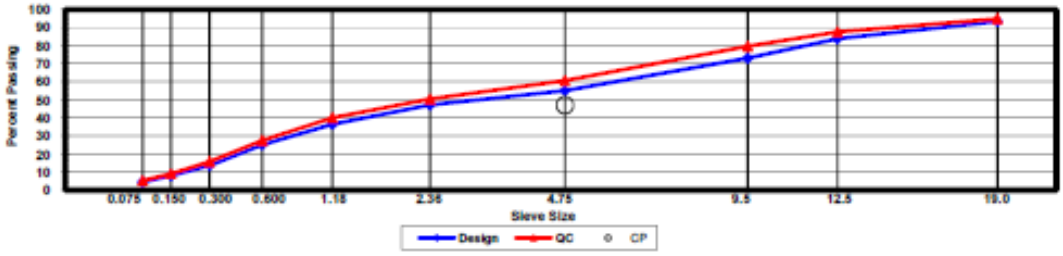

General Notes:

1) Mixes are referenced by quadrant (E=East, N=North, W=West, and S=South), section # (sequential) and sublot (top=1);
3) The total HMA thickness of all structural study sections (N1-N11 and S8-S12) ranges from 5-3/4 to 14 inches by design;
3) All non-structural sections are supprted by a uniform perpetual foundation in order to study surface mix performance;
4) SMA and OGFC refer to stone matrix asphalt and open-graded friction course, respectively; and
5) All liquid asphalt purchased for use in Track reconstruction contained LOF 6500 antistrip additive at a rate of 0.5 percent

Quadrant: S
Section: 12
Sublot: 1

Laboratory Diary

General Description of Mix and Materials

Design Method:	TLA
Compactive Effort:	80 gyrations
Binder Performance Grade:	67-28
Modifier Type:	TLA
Aggregate Type:	Grn/Sand/Lms
Design Gradation Type:	Fine

Avg. Lab Properties of Plant Produced Mix

Sieve Size	Design	QC
25 mm (1"):	100	100
19 mm (3/4"):	100	100
12.5 mm (1/2"):	100	100
9.5 mm (3/8"):	100	100
4.75 mm (#4):	73	83
2.36 mm (#8):	57	61
1.18 mm (#16):	45	47
0.60 mm (#30):	30	32
0.30 mm (#50):	15	16
0.15 mm (#100):	10	9
0.075 mm (#200):	6.5	6.1
Binder Content (Pb):	5.7	6.1
Eff. Binder Content (Pbe):	5.0	5.5
Dust-to-Binder Ratio:	1.3	1.1
Rice Gravity (Gmm):	2.481	2.473
Avg. Bulk Gravity (Gmb):	2.382	2.361
Avg Air Voids (Va):	4.0	4.5
Agg. Bulk Gravity (Gsb):	2.659	2.675
Avg VMA:	15.5	17.2
Avg. VFA:	74	74

Construction Diary

Relevant Conditions for Construction

Completion Date:	August 10, 2009
24 Hour High Temperature (F):	94
24 Hour Low Temperature (F):	75
24 Hour Rainfall (in):	0.00
Planned Subot Lift Thickness (in):	1.3
Paving Machine:	Roadtec

Plant Configuration and Placement Details

Component	% Setting
Asphalt Content (Plant Setting)	5.9
89 Columbus Granite	36.0
8910 Opelika Limestone Screenings	23.0
M10 Columbus Granite	10.0
Shorter Coarse Sand	31.0
TLA	25.0
As-Built Sublot Lift Thickness (in):	1.4
Total Thickness of All 2009 Sublots (in):	6.9
Approx. Underlying HMA Thickness (in):	0.0
Type of Tack Coat Utilized:	PG67-22
Target Tack Application Rate (gal/sy):	0.03
Approx. Avg. Temperature at Plant (F):	335
Avg. Measured Mat Compaction:	94.5%

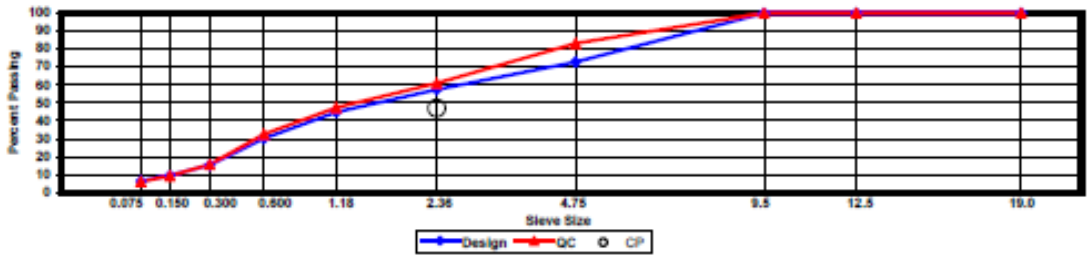

General Notes:

1) Mixes are referenced by quadrant (E=East, N=North, W=West, and S=South), section # (sequential) and sublot (top=1);
3) The total HMA thickness of all structural study sections (N1-N11 and S8-S12) ranges from 5-3/4 to 14 inches by design;
3) All non-structural sections are supprted by a uniform perpetual foundation in order to study surface mix performance;
4) SMA and OGFC refer to stone matrix asphalt and open-graded friction course, respectively; and
5) All liquid asphalt purchased for use in Track reconstruction contained LOF 6500 antistrip additive at a rate of 0.5 percent

Quadrant: S
Section: 12
Sublot: 2

Laboratory Diary

General Desccription of Mix and Materials

Design Method:	TLA
Compactive Effort:	80 gyrations
Binder Performance Grade:	67-28
Modifier Type:	TLA
Aggregate Type:	Lms/Sand/Grn
Design Gradation Type:	Fine

Avg. Lab Properties of Plant Produced Mix

Sieve Size	Design	QC
25 mm (1"):	100	99
19 mm (3/4"):	93	94
12.5 mm (1/2"):	82	84
9.5 mm (3/8"):	71	74
4.75 mm (#4):	52	57
2.36 mm (#8):	45	46
1.18 mm (#16):	35	36
0.60 mm (#30):	24	24
0.30 mm (#50):	12	12
0.15 mm (#100):	7	7
0.075 mm (#200):	3.9	4.4
Binder Content (Pb):	4.7	4.7
Eff. Binder Content (Pbe):	4.4	4.5
Dust-to-Binder Ratio:	0.9	1.0
Rice Gravity (Gmm):	2.557	2.534
Avg. Bulk Gravity (Gmb):	2.468	2.421
Avg Air Voids (Va):	3.5	4.5
Agg. Bulk Gravity (Gsb):	2.737	2.715
Avg VMA:	14.0	15.0
Avg. VFA:	75	70

Construction Diary

Relevant Conditions for Construction

Completion Date:	August 7, 2009
24 Hour High Temperature (F):	94
24 Hour Low Temperature (F):	70
24 Hour Rainfall (in):	0.00
Planned Subot Lift Thickness (in):	2.8
Paving Machine:	Roadtec

Plant Configuration and Placement Details

Component	% Setting
Asphalt Content (Plant Setting)	4.8
78 Opelika Limestone	30.0
57 Opelika Limestone	18.0
M10 Columbus Granite	25.0
Shorter Coarse Sand	27.0
TLA	25.0

As-Built Sublot Lift Thickness (in):	2.9
Total Thickness of All 2009 Sublots (in):	6.9
Approx. Underlying HMA Thickness (in):	0.0
Type of Tack Coat Utilized:	NTSS-1HM
Target Tack Application Rate (gal/sy):	0.03
Approx. Avg. Temperature at Plant (F):	335
Avg. Measured Mat Compaction:	95.2%

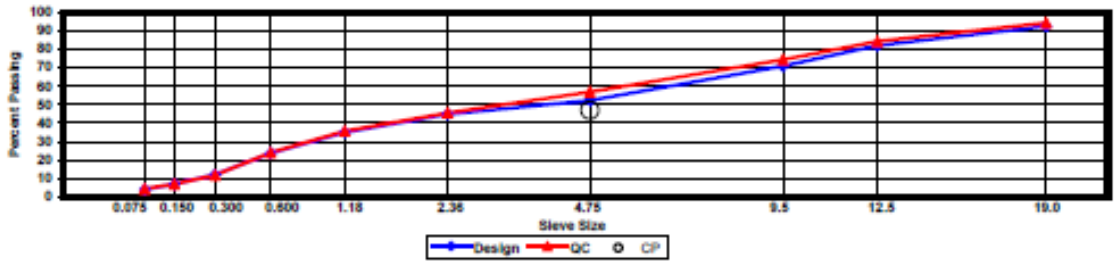

General Notes:

1) Mixes are referenced by quadrant (E=East, N=North, W=West, and S=South), section # (sequential) and sublot (top=1);
3) The total HMA thickness of all structural study sections (N1-N11 and S8-S12) ranges from 5-3/4 to 14 inches by design;
3) All non-structural sections are supprted by a uniform perpetual foundation in order to study surface mix performance;
4) SMA and OGFC refer to stone matrix asphalt and open-graded friction course, respectively; and
5) All liquid asphalt purchased for use in Track reconstruction contained LOF 6500 antistrip additive at a rate of 0.5 percent

Quadrant: S
Section: 12
Sublot: 3

Laboratory Diary

General Description of Mix and Materials

Design Method:	TLA
Compactive Effort:	80 gyrations
Binder Performance Grade:	67-28
Modifier Type:	TLA
Aggregate Type:	Lms/Sand/Gm
Design Gradation Type:	Fine

Avg. Lab Properties of Plant Produced Mix

Sieve Size	Design	QC
25 mm (1"):	100	99
19 mm (3/4"):	93	93
12.5 mm (1/2"):	82	85
9.5 mm (3/8"):	71	74
4.75 mm (#4):	52	57
2.36 mm (#8):	45	45
1.18 mm (#16):	35	36
0.60 mm (#30):	24	25
0.30 mm (#50):	12	12
0.15 mm (#100):	7	7
0.075 mm (#200):	3.9	4.9
Binder Content (Pb):	4.7	4.9
Eff. Binder Content (Pbe):	4.4	4.7
Dust-to-Binder Ratio:	0.9	1.1
Rice Gravity (Gmm):	2.557	2.533
Avg. Bulk Gravity (Gmb):	2.468	2.434
Avg Air Voids (Va):	3.5	3.9
Agg. Bulk Gravity (Gsb):	2.737	2.722
Avg VMA:	14.0	14.9
Avg. VFA:	75	74

Construction Diary

Relevant Conditions for Construction

Completion Date:	August 7, 2009
24 Hour High Temperature (F):	94
24 Hour Low Temperature (F):	70
24 Hour Rainfall (in):	0.00
Planned Subot Lift Thickness (in):	3.0
Paving Machine:	Roadtec

Plant Configuration and Placement Details

Component	% Setting
Asphalt Content (Plant Setting)	4.8
78 Opelika Limestone	30.0
57 Opelika Limestone	18.0
M10 Columbus Granite	25.0
Shorter Coarse Sand	27.0
TLA	25.0
As-Built Sublot Lift Thickness (in):	2.6
Total Thickness of All 2009 Sublots (in):	6.9
Approx. Underlying HMA Thickness (in):	0.0
Type of Tack Coat Utilized:	NA
Target Tack Application Rate (gal/sy):	NA
Approx. Avg. Temperature at Plant (F):	335
Avg. Measured Mat Compaction:	93.9%

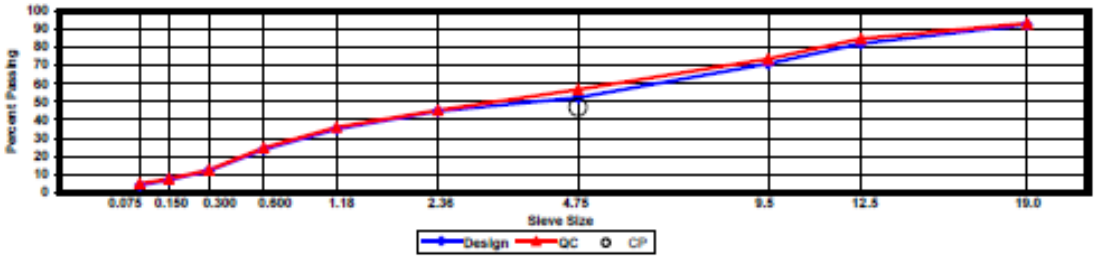

General Notes:

1) Mixes are referenced by quadrant (E=East, N=North, W=West, and S=South), section # (sequential) and sublot (top=1);
3) The total HMA thickness of all structural study sections (N1-N11 and S8-S12) ranges from 5-3/4 to 14 inches by design;
3) All non-structural sections are supprted by a uniform perpetual foundation in order to study surface mix performance;
4) SMA and OGFC refer to stone matrix asphalt and open-graded friction course, respectively; and
5) All liquid asphalt purchased for use in Track reconstruction contained LOF 6500 antistrip additive at a rate of 0.5 percent

APPENDIX B

DYNAMIC MODULUS MASTER CURVE PARAMETERS

Table B.1: Dynamic modulus master curve fitting parameters by section and lift

Year	Section	Lift	$\|E^*\|_{max}$ (ksi)	$\|E^*\|_{min}$ (ksi)	$\beta_{\|E^*\|}$	$\gamma_{\|E^*\|}$	ΔE_a
2006	N1	1	3153.45	12.2515	-0.48490	-0.51437	173446
2006	N1	2	3153.45	12.2515	-0.48490	-0.51437	173446
2006	N1	3	3108.02	16.9892	-0.44890	-0.55771	183418
2006	N2	1	3151.62	6.5469	-0.67434	-0.45750	189759
2006	N2	2	3151.62	6.5469	-0.67434	-0.45750	189759
2006	N2	3	3108.02	16.9892	-0.44890	-0.55771	183418
2006	N8	1	3200.01	26.0446	-0.21065	-0.56947	184441
2006	N8	2	3275.35	18.5746	-0.52847	-0.55186	177544
2006	N8	3	3324.36	15.9505	-0.79394	-0.52042	187967
2006	N8	4	3199.01	1.4703	-0.79536	-0.45638	174143
2006	N9	1	3200.01	26.0446	-0.21065	-0.56947	184441
2006	N9	2	3275.35	18.5746	-0.52847	-0.55186	177544
2006	N9	3	3324.36	15.9505	-0.79394	-0.52042	187967
2006	N9	4	3324.36	15.9505	-0.79394	-0.52042	187967
2006	N9	5	3199.01	1.4703	-0.79536	-0.45638	174143
2009	N5	1	3077.80	6.1206	-0.68194	-0.48215	198848
2009	N5	2	3116.15	20.8315	-1.16723	-0.55371	194599
2009	N5	3	3116.15	20.8315	-1.16723	-0.55371	194599
2009	N5	4	3058.94	11.0581	-0.93074	-0.51905	194778
2009	N6	1	3077.80	6.1206	-0.68194	-0.48215	198848
2009	N6	2	3116.15	20.8315	-1.16723	-0.55371	194599
2009	N6	3	3058.94	11.0581	-0.93074	-0.51905	194778
2009	N7	1	3069.92	5.0225	-1.21839	-0.41255	212277
2009	N7	2	3171.23	8.8627	-0.94238	-0.50426	199863
2009	N7	3	3171.23	8.8627	-0.94238	-0.50426	199863
2009	N9	1	3200.01	26.0446	-0.21065	-0.56947	184441
2009	N9	2	3275.35	18.5746	-0.52847	-0.55186	177544
2009	N9	3	3324.36	15.9505	-0.79394	-0.52042	187967
2009	N9	4	3324.36	15.9505	-0.79394	-0.52042	187967
2009	N9	5	3199.01	1.4703	-0.79536	-0.45638	174143
2009	N10	1	3120.90	2.8804	-1.32794	-0.46090	200495
2009	N10	2	3210.41	10.0223	-1.61924	-0.48190	202316
2009	N10	3	3210.41	10.0223	-1.61924	-0.48190	202316
2009	N11	1	3131.28	2.9588	-1.23474	-0.48011	193601
2009	N11	2	3198.51	7.0638	-1.46638	-0.50342	196269
2009	N11	3	3198.51	7.0638	-1.46638	-0.50342	196269
2009	S9	1	3077.80	6.1206	-0.68194	-0.48215	198848
2009	S9	2	3189.49	8.8575	-1.13275	-0.47236	198828
2009	S9	3	3177.54	6.5248	-0.97379	-0.52221	178209
2009	S10	1	3091.29	8.8030	-0.59337	-0.52043	196110
2009	S10	2	3206.25	7.9263	-0.89651	-0.50838	194852

Year	Section	Lift	Max |E*| (ksi)	Min |E*| (ksi)	β	γ	ΔE_a
2009	S10	3	3220.34	7.3056	-0.88260	-0.55914	170475
2009	S11	1	3061.17	9.2506	-0.41207	-0.54640	197466
2009	S11	2	3197.85	9.1633	-0.65187	-0.56096	180094
2009	S11	3	3190.01	7.8541	-0.83602	-0.52289	198519
2009	S12	1	3085.15	6.2547	-0.85176	-0.56174	184189
2009	S12	2	3151.74	11.7112	-1.05119	-0.55833	192917
2009	S12	3	3151.74	11.7112	-1.05119	-0.55833	192917

APPENDIX C

DYNAMIC SHEAR MODULUS MASTER CURVE PARAMETERS

Table C.1: Dynamic shear modulus master curve fitting parameters by section and lift

Year	Section	Lift	f_c	k	m_e	C_1	C_2
2006	N1	1	7.2416E-08	2.3883	0.08268	13.7631	116.887
2006	N1	2	7.2416E-08	2.3883	0.08268	13.7631	116.887
2006	N1	3	0.00044	1.4739	0.09071	17.3488	150.184
2006	N2	1	0.00457	1.1076	0.08414	10.6846	73.549
2006	N2	2	0.00457	1.1076	0.08414	10.6846	73.549
2006	N2	3	0.00044	1.4739	0.09071	17.3488	150.184
2006	N8	1	1.6833E-07	2.0390	0.08106	17.8700	149.105
2006	N8	2	1.6833E-07	2.0390	0.08106	17.8700	149.105
2006	N8	3	186.722	0.7504	0.11852	23.8849	216.356
2006	N8	4	2.2933	1.1057	0.11350	7.4792	71.741
2006	N9	1	1.6833E-07	2.0390	0.08106	17.8700	149.105
2006	N9	2	1.6833E-07	2.0390	0.08106	17.8700	149.105
2006	N9	3	186.722	0.7504	0.11852	23.8849	216.356
2006	N9	4	186.722	0.7504	0.11852	23.8849	216.356
2006	N9	5	2.2933	1.1057	0.11350	7.4792	71.741
2009	N5	1	0.61063	0.1273	1.18821	17.2716	149.705
2009	N5	2	0.27471	0.1222	1.21480	14.3698	119.775
2009	N5	3	0.27471	0.1222	1.21480	14.3698	119.775
2009	N5	4	1.4244	0.1309	1.14818	15.5013	134.316
2009	N6	1	0.61063	0.1273	1.18821	17.2716	149.705
2009	N6	2	0.27471	0.1222	1.21480	14.3698	119.775
2009	N6	3	1.4244	0.1309	1.14818	15.5013	134.316
2009	N7	1	287619	1.3110	0.49998	8.4089	45.607
2009	N7	2	287619	1.3110	0.49998	8.4089	45.607
2009	N7	3	287619	1.3110	0.49998	8.4089	45.607
2009	N9	1	1.6833E-07	2.0390	0.08106	17.8700	149.105
2009	N9	2	1.6833E-07	2.0390	0.08106	17.8700	149.105
2009	N9	3	186.722	0.7504	0.11852	23.8849	216.356
2009	N9	4	186.722	0.7504	0.11852	23.8849	216.356
2009	N9	5	2.2933	1.1057	0.11350	7.4792	71.741
2009	N10	1	0.02167	0.1110	1.06370	31.5280	255.552
2009	N10	2	0.14052	0.1160	0.86545	110.7931	908.838
2009	N10	3	0.14052	0.1160	0.86545	110.7931	908.838
2009	N11	1	0.17850	0.1203	1.00542	27.5737	223.694
2009	N11	2	0.01452	0.1091	1.03005	40.4620	324.899
2009	N11	3	0.01452	0.1091	1.03005	40.4620	324.899
2009	S9	1	90.647	0.1431	0.80619	18.7539	164.279
2009	S9	2	95.027	0.1481	0.77346	17.2116	140.433
2009	S9	3	0.06432	0.1171	1.20582	19.3601	159.895
2009	S10	1	71.981	0.1478	0.80602	17.5386	144.205
2009	S10	2	56.495	0.1415	0.76630	17.1095	136.206
2009	S10	3	0.35163	0.1240	1.11898	26.5075	227.293

Year	Section	Lift	f_c	k	m_e	C_1	C_2
2009	S11	1	143.328	0.1493	0.81344	17.0336	143.466
2009	S11	2	118.258	0.1491	0.78419	18.1580	149.320
2009	S11	3	0.09870	0.1206	1.24448	15.3782	124.872
2009	S12	1	11.267	0.1505	0.87501	25.2123	207.692
2009	S12	2	8.0719	0.1386	0.90201	16.9651	140.137
2009	S12	3	8.0719	0.1386	0.90201	16.9651	140.137

APPENDIX D

FIELD-CALIBRATED MASTER CURVES

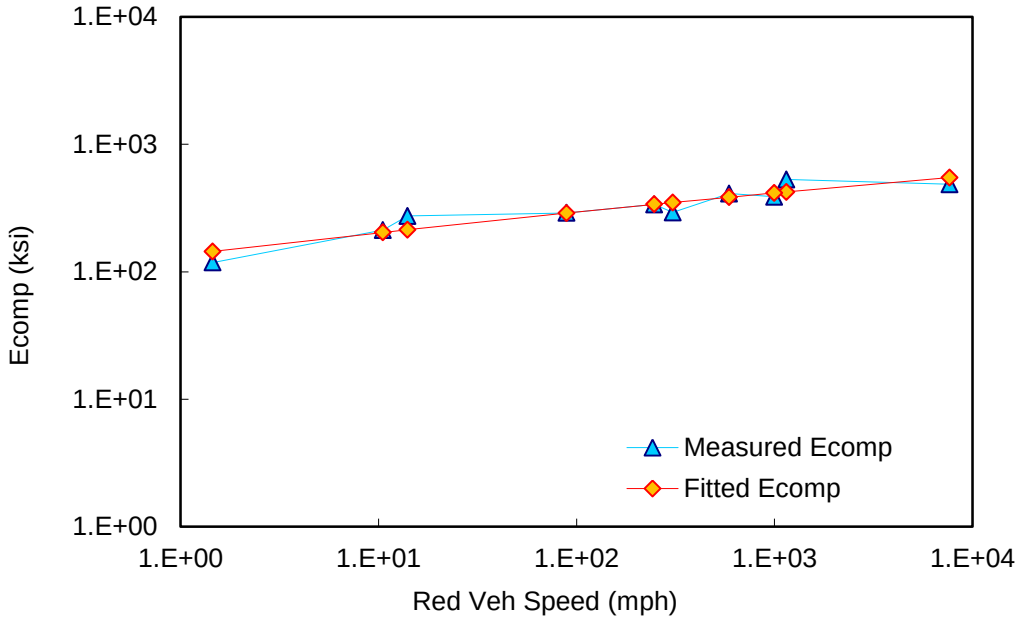

Figure D.1: Field-calibrated master curve, N1.

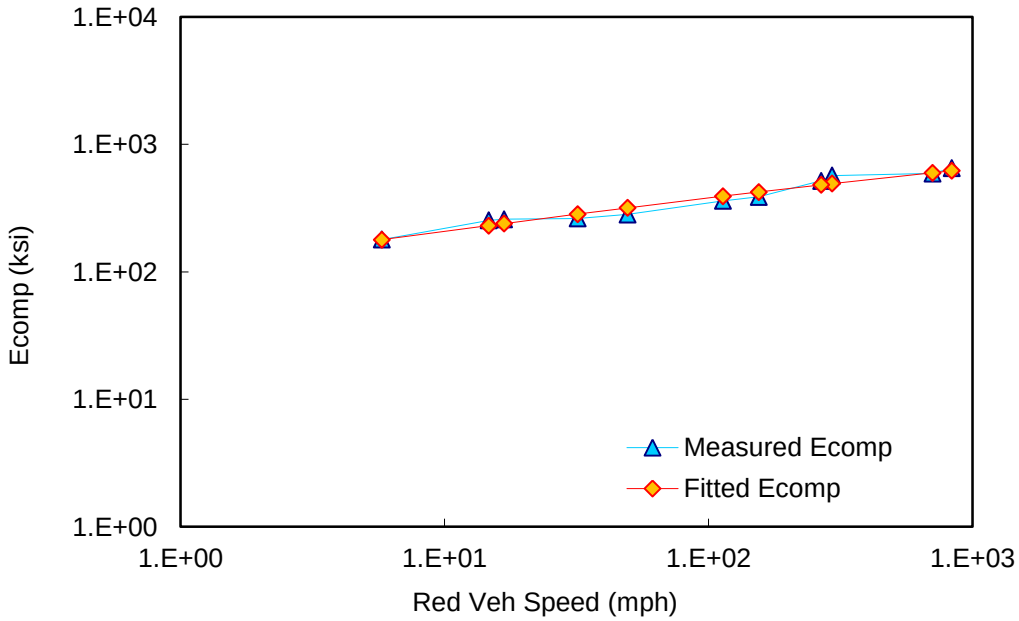

Figure D.2: Field-calibrated master curve, N2.

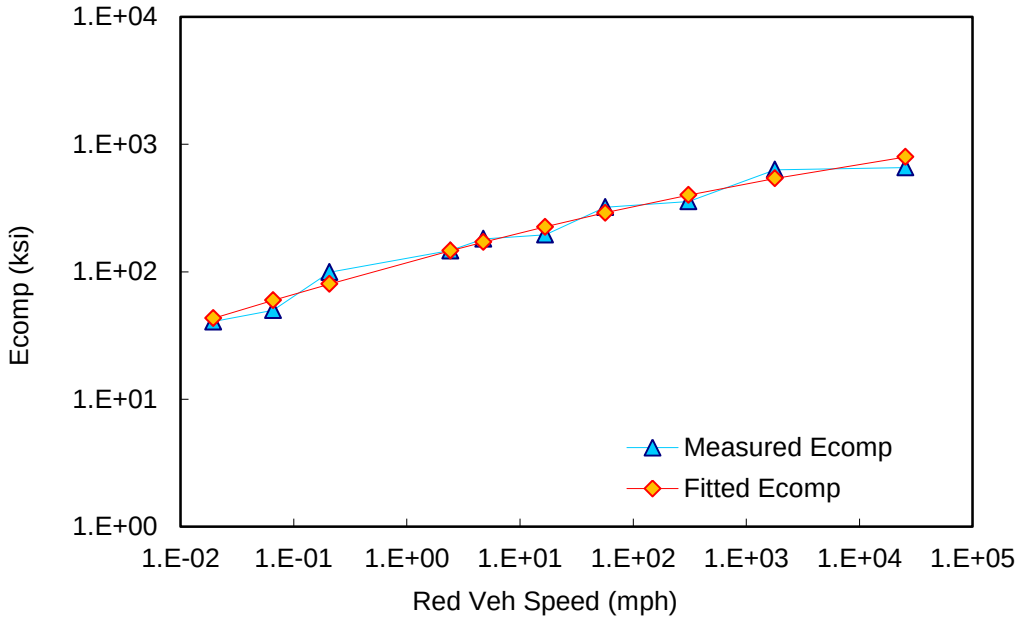

Figure D.3: Field-calibrated master curve, N8.

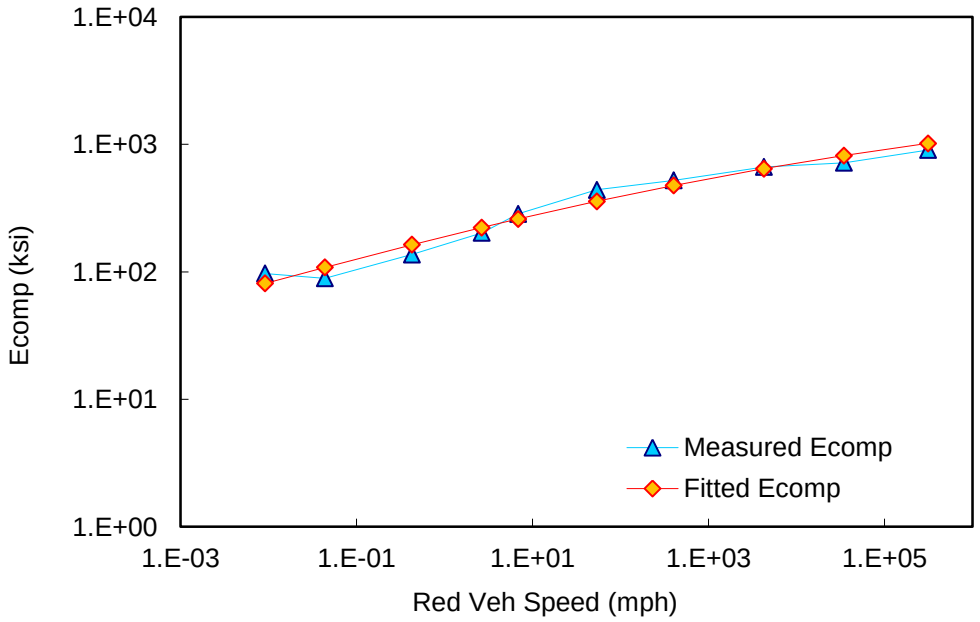

Figure D.4: Field-calibrated master curve, N9 (2006).

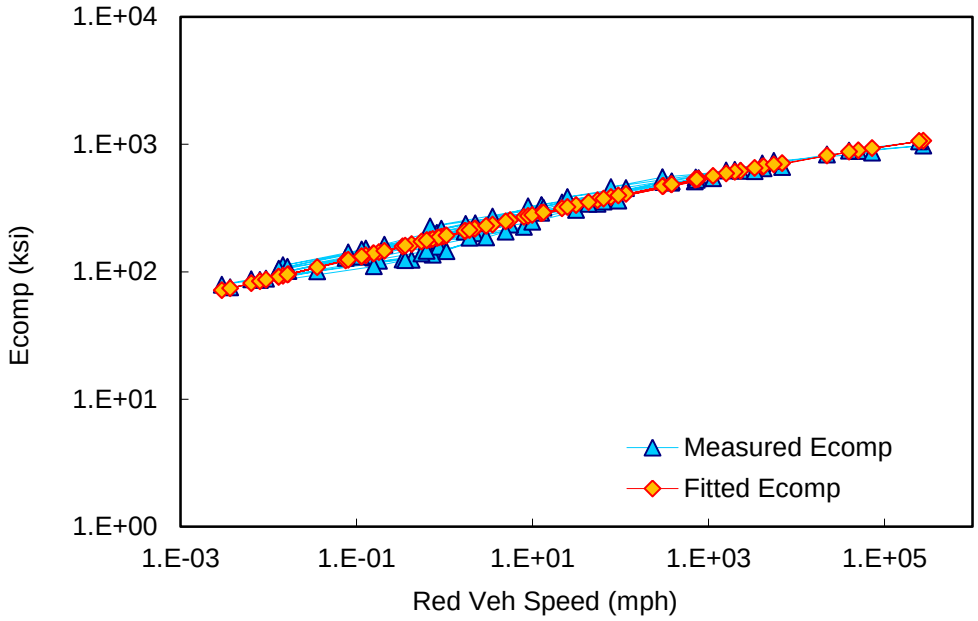

Figure D.5: Field-calibrated master curve, N5.

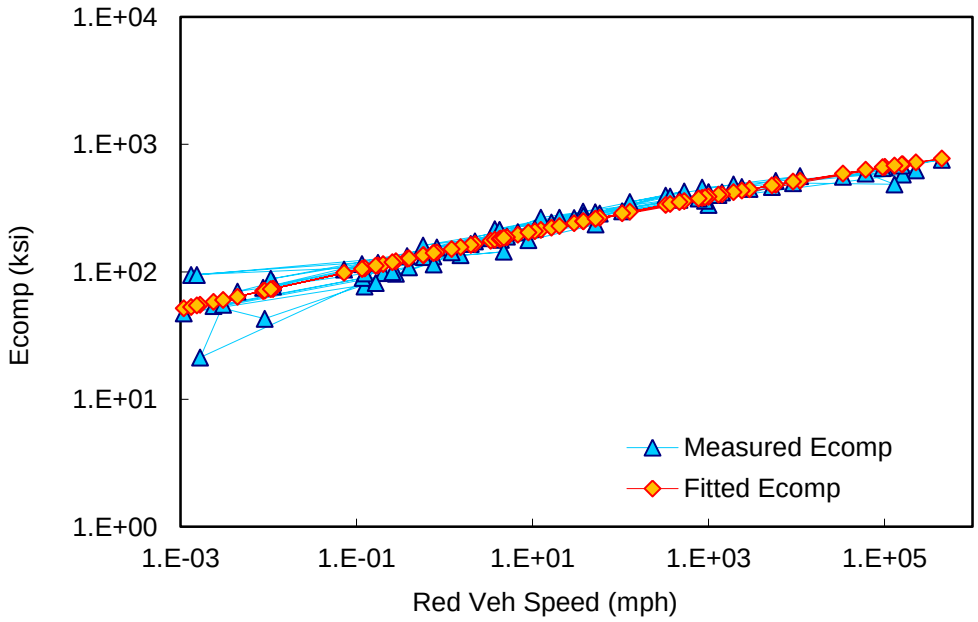

Figure D.6: Field-calibrated master curve, N6.

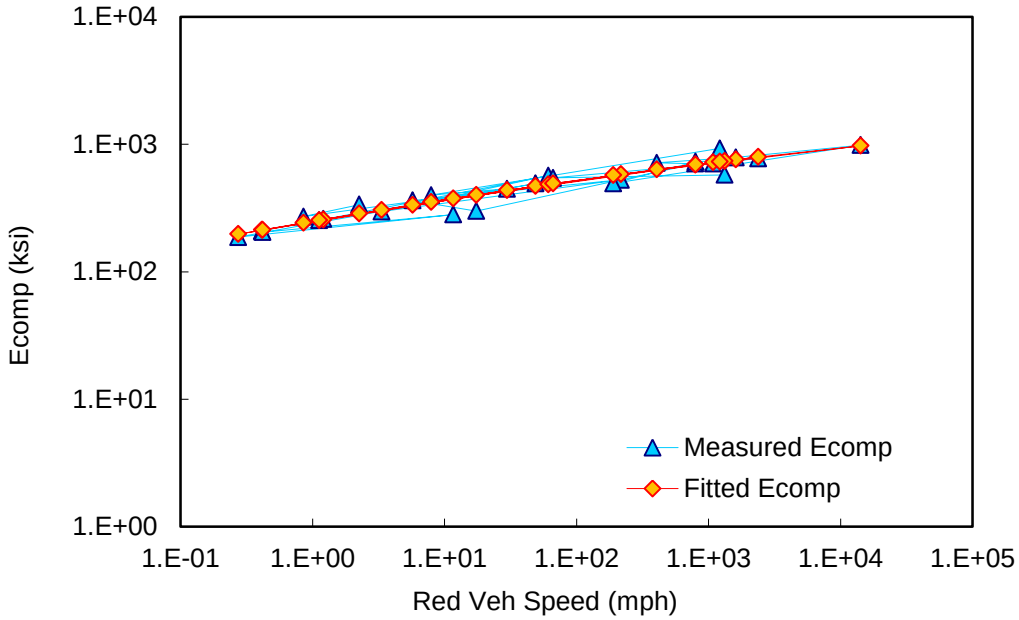

Figure D.7: Field-calibrated master curve, N7.

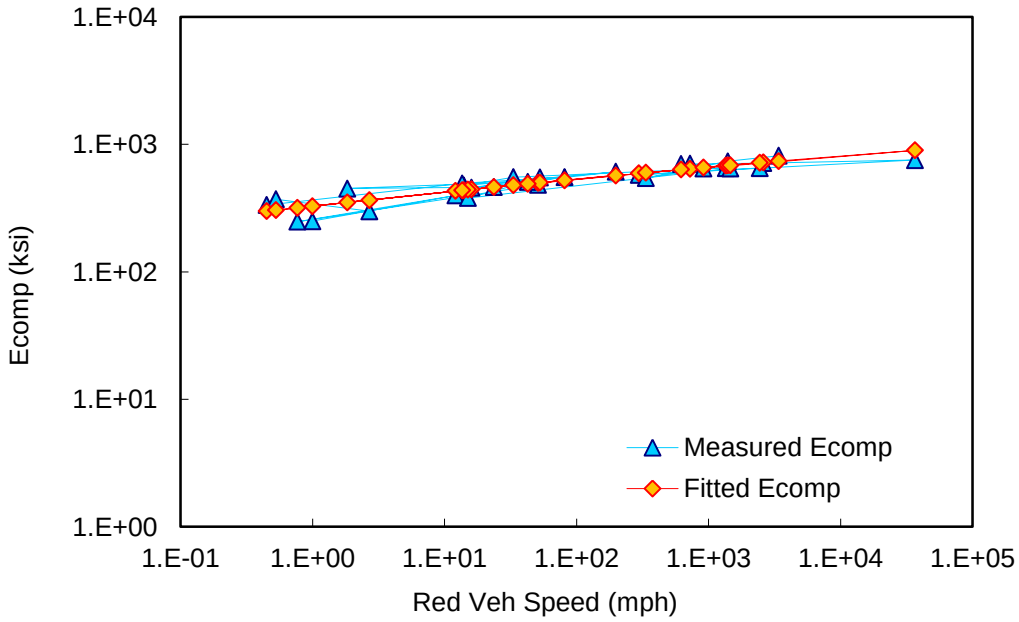

Figure D.8: Field-calibrated master curve, N9 (2009).

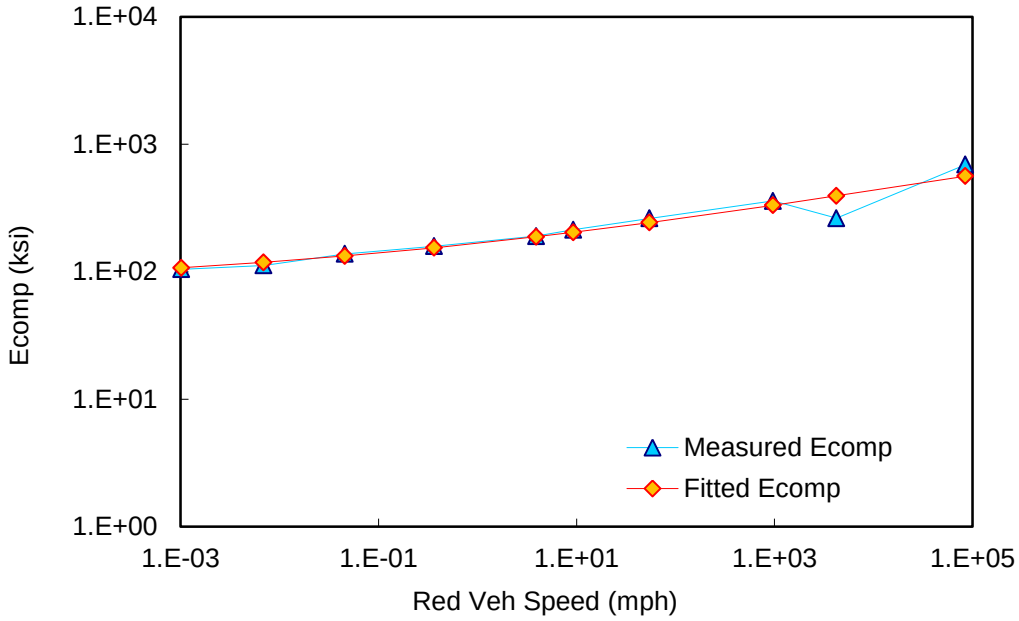

Figure D.9: Field-calibrated master curve, N10.

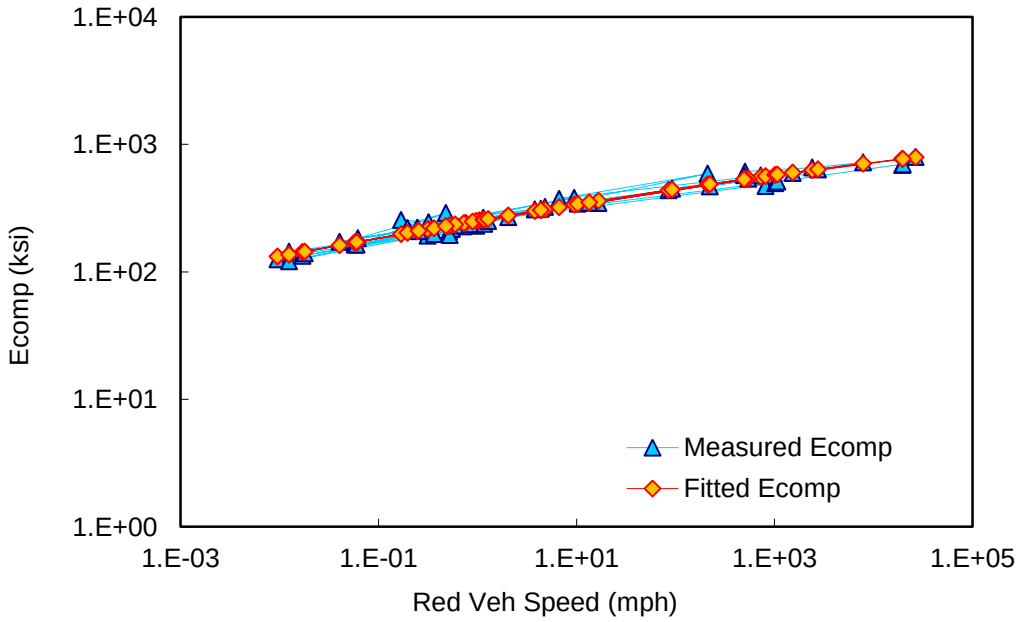

Figure D.10: Field-calibrated master curve, N11.

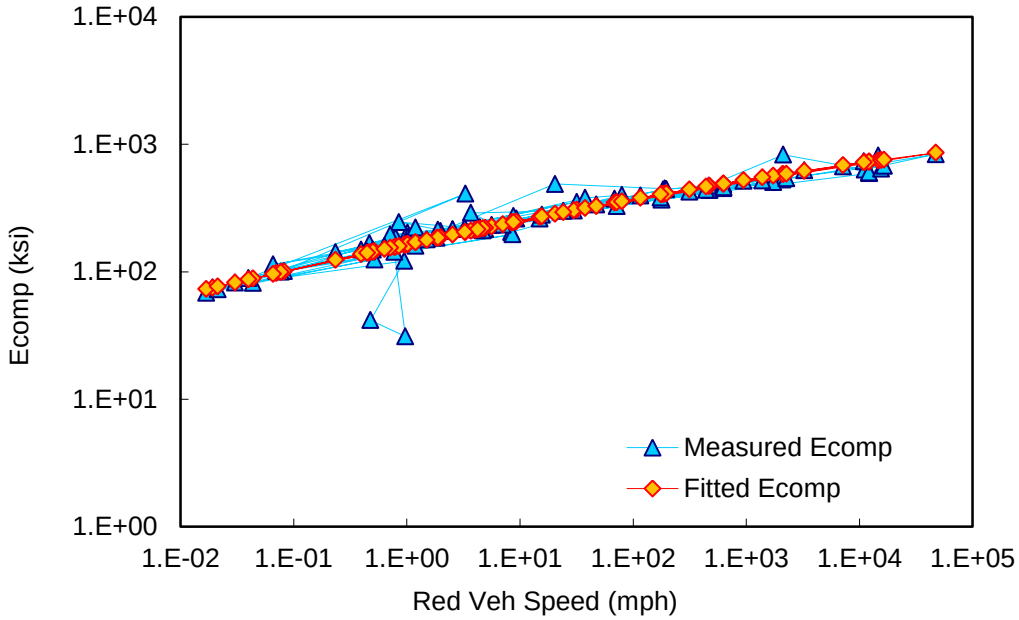

Figure D.11: Field-calibrated master curve, S9.

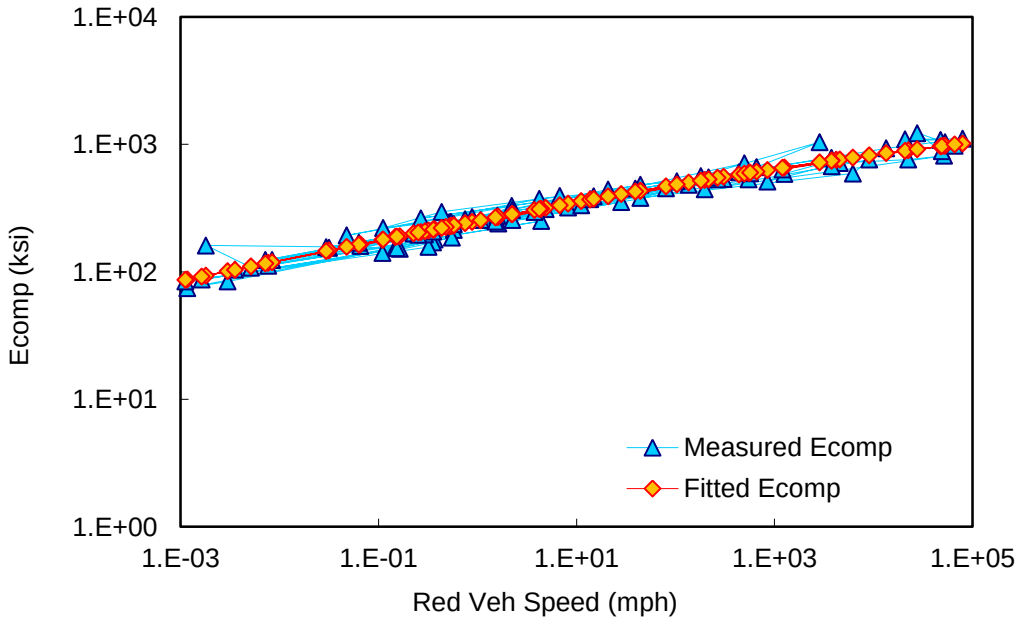

Figure D.12: Field-calibrated master curve, S10.

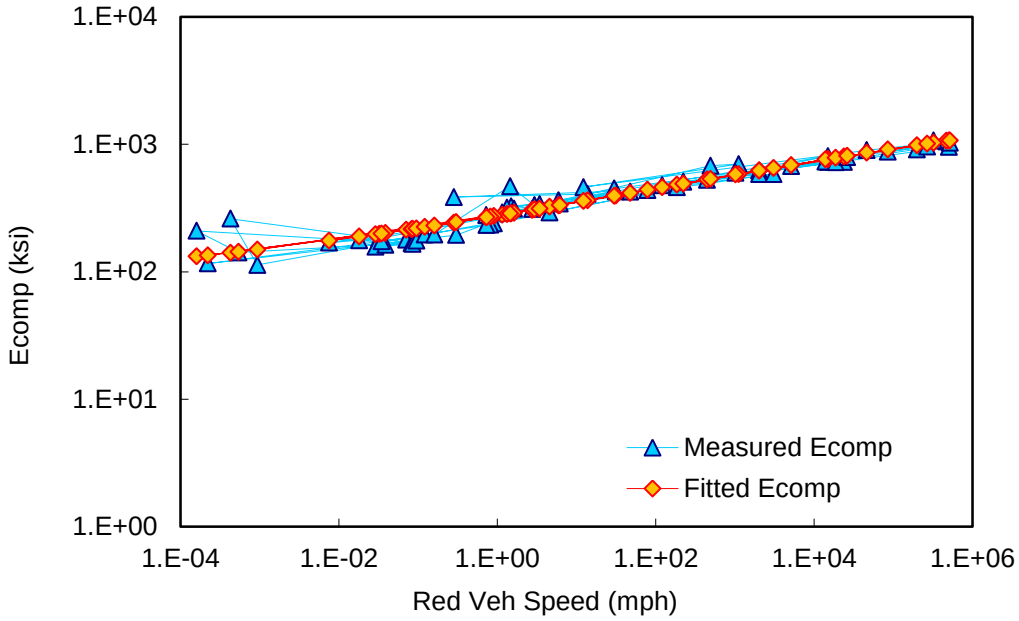

Figure D.13: Field-calibrated master curve, S11.

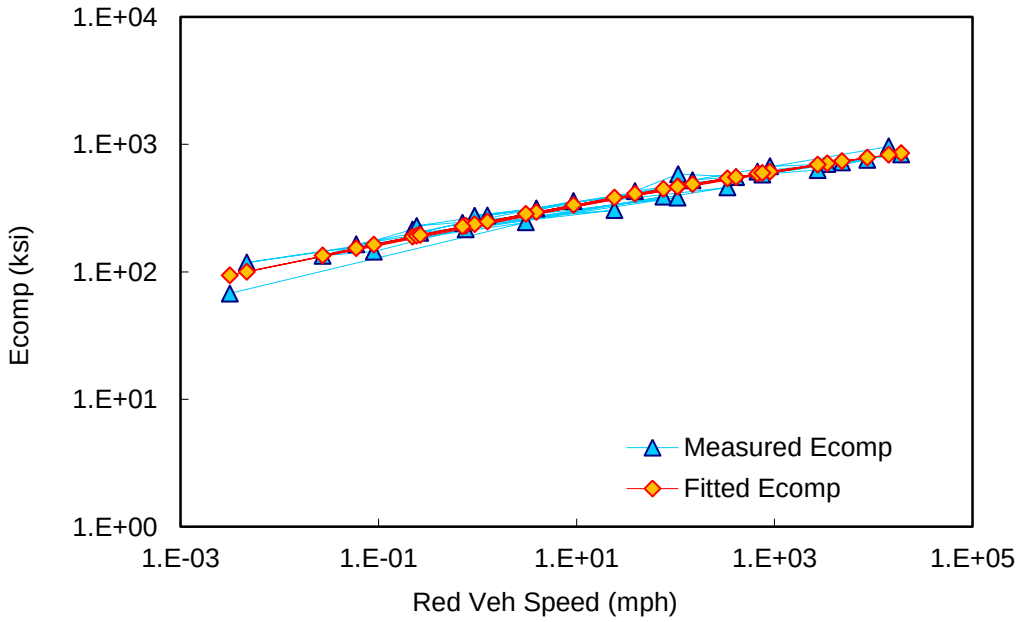

Figure D.14: Field-calibrated master curve, S12.